University of Alberta

Analysis of Retinal Degeneration Using a Model of Human Retinal Disease: Focus on the *in vivo* and *in vitro* Molecular Characterization of the Novel Gene KCTD8

by

Rhonda Michele Kelln ©

A thesis submitted to the Faculty of Graduate Studies and Research
in partial fulfillment of the requirements for the degree of

Doctor of Philosophy
in
Molecular Biology and Genetics

Department of Biological Sciences

Edmonton, Alberta
Spring 2007

Library and
Archives Canada

Published Heritage
Branch

395 Wellington Street
Ottawa ON K1A 0N4
Canada

Bibliothèque et
Archives Canada

Direction du
Patrimoine de l'édition

395, rue Wellington
Ottawa ON K1A 0N4
Canada

Your file Votre référence
ISBN: 978-0-494-29697-4
Our file Notre référence
ISBN: 978-0-494-29697-4

NOTICE:
The author has granted a non-exclusive license allowing Library and Archives Canada to reproduce, publish, archive, preserve, conserve, communicate to the public by telecommunication or on the Internet, loan, distribute and sell theses worldwide, for commercial or non-commercial purposes, in microform, paper, electronic and/or any other formats.

The author retains copyright ownership and moral rights in this thesis. Neither the thesis nor substantial extracts from it may be printed or otherwise reproduced without the author's permission.

AVIS:
L'auteur a accordé une licence non exclusive permettant à la Bibliothèque et Archives Canada de reproduire, publier, archiver, sauvegarder, conserver, transmettre au public par télécommunication ou par l'Internet, prêter, distribuer et vendre des thèses partout dans le monde, à des fins commerciales ou autres, sur support microforme, papier, électronique et/ou autres formats.

L'auteur conserve la propriété du droit d'auteur et des droits moraux qui protège cette thèse. Ni la thèse ni des extraits substantiels de celle-ci ne doivent être imprimés ou autrement reproduits sans son autorisation.

In compliance with the Canadian Privacy Act some supporting forms may have been removed from this thesis.

While these forms may be included in the document page count, their removal does not represent any loss of content from the thesis.

Conformément à la loi canadienne sur la protection de la vie privée, quelques formulaires secondaires ont été enlevés de cette thèse.

Bien que ces formulaires aient inclus dans la pagination, il n'y aura aucun contenu manquant.

ABSTRACT

Retinal degeneration encompasses a large number of disorders resulting in vision loss. The use of animal models to study human retinal disease has been invaluable in understanding the process of visual cell loss. One common feature between human retinal dystrophies and the light-induced retinal degeneration (LIRD) animal model is that both result in visual cell loss via apoptosis. The use of the LIRD model in rats, a well-characterized model of human retinal disease, facilitates the study of retinal disease by studying the molecular changes that take place during the degeneration process.

In order to gain a better understanding of the molecular phenotype during LIRD, I performed a differential cDNA library screen from light-treated retinas representing the oxidative stress phase of LIRD. A number of genes were identified which were either upregulated or downregulated in response to intense light exposure. T-cadherin, which was isolated from this screen, was further analyzed due to the number of cadherin family members that have been implicated in retinal disease. T-cadherin was shown to be upregulated after prolonged light exposure and was found to be expressed in the Müller cells of the retina, further supporting the idea of signaling pathways between the inner and outer retina during retinal degeneration.

The main focus of the thesis was on the characterization of a novel gene isolated from the cDNA library screen, which demonstrated significant homology to the mouse potassium channel tetramerization containing 8 (KCTD8) gene. Bioinformatic analysis of rat KCTD8 identified three conserved domains: a BTB/POZ/T1 domain and two nuclear localization signals (NLSs). The functionality of these two NLSs was studied by mutagenesis and subcellular localization in mammalian cell culture. It was found that the

KCTD8 protein binds to α-tubulin and co-localizes with microtubules. Nuclear localization of KCTD8 was observed in a subset of cells treated with chemicals known to induce oxidative stress.

These studies provide further molecular insight into the process of retinal degeneration. In addition, the characterization of two genes involved in retinal degeneration provides additional avenues of study to gain a better understanding of the molecular events involved in retinal degeneration and apoptosis.

ACKNOWLEDGEMENTS

This thesis would not be possible without the support, guidance and assistance of many. Foremost I would like to thank my supervisor, Dr. Paul Wong, for always setting the bar high and never accepting anything less. By doing so you helped me to achieve more than I thought was possible. Thank you for your guidance and advice over the years and for the numerous opportunities you afforded me. I am forever grateful. To Micah Chrenek, thank you for your countless hours of help over the years, especially with all the cell culture work and for keeping me company during the long hours in the lab in Atlanta. Without your advice and assistance my thesis would not be what it is. Thank you to Michelle Patterson and Jadwiga Stepczynski for their help and guidance in the early part of my project and for creating the cDNA library and helping me with the library screen. As well, many thanks to Pam Lagali for her insightful chats and endless advice. You are a wealth of knowledge. Also, thanks to Brian Maciejko for the technical advice, the music and for always making the lab an enjoyable place.

I would also like to express my gratitude to my co-supervisor, Dr. Shelagh Campbell, for her guidance over the years and also for providing me with my first experience of real research as an undergraduate student in her lab. I would also like to thank my committee members Dr. Julia Foght, Dr. Susan Andew, and Dr. Diane Borst for their time and effort in reading my thesis and providing me with feedback as well as for their advice and assistance over the years.

I am indebted to Dr. Daniel Organisciak, Ruth Darrow and Linda Barsalou for providing me with retinal tissue and for their guidance and support throughout my degree. I am also grateful to Dr. Radha Ayyagari and Dr. Vidyullatha Vasireddy for their help and advice in the early stages of the cell culture work. Thank you to Dr. Machelle Pardue and Tiffany Walker for performing the immunohistochemistry on the RCS rat retinas. Thank you to Laith Dabbagh for the sectioning of the light treated rat retinas for immunohistochemistry. Dr. Rakesh Bhatnagar, Jack Scott and Randy Mandryk at the Advance Microscopy Facility for their technical assistance and advice with the microscopy work and Pat Murray and Lisa Ostafichuk in the Molecular Biology Service Unit for running numerous sequence reactions for me. Thank you.

Of course none of this would have been possible without the support of my family and friends. To my parents, Ron and Sharon Kelln, and to my sister Nancy, thank you for all your support despite wondering why I was still in school. Your love and encouragement over the years is greatly appreciated. Thank you also to Christine Walker for the scientific as well as non-scientific discussions and for being a good listener and a great friend.

Lastly, but certainly not least, this thesis would not be possible without my husband, Scott Milligan, who has supported me every step of the way. His patience, kindness, and love were instrumental in my success and for that I dedicate this thesis to him.

TABLE OF CONTENTS

Chapter **Page**

1 INTRODUCTION **1**

1.1 The Mammalian Eye **2**
  1.1.1 The Retina 3
    1.1.1.1 Cell types and spatial organization of the retina 3
    1.1.1.2 Photoreceptors 4

1.2 Degenerative Diseases Affecting the Retina **5**

1.3 Apoptosis in Retinal Degeneration **7**

1.4 Genetic Models of Retinal Degeneration **8**

1.5 Induced Models of Retinal Degeneration **10**
  1.5.1 Advantages of studying light-induced retinal degeneration 10
  1.5.2 The use of LIRD in rodents as a model system for human disease 11
  1.5.3 Gene expression changes during light-induced retinal degeneration 12
  1.5.4 Practical considerations in the study of light-induced retinal degeneration . 14
    1.5.4.1 Wavelength of light 14
    1.5.4.2 Light exposure duration and intensity 15
    1.5.4.3 Rearing conditions 16
    1.5.4.4 Time of light exposure 16
  1.5.5 The role of oxidative stress in light-induced retinal degeneration 17
  1.5.6 Stages of degeneration in the light-induced retinal degeneration model 18

1.6 Focus of the Thesis **20**

1.7 References **30**

2 DIFFERENTIAL SCREENING FOR GENES INVOLVED IN LIGHT-INDUCED RETINAL DEGENERATION, IDENTIFICATION AND CHARACTERIZATION OF T-CADHERIN 41

2.1 Introduction 42

2.2 Materials and Methods 44
  2.2.1 Animals 44
  2.2.2 RNA isolation 45
  2.2.3 cDNA library construction 45
  2.2.4 cDNA library screening: 45
  2.2.5 Sequencing 47
  2.2.6 Northern analysis 47
  2.2.7 Western analysis 48
  2.2.8 Northern and western blot image analysis 48
  2.2.9 Immunohistochemistry 49

2.3 Results 49
  2.3.1 Isolation of clones 49
  2.3.2 Expression analysis 50
  2.3.3 Sequence characterization 50
  2.3.4 Expression of rat T-cadherin in normal tissues 51
  2.3.5 Rat T-cadherin RNA is upregulated in the retina at peak levels of oxidative stress 52
  2.3.6 T-cadherin protein levels are upregulated when the retina is under a high level of oxidative stress 52
  2.3.7 T-cadherin is localized to the Müller cells of the retina 53

2.4 Discussion 53

2.5 References 72

3 IDENTIFICATION AND CHARACTERIZATION OF RAT KCTD8 80

3.1 Introduction **81**

3.2 Materials and Methods **82**
- 3.2.1 Animals 82
- 3.2.2 RNA isolation and cDNA library screening 82
- 3.2.3 Protein isolation 83
- 3.2.4 Obtaining the full-length sequence of KCTD8 83
- 3.2.5 KCTD8 DNA and protein sequence analysis 84
- 3.2.6 Zooblot analysis 85
- 3.2.7 Northern blot analysis 85
- 3.2.8 Production of a KCTD8 antibody 85
- 3.2.9 Peptide competition assay and western blot analysis 86

3.3 Results **87**
- 3.3.1 Isolation of rat KCTD8 cDNA 87
- 3.3.2 KCTD8 genomic structure 87
- 3.3.3 Sequence conservation of KCTD8 88
- 3.3.4 KCTD8 protein sequence analysis 88
- 3.3.5 Tissue distribution of KCTD8 89
- 3.3.6 Expression analysis of KCTD8 during LIRD 90

3.4 Discussion **91**

3.5 References **112**

4 FUNCTIONAL ANALYSIS OF THE KCTD8 PROTEIN BY MUTAGENESIS AND SUBCELLULAR LOCALIZATION **118**

4.1 Introduction **119**

4.2 Materials and Methods **120**
- 4.2.1 Animals 120
- 4.2.2 KCTD8 subcloning and site-directed mutagenesis 120
- 4.2.3 Mammalian cell culture and transfection 122

4.2.4 Cell treatments and immunocytochemistry 122
4.2.5 Immunoblotting and co-immunoprecipitation 123
4.2.6 Immunohistochemistry 125

4.3 Results 126
4.3.1 Expression of GFP-KCTD8 fusion proteins in COS-7 cells 126
4.3.2 Subcellular localization of the wild-type and mutant KCTD8 in COS-7 cells 127
4.3.3 KCTD8 is colocalized and associates with α-tubulin in COS-7 cells 128
4.3.4 Localization of wild-type KCTD8 to microtubules is disrupted in colcemid treated COS-7 cells 130
4.3.5 Immunolocalization of KCTD8 in the rat retina 131
4.3.6 KCTD8 is colocalized and associates with α-tubulin in the rat retina 131

4.4 Discussion 133

4.5 References 161

5 SUBCELLULAR LOCALIZATION OF THE KCTD8 PROTEIN IN RESPONSE TO OXIDATIVE STRESS 165

5.1 Introduction 166

5.2 Materials and Methods 167
5.2.1 KCTD8 subcloning and site-directed mutagenesis 167
5.2.2 Mammalian cell culture and transfection 168
5.2.3 Cell treatments and immunocytochemistry 168
5.2.4 Animals 169
5.2.5 Immunohistochemistry 169
5.2.6 Statistical analysis 170

5.3 Results 170
5.3.1 Cell treatments result in nuclear condensation and characteristic pyknotic nuclei 170

5.3.2 Oxidative stress results in nuclear localization of wild-type KCTD8 170
5.3.3 KCTD8 becomes nuclear localized in response to cellular stress and degeneration in the retina 174

5.4 Discussion **175**

5.5 References **212**

6 SUMMARY AND CONCLUSIONS **218**

6.1 Summary and Conclusions **219**

6.2 References **225**

LIST OF FIGURES

Figure **Page**

Figure 1.1 – Schematic diagram of the adult human eye. 22

Figure 1.2 – Cellular layers of the retina. 23

Figure 1.3 – Rod photoreceptor cell phototransduction in the vertebrate retina 25

Figure 1.4 – Schematic diagram of rod and cone photoreceptor cells. 27

Figure 1.5 – Morphological changes that occur in a cell undergoing apoptosis 28

Figure 1.6 – Stages of degeneration in the light-induced retinal degeneration model 29

Figure 2.1 - Northern blot analysis of a subset of the putative differentially expressed clones isolated from the cDNA library screen. 59

Figure 2.2 - Graphical analysis of the northern blot profiles. 60

Figure 2.3 - Functional categorization of the differentially expressed clones. 67

Figure 2.4 - Multiple tissue northern analysis of rat T-cadherin. 68

Figure 2.5 - Northern blot analysis of rat T-cadherin expression during LIRD. 69

Figure 2.6 - Western analysis of rat T-cadherin during LIRD. 70

Figure 2.7 - Immunolocalization of T-cadherin on retina sections. 71

Figure 3.1 - Nucleotide and deduced amino acid sequence of the rat KCTD8 cDNA. 96

Figure 3.2 - Gene and protein structure of rat KCTD8. 99

Figure 3.3 - Protein sequence alignment of rat KCTD8 and homologues identified in other species. 100

Figure 3.4 – Protein conservation of KCTD8 in bacteria and eukaryotes. 103

Figure 3.5 - Genomic conservation of KCTD8 104

Figure 3.6 - Hydropathy plot analysis of KCTD8. 105

Figure 3.7 - Multiple tissue northern blot analysis of rat KCTD8. 106

Figure 3.8 – Expression analysis of rat KCTD8 during LIRD. 107

Figure 3.9 - Western blot analysis of KCTD8. 109

Figure 4.1 - GFP-tagged KCTD8 expression constructs for cell transfections. 138

Figure 4.2 - Immunoblot analysis of GFP-KCTD8 fusion proteins expressed in COS-7 cells transfected with wild-type and mutant pEGFP-KCTD8 constructs. 140

Figure 4.3 - Representative immunofluorescent images showing the subcellular localization of wild-type and mutant GFP-tagged KCTD8 fusion proteins in transfected COS-7 cells. 142

Figure 4.4 - Analysis of cellular localization of wild-type and mutant GFP-KCTD8 fusion protein in transfected COS-7 cells treated with leptomycin. 144

Figure 4.5 – Representative immunofluorescent images of COS-7 cells labeled with various cellular markers. 146

Figure 4.6 - Representative immunofluorescent images showing co-localization of the wild-type GFP-KCTD8 with α-tubulin. 148

Figure 4.7 - Co-immunoprecipitation (co-IP) showing association of KCTD8 with α-tubulin in transfected COS-7 cells. 149

Figure 4.8 - Representative images showing subcellular localization of colcemid treated COS-7 cells transfected with wild-type and mutant GFP-KCTD8 fusion proteins. 151

Figure 4.9 – Optical sections of wild-type and mutant KCTD8 transfected COS-7 cells treated with 5 μM colcemid. 153

Figure 4.10 - Immunohistochemical localization of KCTD8 in the rat retina. 155

Figure 4.11 - Co-localization of KCTD8 with α-tubulin in the dark-reared rat retina. 158

Figure 4.12 - Co-immunoprecipitation showing association of α-tubulin with KCTD8 in the dark-reared rat retina. 160

Figure 5.1 – Comparison of nuclear morphology of untreated cells with cells treated with hydrogen peroxide, paraquat and staurosporine. 182

Figure 5.2 – Comparison of cell nuclei diameter when COS-7 cells are treated with hydrogen peroxide, staurosporine and paraquat. 184

Figure 5.3 – Immunofluorescent images of COS-7 cells transfected with wild-type and NLS mutant pEGFP-KCTD8 constructs and treated with 300 μM hydrogen peroxide for 6 hours. 186

Figure 5.4 – Immunofluorescent images of COS-7 cells transfected with wild-type and NLS mutant pEGFP-KCTD8 constructs and treated with 600 μM hydrogen peroxide for 6 hours. 188

Figure 5.5 – Immunofluorescent images of COS-7 cells transfected with wild-type and NLS mutant pEGFP-KCTD8 constructs and treated with 1 mM hydrogen peroxide for 6 hours. 190

Figure 5.6 – Representative immunofluorescent images showing the subcellular localization of wild-type and NLS mutant GFP-tagged KCTD8 constructs in cells treated with 100 μM, 200 μM or 300 μM paraquat for 6 hours. 192

Figure 5.7 – Representative images showing subcellular localization of COS-7 cells transfected with wild-type and mutant pEGFP-KCTD8 constructs and treated with 100 μM paraquat for 48 hours. 194

Figure 5.8 - Representative images showing subcellular localization of COS-7 cells transfected with wild-type and mutant pEGFP-KCTD8 constructs and treated with 200 μM paraquat for 48 hours. 196

Figure 5.9 – Representative images showing subcellular localization of COS-7 cells transfected with wild-type and mutant pEGFP-KCTD8 constructs and treated with 300 μM paraquat for 48 hours. 198

Figure 5.10 – Analysis of cellular localization of wild-type and NLS mutant GFP-KCTD8 fusion proteins in transfected COS-7 cells treated with 1 μM staurosporine. 200

Figure 5.11 – Analysis of cellular localization of wild-type and NLS mutant GFP-KCTD8 fusion proteins in transfected COS-7 cells treated with 3 μM staurosporine. 202

Figure 5.12 – Immunohistochemical localization of KCTD8 in dark-reared and light-induced retinal degenerative rat retinas.......... 204

Figure 5.13 – Co-localization of KCTD8 with α-tubulin in dark-reared and light-induced retinal degenerative rat retinas. 207

Figure 5.14 – Immunolocalization of KCTD8 in wild-type and RCS rat retinas. 210

LIST OF TABLES

Table **Page**

Table 2.1 - Clones isolated from the differential cDNA library screen. 62

LIST OF ABBREVIATIONS

AIF	apoptosis inducing factor
AMD	age-related macular degeneration
AP-1	activator protein-1
ARVO	Association for Research in Vision and Ophthalmology
ATG	start codon
Bcl-2	B-cell leukemia/lymphoma 2
Bcl-xl	Bcl-2 associated X protein long isoform/short isoform
BDNF	brain-derived neurotrophic factor
bFGF	basic fibroblast growth factor
BLAST	Basic Local Alignment Search Tool
bp	base pair
BTB/POZ	broad complex tramtrack bric-a-brac/pox-virus and zinc finger
Ca^+	calcium ion
CDD	Conserved Domain Database
cDNA	complementary DNA
c-fos	cellular Finkel-Biskis-Jinkins (FBJ) murine osteosarcoma virus oncogene homolog
cGMP	cyclin guanosine monophosphate
c-Jun	proto-oncogene jun
CLU	clusterin
CMV	cytomegalovirus
c-myc	cellular myelocytomatosis oncogene
CNTF	ciliary neurotrophic factor
CO_2	carbon dioxide
co-IP	co-immunoprecipitation

COS-7	African green monkey SV40-transformed kidney fibroblast cell line
cpm	counts per minute
DAPI	4',6'-diamidino-2-phenylindole
dATP	deoxyadenosine-5'-triphosphate
dCTP	deoxycytidine-5'-triphosphate
DEPC	diethylpyrocarbonate
dex	dexter
dGTP	deoxyguanosine-5'-triphosphate
DMEM	Dulbecco's modified Eagles medium
DMTU	dimethylthiourea
DNA	deoxyribonucleic acid
dNTPs	deoxyribonucleoside triphosphates
DP	guanosine diphosphate
EA.hy926	human umbilical vein-derived endothelial cell line
ECL	enhanced chemiluminescence
ELISA	enzyme linked immunosorbent assay
E_m	membrane potential
EndoG	endonuclease G
Erk1/2	extracellular signal-regulated kinase 1 and 2
EST	expressed sequence tag
E-value	expectation value
g	acceleration due to gravity
GC	guanylate cyclase
GCAP	guanylate cyclase-activating protein
GCL	ganglion cell layer
GFP	green fluorescent protein

6

GPI	glycosylphosphatidylinositol
GTP	guanosine triphosphate
H^+	proton
H_2O_2	hydrogen peroxide
HCL	hydrochloric acid
HEK293	human embryonic kidney epithelial cell line
HJMD	hypotrichosis associated with juvenile macular dystrophy
HO-1	heme oxygenase-1
hr	hour
HRP	horseradish peroxidase
HUVEC	human umbilical vein endothelial cells
IgG	immunoglobulin G
I-κB	inhibitor of NFκB
ILM	inner limiting membrane
INL	inner nuclear layer
IPL	inner plexiform layer
IPM	interphotoreceptor matrix
IRBP	interphotoreceptor retinoid binding protein
IS	inner segment
K^+	potassium ion
kb	kilobase
KCTD	potassium channel tetramerization domain containing
kDa	kilodaltons
LDL	low-density lipoprotein
LIRD	light-induced retinal degeneration
lov	leftover

M	molar
MAP	multiple antigenic peptide
Mertk	receptor tyrosine kinase gene
μg	microgram
$MgCl_2$	magnesium chloride
MIZ-1	Myc-interacting protein 1
μl	microlitre
ml	millilitre
μm	micrometer
mM	millimolar
MOI	multiplicity of infection
mRNA	messenger RNA
Na^+	sodium ion
NaCl	sodium chloride
NADPH	nicotinamide adenine dinucleotide phosphate
NCBI	National Center for Biotechnology Information
NES	nuclear export signal
NFκB	nuclear factor of kappa B
NLS	nuclear localization signal
nm	nanometer
^oC	degrees Celsius
OCT	optimal cutting temperature compound
OLM	outer limiting membrane
ONL	outer nuclear layer
OPL	outer plexiform layer
ORF	open reading frame

OS	outer segment
p53	tumor protein 53
PAGE	polyacrylamide gel electrophoresis
PANTHER	Protein Analysis Through Evolutionary Relationships
pat7	pattern7
PBS	phosphate buffered saline
PCR	polymerase chain reaction
PDE	cGMP-phosphodiesterase
PMSF	phenylmethylsulfonyl fluoride
prCAD	gene encoding protocadherin-21
PTHrP	parathyroid hormone-related protein
PUFA	polyunsaturated fatty acids
RACE	rapid amplification of cDNA ends
rcd1	rod-cone dysplasia type 1
RCS	Royal College of Surgeons
rd	retinal degeneration
rds	retinal degeneration slow
RhoK	rhodopsin kinase
RIPA	radioimmunoprecipitation
RNA	ribonucleic acid
ron	right on
RP	Retinitis Pigmentosa
RPE	retinal pigment epithelium
SDS	sodium dodecyl sulfate
SM	storage media
SSC	sodium chloride, tri-sodium citrate

STRING	Search Tool for the Retrieval of Interacting Genes/proteins
T1	tetramerization domain
TAG	stop codon
TBS	Tris buffered saline
TBS-T	0.1% Tween-20 (v/v) in TBS
TNF-α	tumor necrosis factor alpha
Tris	tris(hydroxymethyl)aminomethane
TRPM-2	testosterone-repressed prostate message 2
TSS	transcription start site
TUNEL	terminal UTP nick end labeling
USH1D	Usher syndrome type 1D
USH1F	Usher syndrome type 1F
UTR	untranslated region
UV	ultraviolet
v/v	volume/volume
w/v	weight/volume
XIAP	X-linked inhibitor of apoptosis protein

Chapter 1

Introduction

Light-induced retinal degeneration (LIRD) in rodents is a model system to study the process of retinal degeneration and is an animal model system for aspects of human retinal disease [1]. LIRD is different from other animal models of retinal disease in that it relies on an external stimulus, light, to illicit the dystrophic phenotype in the retina of animals as opposed to an internal stimulus, such as a genetic defect.

Excessive light exposure is believed to overwhelm the endogenous antioxidant mechanisms of the retina resulting in oxidative stress mediated active cell death of the photoreceptor cells of the retina, leading to blindness. The actual mechanism of cell loss in LIRD, the process from which a normal retina is transformed to a degenerative one, is not well understood. The major focus of my research has been to molecularly dissect out aspects of the LIRD process and attempt to understand their part in the degenerative process as a whole.

1.1 THE MAMMALIAN EYE

The mammalian eye is a complex, highly specialized organ composed of many different tissues and cell types, all of which need to correctly interact in a coordinated fashion for vision to occur. The formation of the eye during embryogenesis involves two of the three embryonic cellular layers: the ectoderm, which gives rise to the nervous system, the epithelial layers and the major parts of the eye; and the mesodermal derivatives giving rise to the orbital bones, the extraocular muscles, and the blood vessels of the eye [2]. The eye is made up of many different structures that are all important for the visual process. The process of vision in the fully developed eye is initiated when light enters the eye through the cornea then passes through the iris to the lens (Figure 1.1) [3]. The cornea along with the lens focus the light onto the retina, located at the anterior of the eye. The retina is a thin tissue that contains photopigments within specialized cells called photoreceptors. The energy transfer between photons of light and the photopigments of the retina is the initial and essential process for sight. The retina, which is part of the central nervous system, can be considered the most important functional and complex element of the eye. The vertebrate retina consists of three layers of nerve cell bodies and two layers of synapses that, similar to other sensory systems in the body, interact through synaptic connections to convey information via the optic nerve to the lateral geniculate body in the brain, which then sends the sensory impulse to the cerebral cortex [4].

1.1.1 The Retina

1.1.1.1 Cell types and spatial organization of the retina

The construction of all vertebrate retinas follows the same basic organizational design (Figure 1.2). At the far posterior of the eye, furthest from the cornea and incoming light, is the retinal pigment epithelium (RPE). The RPE lies between the outer segments of the photoreceptor cells and Bruch's membrane of the choroid and consists of a layer of cells that, in pigmented mammals, contain melanin [2]. Although the RPE is not directly involved in the neural events of vision, it is critical for normal photoreceptor cell function and survival [2, 5]. The RPE closely associates with the outer segments of the photoreceptor cells and functions in the maintenance of photoreceptor cells by phagocytosing the shed outer segments for photoreceptor renewal, regeneration of the bleached visual pigments caused by phototransduction, absorption of stray light by the melanin pigment in the RPE cell, and the scavenging of free radicals [5].

Anterior to the RPE is the outer nuclear layer (ONL), which contains the cell bodies of the photoreceptor cells [2]. The RPE and the ONL are separated by, first, the outer segment disks of the photoreceptor cells, followed by the inner segment disks of the photoreceptor cells. The outer segments of the photoreceptor cells contain the photopigments necessary for the absorption of light. The inner segments contain the mitochondria of the cells and as such are the metabolic center of the cell. The ONL contains, as the name suggest, the nuclei of the photoreceptor cells. Projecting towards the inner retina, away from the RPE, are the photoreceptor cell axons, which form synapses with the bipolar and horizontal cells of the retina to make up the outer plexiform layer (OPL).

The nuclei of the bipolar and horizontal cells along with the nuclei of the amacrine cells and Müller cells, the main glial cells of the retina, are found in the inner nuclear layer (INL) [2]. Next to the INL, working toward the anterior of the eye, is the inner plexiform layer (IPL). It is here that the axon terminals of the bipolar, amacrine, and interplexiform cells form connections with the ganglion cell dendrites. The ganglion cell layer (GCL) makes up the next nuclear layer towards the inner retina. This layer contains the cell bodies of the ganglion cells as well as displaced amacrine cells [4]. The axons of the ganglion cells lie in the next layer inward, the nerve fiber layer, in which a convergence of the axons of the ganglion cells from all parts of the retina innervate the optic nerve. The final, innermost layer of the retina is the inner limiting membrane (ILM), which contains the terminal expansions of the Müller cells.

The purpose of these many layers and cell types in the retina is to process and convey the information from the photoreceptor cells to the brain. In the retina this information processing occurs by both vertical and lateral pathways [2]. In the simplest of vertical pathways, the signal from the photoreceptor cells is passed to the bipolar cells, which in turn conveys the information to the ganglion cells that then transmit that information via the optic nerve to the brain. The function of the lateral pathways in the retina is to connect neighbouring parts of the retina. This is achieved by both the horizontal cells, which are involved in making connections between photoreceptor cells in the outer retina; and the amacrine cells, which function in the inner retina by making connections between vertical pathways where the bipolar and ganglion cells interact [2].

1.1.1.2 Photoreceptors

The cells of the retina that are responsible for capture of the visual stimulus and conversion into nerve signals are the photoreceptor cells. The transfer of energy from the photons to photopigments, a process known as phototransduction (Figure 1.3), is necessary for vision to occur. The major parts of a photoreceptor cell consist of: an outer segment, which contains the photopigment; an inner segment that contains the mitochondria; a nucleus; and a synaptic terminal (Figure 1.4) [6]. Each photoreceptor contains a specific photopigment opsin that differs with respect to the wavelength of light it absorbs. Each photopigment consists of a chromophore, 11-*cis*-retinal, which is a vitamin A derivative, attached to an opsin.

Two groups of photoreceptor cells exist in the mammalian retina, cones and rods. The main structural difference between rods and cones is that rods are cylindrically shaped whereas cones are conically shaped [2]. There are three types of cone photoreceptors in the human retina that contain one of three photopigments – red, blue, or green [2]. The designation of red, blue, or green cone photoreceptors is based on the wavelength of light that is absorbed with peak absorption at 420 nm for blue cones, 531 nm for green cones, and 588 nm for red cones [4]. Cone photoreceptors are responsible for vision in bright illumination. On the other hand, there is only one type of rod photoreceptor, which contains the photopigment rhodopsin, with peak absorption of 496 nm, and is responsible for vision in dim lit conditions.

While light absorption by the photoreceptor outer segments is essential for vision, this process also damages them. Replacement of rod outer segments occurs daily when the outer segments shed their tips, which are then phagocytosed by the RPE [2]. New disks are formed at the base of the outer segments to replace the damaged, shed disks. Shedding of outer segment disks is not a continuous process and is in fact coupled to circadian rhythm resulting in rod tips usually being shed in the early morning and cone tips usually being shed in the evening [2, 4].

1.2 DEGENERATIVE DISEASES AFFECTING THE RETINA

The integrity of the photoreceptor cells and the proper functioning of the phototransduction cascade are essential to the visual process. As such, any defect in these critical retina components can have a profound effect on vision as well as the survival and maintenance of the photoreceptor cells. Any defect in photoreceptor integrity or function can lead to degeneration of not only the defective cells but also surrounding functioning cells leading to widespread retinal degeneration and blindness. The two main classes of human retinal dystrophies are classified based on the localization of the degeneration in the retina. Degenerations involving loss of peripheral rod cells are classified as peripheral dystrophies, such as Retinitis Pigmentosa (RP), and degenerations involving the loss of central cone photoreceptor cells located in the macular region of the retina are classified as Macular Degenerations [7].

RP is a term used to describe a large group of phenotypic and heterogeneous disorders, which represent the most common inherited form of human visual disorders with a prevalence of approximately 1/3500 [8]. RP primarily affects rod photoreceptors in the periphery of the retina affecting night vision and causing a loss of the peripheral visual field. In most cases, degeneration of the rod photoreceptor cells is accompanied by the eventual loss of cone photoreceptor cells resulting in the loss of central vision in addition to peripheral vision. The subsequent degeneration of the cone cells suggests that degenerating rod photoreceptor cells induce cell death in neighbouring normal cells [9]. Photoreceptor cell loss in RP is known to occur primarily through programmed cell death (apoptosis) [10]. Due to the heterogeneous nature of RP, numerous genes have been identified to be involved in the disease. These genes can be placed into one of four categories: 1) proteins related to phototransduction processes; 2) photoreceptor structural proteins; 3) proteins involved in photoreceptor and RPE metabolism; and 4) proteins that regulate gene expression, such as transcription factors. This myriad of defects involved in such a complex disease makes prevention of such a disease quite difficult.

In contrast to the initial loss of peripheral vision in RP, macular degeneration involves the loss of central vision caused by degeneration of the cone-rich central region of the retina, the macula, as well as the RPE [11]. Macular degeneration is characterized by lipofuscin (oxidized lipid) accumulation in the RPE suggesting that oxidative stress may play a role in the degeneration of the retina [12, 13]. The outer segments of photoreceptor cells contain a high concentration of polyunsaturated fatty acids (PUFAs) in the membrane. Being that the eye is an oxygen rich environment, it is believed that oxidation of PUFAs may be a contributing factor, if not a causative factor of the disease [14]. While treatment with anti-oxidants would be expected to slow the progression of the disease, additional studies of this sort are required before widespread anti-oxidant treatment is recommended [15]. Age-related macular degeneration (AMD) is the leading cause of vision loss in North American's over the age of 50 [16] and this number is expected to increase in the coming years due to the increasing longevity of the senior population.

To date, inherited retinal degenerations have been linked to 177 loci and 124 disease-causing genes have been identified [17]. In the case of inherited photoreceptor degenerations, apoptosis has been found to play a significant role in the loss of visual cells in RP [18] and AMD [19]. It is highly unlikely that there are 177 separate gene-specific preapoptotic pathways leading to inherited photoreceptor apoptosis. Instead, the more plausible scenario is that there are relatively few preapoptotic pathways that are shared by the numerous inherited retinal disorders and that these pathways converge at some point resulting in one or a few common photoreceptor apoptotic pathways. Thus, by studying the general process of photoreceptor degeneration we will gain a better understanding of the general mechanisms involved in a variety of inherited retinal dystrophies.

1.3 APOPTOSIS IN RETINAL DEGENERATION

Studies of different animal models of retinal degeneration have all demonstrated that photoreceptor cells die via an apoptotic pathway [20-24]. The process of programmed cell death is an integral part of normal cellular function in that it regulates cell number as well as eliminates abnormal or dysfunctional cells. Specific morphological changes of the cell are associated with the process of apoptosis [25-27], most of which can be viewed by histological examination. In early apoptosis, cells round up resulting in loss of contact with neighbouring cells and cell shrinkage is also observed (Figure 1.5B). Blebs in the plasma membrane occur, and in the cytoplasm dilatation of the endoplasmic reticulum occurs. There is condensation of the cell nucleus and fragmentation of chromatin by endonucleases, which can be observed experimentally as a DNA laddering pattern by gel electrophoresis [28]. The condensed nucleus then breaks up into several fragments and the entire cell condenses and eventually forms what are known as apoptotic bodies (Figure 1.5C) [25, 26]. These apoptotic bodies send signals that result in engulfment by neighbouring cells and as a result, apoptosis occurs without leakage of cellular content or an inflammatory response (Figure 1.5D and 1.5E).

The underlying molecular events that occur during apoptosis to signal the cell to die are much more complex. Apoptosis is known to occur by both an extrinsic pathway, involving receptors on the plasma membrane that signal the apoptotic process, and an intrinsic pathway, which involves apoptotic signaling from the mitochondria [29, 30]. In both cases, apoptosis occurs through complex signaling pathways that converge at the level of caspases, specific proteases that cleave cellular substrates. To add to the complexity of apoptosis, caspase-independent mechanisms of proteolytic degradation have been observed. Many non-caspase proteases have been found to be involved in the apoptotic process in conjunction or independent of caspases, including cathepsins, calpains, granzymes A and B, serine proteases and proteasomes [31-34]. As well, the caspase-independent death effectors apoptosis inducing factor (AIF) [35] and endonuclease G (EndoG) [36, 37] may be released from the mitochondria in a caspase-independent mechanism to bring about apoptosis. In the case of LIRD in rats, we have found that, under our experimental conditions, cell loss is mediated by an oxidative stress induced caspase-dependent active cell death process [38]. The complexity of alternative apoptotic processes contributes to the difficulty in fully understanding cell death.

A second type of cell death, which is morphologically quite different from apoptosis, is that of necrosis. Unlike the programmed nature of apoptosis, necrotic cell death is generally believed to be a passive process involving the chaotic breakdown of the cell [39]. Necrosis is morphologically distinct from apoptosis in that it involves the swelling of the cell, clumping and random degradation of DNA, destruction of cellular organelles, and rupture of the plasma membrane resulting in leakage of cell content and an inflammatory response. The process of necrosis requires minimal energy and does not involve *de novo* RNA and protein synthesis.

1.4 GENETIC MODELS OF RETINAL DEGENERATION

The study of photoreceptor cell death in human retinal diseases is complicated by the lack of retinal tissues from RP and macular degeneration patients that are still in the tissue state of actively undergoing retinal degeneration. This is largely a result of retinal disorders not being lethal; thus, when tissue becomes obtainable the retina is fully degenerated, making it difficult to study the process of photoreceptor cell death in these patients. The use of animal models, therefore, that carry spontaneous or engineered mutations known to cause retinal disease in humans are of great value in attempting to understand the process of cell death in human retinal disease. Numerous spontaneous models of retinal degeneration have been identified including the rd [40] and rds mouse [41], the RCS rat [42], and several canine lines [43, 44], to name a few. Naturally occurring models of retinal disease are not available for all known mutations in human retinal dystrophies; therefore, transgenic and knockout techniques have been used to develop additional animal models of retinal disease. Since numerous human retinal diseases involve defects in the visual pigment of rod cells, rhodopsin, a number of transgenic and knockout animal models, involving mice, rats, and pigs, have been developed to study the process of retinal degeneration resulting from defects in the rhodopsin gene [44]. One setback to the study of knockout model systems is that a number of retinal diseases involve missense mutations usually resulting in partial transcription and translation of the gene, albeit the protein does not function normally. Knockout models deal with null mutations rather than missense mutations; therefore, the study of knockout models is not ideal for the understanding of the gene defect in humans. Knockout models do not allow for the analysis of the specific defect seen in human retinal diseases given that a number of retinal diseases are not due to complete loss of gene function.

The use of animal model systems has provided some clues as to the possible process of retinal degeneration in human retinal dystrophies. The studies of the rds mouse and mice expressing Pro347Ser mutant rhodopsin have shown that faulty disc morphogenesis can lead to cell death of photoreceptor cells [45, 46]. Results such as these stresses the importance of proper photoreceptor cell formation in preventing retinal degeneration.

A second mechanism of photoreceptor cell loss identified from the study of genetic model systems is that of metabolic overload. This phenomenon has been observed in rd mice, rcd1 dogs, and mice deficient in γ-PDE [47, 48]. In all cases, animals have an elevated level of cGMP resulting in increased conductance through the open cGMP-gated channels in the outer segments of the photoreceptor cells. This would cause an influx of Na^+ and Ca^+ ions resulting in metabolic overload of the cell. In addition, growing evidence suggest that a prolonged change in intracellular calcium concentration could lead to apoptosis [20, 49].

The close association of the RPE with the photoreceptor cells and its importance in the proper functioning and survival of photoreceptors makes it a likely factor in photoreceptor degeneration. As such, dysfunction in the RPE has been found in numerous animal models including the RCS rat [50] and Rpe65 knockout mouse [51]. Although different defects are involved, in both cases disruption of RPE function leads to photoreceptor cell degeneration.

The fourth mechanism identified from the study of genetic animal models is that of constitutive activation of the phototransduction cascade. This has been observed in the arrestin and rhodopsin kinase (RhoK) knockout mice [52, 53]. Both arrestin and RhoK are necessary for the termination of the phototransduction cascade. Chronic activation of the phototransduction cascade leads to photoreceptor cell death, however the mechanism by which this occurs is unknown. Human retinal disorders such as Oguchi disease caused by mutations in RhoK and possibly arrestin [54, 55], recessive RP due to mutations in the α subunit of PDE [56], and Leber's congenital amaurosis resulting from mutations in the retinal guanylate cyclase [57] are all thought to result from chronic activation of the phototransduction cascade. These findings have lead to the development of the "equivalent-light" hypothesis, which suggests that the mechanism of photoreceptor degeneration in retinal dystrophies resulting from constitutive activation of the visual cascade may be similar to the degeneration observed with continuous light exposure [58, 59].

1.5 INDUCED MODELS OF RETINAL DEGENERATION

The most extensively studied model of induced retinal degeneration is the LIRD model. The damaging effects of visible light were first described by Noell *et al.* in 1966 [1]. Since this time, many light damage models have been developed using different animal models and various wavelengths of light and duration. Although the variety of LIRD model systems leads to a difficulty in comparison of the various systems, the general goal of understanding photoreceptor cell death by apoptosis is still maintained. As well, all model systems rely on the basic principle of exposing animals to intense light resulting in degeneration of the photoreceptor cells via apoptosis.

1.5.1 Advantages of studying light-induced retinal degeneration

As mentioned above, many genetic model systems exist for the study of retinal degeneration. While these model systems have provided insight into the mechanisms of photoreceptor cell death underlying specific inherited human retinal diseases, the study of photoreceptor apoptosis by induced light affords some advantages to the study of retinal degeneration that genetic model systems can not [60]. First, light exposure results in synchronized photoreceptor apoptosis resulting in cells passing through the various apoptotic stages at roughly the same time. This is essential in studying gene expression changes associated with photoreceptor cell death and also allows for various durations of light exposure to be broken down into different phases of degeneration. In the case of genetic model systems, the stages of photoreceptor degeneration are usually quite varied between cells and in most cases not all cells are affected resulting in difficulty when characterizing the molecular changes involved in photoreceptor degeneration. Secondly, the degeneration process in light exposed animals occurs much faster than the degeneration in genetic model systems [60]. In addition, the use of adult animals in the light-induced model system allows for the retina to be fully developed before degeneration occurs, enabling the study of degeneration from an adult photoreceptor cell state. In many of the genetic model systems, photoreceptor cells begin to degenerate shortly after birth or do not develop normally before retinal degeneration occurs. Third, the extent of photoreceptor degeneration can be easily manipulated by varying the duration of the light exposure, thus allowing analysis of the molecular events that occur at different stages of degeneration.

1.5.2 The use of LIRD in rodents as a model system for human disease

Although the light damage model involves induction of the degeneration process by an external stimulus and may seem quite removed from the genetic defects involved in human retinal dystrophies, photoreceptor degeneration in a number of human retinal diseases and genetic animal model systems has been shown to be accelerated by the presence of light, suggesting that light may be a co-factor in many retinal diseases [61]. As such, the study of LIRD may not represent just an artificial stimulus. Since LIRD does not involve specific gene defects known to result in specific human retinal disease, this model system affords itself more to the study of the degeneration process involved in a variety of retinal diseases. As a result, the study of the LIRD model system provides more of an understanding of the overall molecular events involved in photoreceptor cell death.

In our system, LIRD primarily targets rod photoreceptors, making it an ideal model system for the study of RP. Patients with RP experience visual loss in the peripheral retina due to the degeneration of the rod photoreceptor cells. Approximately 30-40% of patients with autosomal dominant RP have a mutation in the rhodopsin gene [17]. Being that LIRD primarily targets the rhodopsin photopigment, this model system lends itself well to the study of rhodopsin-mediated cell death. The identification of the processes involved in rod photoreceptor cell loss due to LIRD can be extrapolated to determine a possible mechanism of how the rod photoreceptor cells are lost in patients with RP.

AMD is believed to primarily affect the cone photoreceptor cells in the central macular and foveal region of the human retina. Since only primates and birds have a macular region [2], the development of animal model systems to study macular degeneration is difficult. However, there are many similarities between LIRD in rodents and macular degeneration in humans allowing the use of LIRD as a pseudo-model system for the study of AMD. The only rod-free zone in the human macula lies in the central 0.35 mm visual field [62]. In an ellipsoid ring at 3-5 mm is the parafovea, which is a rod-dominated region [62]. In AMD, rod photoreceptor cell loss has been shown to occur prior to the loss of cone photoreceptor cells [63]. Although loss of rod cells is a natural part of aging, the rod densities in patients with AMD has been found to be reduced by an additional 30-40% over the normal aging loss [64]. As such, it appears that early rod loss is an important underlying factor of AMD. Similarly to RP and LIRD, rod photoreceptor cell loss in AMD occurs by apoptosis. In addition, the accumulation of lipofuscin in AMD due to oxidation of the high proportion of polyunsaturated fatty acids in the retina suggests that AMD may involve an oxidative stress component [13, 65]. Similarly, LIRD has also been found to be mediated by oxidative stress, as discussed below. Therefore, although LIRD is not a direct model for AMD, the similarities that exist with respect to the degeneration of the photoreceptor cells in both cases suggests that the mechanism of cell death in the LIRD model may be similar to that of AMD.

1.5.3 Gene expression changes during light-induced retinal degeneration

As a result of photoreceptor cell death in LIRD it is expected that there would be changes in retinal gene expression during the degeneration process. However, due to the diversity of light damage model systems, the correlation of the findings from one experimental system to the other is not always relevant. In any event, it appears that the initiating factor in all light damage models is that of rhodopsin activation [66, 67]. There appears to be, at least in the case of white light treatment, two apoptotic pathways leading to LIRD. In long-term, low-level white light exposure the activation of transducin, and thus the phototransduction cascade, is essential for mediating photoreceptor cell death [68]. In contrast, short-term, bright white light exposures leading to photoreceptor cell death does not rely on the presence of transducin and the phototransduction cascade, as is evident by photoreceptor degeneration in transducin knockout mice [68]. In the case of bright white light exposure, photoreceptor cell death is mediated by the transcription factor AP-1 (activator protein-1) [68, 69]. AP-1 is a heterodimer consisting mainly of c-Fos and c-Jun [69, 70]. Both c-Fos and c-Jun have been found to be upregulated in response to white light and this induction of gene expression precedes the light-induced increase in AP-1 DNA binding activity [71].

In mice exposed to green light, NFκB p65 was found to be co-localized with TUNEL (Terminal deoxynucleotidyl transferase Biotin-dUTP Nick End Labeling) in light-treated photoreceptor cells suggesting that NFκB may play a neuroprotective role in light-induced photoreceptor degeneration [72]. In addition, XIAP and Bcl-xl, two NFκB-regulated anti-apoptotic proteins, were found to increase after light-exposure further supporting the hypothesis that NFκB plays an anti-apoptotic role in LIRD.

With respect to caspases, cysteine proteases involved in mediated apoptosis, their role in LIRD is more controversial. Studies in our lab as well as others have shown an induction of caspase-1 [38, 71, 72] and caspase-3 [38, 73] in response to light exposures in both rats and mice. In contrast, other findings have shown that light-induced photoreceptor apoptosis occurs independently of caspase-1, -3, -7, -8, or -9 activation (cleavage) in mice [74, 75]. This may indicate that different light exposures trigger different cell death pathways, further adding to the complexity of cell death in LIRD.

Coordinated gene expression has also been observed in green light mediated retinal degeneration. Ribosomal binding proteins, regulators of gene expression at the translational level, have been found to have altered levels of expression during LIRD [76]. In addition, there is an increase in the crystallin content of the retina in light exposed rats suggesting that crystallins function in protecting the photoreceptor cells from light damage [77, 78].

It is clear that there are different mechanisms and pathways involved in the damage induction with the various light damage models. However, the consistency that all models appear to be initiated with rhodopsin bleaching and all involve the eventual apoptotic loss of rod photoreceptor cells suggests that at some point in the degeneration process these pathways converge.

1.5.4 Practical considerations in the study of light-induced retinal degeneration

1.5.4.1 Wavelength of light

Numerous factors affect the response of the retina to the light stimulus. To begin with, the wavelength of light affects which photoreceptor cells, rods or cones, are most susceptible to the light insult and is probably the most important consideration in light damage studies. Variation in the wavelength of light used to elicit damage is one of the main differences in the various LIRD model systems. Although the light damage systems developed in rodents are mainly used to study the process of rod photoreceptor degeneration, the various wavelengths of light used usually overlap with the absorbance spectrum of the cones. Since rats and mice are nocturnal animals, their retinas mainly consist of rod photoreceptors. Photoreceptor counts in albino rats have shown that only 1% of the entire photoreceptor population consists of cones [79, 80], which have their peak absorbencies at 359 nm for rat UV pigment and 509 nm for M-cone pigment [81]. Due to the low cone population in rodents, any cone degeneration as a result of the light insult would account for minimal changes in the overall integrity of the retina.

Fluorescent white light is used mainly because it most closely mimics the wavelength of light we are exposed to daily. This is important when studying the effects of light as a co-factor in retinal disease. However, the use of white light to study the molecular events of photoreceptor degeneration is complicated by the wide spectrum of wavelengths present, which simultaneously affect both rods and cones.

Narrow band blue light (403±10 nm) is also used for the study of LIRD. This particular wavelength of light induces damage to both rods and blue-UV light sensitive cones as well as the RPE [1, 82]. While this type of induced retinal degeneration is initiated by the absorption of photons by rhodopsin, the extent of degeneration is greater with blue light exposed animals than with most other wavelengths of light due to the photoreversal of rhodopsin bleaching, a photochemical process induced by blue light [83, 84]. This process results in a regeneration of unbleached rhodopsin, providing a pool of unbleached rhodopsin available to absorb additional photons resulting in an enhanced progression of photoreceptor apoptosis.

In contrast, broadband green light (490-580 nm) above 500 nm does not cause photoreversal of rhodopsin; therefore the extent of damage is mainly related to the initial pool of rhodopsin available for bleaching [84]. An additional advantage of using green light is that the wavelength used most closely matches the absorbance spectrum of rhodopsin, of which the peak absorption is 496 nm [1, 85]. Therefore, green light is best suited to the study of rhodopsin-mediated damage. Due to these advantages, we have chosen broadband green light exposure in rats as our model system for studying LIRD.

1.5.4.2 Light exposure duration and intensity

A second factor to consider when studying LIRD is the duration and intensity of the light. Since photoreceptor cell damage by light is a photochemical process, it is expected that variations in the light intensity and duration would result in varying degrees of retinal degeneration. Studies have shown that increasing the duration of light exposure increases the number of retinal DNA strand breaks, as analyzed by alkaline gel electrophoresis [86]. In addition, histological analysis of light exposed retinas showed an increase in pyknotic nuclei in the outer nuclear layer with increasing duration of light exposure [87]. This simple manipulation of light intensity and exposure times facilitates the study of various phases of retinal degeneration. In the model system we use, we maintain the intensity of green light at 1200-1400 lux[1] but vary the exposure times allowing us to divide our LIRD model system into various phases of degeneration (see below), with short light exposures representing the beginnings of the apoptotic process and longer light exposures representing a retinal environment actively undergoing programmed cell death [88].

---

[1] Definition of lux - a unit of illumination equal to the direct illumination on a surface that is everywhere one meter from a uniform point source of one candle intensity or equal to one lumen per square meter. http://www.m-w.com, Merriam-Webster Online, August 2006

1.5.4.3 Rearing conditions

Since we are studying retinal cell loss due to light exposure, the illumination levels the animals are maintained in prior to damaging light treatment is an important consideration. Studies have found that rats reared under cyclic light conditions (12 hour light/12 hour dark) are less susceptible to light-induced damage than rats reared in the dark [89-91]. This protective effect due to cyclic rearing is believed to be the result of a process called photostasis, where the photoreceptor cells regulate their steady-state levels of rhodopsin bleaching as an adaptive mechanism to prevent cell degeneration [92]. In addition, the rod outer segments of dark-reared rats have been found to contain more rhodopsin per eye, which is more tightly packed than in cyclic reared rats [93, 94]. The increased rhodopsin levels in dark-reared rats contribute to their increased susceptibility to light damage by providing a greater pool of rhodopsin available for bleaching by the light stimulus. In our model system we use rats that are purchased as weanlings and are maintained in the dark until 60 days of age, allowing approximately four rod renewal cycles prior to light exposure [95].

1.5.4.4 Time of light exposure

To maintain consistency between experiments, light exposures of the animals should be conducted at the same time of day. This is especially relevant in the rat since there is a circadian-dependent susceptibility to light damage [96, 97]. Rats exposed to intense light at 1 am have a 1-2 fold increase in photoreceptor cell damage as compared to rats exposed at 9 am [96, 97]. In addition, rats exposed at 5 pm have little light-induced cell damage suggesting that the molecular environment in the retina at 5 pm elicits a protective effect. Although different times of day have an effect on retinal susceptibility to the light insult, the choice of time of day to initiate the light exposures is more so based on convenience. As long as the time at which the light exposure is initiated is maintained between experiments, experimental data will be comparable. In our model system all light treatments are initiated at 9 am.

1.5.5 The role of oxidative stress in light-induced retinal degeneration

There is growing evidence that photoreceptor cell death as a result of exposure to intense light is oxidative stress mediated and, at least in the case of blue light exposures, the generation of reactive oxygen species is mediated by mitochondrial electron transport [98]. Changes in expression levels of various genes have indicated a role for reactive oxygen species in the process of light-induced damage. Studies have shown an increase in heme oxygenase-1 (HO-1) expression levels in the retina after 12 or more hours of light exposure, suggesting that the retina is experiencing an oxidative stress environment [99]. In addition, the levels of ascorbic acid, an endogenous antioxidant found in the retina, are found to decrease in retinas of rats exposed to light [100]. Supplementation of rats with ascorbic acid was shown to reduce the amount of photoreceptor cell loss [100-104]. The use of exogenous antioxidant supplements to reduce visual cell loss are also indicative of a role of reactive oxygen species in photoreceptor cell loss as a result of light exposure. The synthetic antioxidant dimethylthiourea (DMTU) has been found to reduce visual cell loss in rats but only if the treatment is given prior to the light insult [86, 105, 106], suggesting that generation of reactive oxygen species is an early event in photoreceptor cell loss. As well, use of the radioprotective dye WR-77913, a singlet oxygen scavenger, has been found to protect against light-induced membrane disruptions in the outer segments of the rat retina [107]. Transgenic expression of thioredoxin, a regulator of endogenous reduction-oxidation [108], or use of recombinant thioredoxin in mice exposed to high intensity white light was also found to confer photoreceptor cell protection by reducing oxidative stress [109, 110]. Reactive oxygen species and protection from photooxidation with antioxidants have been found for light damage models using white light, broadband green light, and narrow band blue light, suggesting that independent of the wavelength of light used, photoreceptor cells degenerate as a result of the light stimulus causing oxidative stress induced apoptosis.

The finding that reactive oxygen species play a role in light-induced degeneration of the retina is not surprising. As a whole, the retina is quite susceptible to oxidative stress due to its high oxygen consumption, the high proportion of polyunsaturated fatty acids in the retina, and the fact that the retina is exposed to visible light on a daily basis. The involvement of oxidative stress in light-induced degeneration of the retina has lead to the hypothesis that reactive oxygen species, such as superoxide, singlet oxygen, hydrogen peroxide, hydroxyl radicals, and nitric oxide, function as diffusible phototoxic substances, which radiate from damaged cells affecting surrounding cells and causing an overall irreversible visual cell loss [85]. The involvement of oxidative stress in LIRD lends the study of these model systems well to the study of not only rod related degenerations such as Retinitis Pigmentosa but also to the study of age-related macular degeneration, which is known to involve an oxidative stress mediated degeneration of the cone rich fovea [13, 14, 111].

1.5.6 Stages of degeneration in the light-induced retinal degeneration model

An advantage to using controlled light exposures to elicit degeneration of the photoreceptor cells in the retina is that by altering the intensity or duration of the light exposure one can fairly easily control the amount of degeneration that occurs. In our model system we use a constant light intensity of 1200-1400 lux (490-580 nm) and vary the amount of degeneration by varying the duration of the exposure times. This allows us to produce predictable and reproducible degeneration of the retina. The various exposure times used can be divided into various phases of degeneration based on analysis of the expression levels of various marker genes: interphotoreceptor retinoid binding protein (IRBP); heme-oxygenase 1 (HO-1); and testosterone-repressed prostate message 2 (TRPM-2)/clusterin (CLU) (Figure 1.6) [88]. IRBP functions in the regeneration of rhodopsin in the visual cycle and therefore is important for retinol transport between the photoreceptor cells and the neighbouring RPE [112]. The expression levels of IRBP were used as a marker of normal retinal function. As such, the highest level of IRBP expression is seen in untreated, dark-reared rats. As the duration of light exposure increases there is a decrease in IRBP levels indicating that there is a loss of normal photoreceptor cell function due to the cells beginning the apoptotic process. HO-1 expression was used as a marker for oxidative stress in the degenerating retina [99, 113]. Therefore, the duration of light in which the highest level of HO-1 expression is seen correlates with the highest level of oxidative stress in the retina. As such, increasing durations of light exposure results in increased expression in HO-1. TRPM2/CLU was used as a marker of cellular recovery. Increased TRPM2/CLU expression is found in response to the post-apoptotic recovery of surviving cells [88]. As such, the highest level of expression of TRPM2/CLU in our light damage model system is seen when rats are placed in the dark after extended light treatment in order to allow recovery of surviving photoreceptor cells.

Based on the expression of these marker genes the LIRD profile can be divided into four phases: 1) commitment; 2) execution; 3) stress response; and 4) survival response [88]. Four hours of light treatment represents the commitment phase of degeneration. At this stage the rod photoreceptor cells begin to initiate the sequence of events necessary to undergo programmed cell death; however, the cells are not actively undergoing apoptosis at this stage as evidenced by the absence of DNA fragmentation ladders after 4 hours of light exposure. If allowed a two week dark recovery period following the light insult, it was found that 80% of the photoreceptor cells were lost suggesting that a 4 hour light treatment is sufficient to initiate the apoptotic process and commit the photoreceptor cells to undergo cell death [114]. Expression levels of the marker genes at an 8 hour light treatment indicates a further decrease in IRBP expression representative of a loss of photoreceptor cells as well as an increase in HO-1 expression, indicative of an increase in oxidative stress at this time point. This time point is referred to as the execution phase due to active photoreceptor cell death. The process of apoptosis at this time point is also confirmed by the appearance of DNA fragmentation ladders immediately following the 8 hour light insult [86]. Sixteen hours of light exposure is the time point, in our model system, where the highest level of HO-1 expression is observed. In conjunction with this is a low level of both IRBP and TRPM2/CLU. As such, this stage of the degeneration profile is referred to as the stress response phase due to the high oxidative stress environment resulting in apoptosis of the photoreceptor cells. The final phase of the degeneration profile is that of the survival response phase. Animals in this stage are allowed a 24 hour dark recovery period following 12 hours of light exposure. It is at this time point where a change in expression of genes responsible for recovery from apoptosis becomes apparent. As a result, the highest level of TRPM2/CLU expression, a marker for cellular recovery, is observed.

1.6 FOCUS OF THE THESIS

Hypothesis 1: LIRD is a multifaceted process involving numerous changes in the molecular phenotype of the retina
Hypothesis 2: Alterations in KCTD8 expression and localization defines one aspect of the LIRD molecular phenotype.

The work outlined in this thesis was initiated with the primary goal of further understanding the molecular mechanisms involved in LIRD, which can then be correlated to the mechanisms involved in human retinal disease progression leading to blindness. As a result of this original objective, genes that possess the potential to be involved in the retinal degeneration process were isolated and identified through a differential cDNA library screening strategy. Chapter 2 outlines this process and the resultant genes isolated. In addition to the overall analysis of the gene expression profile during high oxidative stress in the retina, the characterization of T-cadherin is also outlined in this chapter. The analysis of T-cadherin, a novel member of the cadherin superfamily, was undertaken in response to a number of cadherin family members found as retinal disease genes or have been shown to have a role in the retinal degeneration process. In addition to the characterization of T-cadherin, a novel gene that was isolated from the cDNA library screen and thus has the potential to be involved in the retinal degeneration process was chosen for further characterization. The preliminary characterization of this novel gene, KCTD8 (originally referred to arbitrarily as 1363), encompasses chapter 3. The bioinformatic characterization of this gene led to the discovery of three putative conserved domains within the protein – a BTB/POZ/T1 domain and two nuclear localization signals (NLSs). Chapter 4 describes the analysis of the functionality of the putative NLSs by studying the cellular localization of the wild-type and NLS mutant KCTD8, *in vitro* and *in vivo*. Finally, being that this gene was isolated from a screen for genes involved in LIRD, a process known to involve oxidative stress mediated apoptosis, the cellular localization of wild-type and NLS mutant KCTD8 was analyzed, *in vivo* and *in vitro*, in response to a number of oxidative stress stimuli.

These studies follow the characterization of a gene from the initial isolation of a partial cDNA sequence to obtaining the full-length sequence and using the limited data available from simple sequence analysis to design a molecular approach in order to ascertain information as to the function of this gene in general as well as during retinal degeneration.

Figure 1.1 – Schematic diagram of the adult human eye.

Figure taken from http://webvision.med.utah.edu/.

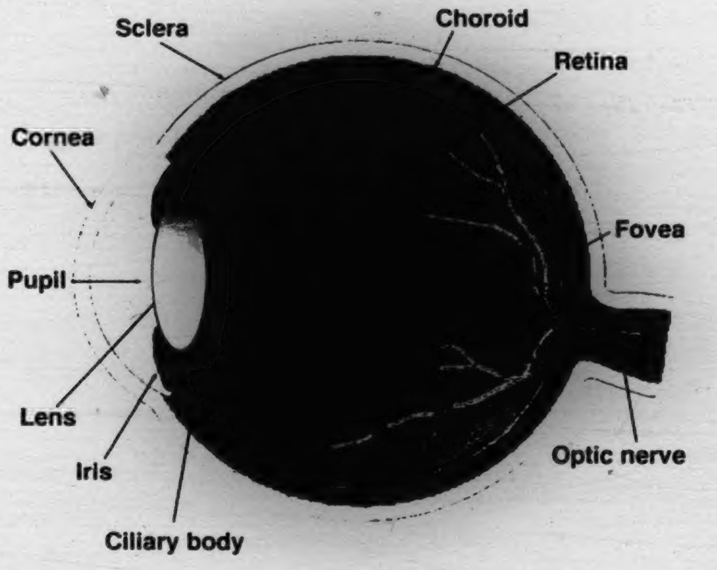

Figure 1.2 – Cellular layers of the retina.

A) Schematic diagram illustrating the various cellular layers and organization of the retina. B) Light micrograph of a vertical cross-section through the retina. OLM, outer limiting membrane; ONL, outer nuclear layer; OPL, outer plexiform layer; INL, inner nuclear layer; IPL, inner plexiform layer; GCL, ganglion cell layer; ILM, inner limiting membrane. Figure adapted from http://webvision.med.utah.edu/.

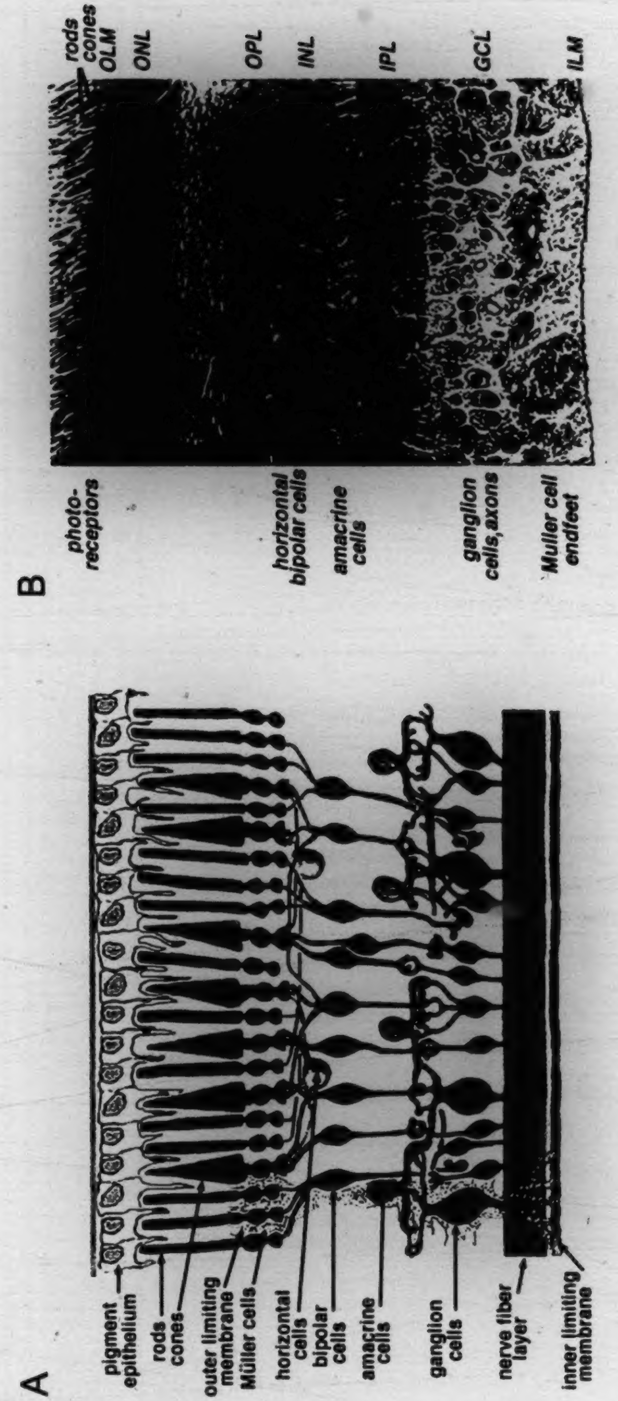
A
pigment epithelium
rods
cones
outer limiting membrane
Müller cells
horizontal cells
bipolar cells
amacrine cells
ganglion cells
nerve fiber layer
inner limiting membrane
B
photo-receptors
horizontal
bipolar cells
amacrine cells
ganglion cells, axons
Muller cell endfeet
rods
cones
OLM
ONL
OPL
INL
IPL
GCL
ILM

Figure 1.3 – Rod photoreceptor cell phototransduction in the vertebrate retina.

A) When a photon of light enters the eye, it is absorbed by the photopigment, rhodopsin, in the outer segment (OS) of rod photoreceptor cells. Rhodopsin consists of an opsin protein chemically linked to a chromophore, 11-cis-retinal. When light is absorbed, the 11-cis retinal is converted to an all-trans retinal; this structural change activates rhodopsin (R^*). R* binds to and activates the trimeric G protein transducin ($T\alpha^*$). $T\alpha^*$ activates the membrane-associated cyclic guanosine monophosphate (cGMP) phosphodiesterase (PDE) (PDE^*, activated phosphodiesterase). PDE^* converts cGMP to 5'-GMP thus reducing the intracellular cGMP concentration. cGMP binds to the ligand-gated channels in the OS membrane. Decreased cGMP concentrations result in the closing of the membrane channels, a decrease in Na^+ ion influx, generation of a negative membrane potential and a hyperpolarization of the rod photoreceptor cell. (B). The end result of the cascade is a decrease in the rate of glutamate release, a neurotransmitter, a change in the membrane polarity of the downstream neurons that synapse with the photoreceptor cells and eventually transmission of the visual signal to the brain [2].

In order to return the rod photoreceptor cell to its native depolarized state, R* must be phosphorylated by rhodopsin kinase. This causes a structural change in R* so that arrestin can bind to R*, blocking R* and $T\alpha^*$ interactions. This subsequently leads to the inactivation of PDE*, restoration of cellular cGMP levels, and the re-opening of the cGMP gated membrane channels. Once R* has been blocked from further interactions with transducin, all-trans retinal dissociates from rhodopsin and the photopigment is then said to be bleached. Bleached photopigment is unable to absorb photons of light. The dissociated all-trans retinal is regenerated in the RPE via conversion to 11-cis retinal, which is then able to recombine with rhodopsin and absorb another photon of light to re-initiate the phototransduction cascade.

B) Changes in Na^+ and K^+ currents in rod photoreceptor cells between photoreceptors in the dark and with light stimulus. In the dark, the channels in the photoreceptor outer segments are open, allowing flow of Na^+ into the cell. In the presence of light, the channels close, reducing the amount of Na^+ entering the cell. The efflux of K^+ from the inner segments remains constant resulting in hyperpolarization of the cell in the presence of light.

DP, guanosine diphosphate; GTP, guanosine triphosphate; cGMP, cyclin guanosine monophosphate; PDE, cGMP-phosphodiesterase; GC, guanylate cyclase; GCAP, guanylate cyclase-activating protein; Ca, calcium; H^+, proton; IPM, interphotoreceptor matrix; Na^+, sodium ion; K^+, potassium ion; E_m, membrane potential.

A: Image adapted from ref [115].

B: Image taken from http://soma.npa.uiuc.edu/courses/bio303/Ch11.html

A

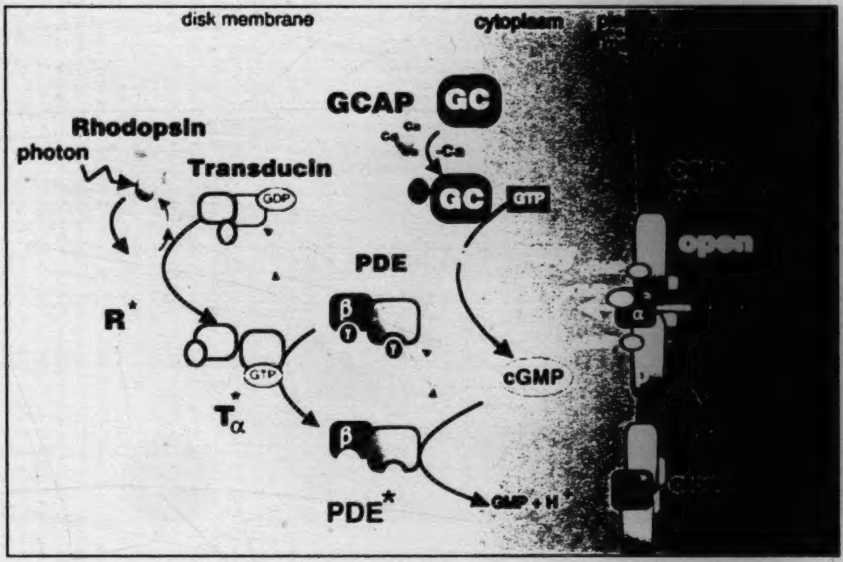

B

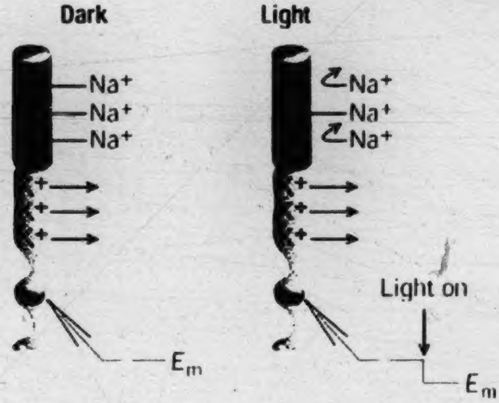

Figure 1.4 – Schematic diagram of rod and cone photoreceptor cells.

Image adapted from http://www.fz-juelich.de/ibi/ibi-1/Photoreception/

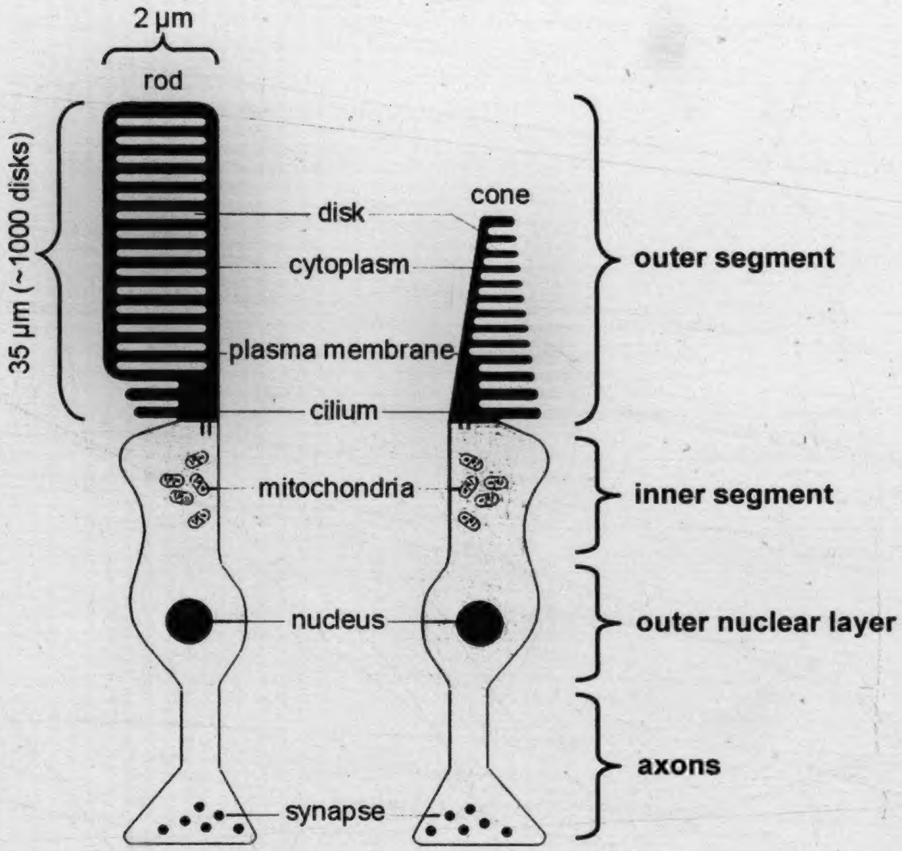

Figure 1.5 – Morphological changes that occur in a cell undergoing apoptosis.
A) Normal cellular morphology showing cell-cell and cell-matrix contacts. B) Cellular and nuclear condensation and fragmentation of chromatin. C) Disassembly of the cell and formation of apoptotic bodies. Phagocytosis of apoptotic bodies by neighbouring cells (D) and phagocytes (E). Image courtesy of Dr. Paul Wong, Emory University.

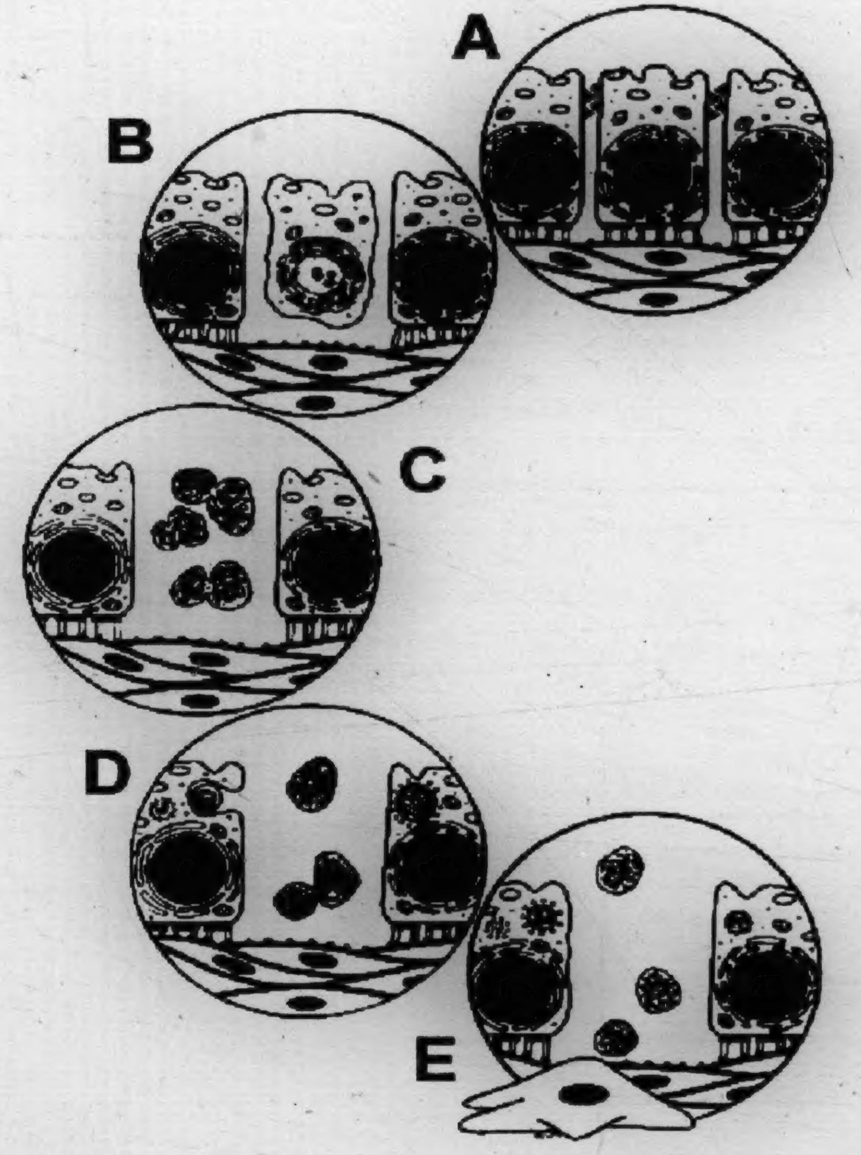

Figure 1.6 – Stages of degeneration in the light-induced retinal degeneration model. A) Northern blot analysis of IRBP, HO-1, and CLU from dark-reared and light exposed rat retinas. 18S ribosomal RNA bands are shown as a loading control. B) Graphical analysis of the expression levels shown on the corresponding northern blots. Expression levels were normalized to the 18S ribosomal RNA. Based on the expression profiles of these genes, the apoptotic pathway observed in LIRD can be divided into five stages: normal; commitment; execution; stress response; and survival response. Figure adapted from reference [88].

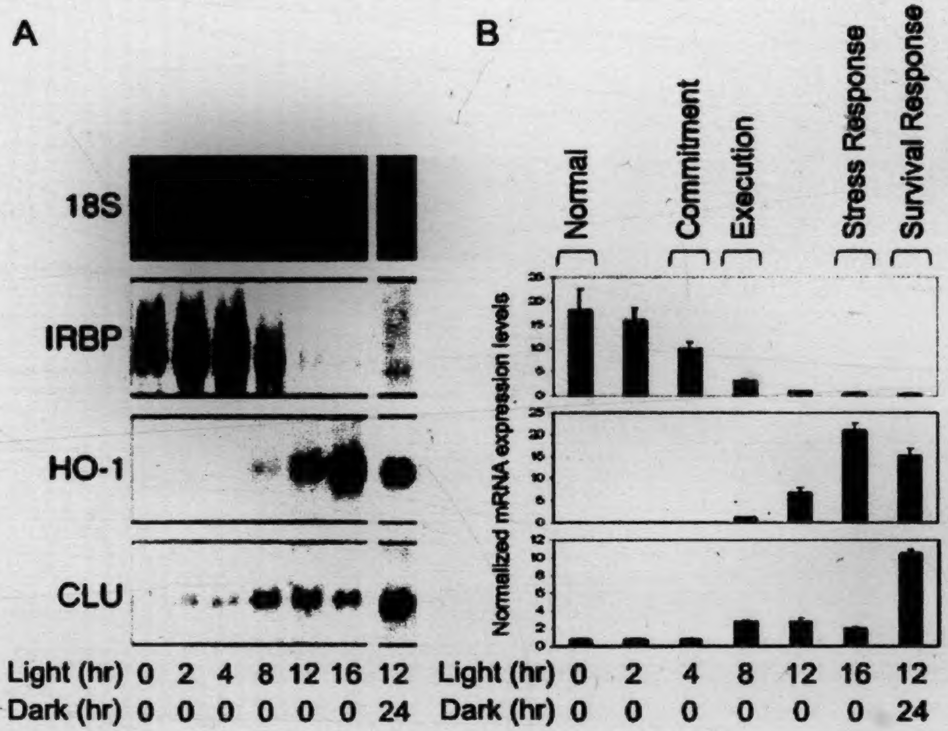

1.7 REFERENCES

1. Noell, W.K., Walker, V.S., Kang, B.S. and Berman, S. (1966) Retinal damage by light in rats. *Investigative Ophthalmology,* **5,** 450-472.
2. Oyster, C.W. (1999) The human eye: structure and function. In. Sinauer Associates, Sunderland, MA, pp. 60-61; 545-648.
3. Hubel, D.H. (1988) Eye, brain, and vision. In. Scientific American Library, New York, NY, pp. 59-71.
4. Sharma, R.K., Ehinger, B.E.J. (2003) Development and Structure of the Retina. In Kaufman, P.L., Alm, A. (ed.), *Adler's Physiology of the Eye.* 10th ed. Mosby, St. Louis, MO, pp. 319-440.
5. la Cour, M. (2003) The Retinal Pigment Epithelium. In Kaufman, P.L., Alm, A. (ed.), *Adler's Physiology of the Eye.* Tenth ed. Mosby, St. Louis, MO, pp. 348-357.
6. Rhoades, R., Pflanzer, R. (1996) Sensory systems. In *Human Physiology.* 3rd ed. Saunders College Publishing, Fort Worth, TX, pp. 269-272.
7. Bessant, D.A.R., Kaushal, S., Bhattacharya, S.S. (2003) Genetics and Biology of the Inherited Retinal Dystrophies. In Kaufman, P.L.a.A., A. (ed.), *Adler's Physiology of the Eye.* 10th ed. Mosby, St. Louis, MO, pp. 358-381.
8. Rivolta, C., Sharon, D., DeAngelis, M.M. and Dryja, T.P. (2002) Retinitis pigmentosa and allied diseases: numerous diseases, genes, and inheritance patterns. *Hum Mol Genet,* **11,** 1219-27.
9. Huang, P.C., Gaitan, A.E., Hao, Y., Petters, R.M. and Wong, F. (1993) Cellular interactions implicated in the mechanism of photoreceptor degeneration in transgenic mice expressing a mutant rhodopsin gene. *Proc Natl Acad Sci U S A,* **90,** 8484-8.
10. Reme, C.E., Grimm, C., Hafezi, F., Marti, A. and Wenzel, A. (1998) Apoptotic cell death in retinal degenerations. *Prog Retin Eye Res,* **17,** 443-64.
11. Zhang, K., Nguyen, T.H., Crandall, A. and Donoso, L.A. (1995) Genetic and molecular studies of macular dystrophies: recent developments. *Surv Ophthalmol,* **40,** 51-61.

12. Young, R.W. (1988) Solar radiation and age-related macular degeneration. *Surv Ophthalmol,* **32,** 252-69.

13. Beatty, S., Koh, H., Phil, M., Henson, D. and Boulton, M. (2000) The role of oxidative stress in the pathogenesis of age-related macular degeneration. *Surv Ophthalmol,* **45,** 115-34.

14. Winkler, B.S., Boulton, M.E., Gottsch, J.D. and Sternberg, P. (1999) Oxidative damage and age-related macular degeneration. *Mol Vis,* **5,** 32.

15. Evans, J.R. (2006) Antioxidant vitamin and mineral supplements for slowing the progression of age-related macular degeneration. *Cochrane Database Syst Rev,* CD000254.

16. http://www.cnib.ca/ (August 2006) Canadian National Institute for the Blind website.

17. http://www.sph.uth.tmc.edu/Retnet/ (August 2006) RetNet - Retinal Information Network.

18. van Soest, S., Westerveld, A., de Jong, P.T., Bleeker-Wagemakers, E.M. and Bergen, A.A. (1999) Retinitis pigmentosa: defined from a molecular point of view. *Surv Ophthalmol,* **43,** 321-34.

19. Dunaief, J.L., Dentchev, T., Ying, G.S. and Milam, A.H. (2002) The role of apoptosis in age-related macular degeneration. *Arch Ophthalmol,* **120,** 1435-42.

20. Chang, G.Q., Hao, Y. and Wong, F. (1993) Apoptosis: final common pathway of photoreceptor death in rd, rds, and rhodopsin mutant mice. *Neuron,* **11,** 595-605.

21. Portera-Cailliau, C., Sung, C.H., Nathans, J. and Adler, R. (1994) Apoptotic photoreceptor cell death in mouse models of retinitis pigmentosa. *Proc Natl Acad Sci U S A,* **91,** 974-8.

22. Abler, A.S., Chang, C.J., Ful, J., Tso, M.O. and Lam, T.T. (1996) Photic injury triggers apoptosis of photoreceptor cells. *Res Commun Mol Pathol Pharmacol,* **92,** 177-89.

23. Molthagen, M., Schachner, M. and Bartsch, U. (1996) Apoptotic cell death of photoreceptor cells in mice deficient for the adhesion molecule on glia (AMOG, the beta 2- subunit of the Na, K-ATPase). *J Neurocytol,* **25,** 243-55.

24. Tso, M.O., Zhang, C., Abler, A.S., Chang, C.J., Wong, F., Chang, G.Q. and Lam, T.T. (1994) Apoptosis leads to photoreceptor degeneration in inherited retinal dystrophy of RCS rats. *Invest Ophthalmol Vis Sci,* **35,** 2693-9.

25. Kerr, J.F., Wyllie, A.H. and Currie, A.R. (1972) Apoptosis: a basic biological phenomenon with wide-ranging implications in tissue kinetics. *Br J Cancer,* **26,** 239-57.

26. Hacker, G. (2000) The morphology of apoptosis. *Cell Tissue Res,* **301,** 5-17.

27. Young, R.W. (1984) Cell death during differentiation of the retina in the mouse. *J Comp Neurol,* **229,** 362-73.

28. Wyllie, A.H. (1980) Glucocorticoid-induced thymocyte apoptosis is associated with endogenous endonuclease activation. *Nature,* **284,** 555-6.

29. Schultz, D.R. and Harrington, W.J., Jr. (2003) Apoptosis: programmed cell death at a molecular level. *Semin Arthritis Rheum,* **32,** 345-69.

30. Lawen, A. (2003) Apoptosis-an introduction. *Bioessays,* **25,** 888-96.

31. Wright, S.C., Wei, Q.S., Zhong, J., Zheng, H., Kinder, D.H. and Larrick, J.W. (1994) Purification of a 24-kD protease from apoptotic tumor cells that activates DNA fragmentation. *J Exp Med,* **180,** 2113-23.

32. Johnson, D.E. (2000) Noncaspase proteases in apoptosis. *Leukemia,* **14,** 1695-703.

33. Altairac, S., Wright, S.C., Courtois, Y. and Torriglia, A. (2003) L-DNase II activation by the 24 kDa apoptotic protease (AP24) in TNFalpha-induced apoptosis. *Cell Death Differ,* **10,** 1109-11.

34. Friedman, J. and Xue, D. (2004) To live or die by the sword: the regulation of apoptosis by the proteasome. *Dev Cell,* **6,** 460-1.

35. Susin, S.A., Lorenzo, H.K., Zamzami, N., Marzo, I., Snow, B.E., Brothers, G.M., Mangion, J., Jacotot, E., Costantini, P., Loeffler, M., Larochette, N., Goodlett, D.R., Aebersold, R., Siderovski, D.P., Penninger, J.M. and Kroemer, G. (1999) Molecular characterization of mitochondrial apoptosis-inducing factor. *Nature,* **397,** 441-6.

36. Li, L.Y., Luo, X. and Wang, X. (2001) Endonuclease G is an apoptotic DNase when released from mitochondria. *Nature,* **412,** 95-9.

37. van Loo, G., Schotte, P., van Gurp, M., Demol, H., Hoorelbeke, B., Gevaert, K., Rodriguez, I., Ruiz-Carrillo, A., Vandekerckhove, J., Declercq, W., Beyaert, R. and Vandenabeele, P. (2001) Endonuclease G: a mitochondrial protein released in apoptosis and involved in caspase-independent DNA degradation. *Cell Death Differ,* **8,** 1136-42.

38. Patterson, M., Organisciak, D.T., Kelln, R.M., Grewal, R., McDonald, B., Darrow, R., Barsalou, L., Wong, P. (In preparation) Activation of caspases during light-induced retinal degeneration.

39. Syntichaki, P. and Tavernarakis, N. (2002) Death by necrosis. Uncontrollable catastrophe, or is there order behind the chaos? *EMBO Rep,* **3,** 604-9.

40. Bowes, C., Li, T., Danciger, M., Baxter, L.C., Applebury, M.L. and Farber, D.B. (1990) Retinal degeneration in the rd mouse is caused by a defect in the beta subunit of rod cGMP-phosphodiesterase. *Nature,* **347,** 677-80.

41. Hawkins, R.K., Jansen, H.G. and Sanyal, S. (1985) Development and degeneration of retina in rds mutant mice: photoreceptor abnormalities in the heterozygotes. *Exp Eye Res,* **41,** 701-20.

42. Strauss, O., Stumpff, F., Mergler, S., Wienrich, M. and Wiederholt, M. (1998) The Royal College of Surgeons rat: an animal model for inherited retinal degeneration with a still unknown genetic defect. *Acta Anat (Basel),* **162,** 101-11.

43. Petersen-Jones, S.M. (1998) Animal models of human retinal dystrophies. *Eye,* **12 (Pt 3b),** 566-70.

44. Pierce, E.A. (2001) Pathways to photoreceptor cell death in inherited retinal degenerations. *Bioessays,* **23,** 605-18.

45. Molday, R.S. (1998) Photoreceptor membrane proteins, phototransduction, and retinal degenerative diseases. The Friedenwald Lecture. *Invest Ophthalmol Vis Sci,* **39,** 2491-513.

46. Li, T., Snyder, W.K., Olsson, J.E. and Dryja, T.P. (1996) Transgenic mice carrying the dominant rhodopsin mutation P347S: evidence for defective vectorial transport of rhodopsin to the outer segments. *Proc Natl Acad Sci U S A,* **93,** 14176-81.

47. Travis, G.H. (1998) Mechanisms of cell death in the inherited retinal degenerations. *Am J Hum Genet,* **62,** 503-8.

48. Tsang, S.H., Gouras, P., Yamashita, C.K., Kjeldbye, H., Fisher, J., Farber, D.B. and Goff, S.P. (1996) Retinal degeneration in mice lacking the gamma subunit of the rod cGMP phosphodiesterase. *Science,* **272,** 1026-9.

49. Fain, G.L. (2006) Why photoreceptors die (and why they don't). *Bioessays,* **28,** 344-54.

50. D'Cruz, P.M., Yasumura, D., Weir, J., Matthes, M.T., Abderrahim, H., LaVail, M.M. and Vollrath, D. (2000) Mutation of the receptor tyrosine kinase gene Mertk in the retinal dystrophic RCS rat. *Hum Mol Genet,* **9,** 645-51.

51. Redmond, T.M., Yu, S., Lee, E., Bok, D., Hamasaki, D., Chen, N., Goletz, P., Ma, J.X., Crouch, R.K. and Pfeifer, K. (1998) Rpe65 is necessary for production of 11-cis-vitamin A in the retinal visual cycle. *Nat Genet,* **20,** 344-51.

52. Chen, J., Simon, M.I., Matthes, M.T., Yasumura, D. and LaVail, M.M. (1999) Increased susceptibility to light damage in an arrestin knockout mouse model of Oguchi disease (stationary night blindness). *Invest Ophthalmol Vis Sci,* **40,** 2978-82.

53. Chen, C.K., Burns, M.E., Spencer, M., Niemi, G.A., Chen, J., Hurley, J.B., Baylor, D.A. and Simon, M.I. (1999) Abnormal photoresponses and light-induced apoptosis in rods lacking rhodopsin kinase. *Proc Natl Acad Sci U S A,* **96,** 3718-22.

54. Fuchs, S., Nakazawa, M., Maw, M., Tamai, M., Oguchi, Y. and Gal, A. (1995) A homozygous 1-base pair deletion in the arrestin gene is a frequent cause of Oguchi disease in Japanese. *Nat Genet,* **10,** 360-2.

55. Yamamoto, S., Sippel, K.C., Berson, E.L. and Dryja, T.P. (1997) Defects in the rhodopsin kinase gene in the Oguchi form of stationary night blindness. *Nat Genet,* **15,** 175-8.

56. Dryja, T.P., Finn, J.T., Peng, Y.W., McGee, T.L., Berson, E.L. and Yau, K.W. (1995) Mutations in the gene encoding the alpha subunit of the rod cGMP-gated channel in autosomal recessive retinitis pigmentosa. *Proc Natl Acad Sci U S A,* **92,** 10177-81.

57. Perrault, I., Rozet, J.M., Calvas, P., Gerber, S., Camuzat, A., Dollfus, H., Chatelin, S., Souied, E., Ghazi, I., Leowski, C., Bonnemaison, M., Le Paslier, D., Frezal, J., Dufier, J.L., Pittler, S., Munnich, A. and Kaplan, J. (1996) Retinal-specific guanylate cyclase gene mutations in Leber's congenital amaurosis. *Nat Genet,* **14,** 461-4.

58. Fain, G.L. and Lisman, J.E. (1999) Light, Ca2+, and photoreceptor death: new evidence for the equivalent-light hypothesis from arrestin knockout mice. *Invest Ophthalmol Vis Sci,* **40,** 2770-2.

59. Lisman, J. and Fain, G. (1995) Support for the equivalent light hypothesis for RP. *Nat Med,* **1,** 1254-5.

60. Wenzel, A., Grimm, C., Samardzija, M. and Reme, C.E. (2005) Molecular mechanisms of light-induced photoreceptor apoptosis and neuroprotection for retinal degeneration. *Prog Retin Eye Res,* **24,** 275-306.

61. Paskowitz, D.M., LaVail, M.M. and Duncan, J.L. (2006) Light and inherited retinal degeneration. *Br J Ophthalmol,* **90,** 1060-6.

62. Curcio, C.A., Sloan, K.R., Kalina, R.E. and Hendrickson, A.E. (1990) Human photoreceptor topography. *J Comp Neurol,* **292,** 497-523.

63. Curcio, C.A., Medeiros, N.E. and Millican, C.L. (1996) Photoreceptor loss in age-related macular degeneration. *Invest Ophthalmol Vis Sci,* **37,** 1236-49.

64. Curcio, C.A. (2001) Photoreceptor topography in ageing and age-related maculopathy. *Eye,* **15,** 376-83.

65. Kopitz, J., Holz, F.G., Kaemmerer, E. and Schutt, F. (2004) Lipids and lipid peroxidation products in the pathogenesis of age-related macular degeneration. *Biochimie,* **86,** 825-31.

66. Grimm, C., Wenzel, A., Hafezi, F., Yu, S., Redmond, T.M. and Reme, C.E. (2000) Protection of Rpe65-deficient mice identifies rhodopsin as a mediator of light-induced retinal degeneration. *Nat Genet,* **25,** 63-6.

67. Reme, C.E. (2005) The dark side of light: rhodopsin and the silent death of vision the proctor lecture. *Invest Ophthalmol Vis Sci,* **46,** 2671-82.

68. Hao, W., Wenzel, A., Obin, M.S., Chen, C.K., Brill, E., Krasnoperova, N.V., Eversole-Cire, P., Kleyner, Y., Taylor, A., Simon, M.I., Grimm, C., Reme, C.E.

and Lem, J. (2002) Evidence for two apoptotic pathways in light-induced retinal degeneration. *Nat Genet,* **32,** 254-60.

69. Wenzel, A., Grimm, C., Marti, A., Kueng-Hitz, N., Hafezi, F., Niemeyer, G. and Reme, C.E. (2000) c-fos controls the "private pathway" of light-induced apoptosis of retinal photoreceptors. *J Neurosci,* **20,** 81-8.

70. Hafezi, F., Marti, A., Grimm, C., Wenzel, A. and Reme, C.E. (1999) Differential DNA binding activities of the transcription factors AP-1 and Oct-1 during light-induced apoptosis of photoreceptors. *Vision Res,* **39,** 2511-8.

71. Grimm, C., Wenzel, A., Hafezi, F. and Reme, C.E. (2000) Gene expression in the mouse retina: the effect of damaging light. *Mol Vis,* **6,** 252-60.

72. Wu, T., Chiang, S.K., Chau, F.Y. and Tso, M.O. (2003) Light-induced photoreceptor degeneration may involve the NF kappa B/caspase-1 pathway in vivo. *Brain Res,* **967,** 19-26.

73. Wu, J., Gorman, A., Zhou, X., Sandra, C. and Chen, E. (2002) Involvement of caspase-3 in photoreceptor cell apoptosis induced by in vivo blue light exposure. *Invest Ophthalmol Vis Sci,* **43,** 3349-54.

74. Donovan, M., Carmody, R.J. and Cotter, T.G. (2001) Light-induced photoreceptor apoptosis in vivo requires neuronal nitric-oxide synthase and guanylate cyclase activity and is caspase-3-independent. *J Biol Chem,* **276,** 23000-8.

75. Donovan, M. and Cotter, T.G. (2002) Caspase-independent photoreceptor apoptosis in vivo and differential expression of apoptotic protease activating factor-1 and caspase-3 during retinal development. *Cell Death Differ,* **9,** 1220-31.

76. Grewal, R., Stepczynski, J., Kelln, R., Erickson, T., Darrow, R., Barsalou, L., Patterson, M., Organisciak, D.T. and Wong, P. (2004) Coordinated changes in classes of ribosomal protein gene expression is associated with light-induced retinal degeneration. *Invest Ophthalmol Vis Sci,* **45,** 3885-95.

77. Sakaguchi, H., Miyagi, M., Darrow, R.M., Crabb, J.S., Hollyfield, J.G., Organisciak, D.T. and Crabb, J.W. (2003) Intense light exposure changes the crystallin content in retina. *Exp Eye Res,* **76,** 131-3.

78. McDonald, B., Kelln, R.M., Stepczynski, J., Chambers, M.L., Organisciak, D.T., Darrow, R.M., Barsalou, L., Wong, P. (2000) Differential crystallin gene

expression in light-induced retinal degeneration. *Invest Ophthalmol Vis Sci,* **41,** 113.

79. LaVail, M.M. (1976) Survival of some photoreceptors in albino rats following long-term exposures to continuous light. *Invest Ophthalmol Vis Sci,* **15,** 64-70.

80. Szel, A. and Rohlich, P. (1992) Two cone types of rat retina detected by anti-visual pigment antibodies. *Exp Eye Res,* **55,** 47-52.

81. Jacobs, G.H., Fenwick, J.A. and Williams, G.A. (2001) Cone-based vision of rats for ultraviolet and visible lights. *J Exp Biol,* **204,** 2439-2446.

82. Ham, W.T., Jr., Mueller, H.A. and Sliney, D.H. (1976) Retinal sensitivity to damage from short wavelength light. *Nature,* **260,** 153-5.

83. Grimm, C., Reme, C.E., Rol, P.O. and Williams, T.P. (2000) Blue light's effects on rhodopsin: photoreversal of bleaching in living rat eyes. *Invest Ophthalmol Vis Sci,* **41,** 3984-90.

84. Grimm, C., Wenzel, A., Williams, T., Rol, P., Hafezi, F. and Reme, C. (2001) Rhodopsin-mediated blue-light damage to the rat retina: effect of photoreversal of bleaching. *Invest Ophthalmol Vis Sci,* **42,** 497-505.

85. Organisciak, D.T. and Winkler, B.S. (1994) Retinal light damage: practical and theoretical considerations. In Osborne, N. and Chader, G. (eds.), *Progress in Retinal and Eye Research.* Pergamon Press, New York, pp. 1-29.

86. Organisciak, D.T., Kutty, R.K., Leffak, M., Wong, P., Messing, S., Wiggert, B., Darrow, R.M. and Chader, G.J. (1995) Oxidative damage and responses in retinal nuclei arising from intense light exposure. In *Degenerative Diseases of the Retina.* Plenum Press, New York, pp. 19-26.

87. Organisciak, D.T., Jiang, Y.L., Wang, H.M., Pickford, M. and Blanks, J.C. (1989) Retinal light damage in rats exposed to intermittent light. Comparison with continuous light exposure. *Invest Ophthalmol Vis Sci,* **30,** 795-805.

88. Wong, P., Ulyanova, T., Organisciak, D.T., Bennett, S., Lakins, J., Arnold, J.M., Kutty, R.K., Tenniswood, M., vanVeen, T., Darrow, R.M. and Chader, G. (2001) Expression of multiple forms of clusterin during light-induced retinal degeneration. *Current Eye Research,* **23,** 157-165.

89. Penn, J.S., Naash, M.I. and Anderson, R.E. (1987) Effect of light history on retinal antioxidants and light damage susceptibility in the rat. *Exp Eye Res,* **44,** 779-88.

90. Penn, J.S., Tolman, B.L., Thum, L.A. and Koutz, C.A. (1992) Effect of light history on the rat retina: timecourse of morphological adaptation and readaptation. *Neurochem Res,* **17,** 91-9.

91. Li, F., Cao, W. and Anderson, R.E. (2001) Protection of photoreceptor cells in adult rats from light-induced degeneration by adaptation to bright cyclic light. *Exp Eye Res,* **73,** 569-77.

92. Penn, J.S. and Williams, T.P. (1986) Photostasis: regulation of daily photon-catch by rat retinas in response to various cyclic illuminances. *Exp Eye Res,* **43,** 915-28.

93. Noell, W.K., Delmelle, M.C. and Albrecht, R. (1971) Vitamin A deficiency effect on retina: dependence on light. *Science,* **172,** 72-5.

94. Organisciak, D.T. and Noell, W.K. (1977) The rod outer segment phospholipid/opsin ratio of rats maintained in darkness or cyclic light. *Invest Ophthalmol Vis Sci,* **16,** 188-90.

95. Organisciak, D.T., Darrow, R.M. and Barsalou, L.S. (2003) Light-induced retinal degeneration. In Levin, L.A. and Di Polo, A. (eds.), *Ocular Neuroprotection.* Marcel Dekker, p. 344.

96. Vaughan, D.K., Nemke, J.L., Fliesler, S.J., Darrow, R.M. and Organisciak, D.T. (2002) Evidence for a circadian rhythm of susceptibility to retinal light damage. *Photochem Photobiol,* **75,** 547-53.

97. Organisciak, D.T., Darrow, R.M., Barsalou, L., Kutty, R.K. and Wiggert, B. (2000) Circadian-dependent retinal light damage in rats. *Invest Ophthalmol Vis Sci,* **41,** 3694-701.

98. Yang, J.H., Basinger, S.F., Gross, R.L. and Wu, S.M. (2003) Blue light-induced generation of reactive oxygen species in photoreceptor ellipsoids requires mitochondrial electron transport. *Invest Ophthalmol Vis Sci,* **44,** 1312-9.

99. Kutty, R.K., Kutty, G., Wiggert, B., Chader, G.J., Darrow, R.M. and Organisciak, D.T. (1995) Induction of heme oxygenase 1 in the retina by intense visible light:

suppression by the antioxidant dimethylthiourea. *Proc Natl Acad Sci U S A,* **92,** 1177-81.

100. Organisciak, D.T., Wang, H.M. and Kou, A.L. (1984) Ascorbate and glutathione levels in the developing normal and dystrophic rat retina: effect of intense light exposure. *Curr Eye Res,* **3,** 257-67.

101. Organisciak, D.T., Wang, H.M., Li, Z.Y. and Tso, M.O. (1985) The protective effect of ascorbate in retinal light damage of rats. *Invest Ophthalmol Vis Sci,* **26,** 1580-8.

102. Organisciak, D.T., Jiang, Y.L., Wang, H.M. and Bicknell, I. (1990) The protective effect of ascorbic acid in retinal light damage of rats exposed to intermittent light. *Invest Ophthalmol Vis Sci,* **31,** 1195-202.

103. Organisciak, D.T., Wang, H.M. and Noell, W.K. (1987) Aspects of the ascorbate protective mechanism in retinal light damage of rats with normal and reduced ROS docosahexaenoic acid. *Prog Clin Biol Res,* **247,** 455-68.

104. Noell, W.K., Organisciak, D.T., Ando, H., Braniecki, M.A. and Durlin, C. (1987) Ascorbate and dietary protective mechanisms in retinal light damage of rats: electrophysiological, histological and DNA measurements. *Prog Clin Biol Res,* **247,** 469-83.

105. Lam, S., Tso, M.O. and Gurne, D.H. (1990) Amelioration of retinal photic injury in albino rats by dimethylthiourea. *Arch Ophthalmol,* **108,** 1751-7.

106. Organisciak, D.T., Darrow, R.M., Jiang, Y.I., Marak, G.E. and Blanks, J.C. (1992) Protection by dimethylthiourea against retinal light damage in rats. *Invest Ophthalmol Vis Sci,* **33,** 1599-609.

107. Reme, C.E., Braschler, U.F., Roberts, J. and Dillon, J. (1991) Light damage in the rat retina: effect of a radioprotective agent (WR-77913) on acute rod outer segment disk disruptions. *Photochem Photobiol,* **54,** 137-42.

108. Nakamura, H., Nakamura, K. and Yodoi, J. (1997) Redox regulation of cellular activation. *Annu Rev Immunol,* **15,** 351-69.

109. Tanito, M., Masutani, H., Nakamura, H., Ohira, A. and Yodoi, J. (2002) Cytoprotective effect of thioredoxin against retinal photic injury in mice. *Invest Ophthalmol Vis Sci,* **43,** 1162-7.

110. Tanito, M., Masutani, H., Nakamura, H., Oka, S., Ohira, A. and Yodoi, J. (2002) Attenuation of retinal photooxidative damage in thioredoxin transgenic mice. *Neurosci Lett,* **326,** 142-6.

111. Imamura, Y., Noda, S., Hashizume, K., Shinoda, K., Yamaguchi, M., Uchiyama, S., Shimizu, T., Mizushima, Y., Shirasawa, T. and Tsubota, K. (2006) Drusen, choroidal neovascularization, and retinal pigment epithelium dysfunction in SOD1-deficient mice: A model of age-related macular degeneration. *PNAS,* **103,** 11282-11287.

112. Pepperberg, D.R., Okajima, T.L., Wiggert, B., Ripps, H., Crouch, R.K. and Chader, G.J. (1993) Interphotoreceptor retinoid-binding protein (IRBP). Molecular biology and physiological role in the visual cycle of rhodopsin. *Mol Neurobiol,* **7,** 61-85.

113. Stocker, R. (1990) Induction of haem oxygenase as a defence against oxidative stress. *Free Radic Res Commun,* **9,** 101-12.

114. Darrow, R.A., Darrow, R.M. and Organisciak, D.T. (1997) Biochemical characterization of cell specific enzymes in light-exposed rat retinas: oxidative loss of all-trans retinol dehydrogenase activity. *Curr Eye Res,* **16,** 144-51.

115. Polans, A., Baehr, W. and Palczewski, K. (1996) Turned on by Ca2+! The physiology and pathology of Ca(2+)-binding proteins in the retina. *Trends Neurosci,* **19,** 547-54.

Chapter 2

Differential screening for genes involved in light-induced retinal degeneration, identification and characterization of T-cadherin

2.1 INTRODUCTION

Human retinal dystrophies are characterized by progressive photoreceptor cell loss leading to blindness. This retinal degeneration is mediated by an active cell death mechanism that is not fully understood [1, 2]. Studying the light-induced retinal degeneration (LIRD) model system in rats, an accepted animal model for human retinal degenerative disease, enables us to gain insight into the active process of retinal degeneration [3-6]. After a prolonged exposure to light, photoreceptor cells in these animals undergo cellular dysfunction leading to apoptosis [3]. Retinal tissue after prolonged light exposure presents with DNA fragmentation ladders and photoreceptor cells within the retina are TUNEL positive, two hallmarks of apoptosis [5, 7-9].

In the LIRD model system, longer periods of light exposure can be used to drive photoreceptor cells to a more complete state of degeneration [7]. The degenerative process leading to visual cell loss involves an oxidative stress mediated apoptotic pathway, which is initiated by the bleaching of the photopigment rhodopsin [3]. Pretreatment of animals with antioxidants such as dimethylthiourea (DMTU) or ascorbate prior to light exposure reduces the extent of retinal photic injury indicating that oxygen radicals are responsible for mediating or exacerbating the retinal degeneration process [10-14]. Accompanying the progressive states of degeneration seen over a time course of increasing periods of light exposure are alterations in gene expression. Changes in the mRNA expression profile over the course of LIRD have been reported for caspases, c-fos, c-jun, RPE65, a number of ribosomal-binding proteins, clusterin, IRBP, and heme oxygenase-1 (HO-1) [6, 15-18]. In the case of the three latter genes, the relative expression profiles for each are different; each peaking at a different stage of the light damage profile, suggesting that the transformation from a normal retina to a degenerate one is progressive [17]. The simultaneous induction of HO-1 (a marker for oxidative stress) mRNA levels at the same time in which IRBP (a marker for normal photoreceptor function) is markedly suppressed supports the finding that LIRD is driven by photoreceptor cell dysfunction and influenced by the presence of oxidative stress [17].

To further elucidate additional elements relevant to LIRD and to identify possible gene candidates involved in the degeneration process, we performed a differential screen of a retinal cDNA library derived from retinas isolated from rats exposed to prolonged periods of light exposure. We are interested in determining the molecular differences that exist between a normal retina and a degenerating retina. More specifically we are interested in defining the molecular signature after a 16 hour green light exposure. HO-1 mRNA levels peak at 16 hour of light, suggesting that this is the light exposure in which the retina may experience the highest level of oxidative stress over the degeneration time course examined [17]. Use of a differential screening approach between a 16 hour light-treated retina and a dark-reared (no light exposed) retina enables us to obtain a "snapshot" of the gene expression events that change in the process of LIRD, and more specifically, to define genes that may be involved in the protection or conversely the degeneration of the retina in response to a high oxidative stress environment.

In the current communication we present our data on the identification of 105 clones with known identities that were isolated as 16 hour light exposed (as compared to dark-reared retina) differentially expressed genes. A number of the genes isolated were as expected, such as those involved in vision processes and signal transduction. One gene that was isolated from our screen was T-cadherin (H-cadherin, cadherin-13, CDH-13). Cadherins are a large family of adhesion molecules that mediate calcium-dependent cell-cell adhesion. Numerous members of the cadherin family have been implicated in retinal disease [19]. Mutations in cadherin-23 as well as protocadherin-15 have been shown to underlie Usher syndrome type 1D (USH1D) and type 1F (USH1F), respectively [20-23]. Usher syndrome type 1 is the most severe form of the disorder manifesting in severe to profound congenital hearing impairment and retinal degeneration beginning in childhood [24]. Congenital hypotrichosis associated with juvenile macular dystrophy (HJMD), a disease that causes hair loss as well as macular degeneration, has been found to arise as a result of a 1 bp deletion in the cadherin-3 (P-cadherin) gene [25]. prCAD, the gene encoding protocadherin-21, has yet to be implicated in retinal disease; however, it has been shown to be essential in mice for retinal outer segment integrity and photoreceptor survival and is thus a likely candidate for retinal dystrophies [26, 27].

T-cadherin is an unusual member of the cadherin superfamily in that it lacks the typical transmembrane and cytoplasmic domains and instead has a glycosylphosphatidylinositol (GPI) cell membrane anchor [28]. Like classical cadherins, T-cadherin is able to form stable Ca^{2+}-dependent intercellular adhesion [29, 30]. T-cadherin expression has been found to be down-regulated in numerous cancers including breast [31], lung [32], and ovarian [33] cancer. Conversely, T-cadherin expression has been shown to be upregulated in tumor angiogenesis [34]. In the nervous system, T-cadherin is thought to be involved in maintaining neural circuitry, perhaps by negatively regulating neural growth [35]. Although lacking known cellular function, it is speculated that T-cadherin may be involved in cellular signaling [36-39]. Recent data shows that T-cadherin serves as a signaling receptor for low-density lipoprotein (LDL)-dependent mitogenic signal in the vasculature [39]. Recently, T-cadherin was shown to be up-regulated in human umbilical vein endothelial cells (HUVEC) in response to oxidative stress and that overexpression of T-cadherin in HUVEC protects against oxidative stress-induced apoptosis [40].

The number of cadherin genes known or suspected to be involved in retinal disease, as well as the studies so far implicating T-cadherin in cellular signaling and protection from oxidative stress made this gene a good candidate for further characterization during retinal degeneration. Virtually nothing is known about the function of T-cadherin in the retina; therefore, by determining its expression in the retina and during retinal degeneration, as well as its cellular localization in the retina, we will provide insight into the role of T-cadherin in the retina.

2.2 MATERIALS AND METHODS

2.2.1 Animals

Weanling male albino Sprague-Dawley rats from Harlan Inc. (Indianapolis, IN) were maintained in darkness for 40 days. At 60 days of age, rats were exposed to intense visible light for 0, 2, 4, 8 or 16 hours. RNA and protein isolated from the retinas of these animals defined the LIRD time course used in the current study (LIRD profile). Light exposures were started at 9 am and were performed in green #2092 Plexiglass chambers (Dayton Plastics, Dayton, OH) transmitting 490-580 nm light (green light) [3] with an illuminance of 1200 to 1400 lux. The use of green light allows for the targeting of the rod photoreceptor cells since the wavelength of light used is within the absorption spectrum of the rhodopsin photopigment [3]. Rats were sacrificed in carbon dioxide saturated chambers and the retinas were excised and flash frozen on dry ice. The tissues were stored at -80°C until use. For each treatment condition, retinas were obtained and pooled from 5-10 rats. For histological analysis, eyes were enucleated from three animals. In all cases, animals were cared for in accordance with the guidelines defined by the Public Health Service Policy on Humane Care and Use of Laboratory Animals.

2.2.2 RNA isolation

Total RNA was isolated using Trizol (Invitrogen, Carlsbad, CA) according to the manufacturer's protocol. The RNA was ethanol precipitated, dissolved in DEPC-treated water and stored at –80°C until use.

2.2.3 cDNA library construction

Using the Oligotex mRNA Mini Kit (Qiagen, Mississauga, Ontario), poly(A)$^+$ mRNA was isolated from total retinal RNA extracted from rats exposed to 8 hr of light. cDNA was synthesized from retinal poly(A)$^+$ mRNA, ligated, and packaged using the UniZAP-XR cDNA synthesis kit and Gigapack gold III packaging system (Stratagene, La Jolla, CA).

2.2.4 cDNA library screening:

Primary screen: An unamplified cDNA library representative of retinas isolated from animals exposed to 8 hours of green light was constructed using the Lambda Zap vector system (Stratagene, La Jolla, CA) according to manufacturer's instructions. The cDNA library was differentially cross-screened with two different cDNA probes - one probe represented the retinal expressed genes from animals exposed to green light for 16 hours (16 hour light treated retina cDNA probe) and the second probe represented the retinal expressed genes from dark-reared animals ("0 hour" exposed retina cDNA probe). For the cDNA probes, total cDNA was made from purified retinal mRNA using a standard cDNA synthesis kit (Invitrogen, Carlsbad, CA). The cDNA probes were radiolabeled with [α-^{32}P] dCTP, dGTP, and dATP by random primer labeling (Invitrogen, Carlsbad, CA). The mixed cDNA probes were purified to remove unincorporated nucleotides using G-50 Sephadex columns (Roche, Indianapolis, IN). For a given differential screen the same level of radioactivity was used for both probes.

Briefly, aliquots of the unamplified cDNA library were plated with XL1-Blue MRF' bacterial cells (Stratagene, La Jolla, CA) in NZY top agar (85.6 mM NaCL, 8.1 mM $MgSO_4$, 0.5% [w/v] yeast extract, 1% casein hydrolysate, 0.7% agar; pH 7.5) [41] at a MOI (multiplicity of infection) to produce 500-1000 plaques for each NZY agar plate [41]. Duplicate plaque lifts were transferred onto nylon membranes (Dupont, NEN, Boston, MA) and processed according to the manufacturer's protocol. The plaque lifts were pre-hybridized for 4 hours at 65°C in Hybrisol II (Serologicals Corp., Norcross, GA). One set of plaque lifts was hybridized with denatured radiolabeled 16 hour light treated retina cDNA probe (discussed above). The other set of plaque lifts was hybridized with denatured radiolabeled "0 hour" exposed retina cDNA probe. Hybridizations were carried out in Hybrisol II at 65°C for at least 16 hours. The membranes were then washed at 65°C twice in 2X SSC (sodium chloride, tri-sodium citrate) for 15 minutes; once in 2X SSC, 0.1% SDS (sodium dodecyl sulfate) for 30 minutes; and once in 0.1X SSC, 0.1% SDS for 10 minutes. The membranes were then exposed to Kodak X-OMAT film (Eastman Kodak Company, Rochester, New York) at –70°C.

The autoradiographs from the plaque lifts probed with the cDNA derived from the dark-reared rats were compared to the autoradiographs from the plaque lifts probed with the cDNA derived from the 16 hour light-treated rats. Upon visual comparison, phage spots that displayed putative increased or decreased hybridization between the two sets of autoradiographs were matched to plaques on the original NZY (85.6 mM NaCl, 8.1 mM $MgSO_4$, 0.5% [w/v] yeast extract, 1% [w/v] casein hydrolysate, 1.5% [w/v] agar; pH 7.5) plates. The selected plaques were isolated using sterile Pasteur pipettes and placed in SM buffer (0.1M NaCl, 8.1 mM $MgSO_4$, 50 mM Tris-HCl pH 7.5, 2% [w/v] gelatin) containing a few drops of chloroform and stored at 4°C.

Secondary screen: XL1-Blue MRF' host bacteria were added to NZY top agar and plated onto NZY agar plates to create a bacterial lawn. Phage dot analysis was performed [42] using 0.5 μl of each phage stock per spot. The plates were incubated at 37°C overnight. Duplicate plaque lifts were taken as described above. Pre-hybridization, probe preparation, hybridization, washes, and film exposure were performed as described for the primary screen. Clones that retained their differential hybridization status after the secondary screen were further analyzed in the tertiary screen.

Tertiary screen: Polymerase Chain Reaction (PCR) amplification using T7 and T3 primers, which flank the cloning insertion site, was performed on the clones identified from the secondary screen. The PCR products were analyzed by gel electrophoresis to confirm the presence of an insert. 0.5μl of each successfully amplified PCR product was spotted onto a grid drawn on a nylon membrane (Dupont, NEN, Boston, MA) to make a DNA macroarray. The membrane was denatured, neutralized and cross-linked according to the membrane manufacturer's protocol. Pre-hybridization, probe preparation, hybridization, washes, and film exposure were performed as described for the primary screen. Clones that still displayed a differential hybridization pattern were kept for further analysis.

2.2.5 Sequencing

Clones that remained after the tertiary screen were PCR amplified using T7 and T3 primers that flank the cDNA insertion site. PCR products were size fractionated by gel electrophoresis and gel purification of each amplified product was performed using a QIAquick gel extraction kit (Qiagen, Mississauga, Ontario). DNA sequencing was performed on the purified PCR products using the DYEnamic ET terminator cycle sequencing kit (Amersham Pharmacia Biotech, Piscataway, NJ) and either SK primer or T7 primer. Sequencing reactions were electrophoresed on a PE Applied Biosystems 373 automated sequencer. DNA sequences were compared to known sequences in the GenBank database using the BLAST program [43] in order to determine putative identities of the isolated clones. Clones with exact identities were placed into functional groups using the PANTHER classification system [44] based on the biological processes in which they are involved.

2.2.6 Northern analysis

Probes: Probes used for northern analysis were prepared by PCR amplification of the clones isolated from the differential cross-screen as described above. The PCR amplified inserts were size fractionated on an agarose gel and each DNA insert was purified as described above. The purified clone inserts were radioactively labeled using the same random primer labeling technique used to label the cDNA probes defined above, with the exception that only [α-^{32}P] dCTP was used as the radioactive label.

Gel analysis: 4 μg of total RNA from each sample to be screened was electrophoresed on 1% formaldehyde-agarose gels in a formaldehyde running buffer system [41]. Capillary northern transfer of fractionated RNA from the gel onto Genescreen Plus nylon membrane (Dupont, NEN, Boston, MA) was performed according to the manufacturer's protocol. The northern blots were pre-hybridized for 4 hours at 65°C in Hybrisol II (Serologicals Corp., Norcross, GA). Radioactively labeled probes were denatured and added to Hybrisol II at a concentration of 1-2x10^6cpm/ml. Hybridizations and washes were performed using the same conditions used for the plaque lifts. The blots were exposed to Kodak X-OMAT film at –70°C.

2.2.7 Western analysis

Proteins were isolated from the LIRD tissue profile using Trizol (Invitrogen, Carlsbad, CA) according to the manufacturer's protocol. Proteins were separated on SDS-polyacrylamide gels under reducing conditions and electrophoretically transferred to Trans-Blot nitrocellulose membrane (Bio-Rad, Hercules, CA). Blots were blocked in TBS-T (50 mM Tris-HCl, 200 mM NaCl, 1 mM $MgCl_2$; pH 7.4, and 0.1% v/v Tween-20) containing 5% skim milk powder (Difco Laboratories, Livonia, MI) for one hour. Rabbit anti-T-cadherin antibody (Santa Cruz Biotechnology, Santa Cruz, CA) was added to the blocking solution at a 1:200 dilution and incubated for one hour. Blots were washed in TBS-T buffer then incubated with a 1:5000 dilution of donkey anti-rabbit IgG secondary antibody (Amersham Biosciences, Piscataway, NJ) in blocking solution for one hour. Blots were again washed in TBS-T and the signal was detected by ECL detection (Amersham Biosciences, Piscataway, NJ).

2.2.8 Northern and western blot image analysis

The intensity of each resulting band on the autoradiographs or photographs was quantified using either ImageJ [45] or Photoshop 7.0 (Adobe Systems Inc., USA). Similar results were obtained with both programs. On the northern blots, differences in band intensities due to RNA loading were accounted for by normalizing the hybridization intensity with the relative intensity of the 18S ribosomal band in each sample [46]. For the western blots, differences in band intensity due to loading were normalized to an actin control. In all cases, analysis was performed on three replicates and a representative autoradiograph of one of the three replicates is shown. Standard deviation bars indicate the variations in band intensity between each replicate.

2.2.9 Immunohistochemistry

Eyes were enucleated from rats exposed to intense light for various times. The eyes were immersed in 4% paraformaldehyde in PBS at 4°C for 4 hours. Cryopreservation was performed in 30% sucrose in PBS for 12 hours. The eyes were then embedded in OCT (Tissue Tek, Torrence, CA) and stored at –80°C until use. Frozen sections (6 µm) were placed on Superfrost Plus slides (Fisher Scientific, Nepean, ON) and stored at –80°C until use.

Frozen sections were blocked in phosphate buffered saline containing 0.1% Tween 20 (PBS-T) plus 5% skim milk powder (Difco Laboratories, Livonia, MI) for 1 hour at room temperature. The primary antibody, anti-T-cadherin (Santa Cruz Biotechnology, Santa Cruz, CA), was added to the blocking solution at a 1:200 dilution and incubated overnight at 4°C on the slides. The slides were then washed in PBS-T 3 times for 5 minutes at room temperature. A Cy3 conjugated secondary antibody (Jackson Immunoresearch, Westgrove, PA) was diluted 1:1000 in blocking solution and incubated on the slides for one hour. The slides were washed as above then mounted in Aquamount (Lerner Laboratories, Pittsburgh, PA). Fluorescence was visualized by Leica TCS-SP2 Multiphoton Confocal Laser Scanning Microscope. After visualization, coverslips were removed by immersing the slides in PBS. The retina sections were then stained with hematoxylin and eosin (Sigma-Aldrich, St. Louis, MO) and visualized by light microscopy.

2.3 RESULTS

2.3.1 Isolation of clones

The primary differential cross screen of 5700 clones identified 1122 putative differentially expressed genes. After the secondary phage dot screen, 437 clones retained their differential status. The final tertiary screen narrowed the number of differential clones to 105. Thus, ~2% of the initial clones screened displayed a consistent differential expression pattern when comparing the 16 hour light treated retina state with the dark-reared retina state.

2.3.2 Expression analysis

To confirm the differential status of the isolated clones and to validate the screening process, northern analysis was performed on a subset of these genes. Nine clones were used as probes for hybridization to northern blots containing retinal RNA isolated from dark-reared rats and retinal RNA isolated from 16 hour light treated rats (Figure 2.1). The Northern analysis confirmed the differential status of these clones. Five of the clones, 1607, 654, 730, 724, and 1505, displayed increased expression at 16 hours of light exposure whereas three clones, 1193, 689A, and 285, displayed decreased expression at 16h of light exposure (Figure 2.1, Figure 2.2). Clone 836B displays both an increase and a decrease in expression depending on which transcript is analyzed. The largest (3.5 kb) and smallest (0.7 kb) transcripts showed a decrease in expression levels whereas the 2.0 kb transcript shows an increase in expression. Thus all clones examined for differential levels of expression were found to be differentially expressed upon northern analysis and this confirmed the differential pattern of expression observed with the cDNA library screen. This supports the success of our screening strategy.

2.3.3 Sequence characterization

The 105 clones that were consistently differential in expression (16 hour light treated tissue in comparison with dark-reared control retina) throughout the three screening process were subjected to single-pass sequencing in order to generate expressed sequence tags (ESTs) to analyze against the GenBank database of DNA sequences. Putative identities of these clones based on their homology to known genes in the GenBank database are shown in Table 2.1. Based on their putative identities, clones were grouped by the biological process in which they are involved. From the 105 clones isolated, 177 biological process hits were found due to many of the genes having more than one known function. The sequences from the isolated clones have been submitted to GenBank as ESTs (refer to Table 2.1 for accession numbers).

The functional gene category with the highest number of differentially identified clones was that of sensory perception, as expected (Figure 2.3). The second highest category consisted of clones involved in developmental processes, the majority of which were members of the crystallin family of genes. Although 105 clones were characterized by sequencing, a number of them are clones for the same gene. Genes represented by the identification of multiple clones in our screen include Rom-1 (2 clones), polyubiquitin (3 clones), alpha A-crystallin (9 clones), beta A3/A1 crystallin (4 clones), beta B2 crystallin (17 clones), gamma S crystallin (5 clones), and ribosomal protein L9 (2 clones). In total these seven genes represent a total of 42 clones that we isolated in our screen, suggesting that they are not only differentially expressed genes but that they are highly expressed genes as well. The most abundantly identified gene was beta B2 crystallin, for which we isolated 17 clones.

2.3.4 Expression of rat T-cadherin in normal tissues

To determine the tissue expression pattern of rat T-cadherin, northern blot analysis was performed on brain, heart, kidney, liver, lung, muscle, retina, spleen, testes, and thymus tissue from dark-reared rats (Figure 2.4). T-cadherin was found to be highly expressed in the brain, heart and muscle. A lower level of expression was observed in the lung and retina, whereas barely detectable expression levels were seen in the kidney, spleen, testes, and thymus. No expression was detected in the liver by northern blot analysis.

For all tissues except testes, northern analysis detected a transcript of approximately 3.4 kb, the expected size of the T-cadherin transcript based on sequence data in the Genbank database. In the testes there appeared to be no 3.4 kb transcript but instead a smaller transcript of 2.4 kb was observed. This smaller transcript was also seen in the brain in addition to the expected 3.4 kb transcript.

2.3.5 Rat T-cadherin RNA is upregulated in the retina at peak levels of oxidative stress

To determine the expression pattern of T-cadherin during LIRD, we performed northern blot analysis on retinal tissue isolated from rats exposed to various durations of light (Figure 2.5a). In all retinal samples, a single mRNA transcript of the expected 3.4 kb was observed. Expression is seen in all light treatment time points with the highest level of expression occurring at 16 hours of light treatment. Densitometry analysis of the expression levels shows more clearly the expression profile observed over LIRD (Figure 2.5b). In dark-reared animals, there is an appreciable amount of T-cadherin expression. With 2 hours of light exposure the expression level drops slightly then increases slightly with 4 hours of light exposure. The expression levels at 4 hours and 8 hours of light exposure are essentially equal with expression peaking at 16 hours of light exposure. A representative autoradiograph is shown in Figure 2.5a however the analysis was actually performed three times on different northern blots with RNA from different replicates of treated animals with similar results (data not shown).

2.3.6 T-cadherin protein levels are upregulated when the retina is under a high level of oxidative stress

Western analysis of T-cadherin revealed two bands of approximately 130 kDa and 95 kDa corresponding to the precursor and mature forms, respectively, of the T-cadherin protein (Figure 2.6a). Analysis of the band intensities normalized to the actin control show somewhat of a bell curve for the 130 kDa precursor protein with the lowest levels of protein occurring at 0 hour and 16 hour light exposed retinas and a slight peak of the protein levels at 4 hours of light exposure (Figure 2.6b). The 95 kDa mature form of the protein shows very low protein levels at 0 hours, 2 hours, 4 hours, and 8 hours of light exposure. Protein levels significantly increase at 16 hours of light exposure to greater than a 5-fold increase over the other time points. As with the T-cadherin RNA levels, the T-cadherin protein levels also increase at the time point in which the retina is experiencing a high oxidative stress environment. The analysis was performed three times on different western blots with protein from different replicates of treated animals; a representative autoradiograph is shown in Figure 2.6a.

2.3.7 T-cadherin is localized to the Müller cells of the retina

Immunohistochemistry of T-cadherin in retina sections from rats exposed to 0 hours, 4 hours, 8 hours, or 16 hours of light putatively localizes the protein to the Müller cells (Figure 2.7). With 0 hours of light exposure, localization is observed in the Müller end feet and extends into the outer nuclear layer (ONL). With 4 hours and 8 hours of light exposure, the localization becomes more limited to the inner retina and is observed in the Müller end feet and only extends to the outer plexiform layer (OPL). By 16 hours of light exposure the localization becomes more punctate, possibly as a result of the degeneration of the retina. However, localization is still observed mainly in the Müller end feet with localization extending to the OPL, as was observed with 4 hours and 8 hours of light exposure.

2.4 DISCUSSION

There is a growing understanding that the molecular environment that defines a given tissue under any particular biological state is complex. The increase in the number of gene profiling initiatives, whether it is an EST databasing of specialized cDNA libraries or systematic micro-array studies, attest to this fact. By identifying the genes expressed in a particular tissue at a particular time, in our case the retina under an oxidative stress environment, one is able to infer certain assumptions about the molecular environment in that specific tissue state.

We are interested in defining rat retinal expressed genes that are either induced or repressed after retinas are exposed to a prolonged period of light exposure (16 hours) as potential genes whose relative expression defines the retinal response to oxidative stress. By taking a differential approach in screening 5700 clones from an existing light exposed rat retinal cDNA library with a cDNA probe derived from 16 hour light exposed retinas and with a cDNA probe derived from dark-reared retinas, we specifically identified 105 clones that are putatively differentially expressed. By applying our differential approach of clone selection we by passed the sequencing of 5595 clones that are not likely to represent genes whose expression changes after a 16 hour light exposure, clones which would have been sequenced if an EST approach had been used. The success of our differential screen was verified by northern analysis of a subset of the clones isolated. In addition, the identification of multiple clones representing the same gene from an unamplified cDNA library suggests that the identification of the putative differentially expressed genes occurs in a highly selective manner.

Interestingly, rhodopsin, the gene encoding the photopigment of rod photoreceptor cells, was only isolated once from our cDNA library screen. During LIRD, rhodopsin is found to be highly expressed in the dark-reared retina with expression levels decreasing with increasing light exposure, resulting in very low levels of expression by 8 and 16 hours of light exposure (Figure 2.1 clone number 1193 and data not shown). Due to the abundance of rhodopsin in the retina and its differential expression between dark-reared and 16 hour light treated retinas we would expect to isolate numerous clones corresponding to rhodopsin. In the normal human retina it is expected that clones corresponding to rhodopsin would be isolated 4355 times for every million clones screened from a non-normalized retina cDNA library [47]. Therefore, in the LIRD cDNA library in which we screened 5700 clones it is expected, according to the above value, that rhodopsin would be isolated approximately 25 times. However, being that the cDNA library we screened was constructed from 8 hour light exposed rat retinas, in which rhodopsin expression levels are less than in the dark-reared retina, it can be assumed that the lower abundance of the transcript would mean that less than 25 clones of rhodopsin would be isolated. Although the exact number of rhodopsin clones expected from a cDNA library constructed from 8 hour light exposed retina is unclear, we can assume that our sample size of only 5700 clones screened was not large enough to expect that the clones isolated would be representative of the entire population of differentially expressed genes in the retina.

The majority of clones isolated from the screen corresponded to genes involved in visual processes, such as those from the crystallin gene family which also made up a large portion of those clones in the developmental processes category. Due to crystallin genes being well characterized as to their function in lens development [48, 49], the classification system used placed crystallins into the developmental processes category. The identification of such a large number of clones corresponding to five genes of the crystallin gene family, a gene group also associated with heat shock and stress-inducible chaperone proteins, after LIRD is consistent with a tissue that is undergoing high levels of cellular stress. It has been shown that retinal protein levels of nine crystallin species increase upon light exposure in the retina, further supporting a specific role for crystallins in retinal degeneration [50]. Due to changes in the crystallin content in the retina following intense light exposure it has been postulated that crystallins may play a role in protecting photoreceptor cells from light damage, possibly by preventing stress-induced protein aggregation [50, 51]. After 16 hours of light exposure it is expected that a number of genes involved in response to a high cellular stress environment would be isolated as it has been shown that this time point of light exposure results in an increase in HO-1 expression, an indicator of oxidative stress [11, 17].

It is expected that any gene isolated from this screen would somehow help define the degeneration process in the retina. With the number of cadherin family members already found to be involved or implicated in retinal degeneration and retinal disease, our focus of gene characterization from this screen turned to T-cadherin. In humans, T-cadherin has been found to be expressed in a broad range of tissues including brain, lung, heart, muscle, and kidney [31]. This is consistent with our data in the rat, which demonstrates that it is expressed in these tissues as well as in the spleen, testes, thymus, and retina.

With respect to northern analysis during LIRD, the fairly high and approximately equal level of expression seen from dark-reared through to 8 hours of light exposure indicates that there appears to be a basal level of expression of T-cadherin in the dark-reared retina as well as light treated retina in the rat. It is not until a prolonged exposure to light, as in the case with 16 hours of light treatment, that there is an increase in T-cadherin mRNA expression, most likely a result of the oxidative stress environment in the retina and the subsequent degeneration. The same holds true for the protein levels during LIRD; however, there is a larger increase in T-cadherin protein levels at 16 hours of light exposure as compared to dark-reared through to 8 hours of light exposure. Analysis of RNA and protein levels during LIRD indicates that T-cadherin increases at the 16 hour time point when the retina is experiencing a high level of oxidative stress [17], indicating that T-cadherin levels increase in response to an oxidative stress environment. The characterization of T-cadherin during LIRD suggests that it may be involved in either contributing to the degeneration process or imparting protection from the effect of a high oxidative stress environment. These results are supported by the recent work by Joshi *et al.* [40] that showed increased T-cadherin expression in HUVEC cultures under oxidative stress conditions. They also found that overexpression of T-cadherin in HUVEC cultures reduced caspase activation and protected against stress-induced apoptosis. LIRD involves both caspase-dependent [9, 15, 52-57] as well as caspase-independent [57-59] apoptosis. Increases in retinal T-cadherin RNA and protein expression after prolonged light exposure could mediate an attempt to protect against oxidative stress induced caspase-dependent apoptosis.

T-cadherin is a GPI-anchored protein that has previously been found to be associated with lipid rafts [60], which are known to contain other signaling molecules such as G-proteins, *src* kinases, ras proteins, and transmembrane receptors of growth factors [61]. Thus, it is likely that T-cadherin is involved in some sort of signaling pathway. Previous work by Kipmen-Korgun *et al.* [39] involving overexpression of T-cadherin in an HEK293 cell line as well as a human umbilical vein-derived endothelial cell line EA.hy926 found that T-cadherin acts as a physiological signaling receptor for LDL which results in intracellular Ca^{2+} mobilization and a subsequent increase in tyrosine phosphorylation and stimulation of Erk1/2 and translocation of NFκB toward the nucleus resulting in increased cell proliferation. The authors speculated that the LDL-triggered signaling pathway via T-cadherin played a role in cell growth and apoptosis of these cells directly. Although T-cadherin is expressed in a variety of tissues, it is possible that it serves a similar function in those tissues. It is thus plausible that the results by Kipmen-Korgun *et al.*, albeit in kidney and endothelial cell lines, could be extrapolated to the function of T-cadherin in the retina. Taken together with our results showing an upregulation of T-cadherin after prolonged light exposure, and thus during oxidative stress, it is likely that T-cadherin is functioning in a similar cell signaling pathway in the retina as was found in the kidney and endothelial cell lines. Research has found that translocation of NFκB to the nucleus in response to light stress in cultured photoreceptor cells as well as in mice functioned in protecting photoreceptor cells, *in vitro* and *in vivo*, against oxidative stress mediated apoptosis [53, 55, 62]. Therefore T-cadherin may be an upstream activator of cell protection during LIRD.

We have shown that in the retina T-cadherin expression is localized to the Müller cells, the main glial cell type in the mammalian retina. Müller cells play critical roles in the maintenance and function of retinal neurons by regulating the neuronal microenvironment, participating in retinal information processing, and protection of retinal neurons from oxidative stress and free radicals [63]. These results are interesting in light of emerging evidence that neurotrophic factors, such as brain derived neurotrophic factor (BDNF), ciliary neurotrophic factor (CNTF), and basic fibroblast growth factor (bFGF), bind to receptors on the cell surface of Müller cells and mediate rescue of differentiated photoreceptor cells from retinal degeneration [64-67]. This suggests that rescue of photoreceptor cells by neurotrophic factors involves some sort of signaling mechanism between the inner retina and the photoreceptor cells. In fact, HO-1, an anti-oxidant defense factor, has been found to be over-expressed in Müller cells of mouse retina in organ culture exposed to oxidative stress [68]. It is speculated that this induction of HO-1 in Müller cells may be important in protection of photoreceptor cells against oxidative stress. Evidence for glial-neuronal cell interactions in induced and inherited retinal degenerations suggest that photoreceptor cell damage is signaled to the Müller cells which in turn initiate a response to either rescue the photoreceptor cells or accelerate cell death [69-71]. Therefore, the localization of T-cadherin to Müller cells may function in a glial-neuronal signaling pathway during LIRD as a mechanism to protect photoreceptor cells from oxidative stress induced light damage.

Functional classification of the genes isolated in our screen provides a “snapshot” of the gene expression profile occurring after prolonged light exposure, indirectly this gives us information on the state of the molecular environment. In addition, our avenue of research also leads to the characterization of genes not previously characterized with respect to retinal degeneration. This is the first report of the characterization of T-cadherin expression in the retina and during retinal degeneration. Although the data presented here is preliminary, our findings, coupled with previous knowledge of T-cadherin in other systems, provide evidence for a possible protective role of T-cadherin against oxidative stress and apoptosis in the retina. Although further analysis of this possible role for T-cadherin in retina degeneration is required, the numerous other cadherin family members that have been shown to be involved in retinal degeneration make exploring the function of T-cadherin during retinal degeneration a worthwhile future endeavor.

Figure 2.1 - Northern blot analysis of a subset of the putative differentially expressed clones isolated from the cDNA library screen.

Approximately 4µg of total RNA isolated from dark-reared rat retinas or 16 hour light treated retinas were probed with radiolabeled cDNA clone inserts. The cDNA clones used as probes and the observed transcript sizes are shown. The 18S ribosomal band is shown as a RNA loading control for each northern blot. Clone numbers correspond to the following genes: 1193 – rhodopsin; 836B – LIM-kinase 1; 1607 – polyglutamine binding protein 1; 654 – ribosomal protein S7; 730 – ribosomal protein L9; 724B – ribosomal protein L35; 1505 – heat shock protein 86; 689A – beta-catenin binding protein; 285 – ribosomal protein S8.

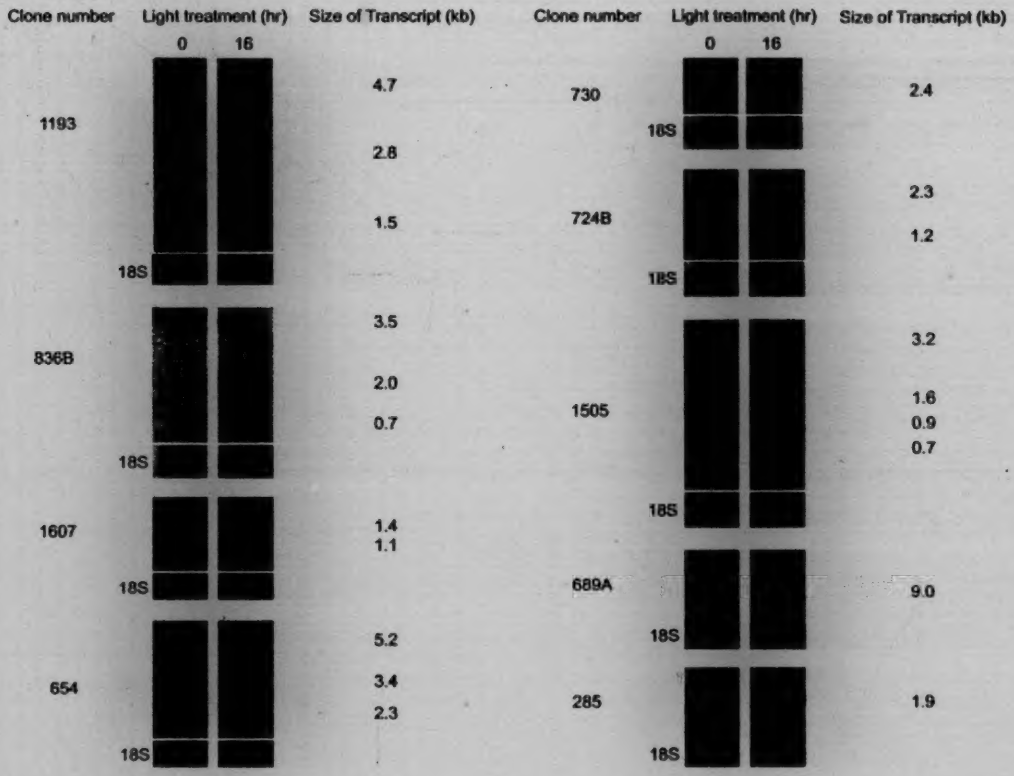

Figure 2.2 - Graphical analysis of the northern blot profiles.

The expression levels on the northern blots represented in Figure 2.1 were normalized to the relative intensity of the corresponding 18S ribosomal band to account for possible differences in band intensities due to RNA loading. For the analysis of each northern blot result, the appropriate exposure in which the intensity of the hybridization was not saturated was used, and not necessarily the exposure shown in Figure 2.1. Quantification of the band intensities was done using Photoshop 7.0 (Adobe Systems Inc., USA). In the case that a given probe detected multiple transcripts, each transcript was analyzed separately. Clone numbers correspond to the following genes: 1193 – rhodopsin; 836B – LIM-kinase 1; 1607 – polyglutamine binding protein 1; 654 – ribosomal protein S7; 730 – ribosomal protein L9; 724B – ribosomal protein L35; 1505 – heat shock protein 86; 689A – beta-catenin binding protein; 285 – ribosomal protein S8.

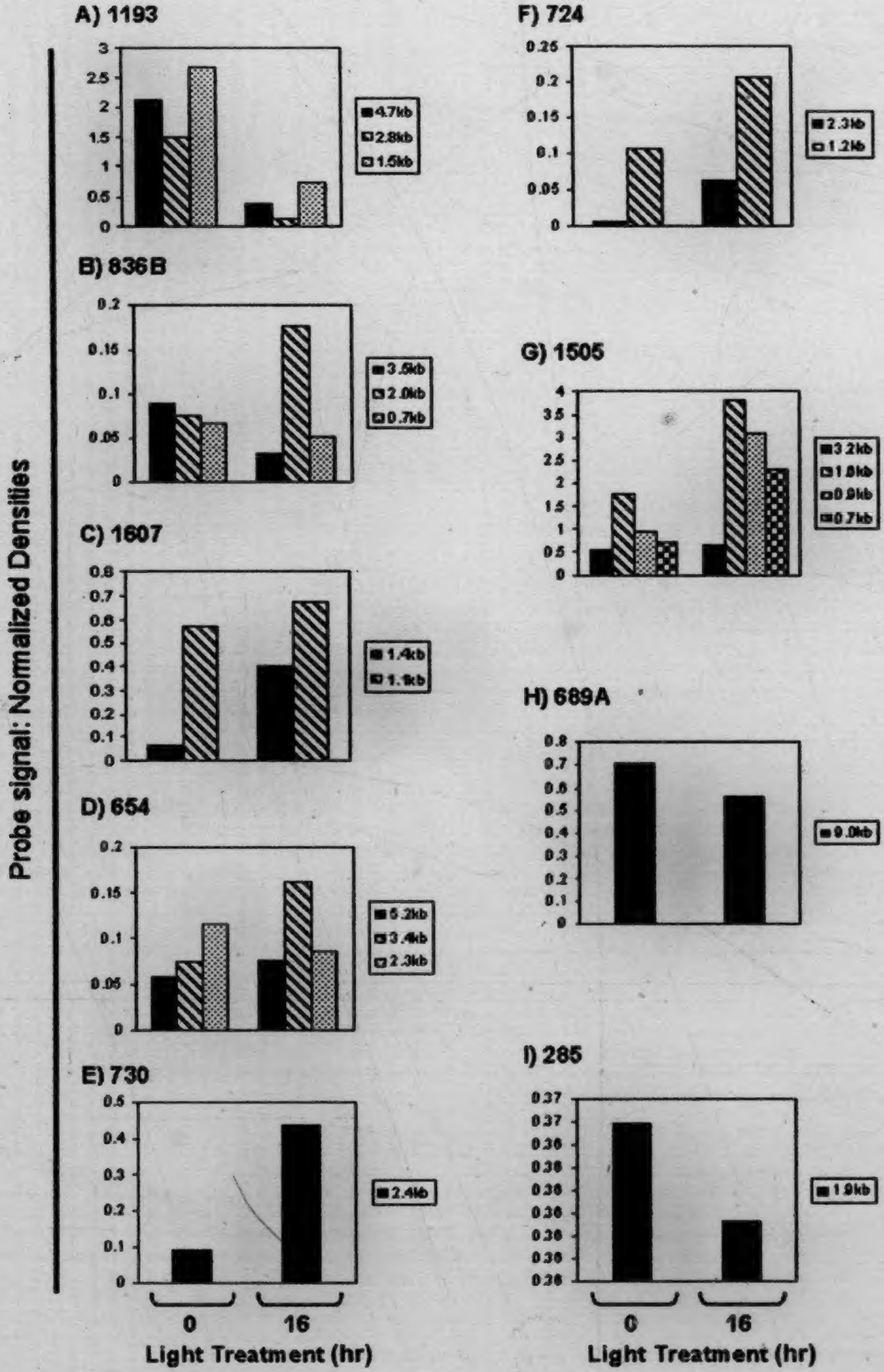

Probe signal: Normalized Densities
A) 1193
4.7kb
2.8kb
1.5kb
B) 836B
3.5kb
2.0kb
0.7kb
C) 1607
1.4kb
1.1kb
D) 654
5.2kb
3.4kb
2.3kb
E) 730
2.4kb
F) 724
2.3kb
1.2kb
G) 1505
3.2kb
1.8kb
0.9kb
0.7kb
H) 689A
9.0kb
I) 285
1.9kb
0
16
Light Treatment (hr)
0
16
Light Treatment (hr)

Table 2.1 - Clones isolated from the differential cDNA library screen.

Clone numbers[*] and GenBank EST accession numbers[†] are listed for the clones isolated from the cDNA library. Blastn searches determined the putative identities of the isolated clones. The significance of the homology between the clone and the known gene from the GenBank database is indicated by the Expect(E)-value[‡]. All clones were categorized by their biological process based on their putative identities.

Clone Number*	GenBank Accession No. for EST†	Homology to known gene	E-Value‡	GenBank Accession No. of homologous gene	Biological Process
3	CA997686	Mus musculus peripherin 2 (Prph2)	1.00E-67	NM 008938.1	Cell adhesion; vision
31	CA997687	Rattus norvegicus CRYBB2 gene (crystallin, beta B2)	0	NM_012937.1	vision; developmental processes
45	CA997688	Rattus norvegicus retinal protein (RRG4)	0	U40999.1	Neurotransmitter release; vision
49	CA997689	Rattus norvegicus mitochondrial cytochrome c oxidase	0	M27315.1	mitochondrial
155	CA997690	Rattus norvegicus mitochondrial cytochrome c oxidase	0	M27315	mitochondrial
285	CA997685	Rat mRNA for ribosomal protein S8	0	X06423.1	protein biosynthesis
286	CA997691	Rattus norvegicus mitochondrial cytochrome c oxidase	0	NC 001665.1	mitochondrial
302	CA997692	Rattus norvegicus Crystallin, alpha polypeptide A (Cryaa)	0	NM 012534.1	Muscle contraction, vision
326	CA997693	Rat mRNA for polyubiquitin	0	D16554.1	proteolysis
413	CA997694	Rattus norvegicus alpha A-crystallin	0	U47922.1	Muscle contraction, vision
440	CA997695	Mus musculus crystallin, gamma S (Crygs)	3.00E-93	NM 009967.1	vision; developmental processes
464A	CA997696	Rattus norvegicus mitochondrial gene for cytochrome b	0	AB033713.1	mitochondrial
464B	CA997697	Rattus norvegicus CRYBB2 gene (crystallin, beta B2)	0	NM 012937.1	vision; developmental processes
498	CA997698	Rattus norvegicus Crystallin, alpha polypeptide A (Cryaa)	0	NM 012534.1	Muscle contraction, vision
566	CA997699	Rattus norvegicus Crystallin, alpha polypeptide A (Cryaa)	0	NM 012534.1	Muscle contraction, vision
584	CA997700	Rattus norvegicus mitochondrial cytochrome oxidase	0	J01435.1	mitochondrial
616	CA997701	Rattus norvegicus alpha B-crystallin	0	S77142.1	Muscle contraction, vision
617	CA997702	Rattus norvegicus CRYBB2 gene (crystallin, beta B2)	5.00E-91	NM_012937.1	vision; developmental processes
626	CA997703	Rat mRNA for beta A3/A1 crystallin	0	X15143.1	vision; developmental processes
653	CA997704	Rattus norvegicus Crystallin, alpha polypeptide A (Cryaa)	0	NM 012534.1	Muscle contraction, vision
654	CA997705	R.rattus mRNA for ribosomal protein S7	0	X53377.1	protein biosynthesis
673A	CA997706	Mus musculus major histocompatibility locus class II region...	1.00E-14	AF050157.1	MHCII-mediated immunity
675A	CA997707	Rattus norvegicus connective tissue growth factor	0	NM_022266.1	receptor protein tyrosine kinase signaling pathway; other receptor mediated signaling pathway; extracellular matrix protein-mediated signaling
676	CA997708	Rattus norvegicus ATPase synthase subunit 6	1.00E-130	AF504920.1	mitochondrial
679	CA997709	Rat mRNA for ribosomal protein L9	0	X51706.1	protein biosynthesis
689A	CA997710	PREDICTED: Rattus norvegicus beta-catenin binding protein	0	XM_573762	mRNA transcription regulation
694B	CA997711	Rattus norvegicus CDK109	0	Y17323.1	mitochondrial
724A	CA997712	Rattus norvegicus CDK109	0	Y17323.1	mitochondrial
724B	CA997713	Rat mRNA for ribosomal protein L35	0	X51705.1	protein metabolism and modification
730	CA997714	Rat mRNA for ribosomal protein L9	0	X51706.1	protein biosynthesis
755	CA997715	Rattus norvegicus alpha A-crystallin	0	U47922.1	Muscle contraction, vision
784	EE683491	Rattus norvegicus sodium-phosphate co-transporter type II (Npt2) gene	1.00E-33	AF156188.1	unclassified
793	CA997716	Rattus norvegicus CDK109	0	Y17323.1	mitochondrial

794A	CA997717	Psammomys obesus (fat sand rat) FIT (FIT) mRNA	e-109	AY611625.1	unclassified
794B	CA997718	Mus musculus BAC clone RP23-314I1 from chromosome 3	2.00E-45	AC135238.4	unclassified
801	CA997719	Rat ribosomal protein L19 mRNA	0	J02650.1	protein biosynthesis
802	CA997720	Mus musculus p300/CBP-associated factor (Pcaf)	0	NM 020005.1	mRNA transcription; chromatin packagin and remodeling
809	CA997721	Human RNA polymerase II 23kD subunit (POLR2)	0	J04965.1	general mRNA transcription activities
827	CA997722	Rattus norvegicus Phototransducing protein, 33 kDa (phosducin)	0	NM 012872.1	G-protein mediated signaling; vision
836A	CA997723	PREDICTED: Rattus norvegicus similar to hypothetical protein FLJ20481	0.00E+00	XM_341747	other metabolism
836B	CA997724	Mus musculus LIM-kinase1 (Limk1) gene, complete cds	3.00E-10	AF139987.1	protein biosynthesis
837	CA997725	Rattus norvegicus CDK109	0	Y17323.1	mitochondrial
968A	CA997726	Rat inositol-1,4,5-triphosphate receptor	0	J05510.1	calcium mediated signaling; cation transport; stress response; neurotransmitter release; other neuronal activity; muscle contraction; cell motility
968B	CA997727	Rattus norvegicus CRYBB2 (crystallin, beta B2)	0	NM 012937.1	vision; developmental processes
973	CA997728	Rat mRNA for beta A3/A1 crystallin	0	X15143.1	vision; developmental processes
1027	CA997729	Rattus norvegicus CRYBB2 gene (crystallin, beta B2)(Crybb2)	0	NM_012937.1	vision; developmental processes
1038	CA997732	Rattus norvegicus CRYBB2 (crystallin, beta B2)	0	NM 012937.1	vision; developmental processes
1047	CA997733	Rat growth and transformation-dependent mRNA	1.00E-103	M17412.1	unclassified
1048	CA997734	Rattus norvegicus CRYBB2 (crystallin, beta B2)	5.00E-80	NM 012937.1	vision; developmental processes
1055A	CA997735	Rattus norvegicus afadin (AF-6)	4.00E-90	NM 013217.1	cell communication; cell adhesion; cell structure
1055B	EE683492	Mus musculus T-cadherin (Cdht), mRNA	e-166	NM 019707.1	cell adhesion-mediated signaling; cell adhesion; oncogenesis
1080	CA997736	Rat mRNA for beta A3/A1 crystallin	0	X15143.1	vision; developmental processes
1085A	CA997737	Mus musculus RNA-binding protein (Tbrbp) mRNA, complete cds	1.00E-29	AF234179.1	DNA recombination; immunity and defense
1085B	CA997738	Rat mRNA for beta A3/A1 crystallin	0	X15143.1	vision; developmental processes
1092B	CA997739	PREDICTED: Rattus norvegicus similar to RIKEN cDNA	0.00E+00	XM_228076	unclassified
1095B	CA997740	Mus musculus gammaS-crystallin (crygs)	e-146	AF032995	vision; developmental processes
1118	CA997741	Rat mRNA for polyubiquitin	0	D16554.1	proteolysis
1123	CA997742	Mus musculus gammaS-crystallin (Crygs)	5.00E-97	AF055703.1	vision; developmental processes
1126	CA997743	Rattus norvegicus CRYBB2 (crystallin, beta B2)	0	NM 012937.1	vision; developmental processes
1128	EE683493	Rattus norvegicus l(3)mbt-like 2 (Drosophila)	0	BC101865	General mRNA transcription activities; cell cycle
1149	CA997744	Rattus norvegicus CDK109	0	Y17323.1	mitochondrial
1161	CA997745	Rattus norvegicus Crystallin, alpha polypeptide A (Cryaa)	0	NM 012534.1	Muscle contraction, vision
1171A	CA997746	Rattus norvegicus CDK109	0	Y17323.1	mitochondrial
1171B	EE683494	Mus musculus phosphodiesterase 6A, cGMP-specific, rod, alpha (Pde6a)	3.00E-17	NM_146086.2	nucleoside, nucleotide and nucleic acid metabolism; vision; signal transduction
1174	CA997747	Rattus norvegicus CRYBB2 (crystallin, beta B2)	0	NM 012937.1	vision; developmental processes

1178A	CA997748	Rattus norvegicus Protein kinase, AMP-activated, gamma (Prkaac)	e-122	NM 013010.1	Fatty acid metabolism; lipid metabolism; protein phosphorylation; other intracellular signaling cascade; stress response
1178B	CA997749	PREDICTED: Mus musculus similar to ring finger protein 170	1.00E-110	XM_001001100.1	Fatty acid metabolism; lipid metabolism; protein phosphorylation; other intracellular signaling cascade; stress response
1180	CA997750	Rattus norvegicus CRYBB2 (crystallin, beta B2)	0	NM 012937.1	vision; developmental processes
1193	CA997751	R.norvegicus mRNA for rhodopsin	0	NM 033441	G-protein mediated signaling; vision
1194A	EE683495	Mus musculus ubiquitin-conjugating enzyme E2I (Ube2i)	0	NM_011665.2	protein modification; meiosis; embryogenesis; determination of dorsal/ventral axis; chromosome segregation; cell proliferation and differentiation
1194B	CA997752	Rattus norvegicus CRYBB2 (crystallin, beta B2)	0	NM 012937.1	vision; developmental processes
1195	CA997753	Mus musculus ubiquitin-conjugating enzyme E2I	0	AK 005058.1	protein modification; meiosis; embryogenesis; determination of dorsal/ventral axis; chromosome segregation; cell proliferation and differentiation
1196	CA997754	Rattus norvegicus ATPase synthase subunit 6	0	AF504920	mitochondrial
1205	CA997755	Rattus norvegicus CRYBB2 (crystallin, beta B2)	0	NM 012937.1	vision; developmental processes
1213	CA997756	Rattus norvegicus Crystallin, alpha polypeptide A (Cryaa)	0	NM 012534.1	Muscle contraction, vision
1217	CA997757	Rattus norvegicus ATPase synthase subunit 6	0	AF504920	mitochondrial
1278	CA997758	Rattus norvegicus CRYBB2 (crystallin, beta B2)	8.00E-12	NM 012937.1	vision; developmental processes
1306	CA997760	Rat mitochondrial 12S and 16S rRNA	0	J01438.1	mitochondrial
1035A	CA997730	Mus musculus crystallin, gamma S (Crygs)	0	NM 009967.1	vision; developmental processes
1035B	CA997731	Rattus norvegicus amyloid beta precursor protein (App)	2.00E-67	AY011335.1	other signal transduction; cell communication; other intracellular protein traffic
1301B	CA997759	Mus musculus, guanine nucleotide binding protein (G protein)	e-125	BC025929.1	G-protein mediated signaling
1356	CA997761	Rattus norvegicus peptidylprolyl isomerase (cyclophilin)-like	1.00E-73	XM_341727	protein folding; nuclear transport; immunity and defense
1363	EE683496	PREDICTED: Rattus norvegicus potassium channel tetramerisation domain containing 8	0.00E+00	XM_001070008.1	cation transport
1365A	CA997762	Rattus norvegicus crystallin, beta B2 (Crybb2)	e-147	NM 012937.1	vision; developmental processes
1365B	CA997763	PREDICTED: Rattus norvegicus similar to RIKEN cDNA 1300010M03	0	XM_343592	unclassified
1367A	CA997764	Rattus norvegicus N-methyl-D-aspartate receptor 1 (Grin1) gene	0	AY157515.1	other receptor mediated signaling pathway; cell communication; cation transport; nerve-nerve synaptic transmission
1367B	CA997765	Mus musculus 2 days pregnant adult female ovary cDNA	4.00E-25	AK054249.1	unclassified
1399A	CA997766	Mus musculus rod outer segment membrane protein 1 (Rom1)	0	NM_009073.1	Cell adhesion; vision
1399B	CA997767	Mus musculus rod outer segment membrane protein 1 (Rom1)	e-101	NM_009073.1	Cell adhesion; vision
1410	CA997768	Rattus norvegicus CRYBB2 (crystallin, beta B2)	0	NM 012937.1	vision; developmental processes
1414	CA997769	Rattus norvegicus CRYBB2 (crystallin, beta B2)	0	NM_012937.1	vision; developmental processes

1415	CA997770	Rattus norvegicus CRYBB2 (crystallin, beta B2)	0	NM 012937.1	vision; developmental processes
1420	CA997771	Rattus norvegicus ATPase synthase subunit 6	0	AF504920	mitochondrial
1423	CA997772	Rattus norvegicus mitochondrial cytochrome oxidase	0	J01435.1	mitochondrial
1425	CA997773	Rat mRNA for polyubiquitin	0	D16554.1	
1431	CA997774	Rattus norvegicus ATPase synthase subunit 6	0	AF504920	mitochondrial
1436	CA997775	Mus musculus crystallin, gamma S (Crygs)	0	NM_009967.1	vision; developmental processes
1440	CA997776	Rattus norvegicus ATPase synthase subunit 6	0	AF504920	mitochondrial
1444	CA997777	Rattus norvegicus alpha A-crystallin	0	U47922.1	Muscle contraction, vision
1448A	CA997778	Rat secretogranin II (SgII)	0	X13618	cell communication
1448B	CA997779	Rattus norvegicus Aldolase C, fructose-biphosphate (Aldoc)	0	NM_012497.1	Glycolysis
1457	CA997780	Rattus norvegicus CDK109	0	Y17323.1	mitochondrial
1480	CA997781	Rattus norvegicus IkBL, vacuolar ATPase NG38, Bat1, and MHC class I antigen	e-105	AF387339.1	nucleoside, nucleotide and nucleic acid metabolism; cation transport
1505	CA997782	Mus musculus heat shock protein, 86 kDa 1 (Hsp86-1)	0	NM_010480.1	protein folding; stress response
1607	CA997783	Mus musculus polyglutamine binding protein 1 (Pqbp1)	0	NM_019478.1	mRNA transcription regulation

Figure 2.3 - Functional categorization of the differentially expressed clones.

The putative clone identities were functionally categorized, based on the PANTHER classification system [44], into twenty different categories based on matches to known sequences in the GenBank database.

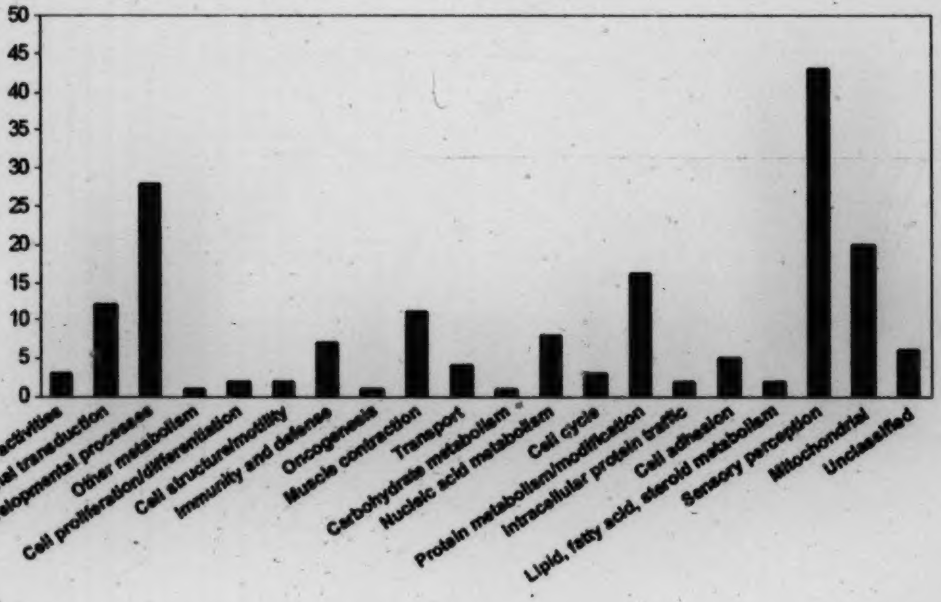

Figure 2.4 - Multiple tissue northern analysis of rat T-cadherin.

A radiolabeled T-cadherin cDNA probe was used to probe 4 μg of total RNA from various rat tissues. The sizes of the observed transcripts are shown on the left of the autoradiograph. The 18S ribosomal band is shown as a loading control.

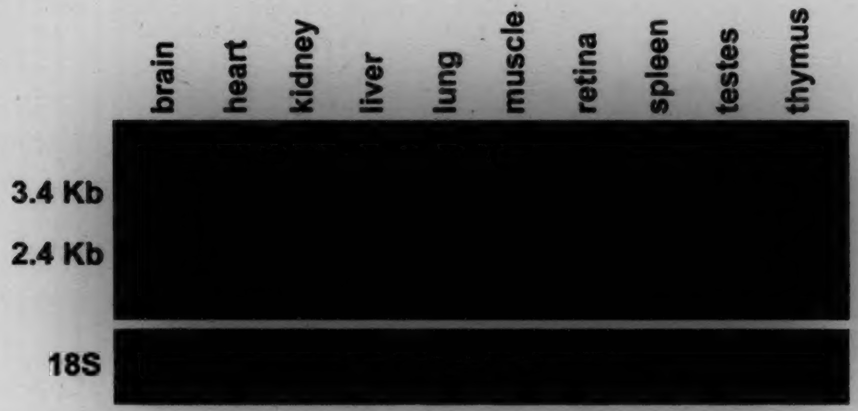

Figure 2.5 - Northern blot analysis of rat T-cadherin expression during LIRD.

A) A radiolabeled T-cadherin cDNA probe was used to probe total RNA from rat retinas exposed to increasing durations of light. The sizes of the observed transcripts are shown on the left of the autoradiograph. Approximately 4 μg of total RNA was loaded in each lane. The 18S ribosomal band is shown as a loading control. B) Graphical analysis of the RNA expression levels on the northern blot. Expression levels are normalized to the 18S ribosomal band.

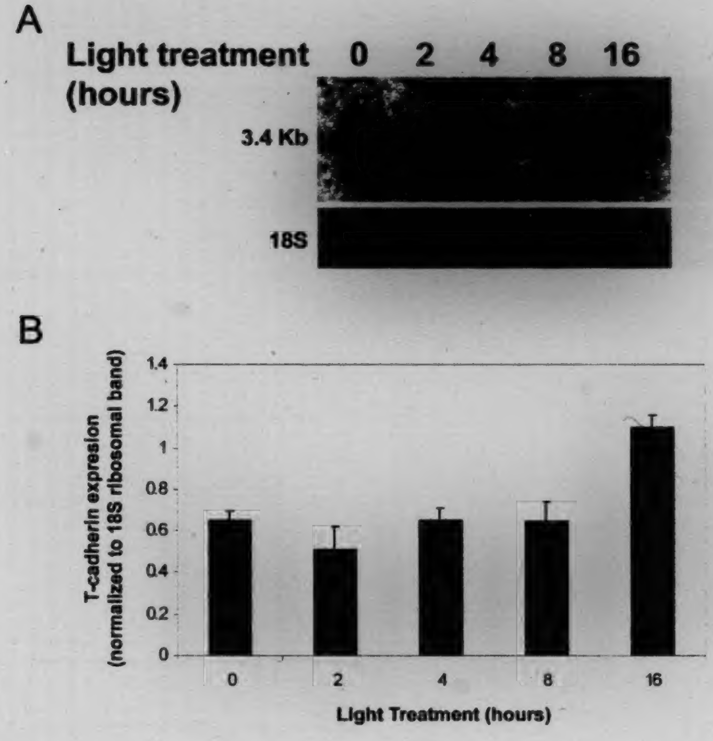

Figure 2.6 - Western analysis of rat T-cadherin during LIRD.

A) A rabbit polyclonal antibody to T-cadherin was used to immunodetect protein from rat retinas exposed to increasing durations of light. Actin immunodetection is shown as a protein loading control. B) Graphical analysis of the levels of T-cadherin protein on the western blot at the varying time points. Protein levels were normalized to actin to account for protein loading variation.

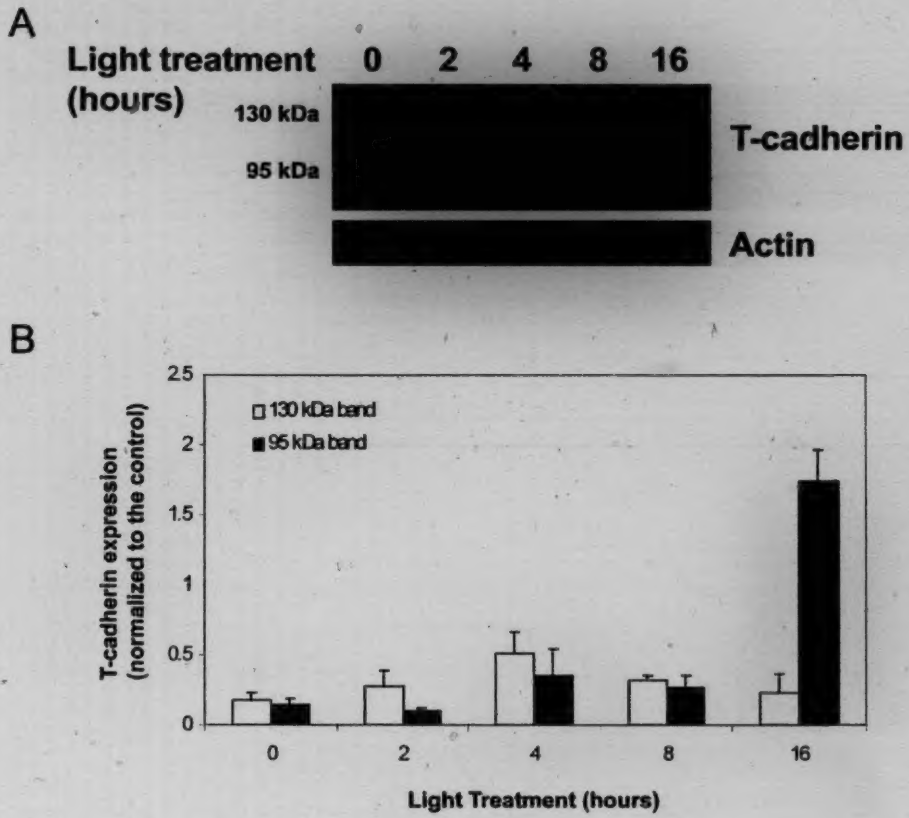

Figure 2.7 - Immunolocalization of T-cadherin on retina sections.

Rat retinas exposed to 0 hr, 4 hr, 8 hr, and 16 hour of light exposure were cryosectioned and immunolabeled with T-cadherin and the primary antibody was detected with a Cy3-conjugated secondary antibody (red). To the right of each fluorescent image is the corresponding section stained with hematoxylin and eosin to show morphology. RPE, retinal pigment epithelium; OS, outer segments; IS, inner segments; ONL, outer nuclear layer; OPL, outer plexiform layer; INL, inner nuclear layer; IPL, inner plexiform layer; GCL, ganglion cell layer. Bar = 40 μm.

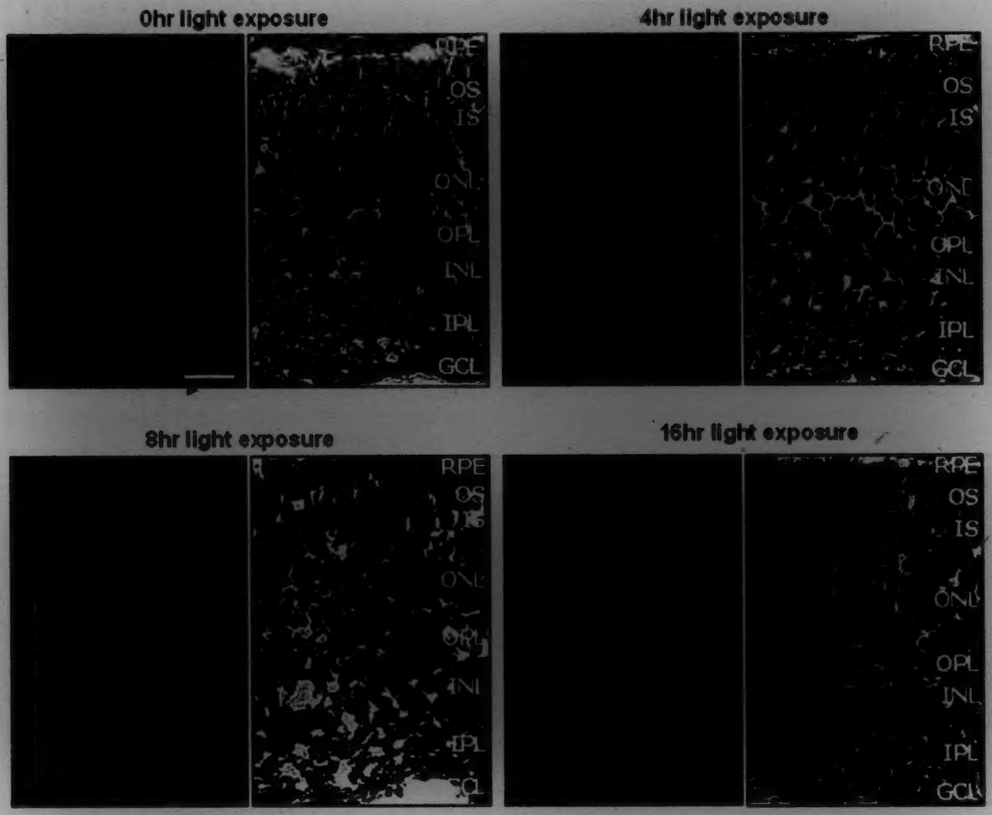

2.5 REFERENCES

1. Naash, M.L., Peachey, N.S., Li, Z.Y., Gryczan, C.C., Goto, Y., Blanks, J., Milam, A.H. and Ripps, H. (1996) Light-induced acceleration of photoreceptor degeneration in transgenic mice expressing mutant rhodopsin. *Invest Ophthalmol Vis Sci,* **37,** 775-82.
2. Wong, P. (1994) Apoptosis, retinitis pigmentosa, and degeneration. *Biochem Cell Biol,* **72,** 489-98.
3. Noell, W.K., Walker, V.S., Kang, B.S. and Berman, S. (1966) Retinal damage by light in rats. *Investigative Ophthalmology,* **5,** 450-472.
4. Organisciak, D.T. and Winkler, B.S. (1994) Retinal light damage: practical and theoretical considerations. In Osborne, N. and Chader, G. (eds.), *Progress in Retinal and Eye Research.* Pergamon Press, New York, pp. 1-29.
5. Reme, C.E., Weller, M., Szezesny, P., Munz, K., Hafezi, F., Rheinboth, J.J. and Clausen, M. (1995) Light-induced apoptosis in the rat retina *in vivo*: morphological features, threshold and time course. In Anderson, R.E., LaVail, M.M. and Hollyfield, J.G. (eds.), *Degenerative Diseases of the Retina.* Plenum Press, New York, pp. 19-25.
6. Wong, P., Kutty, R.K., Darrow, R.M., Shivaram, S., Kutty, G., Fletcher, R.T., Wiggert, B., Chader, G. and Organisciak, D.T. (1994) Changes in clusterin expression associated with light-induced retinal damage in rats. *Biochem Cell Biol,* **72,** 499-503.
7. Organisciak, D.T., Kutty, R.K., Leffak, M., Wong, P., Messing, S., Wiggert, B., Darrow, R.M. and Chader, G.J. (1995) Oxidative damage and responses in retinal nuclei arising from intense light exposure. In *Degenerative Diseases of the Retina.* Plenum Press, New York, pp. 19-26.
8. Shahinfar, S., Edward, D.P. and Tso, M.O. (1991) A pathologic study of photoreceptor cell death in retinal photic injury. *Curr Eye Res,* **10,** 47-59.
9. Abler, A.S., Chang, C.J., Ful, J., Tso, M.O. and Lam, T.T. (1996) Photic injury triggers apoptosis of photoreceptor cells. *Res Commun Mol Pathol Pharmacol,* **92,** 177-89.

10. Organisciak, D.T., Darrow, R.A., Barsalou, L., Darrow, R.M. and Lininger, L.A. (1999) Light-induced damage in the retina: differential effects of dimethylthiourea on photoreceptor survival, apoptosis and DNA oxidation. *Photochem Photobiol,* **70,** 261-8.

11. Kutty, R.K., Kutty, G., Wiggert, B., Chader, G.J., Darrow, R.M. and Organisciak, D.T. (1995) Induction of heme oxygenase 1 in the retina by intense visible light: suppression by the antioxidant dimethylthiourea. *Proc Natl Acad Sci U S A,* **92,** 1177-81.

12. Organisciak, D.T., Wang, H.M., Li, Z.Y. and Tso, M.O. (1985) The protective effect of ascorbate in retinal light damage of rats. *Invest Ophthalmol Vis Sci,* **26,** 1580-8.

13. Wang, M., Lam, T.T., Fu, J. and Tso, M.O. (1995) TEMPOL, a superoxide dismutase mimic, ameliorates light-induced retinal degeneration. *Res Commun Mol Pathol Pharmacol,* **89,** 291-305.

14. Wang, L., Lam, T.T., Lam, K.W. and Tso, M.O. (1994) Correlation of phospholipid hydroperoxide glutathione peroxidase activity to the sensitivity of rat retinas to photic injury. *Ophthalmic Res,* **26,** 60-4.

15. Grimm, C., Wenzel, A., Hafezi, F. and Reme, C.E. (2000) Gene expression in the mouse retina: the effect of damaging light. *Mol Vis,* **6,** 252-60.

16. Grimm, C., Wenzel, A., Hafezi, F., Yu, S., Redmond, T.M. and Reme, C.E. (2000) Protection of Rpe65-deficient mice identifies rhodopsin as a mediator of light-induced retinal degeneration. *Nat Genet,* **25,** 63-6.

17. Wong, P., Ulyanova, T., Organisciak, D.T., Bennett, S., Lakins, J., Arnold, J.M., Kutty, R.K., Tenniswood, M., vanVeen, T., Darrow, R.M. and Chader, G. (2001) Expression of multiple forms of clusterin during light-induced retinal degeneration. *Current Eye Research,* **23,** 157-165.

18. Grewal, R., Stepczynski, J., Kelln, R., Erickson, T., Darrow, R., Barsalou, L., Patterson, M., Organisciak, D.T. and Wong, P. (2004) Coordinated changes in classes of ribosomal protein gene expression is associated with light-induced retinal degeneration. *Invest Ophthalmol Vis Sci,* **45,** 3885-95.

19. Bolz, H., Reiners, J., Wolfrum, U. and Gal, A. (2002) Role of cadherins in Ca2+-mediated cell adhesion and inherited photoreceptor degeneration. *Adv Exp Med Biol,* **514,** 399-410.

20. Bolz, H., von Brederlow, B., Ramirez, A., Bryda, E.C., Kutsche, K., Nothwang, H.G., Seeliger, M., del, C.S.C.M., Vila, M.C., Molina, O.P., Gal, A. and Kubisch, C. (2001) Mutation of CDH23, encoding a new member of the cadherin gene family, causes Usher syndrome type 1D. *Nat Genet,* **27,** 108-12.

21. Bork, J.M., Peters, L.M., Riazuddin, S., Bernstein, S.L., Ahmed, Z.M., Ness, S.L., Polomeno, R., Ramesh, A., Schloss, M., Srisailpathy, C.R., Wayne, S., Bellman, S., Desmukh, D., Ahmed, Z., Khan, S.N., Kaloustian, V.M., Li, X.C., Lalwani, A., Bitner-Glindzicz, M., Nance, W.E., Liu, X.Z., Wistow, G., Smith, R.J., Griffith, A.J., Wilcox, E.R., Friedman, T.B. and Morell, R.J. (2001) Usher syndrome 1D and nonsyndromic autosomal recessive deafness DFNB12 are caused by allelic mutations of the novel cadherin-like gene CDH23. *Am J Hum Genet,* **68,** 26-37.

22. Ahmed, Z.M., Riazuddin, S., Bernstein, S.L., Ahmed, Z., Khan, S., Griffith, A.J., Morell, R.J., Friedman, T.B. and Wilcox, E.R. (2001) Mutations of the protocadherin gene PCDH15 cause Usher syndrome type 1F. *Am J Hum Genet,* **69,** 25-34.

23. Alagramam, K.N., Yuan, H., Kuehn, M.H., Murcia, C.L., Wayne, S., Srisailpathy, C.R., Lowry, R.B., Knaus, R., Van Laer, L., Bernier, F.P., Schwartz, S., Lee, C., Morton, C.C., Mullins, R.F., Ramesh, A., Van Camp, G., Hageman, G.S., Woychik, R.P. and Smith, R.J. (2001) Mutations in the novel protocadherin PCDH15 cause Usher syndrome type 1F. *Hum Mol Genet,* **10,** 1709-18.

24. Kimberling, W.J. and Moller, C. (1995) Clinical and molecular genetics of Usher syndrome. *J Am Acad Audiol,* **6,** 63-72.

25. Sprecher, E., Bergman, R., Richard, G., Lurie, R., Shalev, S., Petronius, D., Shalata, A., Anbinder, Y., Leibu, R., Perlman, I., Cohen, N. and Szargel, R. (2001) Hypotrichosis with juvenile macular dystrophy is caused by a mutation in CDH3, encoding P-cadherin. *Nat Genet,* **29,** 134-6.

26. Rattner, A., Smallwood, P.M., Williams, J., Cooke, C., Savchenko, A., Lyubarsky, A., Pugh, E.N. and Nathans, J. (2001) A photoreceptor-specific cadherin is essential for the structural integrity of the outer segment and for photoreceptor survival. *Neuron,* **32,** 775-86.

27. Bolz, H., Ebermann, I. and Gal, A. (2005) Protocadherin-21 (PCDH21), a candidate gene for human retinal dystrophies. *Mol Vis,* **11,** 929-33.

28. Angst, B.D., Marcozzi, C. and Magee, A.I. (2001) The cadherin superfamily: diversity in form and function. *J Cell Sci,* **114,** 629-41.

29. Vestal, D.J. and Ranscht, B. (1992) Glycosyl phosphatidylinositol--anchored T-cadherin mediates calcium-dependent, homophilic cell adhesion. *J Cell Biol,* **119,** 451-61.

30. Resink, T.J., Kuzmenko, Y.S., Kern, F., Stambolsky, D., Bochkov, V.N., Tkachuk, V.A., Erne, P. and Niermann, T. (1999) LDL binds to surface-expressed human T-cadherin in transfected HEK293 cells and influences homophilic adhesive interactions. *FEBS Lett,* **463,** 29-34.

31. Lee, S.W. (1996) H-cadherin, a novel cadherin with growth inhibitory functions and diminished expression in human breast cancer. *Nat Med,* **2,** 776-82.

32. Sato, M., Mori, Y., Sakurada, A., Fujimura, S. and Horii, A. (1998) The H-cadherin (CDH13) gene is inactivated in human lung cancer. *Hum Genet,* **103,** 96-101.

33. Kawakami, M., Staub, J., Cliby, W., Hartmann, L., Smith, D.I. and Shridhar, V. (1999) Involvement of H-cadherin (CDH13) on 16q in the region of frequent deletion in ovarian cancer. *Int J Oncol,* **15,** 715-20.

34. Wyder, L., Vitaliti, A., Schneider, H., Hebbard, L.W., Moritz, D.R., Wittmer, M., Ajmo, M. and Klemenz, R. (2000) Increased expression of H/T-cadherin in tumor-penetrating blood vessels. *Cancer Res,* **60,** 4682-8.

35. Takeuchi, T., Misaki, A., Liang, S.B., Tachibana, A., Hayashi, N., Sonobe, H. and Ohtsuki, Y. (2000) Expression of T-cadherin (CDH13, H-Cadherin) in human brain and its characteristics as a negative growth regulator of epidermal growth factor in neuroblastoma cells. *J Neurochem,* **74,** 1489-97.

36. Hug, C., Wang, J., Ahmad, N.S., Bogan, J.S., Tsao, T.S. and Lodish, H.F. (2004) T-cadherin is a receptor for hexameric and high-molecular-weight forms of Acrp30/adiponectin. *Proc Natl Acad Sci U S A,* **101,** 10308-13.

37. Ivanov, D.B., Philippova, M.P. and Tkachuk, V.A. (2001) Structure and functions of classical cadherins. *Biochemistry (Mosc),* **66,** 1174-86.

38. Philippova, M.P., Bochkov, V.N., Stambolsky, D.V., Tkachuk, V.A. and Resink, T.J. (1998) T-cadherin and signal-transducing molecules co-localize in caveolin-rich membrane domains of vascular smooth muscle cells. *FEBS Lett,* **429,** 207-10.

39. Kipmen-Korgun, D., Osibow, K., Zoratti, C., Schraml, E., Greilberger, J., Kostner, G.M., Jurgens, G. and Graier, W.F. (2005) T-cadherin mediates low-density lipoprotein-initiated cell proliferation via the Ca(2+)-tyrosine kinase-Erk1/2 pathway. *J Cardiovasc Pharmacol,* **45,** 418-30.

40. Joshi, M.B., Philippova, M., Ivanov, D., Allenspach, R., Erne, P. and Resink, T.J. (2005) T-cadherin protects endothelial cells from oxidative stress-induced apoptosis. *FASEB J,* **19,** 1737-9.

41. Sambrook, J. and Russell, D. (2001) *Molecular cloning : a laboratory manual.* 3rd ed. Cold Spring Harbor Laboratory, Cold Spring Harbor, N.Y.

42. Wong, P., MacDonald, I. and Tenniswood, M. (1989) Use of the polymerase chain reaction for the differential cross screening of libraries cloned into phage-lambda-based vectors. *Gene,* **85,** 59-65.

43. Altschul, S.F., Gish, W., Miller, W., Myers, E.W. and Lipman, D.J. (1990) Basic Local Alignment Search Tool. *Journal of Molecular Biology,* **215,** 403-410.

44. Thomas, P.D., Kejariwal, A., Campbell, M.J., Mi, H., Diemer, K., Guo, N., Ladunga, I., Ulitsky-Lazareva, B., Muruganujan, A., Rabkin, S., Vandergriff, J.A. and Doremieux, O. (2003) PANTHER: a browsable database of gene products organized by biological function, using curated protein family and subfamily classification. *Nucleic Acids Res,* **31,** 334-41.

45. Abramoff, M.D., Magelhaes, P.J., Ram, S.J. (2004) Image Processing with ImageJ. *Biophotonics International,* **11,** 36-42.

46. Correa-Rotter, R., Mariash, C. and Rosenberg, M.E. (1992) Loading and transfer control for Northern hybridization. *BioTechniques,* **12,** 154-158.

47. Hillier, L.D., Lennon, G., Becker, M., Bonaldo, M.F., Chiapelli, B., Chissoe, S., Dietrich, N., DuBuque, T., Favello, A., Gish, W., Hawkins, M., Hultman, M., Kucaba, T., Lacy, M., Le, M., Le, N., Mardis, E., Moore, B., Morris, M., Parsons, J., Prange, C., Rifkin, L., Rohlfing, T., Schellenberg, K., Marra, M. and et al. (1996) Generation and analysis of 280,000 human expressed sequence tags. *Genome Res,* **6,** 807-28.

48. McAvoy, J.W., Chamberlain, C.G., de Iongh, R.U., Hales, A.M. and Lovicu, F.J. (1999) Lens development. *Eye,* **13 (Pt 3b),** 425-37.

49. Reza, H.M. and Yasuda, K. (2004) Lens differentiation and crystallin regulation: a chick model. *Int J Dev Biol,* **48,** 805-17.

50. Sakaguchi, H., Miyagi, M., Darrow, R.M., Crabb, J.S., Hollyfield, J.G., Organisciak, D.T. and Crabb, J.W. (2003) Intense light exposure changes in crystallin content in retina. *Experimental Eye Research,* **76,** 131-133.

51. Organisciak, D. (2006) Genetic, Age and Light Mediated Effects on Crystallin Protein Expression in the Retina. *Photochem Photobiol,* **82,** 1088-1096.

52. Specht, S., Leffak, M., Darrow, R.M. and Organisciak, D.T. (1999) Damage to rat retinal DNA induced in vivo by visible light. *Photochem Photobiol,* **69,** 91-8.

53. Krishnamoorthy, R.R., Crawford, M.J., Chaturvedi, M.M., Jain, S.K., Aggarwal, B.B., Al-Ubaidi, M.R. and Agarwal, N. (1999) Photo-oxidative stress down-modulates the activity of nuclear factor-kappaB via involvement of caspase-1, leading to apoptosis of photoreceptor cells. *J Biol Chem,* **274,** 3734-43.

54. Sparrow, J.R. and Cai, B. (2001) Blue light-induced apoptosis of A2E-containing RPE: involvement of caspase-3 and protection by Bcl-2. *Invest Ophthalmol Vis Sci,* **42,** 1356-62.

55. Wu, T., Chiang, S.K., Chau, F.Y. and Tso, M.O. (2003) Light-induced photoreceptor degeneration may involve the NF kappa B/caspase-1 pathway in vivo. *Brain Res,* **967,** 19-26.

56. Wu, J., Gorman, A., Zhou, X., Sandra, C. and Chen, E. (2002) Involvement of caspase-3 in photoreceptor cell apoptosis induced by in vivo blue light exposure. *Invest Ophthalmol Vis Sci,* **43,** 3349-54.

57. Wenzel, A., Grimm, C., Samardzija, M. and Reme, C.E. (2005) Molecular mechanisms of light-induced photoreceptor apoptosis and neuroprotection for retinal degeneration. *Prog Retin Eye Res,* **24,** 275-306.

58. Li, F., Cao, W. and Anderson, R.E. (2003) Alleviation of constant-light-induced photoreceptor degeneration by adaptation of adult albino rat to bright cyclic light. *Invest Ophthalmol Vis Sci,* **44,** 4968-75.

59. Donovan, M. and Cotter, T.G. (2002) Caspase-independent photoreceptor apoptosis in vivo and differential expression of apoptotic protease activating factor-1 and caspase-3 during retinal development. *Cell Death Differ,* **9,** 1220-31.

60. Doyle, D.D., Goings, G.E., Upshaw-Earley, J., Page, E., Ranscht, B. and Palfrey, H.C. (1998) T-cadherin is a major glycophosphoinositol-anchored protein associated with noncaveolar detergent-insoluble domains of the cardiac sarcolemma. *J Biol Chem,* **273,** 6937-43.

61. Anderson, R.G. (1998) The caveolae membrane system. *Annu Rev Biochem,* **67,** 199-225.

62. Wu, T., Chen, Y., Chiang, S.K. and Tso, M.O. (2002) NF-kappaB activation in light-induced retinal degeneration in a mouse model. *Invest Ophthalmol Vis Sci,* **43,** 2834-40.

63. Bringmann, A., Skatchkov, S.N., Pannicke, T., Biedermann, B., Wolburg, H., Orkand, R.K. and Reichenbach, A. (2000) Muller glial cells in anuran retina. *Microsc Res Tech,* **50,** 384-93.

64. LaVail, M.M., Yasumura, D., Matthes, M.T., Lau-Villacorta, C., Unoki, K., Sung, C.H. and Steinberg, R.H. (1998) Protection of mouse photoreceptors by survival factors in retinal degenerations. *Invest Ophthalmol Vis Sci,* **39,** 592-602.

65. Cayouette, M. and Gravel, C. (1997) Adenovirus-mediated gene transfer of ciliary neurotrophic factor can prevent photoreceptor degeneration in the retinal degeneration (rd) mouse. *Hum Gene Ther,* **8,** 423-30.

66. Wahlin, K.J., Campochiaro, P.A., Zack, D.J. and Adler, R. (2000) Neurotrophic factors cause activation of intracellular signaling pathways in Muller cells and other cells of the inner retina, but not photoreceptors. *Invest Ophthalmol Vis Sci,* **41,** 927-36.

67. Gauthier, R., Joly, S., Pernet, V., Lachapelle, P. and Di Polo, A. (2005) Brain-derived neurotrophic factor gene delivery to muller glia preserves structure and function of light-damaged photoreceptors. *Invest Ophthalmol Vis Sci,* **46,** 3383-92.

68. Ulyanova, T., Szel, A., Kutty, R.K., Wiggert, B., Caffe, A.R., Chader, G.J. and van Veen, T. (2001) Oxidative stress induces heme oxygenase-1 immunoreactivity in Muller cells of mouse retina in organ culture. *Invest Ophthalmol Vis Sci,* **42,** 1370-4.

69. Harada, T., Harada, C., Nakayama, N., Okuyama, S., Yoshida, K., Kohsaka, S., Matsuda, H. and Wada, K. (2000) Modification of glial-neuronal cell interactions prevents photoreceptor apoptosis during light-induced retinal degeneration. *Neuron,* **26,** 533-41.

70. Samardzija, M., Wenzel, A., Aufenberg, S., Thiersch, M., Rem, C. and Grimm, C. (2006) Differential role of Jak-STAT signaling in retinal degenerations. *Faseb J.*

71. Rattner, A. and Nathans, J. (2005) The genomic response to retinal disease and injury: evidence for endothelin signaling from photoreceptors to glia. *J Neurosci,* **25,** 4540-9.

Chapter 3

Identification and Characterization of Rat KCTD8

3.1 INTRODUCTION

Retina dystrophies and degeneration are caused by numerous gene defects as well as environmental factors. Despite this apparent multifaceted process of retinal degeneration, the common end result is visual cell death by apoptosis [1, 2]. Although 158 different gene mutations have been identified which cause retinal dystrophies (RetNet - http://www.sph.uth.tmc.edu/Retnet/home.htm), the intermediary steps between these mutations and the resultant apoptosis of visual cells is not clearly understood. In order to prevent photoreceptor apoptosis, a better understanding of the signaling and cell death mechanisms that lead to visual cell loss is required.

In an effort to elucidate intermediary steps of visual cell loss, we study the light-induced retinal degeneration (LIRD) model system in rodents [3-5]. This involves exposing rats to intense green light, which results in photoreceptor degeneration via apoptosis. Although transgenic animal models that mimic retinal disease are useful for studying the effects of specific gene mutations on retinal degeneration, the LIRD model system affords some advantages to studying the process of retinal cell death that transgenic animal models do not. Most notably, synchronized photoreceptor apoptosis allowing accurate analysis of the molecular steps involved and the ability to vary the duration of light exposure, thus varying the degree of degeneration [5, 6]. To study the molecular mechanisms involved in progressing a retina from a normal, unaffected state to a degenerative state we utilize a differential cDNA library screening approach to identify differentially expressed genes during LIRD. We have isolated and identified a number of genes through this process that may be involved in mediating retinal degeneration in response to light treatment [7, 8].

One such gene isolated in this way initially corresponded to a novel clone matching to only expressed sequence tags (ESTs) in the GenBank database. The gene was arbitrarily given the name 1363, which was the clone number assigned to it when it was isolated from the cDNA library screen. In 2003, a BLAST search of 1363 revealed high homology to the mouse potassium (K$^+$) channel tetramerization domain containing 8 (KCTD8) gene, which was isolated by Okazaki *et al* [9] as part of a mass gene annotation project. The nucleotide homology between the mouse KCTD8 mRNA and the rat 1363 mRNA had an Expect value of 0.0 and an Identities value of 93%. Based on this high homology to the mouse KCTD8 gene, we were confident that 1363 represented the rat homologue of KCTD8. This gene is a member of the KCTD gene family. Despite the HUGO gene name ascribed to this gene, the results presented here suggest that KCTD8 is unlikely to be involved in potassium channel formation. Aside from a conserved N-terminal domain, it contains no additional features of channel proteins. At present, nothing is known about the function of this gene and only limited characterization of the zebrafish homologue is reported in the literature [10]. In this paper, we describe the cloning, *in silico* analysis, and expression during LIRD of rat KCTD8 in an effort to gain a better understanding of its function in general as well as during retinal degeneration.

3.2 MATERIALS AND METHODS

3.2.1 Animals

Male albino Sprague-Dawley rats (Harlan Inc, Indianapolis, IN) were purchased as weanlings and dark-adapted to the age of 60 days before being exposed to intense visible light at a wavelength of 490-580 nm (green light) with an illuminance of 1200 to 1400 lux. Light exposures were started at 9 am for up to 16 hours and were performed in green #2092 Plexiglass chambers (Dayton Plastics, Dayton, OH). Rats were sacrificed in carbon dioxide saturated chambers and retinas excised and flash frozen on dry ice. Tissues were stored at –80°C until use. Each treatment condition consists of pooled retinas from 5-10 rats. Control retinas were obtained from animals maintained in darkness until the age of 60 days old (dark-reared) and sacrificed at 9 am. Three independent sets of animals were used for this study. In all cases, animals were cared for in accordance with the guidelines defined by the Public Health Service Policy on Humane Care and Use of Laboratory Animals.

3.2.2 RNA isolation and cDNA library screening

Total RNA was isolated using Trizol (Invitrogen, Carlsbad, CA) according to the manufacturer's protocol. The RNA was ethanol precipitated, dissolved in DEPC-treated water and stored at –80°C until use. RNA isolated from retinas of light exposed animals defined the LIRD time course used in the current study (LIRD profile).

Synthesis and differential cross-screening of the cDNA library was performed as described in [8].

3.2.3 Protein isolation

The organic layer from the above RNA isolations was used for protein isolation according to the Trizol protocol (Invitrogen). Retinal protein extracts were also prepared from dark-reared rat retinas using RIPA (radioimmunoprecipitation) Lysis Buffer containing PMSF solution, sodium orthovanadate solution, and protease inhibitor cocktail solution supplied with the lysis buffer (Santa Cruz Biotechnology, Santa Cruz, CA). For the RIPA protein extraction, retinal tissue was ground into a powder using liquid nitrogen and a mortar and pestle. Tissues were further homogenized by sonicating the tissue eight times for 10 seconds each time with a 1-minute interval between sonications. The sample was centrifuged at 10,000xg for 10 minutes to pellet the insoluble material and the supernatant was isolated and analyzed for protein content. All steps above were performed at 4°C or on ice. For all proteins, total protein concentration was estimated by the Bradford method [11].

3.2.4 Obtaining the full-length sequence of KCTD8

Rapid amplification of cDNA ends (RACE) was performed using the GeneRacer Kit (Invitrogen) on 5 μg of total retinal RNA isolated from dark-reared rats, according to manufacturer's directions. 5' RACE was performed using the primer GSP1r 5'-tgtggagagctcattgcaggaagtc-3' along with the GeneRacer 5' primer supplied with the kit, which would allow for 226 nucleotides of sequence overlap between the RACE product and the 5' region of the original clone isolated from the cDNA library. Nested PCR was performed using an aliquot of the RACE product as template and using the primer GSP2r 5'-tcccactctcacttcctttgtctgt-3' along with the GeneRacer 5' nested primer, which would allow for 132 nucleotides of sequence overlap between the RACE product and the 5' region of the original clone isolated from the cDNA library. The nested PCR product was gel electrophoresed and gel purified using the QIAquick Gel Extraction kit (Qiagen, Mississauga, ON, Canada). The gel-purified product was ligated into the pCR4-TOPO vector (Invitrogen) according to the manufacturer's protocol. Sequencing of the ligated products was performed using T7 (5’-taatacgactcactataggg-3’) and T3 (5’-attaaccctcactaaaggga-3’) vector-specific primers.

Using the compiled sequence data, primers were designed, ORFf 5’-ccagagagtgccggttgac-3’ and ORFr 5’-tcagttaggcggtgacatgg-3’, in order to amplify the full-length product using Platinum Taq DNA Polymerase (Invitrogen) according to manufacturer’s directions. The resultant product was gel purified, subcloned and sequenced as above. The full-length sequence data confirmed the data complied from the partial KCTD8 cDNA clone isolated from the cDNA library screen and the 5’ RACE products.

3.2.5 KCTD8 DNA and protein sequence analysis

Alignment of the full-length KCTD8 sequence with the rat genome sequence using BLAST revealed the location of the intron-exon boundaries. To confirm this gene structure, PCR primer sets, which flank the proposed exons, were designed and used to amplify these regions from rat genomic DNA. The resultant PCR products were then sequenced. The primer sets used were as follows: GSP4f 5’-gcgaggcagagttcttccagctt-3’, Intron1r 5’-gctgtccccaccctgctgaatac-3’; Intron1f 5’-gggctgtgttgagaatcctggttgtc-3’, GSP2r 5'-tcccactctcacttcctttgtctgt-3'.

The KCTD8 DNA sequence was analyzed for homologues using the blastn search program [12] and prediction of polyadenylation sites within the sequence was performed using the SoftBerry POLYAH program (http://www.softberry.com). An open reading frame (ORF) was found within the predicted KCTD8 mRNA sequence using the ORF finder program (http://www.ncbi.nlm.nih.gov/projects/gorf/). Protein homology and conserved domain searches were performed using the blastp search program and homologous sequences were aligned with ClustalW [12-14]. Search Tool for the Retrieval of Interacting Genes/proteins (STRING) [15-17] was used to bioinformatically determine the level of human KCTD8 protein conservation across both bacteria and eukaryotes. PSORT II (http://psort.hgc.jp/) was used to predict protein sorting signals in the amino acid sequence. Hydropathy plot analysis of the protein was based on the Kyte-Doolittle methodology [18].

3.2.6 Zooblot analysis

[α^{32}P]dCTP-labeled rat KCTD8 probe was generated by random primer labeling using the Random Primers DNA Labeling System (Invitrogen) and purified with G-50 Sephadex columns (Roche Applied Science, Laval, QC). A commercially available Southern blot (Clontech, Palo Alto, CA) containing *Eco*RI-digested genomic DNA from various species (human, monkey, rat, mouse, dog, cow, rabbit, chicken, yeast) was hybridized in Hybrisol II hybridization solution (Serologicals Corporation, Norcross, GA) at 55°C for 16 hours using 10^6 cpm/ml of radioactively labeled, purified probe. The membranes were washed 2X 15 minutes in 2X SSC (sodium chloride, tri-sodium citrate buffer) at 55°C, 1X 30 minutes in 2X SSC, 0.1% SDS (sodium dodecyl sulfate) at 55°C, and 1X 10 minutes in 0.1X SSC, 0.1% SDS at 55°C then exposed to Kodak X-Omat film at –70°C.

3.2.7 Northern blot analysis

Northern blots were prepared using either 5 µg of rat retinal total RNA from the LIRD profile or 5 µg of total RNA isolated from various rat tissues (brain, heart, kidney, liver, lung, muscle, retina, spleen, testes, thymus). For the multiple tissue northern blot, all tissues were isolated from dark reared rats. Radioactive labeling and purification of the KCTD8 probe was performed as above. Hybridization and washing of the blots was performed as above with the exception of the temperature being 65°C. Washed blots were exposed to Kodak X-Omat film at -70°C. Densitometric analysis of the band intensities was done using ImageJ [19]. In all cases, analysis was performed on three replicates and a representative autoradiograph of one of the three replicates is shown. Standard deviation bars indicate the variations in band intensity between each replicate.

3.2.8 Production of a KCTD8 antibody

An anti-KCTD8 antibody was developed by Invitrogen's custom polyclonal antibody service. An 18 amino acid synthetic peptide (NLVNTQQAVSQQPNTLTL) corresponding to amino acids 375-392 of the rat KCTD8 protein was conjugated using Invitrogen's proprietary Multiple Antigenic Peptide (MAP) methodology that presents the peptides in alternate, multiple conformations on a branched lysine core to produce antibodies with greater utility across assays. The conjugated peptide was injected subcutaneously into rabbits for the production of polyclonal antibodies. The peptide antigen was immobilized on an activated support and antibodies were affinity purified by passing antisera through the peptide column and then washing non-specific antibodies off the column. Specific antibodies were eluted via a pH gradient, collected, and stored in a borate buffer (0.125M total borate, pH 8.2). The purified antibody titer was determined with an enzyme linked immunosorbent assay (ELISA).

3.2.9 Peptide competition assay and western blot analysis

Approximately 20 μg of retinal proteins were added to 5X sample buffer (10% [w/v] SDS, 10 mM dithiothreitol, 20% [v/v] glycerol, 0.2 M Tris-HCl, pH 6.8, 0.05% [w/v] bromophenol blue) and electrophoresed on a 10% polyacrylamide gel. Proteins were electrophoretically transferred to Trans-Blot nitrocellulose membrane (Bio-Rad Laboratories, Hercules, CA) using the Mini-Protean 3 apparatus, according to manufacturer's directions (Bio-Rad).

Western blots were blocked against non-specific binding in blocking buffer (TBS-T - 50 mM Tris-HCl, 200 mM NaCl, 1 mM $MgCl_2$ (pH 7.4), and 0.1% v/v Tween-20 + 5% skim milk powder) for 1 hour at room temperature. Following blocking, the blots were incubated with the KCTD8 polyclonal antiserum, diluted 1:1000 in blocking buffer, and incubated for 1 hour at room temperature. For the peptide competition assay, the antibody was incubated with 0 mg, 50 ng, 500 ng, or 5 μg of competing KCTD8 peptide at 4°C overnight, prior to incubation with the western blot. After the primary antibody incubation, the blots were washed 3X in TBS-T at room temperature then incubated with a 1:5000 dilution of horseradish peroxidase-conjugated donkey anti-rabbit secondary antibody (Amersham Biosciences, Piscataway, NJ) for 1 hour at room temperature. Blots were then washed as before. Detection of antibody binding was done using ECL Western Blotting Detection Reagents (Amersham Biosciences) as per manufacturer's directions. The resultant band intensities were analyzed using ImageJ [19]. In all cases, analysis was performed on three replicates and a representative autoradiograph of one of the three replicates is shown. Standard deviation bars indicate the variations in band intensity between each replicate.

3.3 RESULTS

3.3.1 Isolation of rat KCTD8 cDNA

In order to isolate genes that are differentially expressed between an untreated, dark-reared retina and a prolonged light exposed retina, we performed a differential cDNA library screen between dark-reared retinas and retinas exposed to 16 hours of light [8]. Genes isolated from this type of screen have significant potential to be involved in the retinal degeneration process since the genes isolated were either upregulated or down-regulated in response to the light insult.

One clone isolated from this screen initially had no homology to any known genes in the Genbank database and thus was considered novel. Later BLAST searches revealed high homology to the mouse KCTD8 mRNA. Due to the method of the cDNA library construction, the isolated rat clone contained only the 3' end of the gene. 5' RACE PCR was used to obtain the full-length sequence consisting of 2840 bp (Figure 3.1). A putative transcription start site (+1 position) was predicted at the 5' end of the sequence and three poly(A)$^+$ signals [20] were predicted at positions 2181-2186, 2281-2286, and 2340-2345. Bioinformatic analysis of the complete cDNA sequence revealed a 1431 bp open reading frame with the ATG start codon at position 369 and a TAG stop codon at position 1799 encoding a predicted protein product of 476 amino acids. At present, the rat KCTD8 sequence presented here has an expect value of 0.0 and an identities values of 2511/2511 (100%) with the predicted rat KCTD8 sequence in the GenBank database. The predicted sequence in the database was derived using gene prediction methods.

3.3.2 KCTD8 genomic structure

A BLAST search aligned the full-length KCTD8 cDNA sequence to a rat genomic sequence located on chromosome 14. The gene consists of two exons separated by a very large ~240 kb intron (Figure 3.2A). Exon 1 consists of 368 bp of the 5'-UTR in addition to the first 970 bp of the protein coding region of the gene. Exon 2 contains the remaining 461 bp of the coding region as well as 1041 bp of the 3'-UTR. All intron/exon splice junctions conform to consensus sequences for splice donor and acceptor sites (Figure 3.2B) [21].

3.3.3 Sequence conservation of KCTD8

Searches of the protein database using blastp indicated a number of potential KCTD8 homologues (Figure 3.3). The search revealed that the protein is highly conserved between rat and mouse and rat and human, with a percent homology of 97% and 94%, respectively. Sequence homologues were also found for cow, zebrafish, *D. melanogaster* and *C. elegans* with a percent homology to rat KCTD8 of 92%, 76%, 48%, and 44%, respectively. With the exception of the mouse, human and zebrafish homologues, all of the homologues are listed in the NCBI database as either unnamed protein products or predicted similar to potassium channel tetramerization domain containing 8. Analysis of human KCTD8 conservation across eukaryotes and bacteria indicated that KCTD8 is conserved throughout eukaryotes, except fungi. There are no KCTD8 homologues in bacteria (Figure 3.4).

In addition to bioinformatic prediction of homologues, zooblot analysis also showed hybridization of KCTD8 to genomic DNA isolated from human, monkey, rat, mouse, dog, cow, rabbit, chicken, and yeast (Figure 3.5). This data confirms a number of the homologues predicted by bioinformatics as well as identifies other species for which sequence homologues are not yet available in the NCBI database.

3.3.4 KCTD8 protein sequence analysis

The *in silico* translated 476 amino acid KCTD8 protein has a predicted molecular weight of 52.8 kDa and an isoelectric point of 8.54. Analysis of the KCTD8 protein sequence with the NetPhos2.0 program [22] identified a number of putative phosphorylation sites (Figure 3.3), the majority of which are conserved among the different homologues. In addition, three putative O-glycosylated sites and four putative N-glycosylated sites were predicted using NetOGly3.1 [23] and NetNGly1.0, respectively. Hydropathy plot analysis of the KCTD8 amino acid sequence predicts that the protein is mainly hydrophilic with no transmembrane domains (Figure 3.6).

A search of the rat KCTD8 protein against the Conserved Domain Database (CDD) [24] identified a conserved domain in the N-terminal region of the protein corresponding to a potassium (K^+) channel tetramerization domain (Figure 3.2C, Figure 3.3). The K^+ channel tetramerization domain, known as the T1 domain, is distantly related to the BTB/POZ (broad complex tramtrack bric-a-brac/pox-virus and zinc finger) domain, [25] which is a protein-protein interaction motif found at the N-terminus of some transcription factors as well as Shaw-type potassium channels [24, 26]. This domain is highly conserved amongst the KCTD8 homologues identified (Figure 3.3).

Further bioinformatic analysis using the PSORT II program identified two putative nuclear localization signals (NLSs) in the C-terminal region of the KCTD8 protein (Figure 3.2C, Figure 3.3). The pattern7 (pat7) motif is a monopartite basic NLS containing the pattern P followed within 3 residues by a basic segment containing 3 K/R residues out of 4 [27, 28]. In KCTD8 this NLS contains the sequence PERKRQW. The other putative NLS identified in KCTD8 is a bipartite basic NLS which is characterized by a $(K/R)_2\ X_{10\text{-}12}\ (K/R)_{3/5}$ consensus sequence [28, 29]. In KCTD8 this NLS is represented by the sequence RKAPVQWMPPPDKRRNS. The two NLSs identified are highly conserved among human, rat, and mouse homologues. For the cow, zebrafish, *D. melanogaster*, and *C. elegans* homologues, the protein sequences for these species truncates prior to the NLSs. Three leucine-rich nuclear export signals (NES) were also identified in the KCTD8 amino acid sequence [30]; all three of which are conserved among the different homologues (Figure 3). In addition, prediction of cellular localization using PSORT II κ-NN prediction indicates that the protein has a 78% likelihood to be nuclear localized [31].

3.3.5 Tissue distribution of KCTD8

To determine whether KCTD8 is expressed in other tissues, multiple tissue northern analysis of various rat tissues was performed (Figure 3.7). A single transcript of approximately 2.7 kb was observed predominantly in the brain and retina and weakly detectable in the kidney and lung. This transcript size is consistent with the full-length transcript, isolated by RACE, of 2840 bp. In addition to the full-length transcript, an additional smaller transcript of approximately 1.5 kb was observed for the brain tissue. The significance of this smaller transcript in the brain is currently unknown.

3.3.6 Expression analysis of KCTD8 during LIRD

KCTD8 was originally isolated as a differentially expressed clone from the cDNA library screen described in Chapter 2. The macroarray screen (tertiary screen) of the differentially expressed cDNA clones isolated from the library screen indicated that KCTD8 had a slight decrease in expression at 16 hours of light exposure as compared to 0 hours (dark-reared) of light exposure (Figure 3.8A). Northern analysis of KCTD8 during the LIRD profile indicates that the highest level of expression is seen in dark-reared animals with expression levels decreasing upon short light exposure (Figure 3.8B). Expression begins to increase again with 8 and 16 hours of light exposure, a point at which the retina is under oxidative stress. Densitometric analysis of the northern blot profile clearly shows an inverse bell curve of expression over the progression of LIRD (Figure 3.8C). In agreement with the multiple tissue northern analysis, a single transcript of 2.7 kb is seen for the retinal degeneration profile, which corresponds to the full-length sequence.

In contrast to the expression levels seen by northern analysis, western analysis indicates that the protein levels are approximately equal throughout the LIRD profile (Figure 3.9A and 3.9C). Four bands of approximately 96 kDa. 69 kDa, 60 kDa, and 48 kDa were observed on the LIRD western blot of protein extracts resulting from Trizol extraction, a phenol based reagent. The protein levels of all four bands fluctuate slightly between the five time points. In all lanes, the three larger bands are approximately equal density and the smallest band appears much more faint (Figure 3.9A and 3.9C). The peptide competition assay indicates that these four bands are specific to the KCTD8 polyclonal antibody since masking the antigenic sites on the antibody with increased concentration of competing peptide eliminated binding of the antibody to all four bands (Figure 3.9D). Interestingly, different protein extraction methods produced different intensities of the four bands observed by western blot analysis. Using the RIPA isolation method, the 60 kDa band is most prominent with the larger bands being quite faint and the smallest band (48 kDa) being nonexistent (Figure 3.9B). Given that the estimated size of the protein is 52.8 kDa we conclude that the 60kDa protein product is likely to be the least processed version of the protein. Being that Trizol is phenol based, it is more effective at extracting insoluble proteins and will denature lipids in the membrane and hence also membrane bound proteins more efficiently than RIPA buffer. As such, it is likely that the 96 kDa, 69 kDa, and 48 kDa bands represent less soluble forms of post-translationally modified KCTD8 proteins.

3.4 DISCUSSION

The differential screening of a cDNA library to identify genes involved in the retinal degeneration process resulted in the isolation of the rat KCTD8 gene, a previously uncharacterized gene. KCTD8 consists of two exons separated by one intron and spans approximately 242 kb of genomic DNA. The mRNA transcript is 2840 bp in length and encodes a protein of 476 amino acids. Analysis of the genomic conservation of the gene across a wide range of species demonstrates that KCTD8 is evolutionarily conserved from human to yeast. The amino acid sequence of KCTD8 appears to share significant homology with other identified KCTD8 proteins as well as other predicted proteins in *H. sapiens*, *M. musculus*, *B. taurus*, *D. rerio*, *D. melanogaster*, and *C. elegans*. Bioinformatic analysis of the human KCTD8 homologue indicated that it is conserved across eukaryotes, except in yeast. This is in contrast to the experimental zooblot data that indicates hybridization to yeast genomic DNA. This is most likely due to the fact that the protein sequence for yeast KCTD8 is not available in the GenBank database.

Of these homologues, only the zebrafish KCTD8 gene has been analyzed experimentally, by *in situ* hybridization [10]. It was found that the zebrafish KCTD8 gene (also known as *dexter* (*dex*)) is a member of the *leftover* (*lov*)-related gene family, which includes *lov*, *right on* (*ron*), and *dex*. All are members of the KCTD gene family by way of the presence of an N-terminal T1 domain. Lov and Ron proteins are members of the KCTD12 subclass, whereas Dex is a member of the KCTD8 subclass. All three members of the *lov*-related gene family were found to be differently expressed by the left and right habenulae of the zebrafish brain. This asymmetric expression is significant for determining laterality in the zebrafish brain and subsequently influencing the proper development of the formation of midbrain connections. As such, it is plausible that the rat

KCTD8 homologue may have a developmental function in the brain. Multiple tissue northern analysis clearly demonstrates expression of the rat KCTD8 in the brain as well as the retina. However, Gamse *et al.* [10] stated that there were no observed prominent asymmetric differences for the habenular-specific expression of KCTD8 in rats or mice. The authors, however, acknowledged that subtle asymmetric differences cannot yet be ruled out.

Analysis of the rat KCTD8 protein sequence revealed that the protein has 40 potential phosphorylation sites suggesting that the protein is highly phosphorylated. A number of these phosphorylation sites are highly conserved throughout all seven KCTD8 homologues with the highest conservation of sites seen for rat, mouse and human. This high level of phosphorylation could be involved in regulating gene function or in post-translational activation. In addition to the potential phosphorylation sites, a number of conserved predicted glycosylation sites were identified in the protein, suggesting yet another level of post-translational modification that may be essential for proper functioning of the protein. The changes in the molecular weight of the protein due to these predicted post-translational modifications is difficult to determine due the diversity of oligosaccharide structures and the varying degrees of saturation of glycosylation sites, which can result in heterogeneity of the mass and charge of the protein. In addition, phosphorylation can have varying effects on the protein mass as well as structure and has been found to cause gel shifts due to enabling retention of residual structure during SDS-PAGE [32]. However, based on mass alone of post-translational modifications, phosphorylation will add 80 Da per phosphorylation site and N-linked oligosaccharides may contribute 3.5 kDa or more per structure to the mass of the protein [33].

Bioinformatic analysis of the KCTD8 protein identified three potential functional domains – two NLS sites at the C-terminus of the protein and a T1 domain located at the N-terminus. The presence of two potential NLSs suggests that the protein may be localized to the nucleus. In addition, three nuclear export signals were also identified in the protein, further strengthening the hypothesis that the KCTD8 protein may shuttle between the cytoplasm and the nucleus. The KCTD8 homologue in zebrafish, *dex*, however does not possess these two NLS sites; the zebrafish KCTD8 protein product homologue is truncated prior to these sites. However, the nuclear export signals are conserved in the zebrafish homologue. Therefore, the function of the KCTD8 gene in rat, mouse and human may be distinct from the function in cow, zebrafish, *D. melanogaster*, and *C. elegans* due to the lack of the NLSs in the latter. Alternatively, KCTD8 may possess a dual function in higher vertebrates that involves shuttling to the nucleus. At present, the function of these predicted NLSs is being determined.

A third potential function domain identified in the KCTD8 protein is a conserved domain in the N-terminal region of the protein corresponding to a potassium channel tetramerization domain. This suggests that KCTD8 may function in regulating the membrane potential of the cell during degeneration. The K^+ channel tetramerization domain, known as the T1 domain, identified in KCTD8 is a highly conserved cytoplasmic portion at the N-terminal of the voltage-dependent K^+ channel α-subunit [34]. A K^+ channel forms from the association of four identical subunits with each subunit containing six transmembrane domains [35]. Ion channels function in cell signaling by mediating the transmission of electrical signals, most notably in nerve and muscle cells [36]. The T1 domain is believed to have a structural and evolutionary relationship with the BTB/POZ domain [25], which is a protein-protein interaction motif found at the N-terminus of some transcription factors as well as Shaw-type potassium channels [24, 26]. BTB/POZ domains can dimerize with other BTB/POZ domain containing proteins and can also mediate interactions between proteins containing other domains [26, 37, 38]. Proteins with BTB/POZ domains have been shown to be involved in transcription repression/activation, cytoskeletal organization and development [37-40].

Hydropathy plot analysis of KCTD8 does not indicate the presence of any transmembrane domains suggesting it does not function as a conventional K^+ channel. As well, the presence of the two potential NLSs in the KCTD8 protein is contrary to the membrane localization of K^+ channels. Thus, although KCTD8 appears not to be a K^+ channel subunit it may possess a novel function in the regulation of K^+ channels or in protein-protein interactions and perhaps transcription regulation. Despite the unlikely function of KCTD8 in potassium channel formation, the presence alone of the T1 domain in the rat KCTD8 protein, as well as in homologous proteins, has resulted in HUGO gene nomenclature referring to these proteins as "potassium channel tetramerization domain containing 8" (KCTD8) proteins.

Expression analysis of KCTD8 via northern blot indicated that the gene is predominantly expressed in the brain and retina, which is suggestive of a neuronal function for KCTD8. The gene is also expressed to a lesser extent in kidney and liver indicating a more ubiquitous expression pattern. This, however, does not rule out KCTD8 as having a potential function in retinal degeneration. A number of ubiquitously expressed genes have been known to underlie various retinal degenerative disorders [41-45]. During LIRD, KCTD8 displayed an inverse bell curve pattern of expression where the highest levels of expression was seen in dark-reared retinal RNA as well as RNA isolated from rats exposed to 16 hours of light. The time points between zero hours of light exposure and 16 hours of light exposure had very low levels of expression. Sixteen hours of light exposure is the peak of heme oxygenase-1 (HO-1) expression suggesting that the retina is experiencing a high level of oxidative stress at this time point and as a result is undergoing degeneration via apoptosis [46]. This interesting expression pattern of KCTD8 during different phases of LIRD suggests that the gene may have a role in the unaffected retina as well as during later stages of retinal degeneration. At present, it is unclear whether the gene is functioning in the same way during these two very different molecular states or whether the gene has a dual function in which it acts in one way in the unaffected retina and has a different function in the retina under a high level of oxidative stress.

Protein expression levels of KCTD8 during LIRD appear to remain relatively steady during the degeneration process suggesting that a basal level of protein is maintained despite cells of the retina undergoing apoptosis. The finding that the protein extraction method affects the predominance of the bands appearing by western analysis suggests that there are alternate protein isoforms of KCTD8 present in the rat retina. Similar results with respect to the variation of protein isoforms appearing with different protein extraction methods have also been seen for the clusterin protein in the retina [47]. The variation in size of the KCTD8 bands on the western blot may be due to the numerous predicted post-translational modifications of the protein. In any event, the peptide competition assay demonstrates that the KCTD8 polyclonal antibody is specific for all four bands appearing on the western blot and that KCTD8 exists as multiple isoforms.

In conclusion, we have isolated and characterized a novel KCTD family member in the rat retina and during retinal degeneration. The differential level of expression of the transcript during LIRD is suggestive of a role for the gene in retinal degeneration and perhaps retinal disease. Preliminary analysis of the protein suggests that, contrary to the gene name, it is not a typical potassium channel protein. This raises a number of questions as to the function of this gene and the importance and functionality of the T1 domain as well as the NLS signals. Future directions involving the determination of the functionality of the NLS signals, to be discussed in Chapters 4 and 5, as well as the T1 domain may aid in understanding the role KCTD8 in general as well as during retinal degeneration.

Figure 3.1 - Nucleotide and deduced amino acid sequence of the rat KCTD8 cDNA. The numbering of the nucleotide sequence starts at the predicted transcription start site (TSS), which is indicated in bold. Numbering of the protein sequence begins at the translation initiation codon. An asterisk indicates the stop codon of the amino acid sequence. The polyadenylation signals are underlined with a solid line. The sequence of rat KCTD8 has been deposited into the GenBank database under Accession No. EF043041.

```
                                        ↱ +1 TSS
  -33  AGTAGTTAGCGCCGGCGCCAGCGCTCCCGGCTGAGGCGCGCTGGCTCACAAGCAGCCGGGGGTGAGTTTTC  38
   39  TTCGCTCGGGCCCCGCCTCCTGCCCTCCCCTCCCAGAGCCGCGCGCAGCCCCCGAACCTCTCCAAGTCTCT  109
  110  TGTACACTTGCAGTCGGTCGCCCCAAAGGAGCAGCCGAGCTCGCGGAGCTCCATTCCTGAGAGTCTCTCCC  180
  181  CGATGGAGCTCGGGCGACTCCGACGCCGCTGCTGCCCGGAACCCTGAGCAGCGCCGGGTGCCTGGAGGACC  251
  252  GCGCCGGTCAGCCAGAGAGTGCCGGTTGACCGAGCGCACGCCGAGGACCCGAGACCTCGAGGCTCTGGGAA  322
  323  GCGCGCTGTGCGGCTCGCCCGGGTCACCTGGCCGGTGGCGGGACC ATG GCT TTG AAG GAC ACG  386
    1                                                 M   A   L   K   D   T    6

  387  GGC AGC GGC GGC AGC ACC ATC CTC CCG ATC AGC GAG ATG GTG TCC GCG TCC AGC  440
    7   G   S   G   G   S   T   I   L   P   I   S   E   M   V   S   A   S   S   24

  441  TCT CCA GGC GCT CCG CTG GCC GCC GCC CCA GGG CCC TGC GCC CCG TCT CCC TTC  494
   25   S   P   G   A   P   L   A   A   A   P   G   P   C   A   P   S   P   F   42

  495  CCG GAG GTA GTA GAA CTG AAT GTT GGC GGC CAG GTT TAT GTG ACC AAG CAT TCG  548
   43   P   E   V   V   E   L   N   V   G   G   Q   V   Y   V   T   K   H   S   60

  549  ACG TTG CTC AGC GTC CCG GAC AGC ACT CTG GCC AGC ATG TTC TCT CCC TCT AGT  602
   61   T   L   L   S   V   P   D   S   T   L   A   S   M   F   S   P   S   S   78

  603  CCC CGG GGC GGC GCT CGG CGC CGG GGC GAC TTG CCC AGG GAC AGC CGC GCG CGC  656
   79   P   R   G   G   A   R   R   R   G   D   L   P   R   D   S   R   A   R   96

  657  TTC TTC ATC GAC CGC GAC GGC TTC CTC TTT AGG TAC GTG CTG GAT TAC CTG CGC  710
   97   F   F   I   D   R   D   G   F   L   F   R   Y   V   L   D   Y   L   R   114

  711  GAC AAG CAG CTG GCG CTG CCC GAG CAC TTC CCC GAG AAG GAG AGG CTC CTG CGC  764
  115   D   K   Q   L   A   L   P   E   H   F   P   E   K   E   R   L   L   R   132

  765  GAG GCA GAG TTC TTC CAG CTT ACT GAC CTG GTC AAG CTG CTG TCG CCC AAG GTC  818
  133   E   A   E   F   F   Q   L   T   D   L   V   K   L   L   S   P   K   V   150

  819  ACC AAG CAG AAC TCG CTC AAC GAC GAG GGC TGC CAG AGC GAC CTG GAG GAC AAC  872
  151   T   K   Q   N   S   L   N   D   E   G   C   Q   S   D   L   E   D   N   168

  873  CTT TCC CAG GGC AGC AGC GAC GCA CTG CTG CTG CGT GGG GCG GCG GCC GGC GCG  926
  169   L   S   Q   G   S   S   D   A   L   L   L   R   G   A   A   A   G   A   186

  927  CCC TCG AGT TCT GGG GCA CAC GGT GTC AGT GGC GTT GTC AGT GGC GGC AGC GCT  980
  187   P   S   S   S   G   A   H   G   V   S   G   V   V   S   G   G   S   A   204

  981  CCG GAC AAG CGC TCT GGG TTC CTC ACA CTG GGC TAC CGT GGC TCC TAC ACC ACA  1034
  205   P   D   K   R   S   G   F   L   T   L   G   Y   R   G   S   Y   T   T   222

 1035  GTG CGA GAC AAC CAG GCA GAT GCC AAG TTT AGG CGT GTG GCG CGC ATC ATG GTG  1088
  223   V   R   D   N   Q   A   D   A   K   F   R   R   V   A   R   I   M   V   240

 1089  TGC GGG CGC ATA GCC TTG GCC AAG GAG GTC TTT GGG GAC ACT CTT AAT GAG AGT  1142
  241   C   G   R   I   A   L   A   K   E   V   F   G   D   T   L   N   E   S   258

 1143  CGC GAC CCT GAC CGT CAG CCT GAG AAG TAC ACA TCC CGC TTC TAC CTC AAG TTC  1196
  259   R   D   P   D   R   Q   P   E   K   Y   T   S   R   F   Y   L   K   F   276

 1197  ACC TAC TTG GAG CAG GCA TTC GAT CGA CTC TCT GAG GCT GGC TTC CAC ATG GTG  1250
  277   T   Y   L   E   Q   A   F   D   R   L   S   E   A   G   F   H   M   V   294

 1251  GCG TGC AAC TCC TCT GGC ACT GCC GCC TTT GTC AAC CAG TAC CGA GAC GAC AAG  1304
  295   A   C   N   S   S   G   T   A   A   F   V   N   Q   Y   R   D   D   K   312

 1305  ATC TGG AGC AGT TAT ACT GAA TAC ATC TTC TTC CGA CCA CCT CAG AAA ATA GTG  1358
  313   I   W   S   S   Y   T   E   Y   I   F   F   R   P   P   Q   K   I   V   330

 1359  TCA CCC AAA CAA GAA CAT GAA GAC AGG AAA TGT GAC AAA GTC ACA GAC AAA GGA  1412
  331   S   P   K   Q   E   H   E   D   R   K   C   D   K   V   T   D   K   G   348

 1413  AGT GAG AGT GGG ACT TCC TGC AAT GAG CTC TCC ACA TCC AGC TGT GAC AGC CAC  1466
  349   S   E   S   G   T   S   C   N   E   L   S   T   S   S   C   D   S   H   366
```

```
1467  TCA GAG GCC AGC ACT CCA CAG GAC AAC CTG GTC AAC ACT CAG CAG GCT GTA TCT   1520
 367   S   E   A   S   T   P   Q   D   N   L   V   N   T   Q   Q   A   V   S    384

1521  CAG CAG CCT AAC ACC TTA ACC TTG GAT AGA CCC TCC CGG AAA GCC CCT GTT CAG   1574
 385   Q   Q   P   N   T   L   T   L   D   R   P   S   R   K   A   P   V   Q    402

1575  TGG ATG CCG CCA CCA GAC AAG CGC AGA AAC AGT GAA CTC TTT CAG TCA CTC ATC   1628
 403   W   M   P   P   P   D   K   R   R   N   S   E   L   F   Q   S   L   I    420

1629  AGC AAG TCC CGA GAG ACA AAT CTC TCC AAA AAG AAG GTC TGC GAG AAG CTA AGT   1682
 421   S   K   S   R   E   T   N   L   S   K   K   K   V   C   E   K   L   S    438

1683  GTG GAA GAA GAA ATG AAA AAG TGT ATT CAG GAT TTT AAA AAA ATC CAC ATT CCA   1736
 439   V   E   E   E   M   K   K   C   I   Q   D   F   K   K   I   H   I   P    456

1737  GAT TGT TTT CCA GAG CGC AAA CGC CAG TGG CAA TCT GAA CTG CTC CAA AAA TAT   1790
 457   D   C   F   P   E   R   K   R   Q   W   Q   S   E   L   L   Q   K   Y    474

1791  GGG TTG TAG TAATGATGATGTTCTGGGCGTGTTTCGATGGCGTTCAATGTTTACTACCATGTCACCGC   1858
 475   G   L   *                                                                 476

1859  CTAACTGATGGCTGGTGTGATTCTTGCTGCTCTTCCTTTCTGTGAACAGTGGATGTGGACAGTATTTTTT   1929
1930  TTCATTACTTTTATTGTTGTTTTAGAAAGATAATTTTAAAAATGAAACCAACAAGTGTGTATCAAAATGG   2000
2001  TTTAGCTATCTGATTCAAGCCATTTTGTAATAATGAGCGTATAATGTGCATGATCAAGAAACTTAGAATCT   2071
2072  TGATTTTCGAGCTGTGGTTGACTGGACATGTTTGTCATTCTGTAACTCACAAAACAACAAGTTATCATATC   2142
2143  ACACCGATTGAGACAAGAATGTACATGAAAAGACATGAAATAAAAATTTCAACGATGGTTTTAGGACCCAA   2213
2214  ATATACAACTGTTTAAATGTTAATGCATTAAAACAAGTATTATTTTTTGCATGAACACAATGTTACAAATA   2284
2285  AATCTCAAGAAATAGGGAAGAACTGTTTGTGGCTTTGAAAGAAAAAATATTAAAAAATAAAGCAAATATAT   2355
2356  ATATATATGTAATATATATAATAGTTTCAGGCAAAGCCTGTAATTGTAAACTGTCTAGGATTGAACTTTTT   2326
2427  TGTTCCCGATCTGTGGTTCTTTTGTGTAAATGTAAGGTGTTTCCGTATGTTAAGATGGTGTAAATATGCTT   2497
2498  TATTCTGTTATGTTATAGCATCAACATTCATCAATCAAAACTAATCATGAATATTTCTGTGAAATGAGTCT   2568
2569  TTTTACATCAGGCTGTGAAACTCGTATAATGATGATTTAAAAGATTCCATTATCATGTTAATCAAAATAAT   2639
2640  TGAAGGAAATGGCAAAGAGCTTTATGTGTTTATTAAAAATGGAAAATGTATTAGAATTCCTTAATTTCTTC   2710
2711  TGACTTTTCTTTAAAAAATATTTTTTATCATCTTTGATGTTCATTTAAACACCATATTAGAGAATGGTTGA   2781
2782  CAAATTCAAATGTTGGAAAGATTGAACATAATTCAAACTGAGGTAGAGAGCCAGATCGT               2840
```

Figure 3.2 - Gene and protein structure of rat KCTD8.

A) Genomic organization of the KCTD8 gene. Rectangles represent exons with the size of the exon indicated within the rectangle. Open rectangles correspond to the open reading frame while shaded rectangles indicate the 5' and 3' untranslated regions (UTR). The intron is indicated by a solid horizontal line intervening the exons. The size of the intron is indicated below the horizontal solid line. The start (ATG) and stop codons (TAG) of the open reading frame are indicated. B) KCTD8 intron-exon boundary sequence. Sequence corresponding to the intron-flanking exons is indicated in upper case and intron sequence is indicated in lower case. C) Putative conserved domains identified in the KCTD8 protein. Towards the N-terminus of the protein is a BTB/POZ/T1 domain shown with diagonal shading. The C-terminal end of the protein contains two nuclear localization signals (NLS) shown with crosshatch shading.

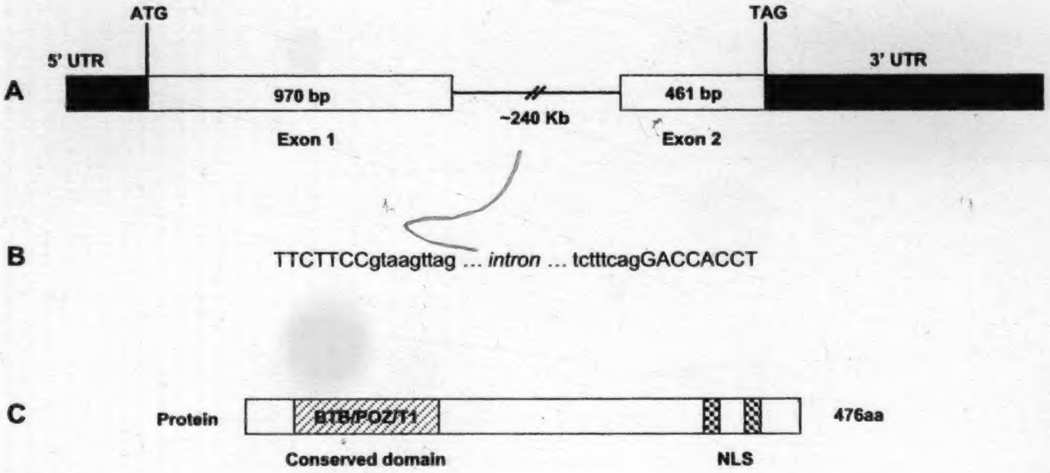

Figure 3.3 - Protein sequence alignment of rat KCTD8 and homologues identified in other species.

The protein sequence of *R. norvegicus* (GenBank Accession No. EF043041), *M. musculus* (GenBank Accession No. NP_780728), *H. sapiens* (GenBank Accession No. NP_938167), *B. taurus* (GenBank Accession No. XP_590048), *D. rerio* (GenBank Accession No. NP_001032318), *D. melanogaster* (GenBank Accession No. NP_650926), and *C. elegans* (GenBank Accession No. T26019) homologues were aligned using ClustalW (version 1.82). Amino acids identical in the sequence of all seven species are shown on a black background. Conserved amino acid substitutions are shaded in gray. Asterisks below the alignment indicate residues that are identical in all seven homologues. The BTB/POZ/T1 domain is outlined with a solid line. The NLS are also outlined, with the pattern7 motif indicated by a dotted line and the bipartite basic NLS outlined with a dashed line. Arrows below the alignment represent the NES. The predicted phosphorylation sites are indicated by arrowheads above the sequence. Three potential O-glycosylation sites were also identified and are indicated by a circle above the sequence. The four predicted N-glycosylation sites are indicated by a square above the sequence.

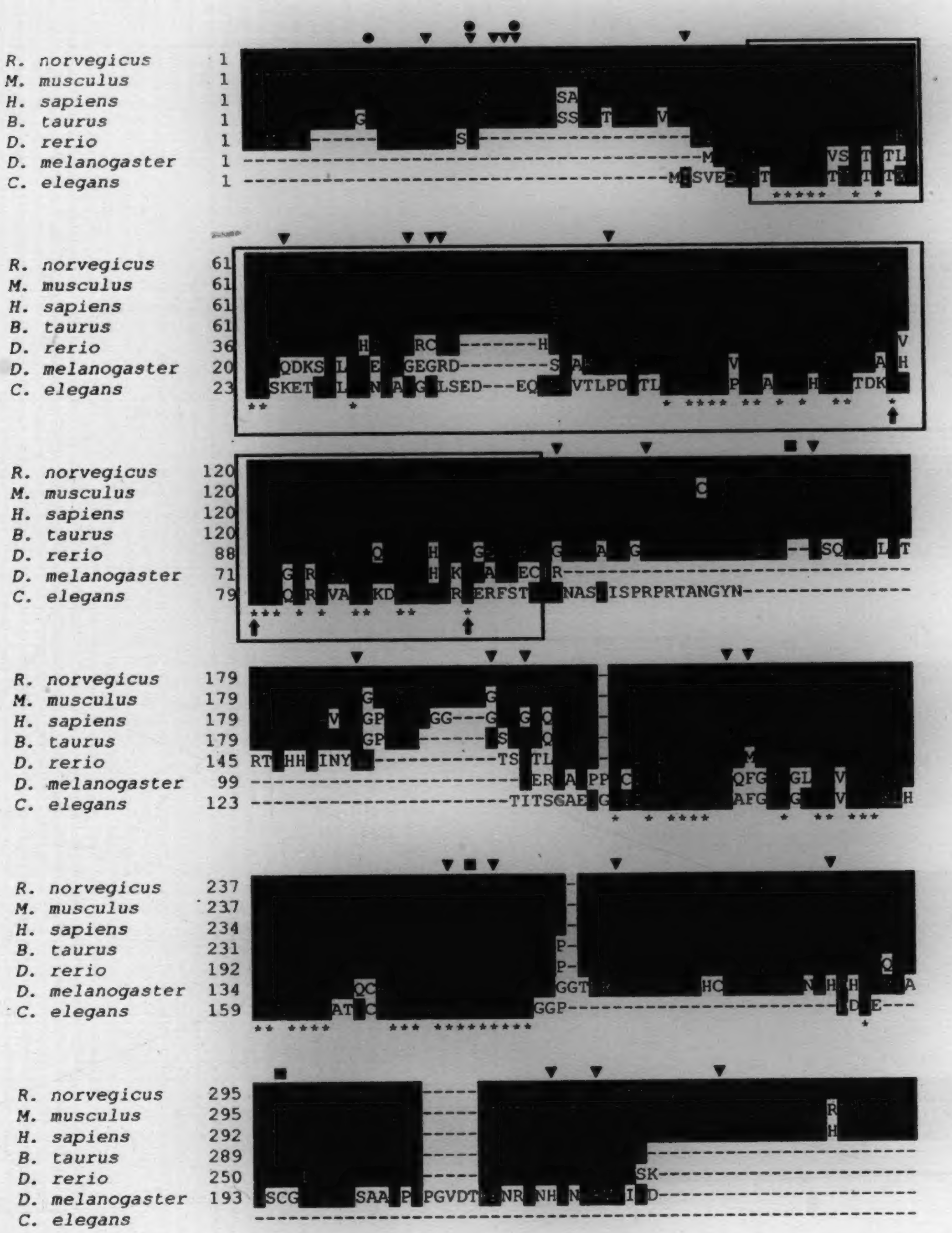
R. norvegicus
M. musculus
H. sapiens
B. taurus
D. rerio
D. melanogaster
C. elegans
ISPRPRTANGYN
TITSGAE
GGP
PGVDT

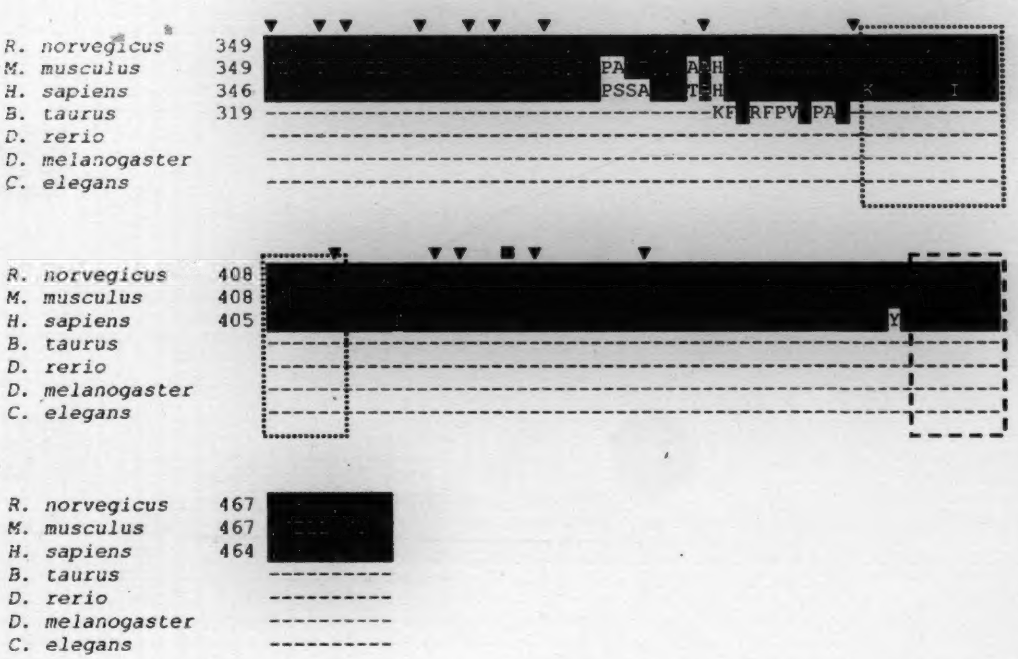
R. norvegicus 349
M. musculus 349
H. sapiens 346
B. taurus 319
D. rerio
D. melanogaster
C. elegans
PA
AH
PSSA
TH
KF
RFPV
PA
K
I
R. norvegicus 408
M. musculus 408
H. sapiens 405
B. taurus
D. rerio
D. melanogaster
C. elegans
Y
R. norvegicus 467
M. musculus 467
H. sapiens 464
B. taurus
D. rerio
D. melanogaster
C. elegans

Figure 3.4 – Protein conservation of KCTD8 in bacteria and eukaryotes.

The protein conservation of human KCTD8 was bioinformatically determined using STRING. The strength of the homology with sequences in other organisms is indicated by a colour grading scheme where white indicates no homology, light red/pink indicates a low level of homology and shades of darker red indicate higher homology.

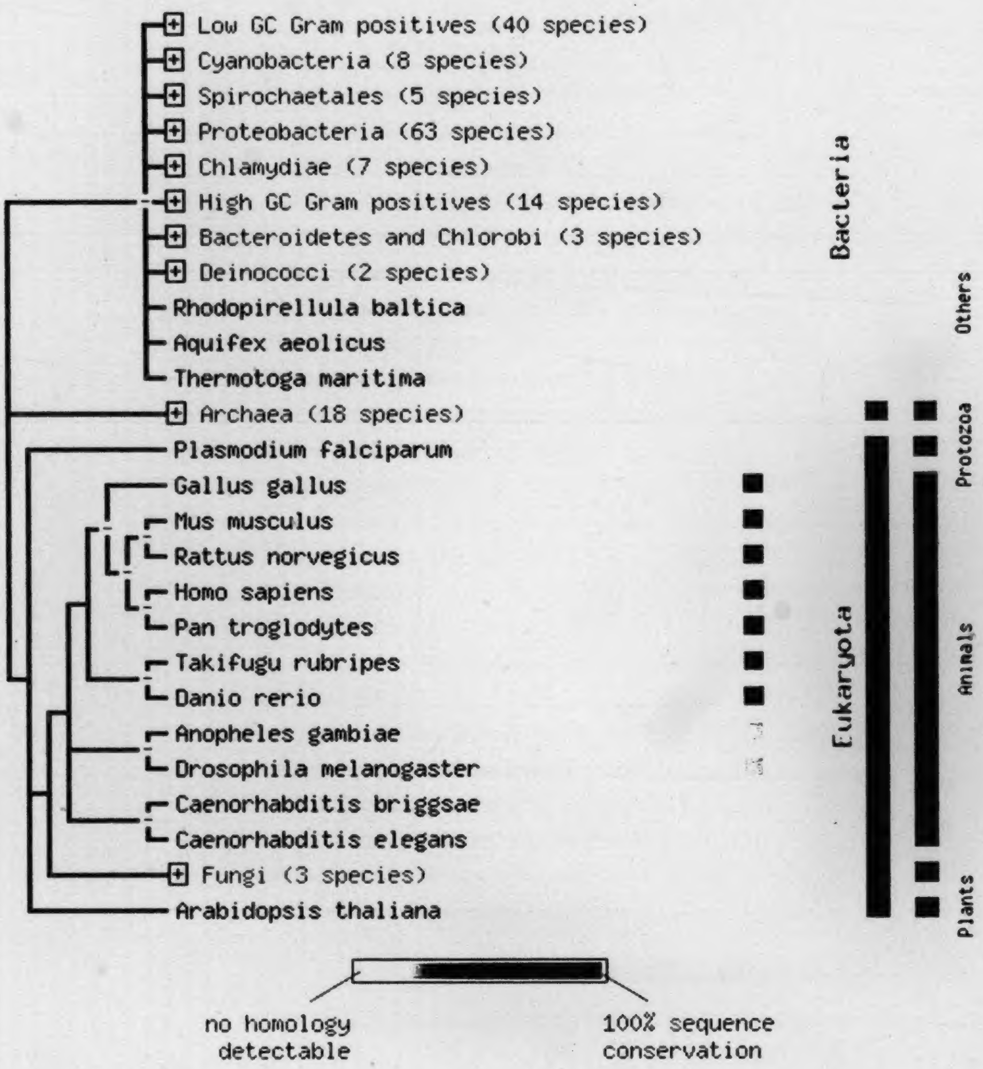

Figure 3.5 - Genomic conservation of KCTD8.

Southern zooblot analysis of genomic DNA from various species was performed to determine evolutionary conservation of KCTD8.

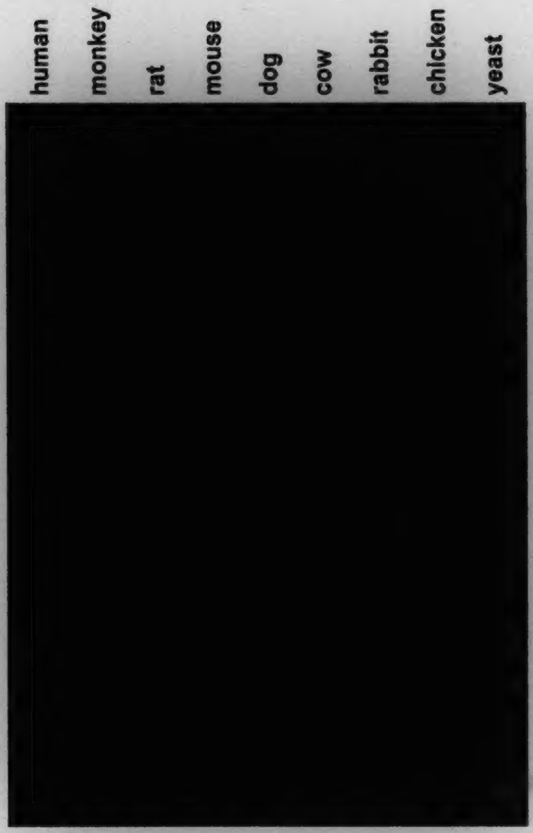

Figure 3.6 - Hydropathy plot analysis of KCTD8.

The KCTD8 protein was analyzed for hydrophobic and hydrophilic regions of the protein as well as for the existence of transmembrane domains. The numbers on the x-axis indicate amino acid residue number and the numbers on the y-axis are a rating of hydrophobicity and hydrophilicity. Peaks above 0.0 indicate hydrophobic regions whereas peaks below 0.0 indicate hydrophilic regions of the protein. Peaks beginning and ending within the hydrophobic region of the plot (0.0 to 4.0 on the y-axis) indicate transmembrane domains, based on the algorithm of Kyte and Doolittle [18]. None of the peaks display a pattern indicative of transmembrane domains.

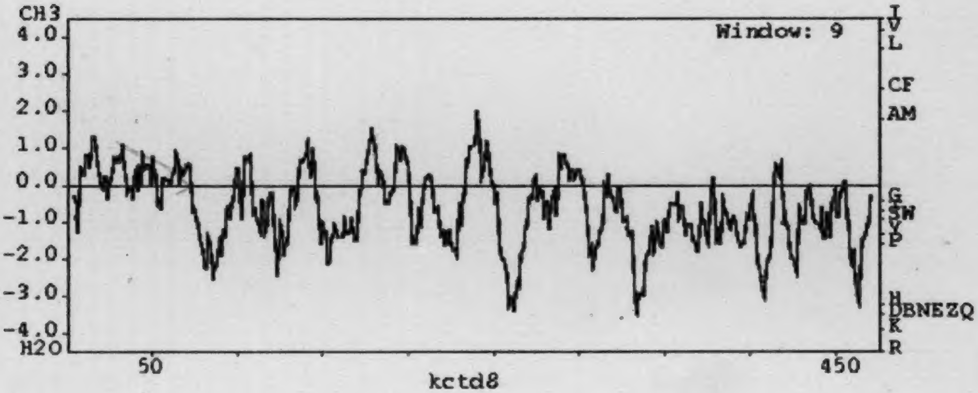

Figure 3.7 - Multiple tissue northern blot analysis of rat KCTD8.

A radiolabeled KCTD8 cDNA probe was used to probe total RNA from various rat tissues. The sizes of the observed transcripts are shown on the left of the autoradiograph. The 18S ribosomal band is shown as a loading control.

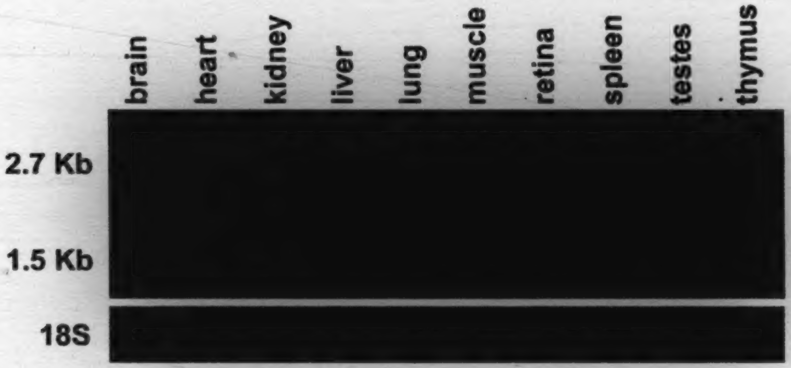

Figure 3.8 – Expression analysis of rat KCTD8 during LIRD.

A) Hybridization levels of the 0 hr (dark-reared) and 16 hour light treated cDNA probes to the KCTD8 PCR product on the macroarray from the tertiary screen of the cDNA library [8]. B) A radiolabeled KCTD8 cDNA probe was used to probe total RNA from rat retinas exposed to increasing durations of light. The size of the observed transcript is shown on the left of the autoradiograph. The 18S ribosomal band is shown as a loading control. C) Graphical analysis of the RNA expression levels on the northern blot. Expression levels are normalized to the 18S ribosomal band.

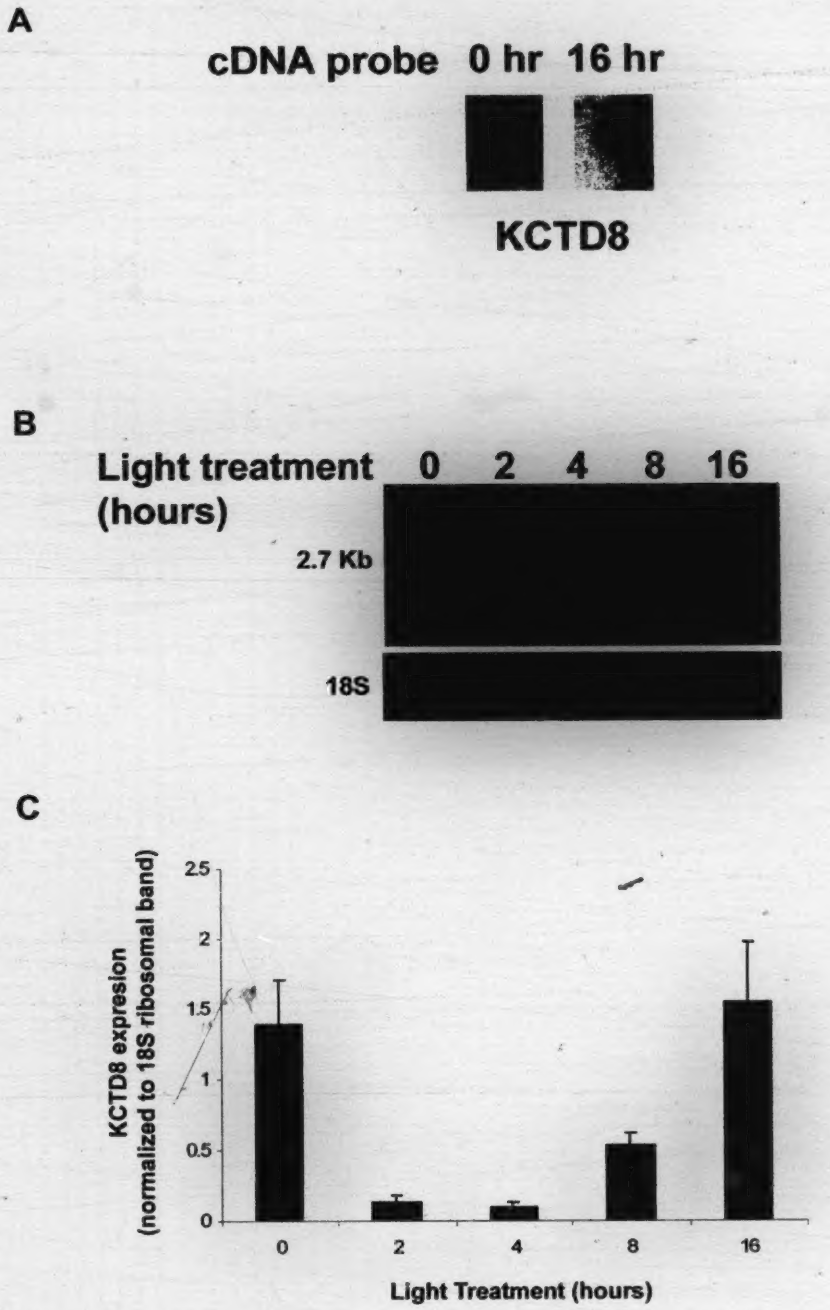
A
cDNA probe
0 hr
16 hr
KCTD8
B
Light treatment (hours)
0
2
4
8
16
2.7 Kb
18S
C
KCTD8 expresion (normalized to 18S ribosomal band)
2.5
2
1.5
1
0.5
0
0
2
4
8
16
Light Treatment (hours)

Figure 3.9 - Western blot analysis of KCTD8.

A polyclonal KCTD8 antibody was used for immunodetection to A) Trizol isolated retinal proteins from rats exposed to increasing durations of light or B) RIPA isolated retinal proteins from dark-reared rats. Sizes of the observed bands are shown between the two figures. C) Graphical analysis of the KCTD8 protein levels observed by the western blot analysis in (A). Expression levels are normalized to β-actin. D) Peptide competition assay in which the KCTD8 antibody was incubated with an increasing amount competing peptide before immunobinding to dark-reared rat retinal proteins. Lane 1: no peptide, Lane 2: 50 ng of peptide, Lane 3: 500 ng peptide, Lane 4: 5 μg peptide. In all three figures, β-actin is shown as a loading control.

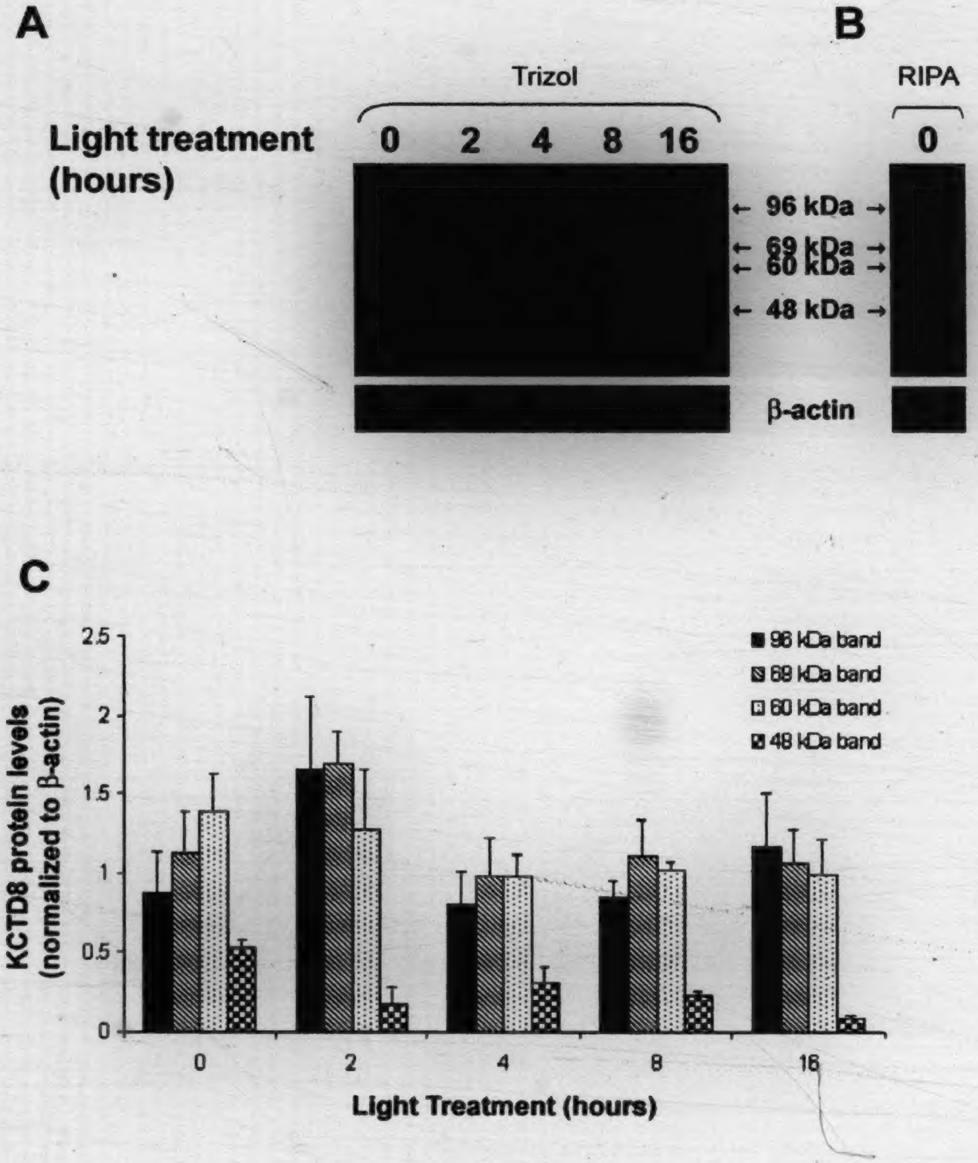
A
B
Trizol
RIPA
Light treatment (hours)
0
2
4
8
16
0
← 96 kDa →
← 69 kDa →
← 60 kDa →
← 48 kDa →
β-actin
C
KCTD8 protein levels (normalized to β-actin)
2.5
2
1.5
1
0.5
0
■ 96 kDa band
▨ 69 kDa band
▤ 60 kDa band
▩ 48 kDa band
0
2
4
8
16
Light Treatment (hours)

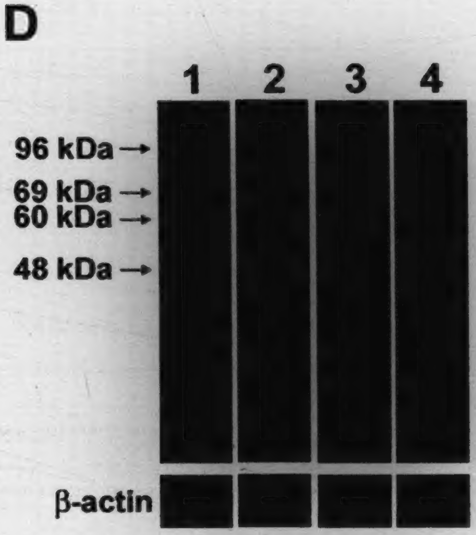
D
1
2
3
4
96 kDa →
69 kDa →
60 kDa →
48 kDa →
β-actin

3.5 REFERENCES

1. Portera-Cailliau, C., Sung, C.H., Nathans, J. and Adler, R. (1994) Apoptotic photoreceptor cell death in mouse models of retinitis pigmentosa. *Proc Natl Acad Sci U S A,* **91,** 974-8.
2. Chang, G.Q., Hao, Y. and Wong, F. (1993) Apoptosis: final common pathway of photoreceptor death in rd, rds, and rhodopsin mutant mice. *Neuron,* **11,** 595-605.
3. Noell, W.K., Walker, V.S., Kang, B.S. and Berman, S. (1966) Retinal damage by light in rats. *Investigative Ophthalmology,* **5,** 450-472.
4. Organisciak, D.T. and Winkler, B.S. (1994) Retinal light damage: practical and theoretical considerations. In Osborne, N. and Chader, G. (eds.), *Progress in Retinal and Eye Research.* Pergamon Press, New York, pp. 1-29.
5. Organisciak, D.T., Darrow, R.M. and Barsalou, L.S. (2003) Light-induced retinal degeneration. In Levin, L.A. and Di Polo, A. (eds.), *Ocular Neuroprotection.* Marcel Dekker, p. 344.
6. Wenzel, A., Grimm, C., Samardzija, M. and Reme, C.E. (2005) Molecular mechanisms of light-induced photoreceptor apoptosis and neuroprotection for retinal degeneration. *Prog Retin Eye Res,* **24,** 275-306.
7. Grewal, R., Stepczynski, J., Kelln, R., Erickson, T., Darrow, R., Barsalou, L., Patterson, M., Organisciak, D.T. and Wong, P. (2004) Coordinated changes in classes of ribosomal protein gene expression is associated with light-induced retinal degeneration. *Invest Ophthalmol Vis Sci,* **45,** 3885-95.
8. Kelln, R.M., Organisciak, D.T., Darrow, R., Wong, P. (In preparation) Identification and characterization of T-cadherin, isolated by a differential screening strategy to identify genes involved in light-induced retinal degeneration.
9. Okazaki, Y. and Furuno, M. and Kasukawa, T. and Adachi, J. and Bono, H. and Kondo, S. and Nikaido, I. and Osato, N. and Saito, R. and Suzuki, H. and Yamanaka, I. and Kiyosawa, H. and Yagi, K. and Tomaru, Y. and Hasegawa, Y. and Nogami, A. and Schonbach, C. and Gojobori, T. and Baldarelli, R. and Hill, D.P. and Bult, C. and Hume, D.A. and Quackenbush, J. and Schriml, L.M. and Kanapin, A. and Matsuda, H. and Batalov, S. and Beisel, K.W. and Blake, J.A. and Bradt, D. and Brusic, V. and Chothia, C. and Corbani, L.E. and Cousins, S.

and Dalla, E. and Dragani, T.A. and Fletcher, C.F. and Forrest, A. and Frazer, K.S. and Gaasterland, T. and Gariboldi, M. and Gissi, C. and Godzik, A. and Gough, J. and Grimmond, S. and Gustincich, S. and Hirokawa, N. and Jackson, I.J. and Jarvis, E.D. and Kanai, A. and Kawaji, H. and Kawasawa, Y. and Kedzierski, R.M. and King, B.L. and Konagaya, A. and Kurochkin, I.V. and Lee, Y. and Lenhard, B. and Lyons, P.A. and Maglott, D.R. and Maltais, L. and Marchionni, L. and McKenzie, L. and Miki, H. and Nagashima, T. and Numata, K. and Okido, T. and Pavan, W.J. and Pertea, G. and Pesole, G. and Petrovsky, N. and Pillai, R. and Pontius, J.U. and Qi, D. and Ramachandran, S. and Ravasi, T. and Reed, J.C. and Reed, D.J. and Reid, J. and Ring, B.Z. and Ringwald, M. and Sandelin, A. and Schneider, C. and Semple, C.A. and Setou, M. and Shimada, K. and Sultana, R. and Takenaka, Y. and Taylor, M.S. and Teasdale, R.D. and Tomita, M. and Verardo, R. and Wagner, L. and Wahlestedt, C. and Wang, Y. and Watanabe, Y. and Wells, C. and Wilming, L.G. and Wynshaw-Boris, A. and Yanagisawa, M. and Yang, I. and Yang, L. and Yuan, Z. and Zavolan, M. and Zhu, Y. and Zimmer, A. and Carninci, P. and Hayatsu, N. and Hirozane-Kishikawa, T. and Konno, H. and Nakamura, M. and Sakazume, N. and Sato, K. and Shiraki, T. and Waki, K. and Kawai, J. and Aizawa, K. and Arakawa, T. and Fukuda, S. and Hara, A. and Hashizume, W. and Imotani, K. and Ishii, Y. and Itoh, M. and Kagawa, I. and Miyazaki, A. and Sakai, K. and Sasaki, D. and Shibata, K. and Shinagawa, A. and Yasunishi, A. and Yoshino, M. and Waterston, R. and Lander, E.S. and Rogers, J. and Birney, E. and Hayashizaki, Y. (2002) Analysis of the mouse transcriptome based on functional annotation of 60,770 full-length cDNAs. *Nature,* **420,** 563-73.

10. Gamse, J.T., Kuan, Y.S., Macurak, M., Brosamle, C., Thisse, B., Thisse, C. and Halpern, M.E. (2005) Directional asymmetry of the zebrafish epithalamus guides dorsoventral innervation of the midbrain target. *Development,* **132,** 4869-81.
11. Kruger, N.J. (1994) The Bradford method for protein quantitation. *Methods Mol Biol,* **32,** 9-15.
12. Altschul, S.F., Gish, W., Miller, W., Myers, E.W. and Lipman, D.J. (1990) Basic Local Alignment Search Tool. *Journal of Molecular Biology,* **215,** 403-410.

13. Marchler-Bauer, A., Anderson, J.B., DeWeese-Scott, C., Fedorova, N.D., Geer, L.Y., He, S., Hurwitz, D.I., Jackson, J.D., Jacobs, A.R., Lanczycki, C.J., Liebert, C.A., Liu, C., Madej, T., Marchler, G.H., Mazumder, R., Nikolskaya, A.N., Panchenko, A.R., Rao, B.S., Shoemaker, B.A., Simonyan, V., Song, J.S., Thiessen, P.A., Vasudevan, S., Wang, Y., Yamashita, R.A., Yin, J.J. and Bryant, S.H. (2003) CDD: a curated Entrez database of conserved domain alignments. *Nucleic Acids Res,* **31,** 383-7.

14. Thompson, J.D., Higgins, D.G. and Gibson, T.J. (1994) CLUSTAL W: improving the sensitivity of progressive multiple sequence alignment through sequence weighting, position-specific gap penalties and weight matrix choice. *Nucleic Acids Res,* **22,** 4673-80.

15. von Mering, C., Jensen, L.J., Snel, B., Hooper, S.D., Krupp, M., Foglierini, M., Jouffre, N., Huynen, M.A. and Bork, P. (2005) STRING: known and predicted protein-protein associations, integrated and transferred across organisms. *Nucleic Acids Res,* **33,** D433-7.

16. von Mering, C., Huynen, M., Jaeggi, D., Schmidt, S., Bork, P. and Snel, B. (2003) STRING: a database of predicted functional associations between proteins. *Nucleic Acids Res,* **31,** 258-61.

17. Snel, B., Lehmann, G., Bork, P. and Huynen, M.A. (2000) STRING: a web-server to retrieve and display the repeatedly occurring neighbourhood of a gene. *Nucleic Acids Res,* **28,** 3442-4.

18. Kyte, J. and Doolittle, R.F. (1982) A simple method for displaying the hydropathic character of a protein. *J Mol Biol,* **157,** 105-32.

19. Abramoff, M.D., Magelhaes, P.J., Ram, S.J. (2004) Image Processing with ImageJ. *Biophotonics International,* **11,** 36-42.

20. Proudfoot, N. (1991) Poly(A) signals. *Cell,* **64,** 671-674.

21. Padgett, R.A., Grabowski, P.J., Konarska, M.M., Seiler, S. and Sharp, P.A. (1986) Splicing of messenger RNA precursors. *Annu Rev Biochem,* **55,** 1119-50.

22. Blom, N., Gammeltoft, S. and Brunak, S. (1999) Sequence and structure-based prediction of eukaryotic protein phosphorylation sites. *J Mol Biol,* **294,** 1351-62.

23. Julenius, K., Molgaard, A., Gupta, R. and Brunak, S. (2005) Prediction, conservation analysis, and structural characterization of mammalian mucin-type O-glycosylation sites. *Glycobiology,* **15,** 153-164.

24. Marchler-Bauer, A., Anderson, J.B., Cherukuri, P.F., DeWeese-Scott, C., Geer, L.Y., Gwadz, M., He, S., Hurwitz, D.I., Jackson, J.D., Ke, Z., Lanczycki, C.J., Liebert, C.A., Liu, C., Lu, F., Marchler, G.H., Mullokandov, M., Shoemaker, B.A., Simonyan, V., Song, J.S., Thiessen, P.A., Yamashita, R.A., Yin, J.J., Zhang, D. and Bryant, S.H. (2005) CDD: a Conserved Domain Database for protein classification. *Nucleic Acids Res,* **33,** D192-6.

25. Aravind, L. and Koonin, E.V. (1999) Fold prediction and evolutionary analysis of the POZ domain: structural and evolutionary relationship with the potassium channel tetramerization domain. *J Mol Biol,* **285,** 1353-61.

26. Bardwell, V.J. and Treisman, R. (1994) The POZ domain: a conserved protein-protein interaction motif. *Genes Dev,* **8,** 1664-77.

27. Hicks, G.R. and Raikhel, N.V. (1995) Protein import into the nucleus: an integrated view. *Annu Rev Cell Dev Biol,* **11,** 155-88.

28. Christophe, D., Christophe-Hobertus, C. and Pichon, B. (2000) Nuclear targeting of proteins: how many different signals? *Cell Signal,* **12,** 337-41.

29. Robbins, J., Dilworth, S.M., Laskey, R.A. and Dingwall, C. (1991) Two interdependent basic domains in nucleoplasmin nuclear targeting sequence: identification of a class of bipartite nuclear targeting sequence. *Cell,* **64,** 615-23.

30. la Cour, T., Kiemer, L., Molgaard, A., Gupta, R., Skriver, K. and Brunak, S. (2004) Analysis and prediction of leucine-rich nuclear export signals. *Protein Eng Des Sel,* **17,** 527-36.

31. Horton, P. and Nakai, K. (1997) Better prediction of protein cellular localization sites with the k nearest neighbors classifier. *Proc Int Conf Intell Syst Mol Biol,* **5,** 147-52.

32. Hawrani, A., Dempsey, C.E., Banfield, M.J., Scott, D.J., Clarke, A.R. and Kenny, B. (2003) Effect of Protein Kinase A-mediated Phosphorylation on the Structure and Association Properties of the Enteropathogenic Escherichia coli Tir Virulence Protein. *J. Biol. Chem.,* **278,** 25839-25846.

33. http://au.expasy.org/tools/findmod/findmod_masses.html (December 2006) ExPASy FindMod tool.

34. Cushman, S.J., Nanao, M.H., Jahng, A.W., DeRubeis, D., Choe, S. and Pfaffinger, P.J. (2000) Voltage dependent activation of potassium channels is coupled to T1 domain structure. *Nat Struct Biol,* **7,** 403-7.

35. Hille, B. (1992) *Ionic Channels of Excitable Membranes.* 2nd ed. Sinauer Associates Inc, Sunderland.

36. Cooper, G.M. and Hausman, R.E. (2004) *The Cell: A molecular approach.* 3rd ed. Sinauer Associates Inc., Sunderland.

37. Dhordain, P., Albagli, O., Ansieau, S., Koken, M.H., Deweindt, C., Quief, S., Lantoine, D., Leutz, A., Kerckaert, J.P. and Leprince, D. (1995) The BTB/POZ domain targets the LAZ3/BCL6 oncoprotein to nuclear dots and mediates homomerisation in vivo. *Oncogene,* **11,** 2689-97.

38. Li, X., Lopez-Guisa, J.M., Ninan, N., Weiner, E.J., Rauscher, F.J., 3rd and Marmorstein, R. (1997) Overexpression, purification, characterization, and crystallization of the BTB/POZ domain from the PLZF oncoprotein. *J Biol Chem,* **272,** 27324-9.

39. Melnick, A., Carlile, G., Ahmad, K.F., Kiang, C.L., Corcoran, C., Bardwell, V., Prive, G.G. and Licht, J.D. (2002) Critical residues within the BTB domain of PLZF and Bcl-6 modulate interaction with corepressors. *Mol Cell Biol,* **22,** 1804-18.

40. Albagli, O., Dhordain, P., Deweindt, C., Lecocq, G. and Leprince, D. (1995) The BTB/POZ domain: a new protein-protein interaction motif common to DNA- and actin-binding proteins. *Cell Growth Differ,* **6,** 1193-8.

41. Inglis-Broadgate, S.L., Ocaka, L., Banerjee, R., Gaasenbeek, M., Chapple, J.P., Cheetham, M.E., Clark, B.J., Hunt, D.M. and Halford, S. (2005) Isolation and characterization of murine Cds (CDP-diacylglycerol synthase) 1 and 2. *Gene,* **356,** 19-31.

42. McKie, A.B., McHale, J.C., Keen, T.J., Tarttelin, E.E., Goliath, R., van Lith-Verhoeven, J.J., Greenberg, J., Ramesar, R.S., Hoyng, C.B., Cremers, F.P., Mackey, D.A., Bhattacharya, S.S., Bird, A.C., Markham, A.F. and Inglehearn,

C.F. (2001) Mutations in the pre-mRNA splicing factor gene PRPC8 in autosomal dominant retinitis pigmentosa (RP13). *Hum Mol Genet,* **10,** 1555-62.

43. Stone, E.M., Lotery, A.J., Munier, F.L., Heon, E., Piguet, B., Guymer, R.H., Vandenburgh, K., Cousin, P., Nishimura, D., Swiderski, R.E., Silvestri, G., Mackey, D.A., Hageman, G.S., Bird, A.C., Sheffield, V.C. and Schorderet, D.F. (1999) A single EFEMP1 mutation associated with both Malattia Leventinese and Doyne honeycomb retinal dystrophy. *Nat Genet,* **22,** 199-202.

44. Gal, A., Li, Y., Thompson, D.A., Weir, J., Orth, U., Jacobson, S.G., Apfelstedt-Sylla, E. and Vollrath, D. (2000) Mutations in MERTK, the human orthologue of the RCS rat retinal dystrophy gene, cause retinitis pigmentosa. *Nat Genet,* **26,** 270-1.

45. Ahmed, Z.M., Riazuddin, S. and Wilcox, E.R. (2003) The molecular genetics of Usher syndrome. *Clin Genet,* **63,** 431-44.

46. Wong, P., Kutty, R.K., Darrow, R.M., Shivaram, S., Kutty, G., Fletcher, R.T., Wiggert, B., Chader, G. and Organisciak, D.T. (1994) Changes in clusterin expression associated with light-induced retinal damage in rats. *Biochem Cell Biol,* **72,** 499-503.

47. Wong, P., Ulyanova, T., Organisciak, D.T., Bennett, S., Lakins, J., Arnold, J.M., Kutty, R.K., Tenniswood, M., vanVeen, T., Darrow, R.M. and Chader, G. (2001) Expression of multiple forms of clusterin during light-induced retinal degeneration. *Current Eye Research,* **23,** 157-165.

Chapter 4

Functional Analysis of the KCTD8 protein by Mutagenesis and Subcellular Localization

4.1 INTRODUCTION

The potassium channel tetramerization domain containing 8 (KCTD8) gene is a member of the KCTD gene family. This family of genes currently consists of 21 members that are grouped together based on the presence of an N-terminal domain that is homologous to the tetramerization domain (T1) of the Shaker class of voltage-gated potassium channels [1-3] and is distantly related to the BTB/POZ (broad complex tramtrack bric-a-brac/pox-virus and zinc finger) domain [4]. Aside from a conserved N-terminal domain, the members of the KCTD gene family contain no additional features of channel proteins. Various KCTD family members are involved in a wide spectrum of cellular functions including: suppression of Hedgehog signaling in medullablastoma [5]; as a transcriptional cofactor [6]; a role in TNF-α-induced DNA replication/repair [7]; and expression in the human fetal cochlea [8].

The rat KCTD8 gene was initially isolated from a screen for genes involved in light-induced retinal degeneration (LIRD) that I did several years ago [9]. In a subsequent study I found that KCTD8 was primarily expressed in the rat retina and brain, suggesting a neuronal function for the gene [10]. During the course of LIRD, KCTD8 was expressed in the unaffected retina (rats reared under strictly dark conditions) as well as in the retina under a high level of oxidative stress after prolonged light exposure. This suggests that KCTD8 may have a dual function wherein it functions in the normal unaffected retina as well as during oxidative stress and active cell death states.

Contrary to the gene name implying that the protein is involved in potassium channel formation, rat KCTD8 does not contain transmembrane domains [10], a hallmark of potassium channel proteins [11]. Additionally, bioinformatic analysis of KCTD8 revealed the presence of two putative nuclear localization signals (NLSs) [10], which is in contrast to the cell membrane localization of channel proteins. Bioinformatic analysis also revealed three putative nuclear export signals (NES) [10], suggesting that KCTD8 may shuttle in and out of the nucleus. To study the functionality of the NLSs and determine the subcellular localization of KCTD8, mammalian expression constructs encoding the KCTD8 protein fused to a green fluorescent protein (GFP) tag [12] were transiently transfected into cultured mammalian cells. In addition, constructs were engineered that contained mutations in one or both NLSs and the subcellular localization of these mutant constructs was also analyzed in cell culture. Since a clone for this gene was initially isolated from a retinal cDNA library, we also examined the localization of KCTD8 in the rat retina. Our results demonstrate that KCTD8 interacts with α-tubulin and microtubules *in vitro* and *in vivo* and that this binding to microtubules is mediated by the NLSs present in the KCTD8 protein.

4.2 MATERIALS AND METHODS

4.2.1 Animals

Male albino Sprague-Dawley rats (Harlan Inc, Indianapolis, IN) were obtained just after weaning and maintained in strict dark conditions until 60 days of age prior to use. Animals were cared for in accordance with the guidelines defined by the ARVO Statement for the Use of Animals in Ophthalmic and Vision Research.

4.2.2 KCTD8 subcloning and site-directed mutagenesis

The entire coding region of wild-type KCTD8 was PCR amplified, using Platinum Taq DNA Polymerase High Fidelity (Invitrogen, Carlsbad, CA), from a pBluescript plasmid containing the full-length sequence using the forward primer 5'-ATATAAGCTTCCATGGCTTTGAAGGACAC -3' and the reverse primer 5'–TTAAGGATCCCACGCCCAGAACATCATCA -3', which contain *Hind*III and *Bam*HI restriction sites, respectively. The PCR product was gel electrophoresed and extracted from the gel using a QIAquick Gel Extraction Kit (Qiagen, Mississauga, ON). The purified product was subcloned into the pDrive cloning vector using the QIAGEN PCR cloning kit, according to the manufacturer's instructions (Qiagen), in order to obtain enough of the cut KCTD8 open reading frame insert for subcloning into the GFP vector. Plasmids containing the correct sized inserts, ~1.7 kb, were confirmed by colony PCR using vector specific primers. The complete open reading frame of KCTD8 was digested out of the pDrive vector using *Hind*III and *Bam*HI and directionally ligated into the corresponding sites of the linearized pEGFP-C1 mammalian expression vector (Clontech Laboratories Inc., Mountain View, CA). Plasmids containing the correct full-length KCTD8 cDNA in-frame with the pEGFP-C1 vector were verified by sequencing.

Mutations in the putative NLSs of KCTD8 were generated by site-directed mutagenesis using the QuikChange Site-Directed Mutagenesis Kit (Stratagene, La Jolla, CA) according to the manufacturer’s protocol. Polyacrylamide gel electrophoresis (PAGE) purified oligonucleotide primers containing the mutated nucleotides were used to introduce the sequence variants. The mutations in the NLS1 site were introduced into the wild-type KCTD8 cDNA sequence using two subsequent mutagenesis reactions. The first reaction used the forward primer 5’–CTTGGATAGACCCTCCGCGGCAGCCCCTGTTCAGTGGATG–3’ and the reverse primer 5’–CATCCACTGAACAGGGGCTGCCGCGGAGGGTCTATCCAAG–3’ to introduce mutations changing codon 397R to 397A and codon 398K to 398A. The product resulting from this reaction was used to introduce a second set of mutations in the NLS1 site. Mutations changing codons 409K to 409A, 410R to 410A, and 411R to 411A were introduced using forward primer 5’–GTGGATGCCGCCACCAGACGCGGCCGCAAACAGTGAACTCTTTCAGTC–3’ and reverse primer 5’-GACTGAAAGAGTTCACTGTTTGCGGCCGCGTCTGGTGGCGGCATCCAC–3’. Mutations in the NLS2 site were introduced into the wild-type KCTD8 cDNA sequence using forward primer 5’-ATTCCAGATTGTTTTCCAGAGGCCGCAGCCCAGTGGCAATCTGAACTGCTC–3’ and reverse primer 5’-GAGCAGTTCAGATTGCCACTGGGCTGCGGCCTCTGGAAAACAATCTGGAAT–3’. Mutations to the NLS2 site changed codons 462R to 462A, 463K to 463A, and 464R to 464A. For the double mutant, in which both NLS sites were mutated (NLS1/2), pEGFP-KCTD8 plasmids that contained mutations in the NLS1 site were used as the template for incorporation of mutations in the NLS2 site, thus creating a plasmid in which both the NLS1 and NLS2 sites were mutated. To determine the sequence integrity, in-frame cloning with the GFP fusion tag, and absence of any sequence artifacts introduced by way of PCR or cloning, the entire KCTD8 cDNA insert for all plasmids was sequence verified. All constructs in the pEGFP vector will be referred to collectively as GFP constructs.

4.2.3 Mammalian cell culture and transfection

African green monkey kidney (COS-7) cells were commercially obtained (American Type Culture Collection, Rockville, MD) and grown in Dulbecco's modified Eagles medium (DMEM) (Invitrogen) supplemented with 10% fetal bovine serum in T-75 flasks with an atmosphere of 10% CO_2 at 37°C. The cells were seeded on Lab-Tek II four-chamber slides (Nalge Nunc, Naperville, IL), grown to a confluence of 80-90%, and then transiently transfected with pEGFP-KCTD8 wild-type or NLS mutant expression constructs or the empty pEGFP-C1 vector. As a control, mock transfections were also performed identical to the other transfections but with the omission of DNA. Transfections were performed using Lipofectamine 2000 transfection reagent (Invitrogen) according to the manufacturer's instructions. Transfected cells were cultured for 48 hours post-transfection and used for immunocytochemistry, immunoblotting, and co-immunoprecipitation.

4.2.4 Cell treatments and immunocytochemistry

Cells transfected with the GFP constructs were treated with 2 μM or 5 μM colcemid or 20 nM leptomycin for 6 hours at 37°C. Untreated control cells were left to incubate for 6 hours at 37°C so that both the untreated and treated cells would be fixed at the same time post-transfection. The cells were fixed by first rinsing in cold phosphate-buffered saline (PBS - 10 mM sodium phosphate, 140 mM NaCl, and 1 mM $MgCl_2$, pH 7.4) and then incubating in absolute methanol at -10°C for 15 minutes and rinsing again in cold PBS. For propidium iodide staining, propidium iodide was obtained from Molecular Probes (Carlsbad, CA) and cells were stained according to the manufacturer's instructions and then mounted in Vectashield mounting medium (Vector Laboratories Inc., Burlingame, CA). For immunocytochemistry, following fixation cells were incubated for 1 hour in blocking solution containing PBS + 10% horse serum. The cells were then incubated for an additional 1 hour with a mouse monoclonal anti-α-tubulin primary antibody or a mouse monoclonal anti-vimentin primary antibody (Abcam, Cambridge, MA) diluted 1:100 in blocking solution. Following washes in PBS, the cells were incubated for 1 hour at room temperature in 5 μg/ml goat anti-mouse IgG Alexa

Fluor 568 secondary antibody (Invitrogen). Cells were washed again in PBS and then mounted in VectaShield mounting medium containing 4',6'-diamidino-2-phenylindole (DAPI) (Vector Laboratories Inc.). Fluorescent images were captured using a Nikon Eclipse E800 epifluorescence microscope with filters B-2A to visualize the GFP fluorescence, G-2A to visualize the propidium iodide and Alexa Fluor 568 fluorescence, and UV-2E/C to visualize the DAPI fluorescence. Confocal images were captured on a Leica TCS-SP2 Spectral Confocal and Multiphoton System using an Argon ion laser for the analysis of GFP and a Helium-Neon ion laser for the analysis of propidium iodide.

Labeling with subcellular markers for the golgi, endoplasmic reticulum, and mitochondria were performed using N-((4-(4,4-difluoro-5-(2-thienyl)-4-bora-3a, 4a-diaza-s-indacene-3-yl)phenoxy)acetyl)shingosine (BODIPY® TR ceramide) (Molecular Probes), ER-Tracker™ Blue-White DPX (Molecular Probes), and Image-iT™ LIVE Mitochondrial and Nuclear Labeling Kit (Molecular Probes), respectively, according to the manufacturer's protocol for labeling fixed cells.

Images were overlaid in Photoshop 7.0 (Adobe Systems Inc., USA) and slight adjustments in levels were performed to reduce background fluorescence, if necessary.

4.2.5 Immunoblotting and co-immunoprecipitation

Cell lysates were prepared from transfected COS-7 cells, dark-reared rat retinal tissue (8 retinas), and rat brain tissue (1 g) using radioimmunoprecipitation (RIPA) buffer (Santa Cruz Biotechnology Inc., Santa Cruz, CA) according to manufacturer's instructions. Proteins were quantified using the Bradford method [13]. Equal concentrations of COS-7 cell lysates were resolved by SDS-PAGE and then transferred to Trans-Blot nitrocellulose membranes (BioRad, Hercules, CA) for western blot analysis. Duplicate blots were incubated for 1 hour at room temperature in blocking solution (TBS-T - 50 mM Tris-HCl, 200 mM NaCl, 1 mM $MgCl_2$ (pH 7.4), and 0.1% v/v Tween-20 + 5% skim milk powder) and then incubated for 1 hour at room temperature with either mouse anti-GFP monoclonal antibody (dilution 1:2500; BD Biosciences, San Diego, CA) or rabbit anti-KCTD8 polyclonal antibody (dilution 1:1000) [10]. The blots were washed three times in TBS-T at room temperature and then incubated for 1 hour at room temperature with the appropriate horseradish peroxidase (HRP)-conjugated secondary antibody – Goat anti-mouse (dilution 1:5000; BD Biosciences) for the GFP antibody and donkey anti-rabbit (dilution 1:5000; Amersham Biosciences, Piscataway, NJ) for the KCTD8 antibody. The blots were washed as above and detection of antibody binding was done using ECL Western Blotting Detection Reagents (Amersham Biosciences) as per manufacturer's instructions.

Co-immunoprecipitation of the transfected COS-7 cell lysates was performed using the Protein G Immunoprecipitation Kit (Sigma-Aldrich, St. Louis, MO) as per manufacturer's instructions. Briefly, 2 mg of each cell lysate was precleared with 30 µl of Protein-G Agarose by incubating for 3 hours at 4°C. The beads were pelleted by centrifugation and the supernatant was collected. The supernatant was incubated overnight at 4°C with 3 µg of anti-rabbit KCTD8 antibody. Protein G beads were added to the cell lysate/antibody mixture and incubated for 3 hours at 4°C. The unbound proteins were eluted from the column by centrifugation and the column was washed six times with 1X IP buffer supplied with the kit. A final wash in 0.1X IP buffer was performed to further remove non-specifically bound proteins. 2X Laemmli sample buffer (125 mM Tris-HCl, pH 6.8, 10% β-Mercaptoethanol, 0.025% (w/v) bromophenol blue, 20% (v/v) glycerol, 4% SDS) was added to the beads and the column was heated at 95°C for 5 minutes and then centrifuged for 30 seconds to dissociate specifically bound proteins from the beads. The eluted immunoprecipitate was divided in two and resolved by duplicate SDS-PAGE gel electrophoresis and electrophoretically transferred to nitrocellulose membranes. An aliquot of each cell lysate used in the co-immunoprecipitation (input protein) was also loaded on the gel. Western blotting was performed as described above with one western blot probed with mouse anti-GFP monoclonal antibody (dilution 1:5000; BD Biosciences) and the other blot probed with mouse anti-tubulin monoclonal antibody (dilution 1:5000; Abcam). For both blots, a 1:5000 dilution of a goat anti-mouse HRP-conjugated secondary antibody (BD Biosciences) was used.

Co-immunoprecipitation of the dark-reared retinal lysate was performed as above with minor changes. Nine hundred micrograms of cell lysate from dark reared rat retina tissue as well as rat brain tissue was used for the preclearance step. As a control, a co-immunoprecipitation was performed with RIPA buffer alone, no protein. After preclearing the lysates, the retinal and brain lysates as well as the RIPA only control were incubated with 3 μg of anti-rabbit KCTD8 polyclonal antibody. An additional control to rule out non-specific binding to rabbit antibodies was performed by incubating 900 μg of the precleared retinal lysate with 3 μg of a rabbit anti-T-cadherin antibody (Santa Cruz). Protein G agarose was then incubated with each cell lysate/antibody mixture. All incubations and washes were done as above. The specifically bound proteins were eluted as above and subjected to SDS-PAGE and electrophoretically transferred onto nitrocellulose membranes. Ten micrograms of each of the cell lysates used in the co-immunoprecipitation (input protein) were also loaded on the gel. Western blotting was performed as above using the mouse anti-α-tubulin monoclonal antibody and the goat anti-mouse HRP-conjugated secondary antibody.

4.2.6 Immunohistochemistry

Dark-reared rats were euthanized in CO_2 saturated chambers and the eyes were enucleated. A small slit was made in the cornea in order for fixative to penetrate the interior of the eye. The eyes were incubated in 4% paraformaldehyde for 10 to 15 minutes prior to the removal of the lens. After the lens was removed, the eyes were incubated in fresh 4% paraformaldehyde for 4 hours at 4°C with gentle agitation. The eyes were washed 3X in PBS and then immersed in 30% sucrose overnight. The cornea was removed and the optic cup was frozen in OCT compound (Electron Microscopy Sciences, Hatfield, PA) and stored at –80°C prior to use. Four micrometer retinal sections were cut at –20°C and placed onto Fisher Superfrost Plus slides (Fisher, Nepean, ON). Slides were stored at –80°C until use.

Frozen slides were thawed and then incubated for 1 hour at room temperature in blocking buffer containing 10% goat serum and 0.05% Tween-20 diluted in SuperBlock buffer in TBS (Pierce Biotechnology Inc., Rockford, IL). After blocking, the slides were incubated in a humidifying chamber at 4°C overnight in blocking buffer containing either 1:100 dilution of rabbit anti-KCTD8 polyclonal antibody alone or a mixture of the KCTD8 antibody and a 1:500 dilution of mouse anti-α-tubulin monoclonal antibody

(Abcam). The slides were washed 3X at room temperature in TBS-T and then incubated for 1 hour with either: a 1:600 dilution of a goat anti-rabbit Oregon Green 514 secondary antibody (Invitrogen), for the single labeled KCTD8 immunohistochemistry; or a Cy3 conjugated AffiniPure F(ab')2 fragment goat anti-rabbit IgG secondary antibody (dilution 1:1000; Jackson ImmunoResearch, West Grove, PA) in conjunction with an Alexa Fluor 488 goat anti-mouse secondary antibody (dilution 1:400; Invitrogen), for the double labeling immunohistochemistry, diluted in blocking buffer. Slides were washed as above and nuclear staining was performed with either propidium iodide (Molecular Probes) or Hoechst 33342 (Invitrogen) according to manufacturer's instructions. Slides were mounted in Vectashield mounting medium (Vector Laboratories Inc.) and visualized with a Leica TCS-SP2 Spectral Confocal and Multiphoton System.

4.3 RESULTS

4.3.1 Expression of GFP-KCTD8 fusion proteins in COS-7 cells

In order to visualize localization of KCTD8 in mammalian cells, wild-type and mutant cDNAs were inserted into the pEGFP-C1 mammalian expression vector (Figure 4.1A). This vector contains the coding sequence for a green fluorescent protein, which was linked to the amino terminus of the KCTD8 protein upon translation of the fusion protein in mammalian cells. The presence of the GFP tag enables visualization of the subcellular localization of the GFP-KCTD8 fusion protein. To determine whether the predicted NLSs function in trafficking the KCTD8 protein to the nucleus, GFP-tagged KCTD8 constructs were made which contained mutations in the basic arginine and lysine residues that signify NLSs. Mutations were introduced by way of site-directed mutagenesis. In total four constructs were made (Figure 4.1B): the wild-type construct containing no mutations; an NLS1 construct which contained mutations in the bipartite NLS; an NLS2 construct which contained mutations in the pat7 NLS; and an NLS1/2 construct which contained mutations in both NLSs. The wild-type GFP-tagged KCTD8 construct as well as the single and double NLS mutant GFP-tagged KCTD8 constructs were transiently transfected into COS-7 cells.

Following transfection, whole cell lysates were prepared and analyzed for the presence of the full-length GFP-KCTD8 fusion proteins (Figure 4.2). Analysis of the lysates was performed with both anti-GFP (Figure 4.2A) and anti-KCTD8 (Figure 4.2B) antibodies. Immunoblot analysis revealed that the size of the wild-type GFP-KCTD8 fusion protein is approximately 95 kDa (Figures 4.2A and 4.2B, lane 3). This size corresponds to the expected size of KCTD8 (~60 kDa) combined with the GFP protein (~30 kDa, Figure 4.2A, lane 2). The sizes of the three mutant GFP-KCTD8 fusion proteins are also approximately 95 kDa due to minimal change in the molecular mass of the proteins from the introduced mutations.

4.3.2 Subcellular localization of the wild-type and mutant KCTD8 in COS-7 cells

Determination of subcellular localization of the wild-type and mutant KCTD8 proteins was analyzed by immunofluorescence microscopy of transiently transfected COS-7 cells (Figure 4.3). In untreated cells, the wild-type KCTD8 construct (pEGFP-KCTD8 wild-type) displayed a filamentous pattern localizing in the cytoplasm of the cell (Figure 4.3G). None of the cells transfected with the wild-type KCTD8 displayed a nuclear localization pattern (Figure 4.3I). With cellular localization of the double mutant construct, pEGFP-KCTD8 NLS1/2, in untreated cells, we consistently observed a punctate pattern within the cytoplasm (Figure 4.3P). Again, none of the cells transfected with the NLS1/2 double mutant construct displayed a nuclear localization pattern (Figure 4.3R). With the single mutant constructs, pEGFP-KCTD8 NLS1 (Figure 4.3J) or pEGFP-KCTD8 NLS2 (Figure 4.3M), a similar pattern emerged for both in which the majority of the cells (approximately 75%) displayed the wild-type filamentous pattern of localization and the remainder of the cells displayed the punctate pattern seen in the double mutant. As with the double mutant and wild-type localization, no nuclear localization was observed with either single mutant construct (Figure 4.3L and Figure 4.3O). The control experiments on mock transfected cells revealed no background green fluorescent staining (Figure 4.3A), and cells transfected with the empty pEGFP-C1 vector exhibited diffused GFP staining (Figure 4.3D) unlike that seen for the wild-type and mutant KCTD8 fusion proteins. Although the wild-type KCTD8 construct did not exhibit nuclear localization, there is a definite difference between the wild-type localization and the double mutant localization. Thus, it appears that mutating both nuclear localization sites results in altered subcellular distribution of the protein as compared to the wild-type KCTD8 localization.

In order to determine whether KCTD8 nuclear localization is transient and had occurred at some point prior to visualization of the cells, the cells were treated with leptomycin, a chemical that inhibits nuclear export [14, 15]. Thus, if the GFP-KCTD8 protein was nuclear localized at some point prior to visualization of the cells it would not be able to be exported back to the cytosol when treated with leptomycin and would remain nuclear. COS-7 cells transfected with wild-type and mutant pEGFP-KCTD8 constructs were treated post-transfection with 20 nM leptomycin (concentration based on published experiments with COS-7 cells [15]) and visualized by fluorescence microscopy for the presence of the GFP fluorescent signal (Figure 4.4). In all transfections - wild-type (Figure 4.4G and 4.4I), single mutant (Figure 4.4J, 4.4L, 4.4M, 4.4O), and double mutant (Figure 4.4P and 4.4R) KCTD8 fusion proteins - the localization observed was the same as for untreated, transfected cells (compare Figure 4.4 with Figure 4.3).

4.3.3 KCTD8 is colocalized and associates with α-tubulin in COS-7 cells

To determine where in the cell the proteins are localizing, transfected, untreated cells were immunolabeled with various subcellular markers (Figures 4.5 and 4.6). Of particular interest was α-tubulin, a subcellular marker for microtubules. The filamentous pattern observed with the wild-type KCTD8 construct appeared similar to that seen for microtubules but not to the other cellular markers tested. To examine the possible co-localization of KCTD8 with microtubules, untreated cells transfected with either wild-type pEGFP-KCTD8 or pEGFP-KCTD8 NLS1/2 constructs were immunolabeled with an α-tubulin antibody and analyzed for co-localization of the GFP signal with the α-tubulin signal. For the wild-type GFP-KCTD8 fusion protein, the fluorescent signal from the GFP-KCTD8 fusion protein co-localized with the signal from α-tubulin (Figure 4.6D, 4.6E, and 4.6F), as is evident by the yellow merged signal in Figure 4.6F. In contrast, the localization of the GFP-KCTD8 NLS1/2 double mutant does not co-localize with α-tubulin (Figure 4.6G, 4.6H, and 4.6I), indicating that by disrupting the NLSs the localization to microtubules is in turn disrupted. The control mock transfection displayed no background GFP fluorescence, as expected (Figure 4.6A and 4.6C).

In Figure 4.6, panel D it appears that there is GFP-KCTD8 protein localizing in the nucleus. However, when panel D is compared to the overlay with α-tubulin (Figure 4.6, panel F) it is clear that the green localization is due to KCTD8 co-localizing with the cytoplasmically localized microtubules that surround the nucleus. This observation would also explain the apparent nuclear localization observed in Figure 4.3 panels I and O. However, definitive confirmation of this observation would require serial optical sections through the z-plane of transfected cells stained with α-tubulin to ensure that the GFP-KCTD8 protein is co-localizing with microtubules in the cytoplasm and is not nuclear localized.

To examine the physical interaction between KCTD8 and α-tubulin, whole cell lysates from COS-7 cells transfected with either wild-type, single mutant, or double mutant pEGFP-KCTD8 constructs were used for co-immunoprecipitation experiments. A polyclonal rabbit anti-KCTD8 antibody was used to immunoprecipitate the GFP-KCTD8 fusion protein from the cell lysates. The immunoprecipitate was then blotted with an antibody against GFP (Figure 4.7A) or α-tubulin (Figure 4.7B). The GFP antibody was used as a control to ensure that the KCTD8 antibody was successful in isolating the GFP-KCTD8 fusion proteins (Figure 4.7A, lanes 9-12). The control cell lysates from mock transfected cells and cells transfected with the empty pEGFP-C1 vector displayed no immunobinding with the GFP antibody, as expected (Figure 4.7A, lanes 7 and 8). The western blot probed with a mouse anti-α-tubulin antibody clearly displays immunobinding to the cell lysate from the wild-type GFP-KCTD8 transfected cells indicating a physical interaction of the KCTD8 protein with the α-tubulin protein (Figure 4.7B, lane 9). The faint bands observed for the cells transfected with the single and double mutant GFP-KCTD8 constructs (Figure 4.7B, lanes 10-12) are due to eluted background protein since bands of the same intensity are seen in the control lanes (Figure 4.7B, lanes 7 and 8), which contain lysate from mock transfected cells and cell lysate from empty pEGFP-C1 vector transfected cells, respectively.

4.3.4 Localization of wild-type KCTD8 to microtubules is disrupted in colcemid treated COS-7 cells

To further confirm the localization of the wild-type KCTD8 to microtubules, transfected cells were treated with either 2 μM or 5 μM colcemid for six hours. Colcemid acts to depolymerize microtubules and limits microtubule formation [16-18]. At the lower concentration of colcemid, 2μM, depolymerization of microtubules was not complete resulting in some intact microtubules. As a result, some of the wild-type pEGFP-KCTD8 transfected cells displayed the normal filamentous pattern seen in untreated cells (compare Figure 4.8H to 4.8G). For the cells transfected with the pEGFP-KCTD8 NLS1/2 double mutant cDNA construct and treated with 2 μM colcemid, there was no change in the localization pattern as compared to the transfected, untreated cells (compare Figure 4.8K to 4.8J). With the higher concentration of colcemid, 5 μM, depolymerization was complete for all transfected cells. Cells with complete depolymerization of microtubules displayed a punctate staining pattern for the wild-type GFP-KCTD8 fusion protein (Figure 4.8I). The staining pattern of the GFP-KCTD8 NLS1/2 fusion protein was not changed with the 5 μM colcemid treatment and appeared identical to the pattern observed in untreated cells (compare Figure 4.8L to 4.8J). Although the pattern of localization for the wild-type KCTD8 transfected cells treated with colcemid appears similar to that seen for the NLS1/2 transfected cells, the two patterns differ slightly. In the cells expressing the GFP-KCTD8 NLS1/2 double mutant fusion protein, the punctate pattern in the cytoplasm shows larger more uniform circular spots, whereas in the wild-type GFP-KCTD8 expressing, colcemid treated cells, the punctate pattern shows smaller more irregular spots, most likely the result of KCTD8 bound to depolymerized microtubules (compare Figures 4.8I and 4.8L).

In a number of the wild-type pEGFP-KCTD8 transfected cells treated with colcemid it appeared that, in addition to the punctate staining in the cytoplasm due to depolymerized microtubules, there was also punctate staining of the GFP signal in the nucleus (Figure 4.8I). In order to analyze whether this staining was in fact nuclear, optical sections along the z-axis of the cell were taken of wild-type pEGFP-KCTD8 transfected cells treated with colcemid (Figure 4.9A). As indicated by the arrowheads in Figure 4.9A, there is in fact punctate GFP-KCTD8 staining in the nucleus of these cells, as is evident by the yellow signal resulting from the merging of the green GFP signal with the red nuclear signal. In contrast, COS-7 cells transfected with the pEGFP-KCTD8 NLS1/2 double mutant construct and treated with colcemid displayed strictly cytoplasmic localization (Figure 4.9B) with none of the cells showing the punctate localization in the nucleus that was observed for the wild-type GFP-KCTD8 transfected cells.

4.3.5 Immunolocalization of KCTD8 in the rat retina

The localization of KCTD8 in the various cellular layers of the rat retina was examined by immunohistochemistry. KCTD8 immunolabeling is observed throughout the various retinal layers with stronger labeling appearing in the inner retina, within the ganglion cell layer, the inner plexiform layer and the inner nuclear layer (Figure 4.10A). Within the ganglion cell layer, KCTD8 appears to be cytoplasmic and nuclear localized as indicated by the arrowheads in Figure 4.10F. The inner nuclear layer also displayed nuclear as well as cytoplasmic localization of KCTD8 (Figure 4.10F, indicated by asterisk). In the outer retina, the KCTD8 immunostaining appeared cytoplasmic within the outer nuclear layer and there was also some immunolabeling in the photoreceptor inner and outer segments (Figure 4.10G and 4.10I). Immunolabeling with the secondary antibody alone displayed a low level of background immunofluorescence in the inner plexiform layer and the photoreceptor inner and outer segments (Figure 4.10J and 4.10L). The level of fluorescence observed with the KCTD8 antibody was significantly higher than the background levels observed with the secondary antibody alone suggesting that the staining observed in the inner plexiform layer and the photoreceptor cells is not due to background immunofluorescence.

4.3.6 KCTD8 is colocalized and associates with α-tubulin in the rat retina

Co-localization of KCTD8 with α-tubulin in the retina was analyzed by immunohistochemistry on retinal sections from rats reared under strictly dark conditions. Retina sections immunolabeled with α-tubulin show strong immunolabeling throughout all layers of the retina, as expected (Figure 4.11A). Immunolabeling with KCTD8 also shows a similar result with localization observed throughout the various retinal layers (Figure 4.11B). When sections immunolabeled with α-tubulin and KCTD8 are merged, there is definite co-localization of the two as shown by the yellow merged signal in Figure 4.11D. The ganglion cell nuclei and the nuclei of the inner nuclear layer are the only areas that do not show co-localization of α-tubulin and KCTD8 due to the nuclear localization of KCTD8 in these layers, as was first seen in Figure 4.9F. Control immunolabeling with the secondary antibodies alone show minimal background fluorescence (Figure 4.11E, 4.11F, and 4.11H) indicating that the detection seen with the α-tubulin and KCTD8 primary antibodies is specific.

To examine the physical interaction between KCTD8 and α-tubulin in retinal cell lysates, co-immunoprecipitation was performed on cell lysates from dark-reared rat retinas. Since previous data had shown that KCTD8 is expressed in the rat brain [10, 19] we also performed the co-IPs using rat brain cell lysates. A negative control using only RIPA buffer, no protein, was also performed to rule out any non-specific binding that may occur. An additional control was performed with another rabbit polyclonal antibody (T-cadherin) to rule out any bands appearing due to non-specific binding to rabbit antibodies. A rabbit anti-KCTD8 polyclonal antibody was used to immunoprecipitate the KCTD8 protein and any binding partners from the cell lysates. The immunoprecipitates were analyzed by western blot analysis using a mouse anti-α-tubulin antibody (Figure 4.12). Bands appearing in the RIPA only eluate (Figure 4.12, lane 4) and the eluate from the co-IP of the retinal lysate with the T-cadherin antibody (Figure 4.12, lane 6) are background immunostaining due to cross-reactivity of the goat anti-mouse secondary antibody (used to detect the α-tubulin primary antibody) with the rabbit anti-KCTD8 antibody used to immunoprecipitate the KCTD8 protein. The 55 kDa band observed in lanes 4 and 6 is the expected size of the rabbit IgG heavy chain protein. The eluate from the co-IP of the rat retina and brain lysates with the KCTD8 antibody show, in addition to the faint 55 kDa band, a band at 57 kDa (Figure 4.12, lanes 5 and 7, indicated by the arrowheads), which is the expected size of α-tubulin. Although the rabbit heavy chain protein and α-tubulin are very close in size, it is clear that the band for α-tubulin in lanes 5 and 7 does not appear in the control lanes 4 and 6, indicating a physical interaction of KCTD8 with α-tubulin in the rat retina and brain.

4.4 DISCUSSION

We have demonstrated, *in vivo* and *in vitro*, that KCTD8 associates with α-tubulin and microtubules and that this association appears to be mediated by the NLS domains present in the KCTD8 protein. Further confirmation of the co-localization with α-tubulin was observed with the disruption of microtubules by the addition of colcemid, which also disrupted the wild-type KCTD8 localization and resulted in punctate nuclear as well as cytoplasmic localization. In addition, retinal localization and co-immunoprecipitation studies confirmed the results of the cell culture studies by showing an association of KCTD8 with α-tubulin in the rat retina.

In recent years our understanding of the role of microtubules in the cell has shifted from one of simple maintenance of cell shape to that of involvement in protein sequestration and transport. p53 has been shown to physically bind to microtubules *in vivo* and *in vitro* in order to facilitate dynein-dependent transport of p53 to the nucleus in response to DNA damage [20]. A similar role of microtubule binding was observed for the parathyroid hormone-related protein (PTHrP) in which the microtubule network actively transports PTHrP toward the nuclear membrane in order for nuclear localization to occur [21]. The involvement of microtubules in regulating nuclear localization of proteins is believed to occur by one of two mechanisms [22]. One mechanism involves active transport of proteins to the nucleus. In this case, an intact microtubule network is needed to transport the protein to the nucleus. Disruption of the microtubule network would lead to a decreased accumulation of the protein in the nucleus. The second mechanism involves sequestration of cellular proteins, thus preventing their accumulation in the nucleus. With this mechanism, disruption of the microtubule network would allow an increased accumulation of the protein in the nucleus due to the protein no longer being sequestered to the microtubules. The latter mechanism of protein sequestration has been implicated in the case of c-myc and MIZ-1 microtubule binding [23-25]. As a result, and in contrast to p53 and PTHrP, the microtubules function in preventing nuclear accumulation c-myc and MIZ-1 rather than facilitate it. Based on the findings that the KCTD8 wild-type protein co-localizes with microtubules in cell culture and in the retina, it is possible that one of the above mechanisms may be involved to either transport the protein to the nucleus or sequester the protein until it is required in the nucleus.

The disruption of the microtubule network by treatment of the cells with colcemid also disrupted the localization of the wild-type KCTD8 protein and resulted in nuclear as well as punctate cytoplasmic localization. The punctate cytoplasmic localization is most likely a result of KCTD8 binding to depolymerized microtubules. This suggests that KCTD8 bound to the microtubules shortly after transfection and before treatment with colcemid and remained bound to the depolymerized microtubules in the presence of colcemid. The observation of nuclear as well as cytoplasmic localization of wild-type KCTD8 in cells treated with colcemid suggests that the binding to microtubules may act to sequester the KCTD8 protein to prevent nuclear accumulation until the protein is required in the nucleus. This type of regulation by microtubule binding would be advantageous for proteins that have multiple functions over time and during the cell cycle, as the cytoskeleton of the cell is quite dynamic. Thus, it is possible that KCTD8 has a dual function in the cell such the binding to microtubules facilitates one function and that nuclear localization, in order to carry out a second function, occurs when the microtubules are depolymerized or in response to some other stimuli. The fact that only a portion of the KCTD8 protein localized to the nucleus upon treatment with colcemid suggests that disruption of the microtubules is not the sole determinant of nuclear localization. As seen by the punctate cytoplasmic staining when the cells are treated with colcemid, KCTD8 remains bound to depolymerized microtubules. It may be such that an additional trigger is required to localize the KCTD8 protein to the nucleus.

In contrast to the wild-type KCTD8 co-localization with α-tubulin in untreated cells, the mutant construct with both NLSs mutated (KCTD8 NLS1/2) did not co-localize with α-tubulin and the cellular localization was not altered when the cells were treated with colcemid. In untreated and colcemid treated cells, the NLS1/2 mutant remained localized as punctate structures in the cytoplasm. Cells transfected with either the KCTD8 NLS1 or KCTD8 NLS2 single mutant constructs displayed a combination of the wild-type KCTD8 localization pattern and the punctate cytoplasmic localization pattern of the KCTD8 NLS1/2 double mutant. Despite the single mutant constructs showing a wild-type localization pattern in cell culture, in the co-immunoprecipitation of the transfected COS-7 cell lysates, none of the cell lysates from the cells transfected with the mutant constructs exhibited an interaction with α-tubulin. This suggests that mutating one or the other NLS may reduce the strength of the binding of KCTD8 to the microtubules, and as such, any association between the single NLS mutant KCTD8 proteins and α-tubulin before the co-immunoprecipitation was not strong enough for α-tubulin to remain bound to the mutant protein after cell lysis.

Typically, proteins that are associated with microtubules do so through a binding domain separate from that of the NLS sites, as is the case with p53 and c-myc [20, 23]. The finding that disrupting the NLS sites in the KCTD8 protein affects the association with microtubules indicates that the signals for nuclear localization may have a dual role in both signaling the protein to the nucleus as well as binding of the protein to microtubules. Recently, Salman *et al.* [26] were able to demonstrate a functional link between the presence of a NLS and dynein-dependent transport along microtubules of a nucleoprotein complex. By the simple presence of NLSs, a protein was able to bind to microtubules and by involvement of dynein the protein was brought toward the nuclear envelope thus enabling nuclear import via the conventional importing-mediated pathway. Due to our observations that the KCTD8 NLS1/2 double mutant does not bind to microtubules and that the single NLS1 or NLS2 mutants only occasionally co-localize with microtubules but not with enough strength to observe this interaction by co-IP, a similar role in which the NLSs in KCTD8 may mediate binding to microtubules is plausible. However, the possibility of an intermediary binding partner which links the KCTD8 protein via the NLS sites to the microtubules can not be ruled out.

The presence of two NLSs within the wild-type KCTD8 protein and the binding of KCTD8 to microtubules as a possible mechanism of transport to the nuclear envelope for import into the nucleus indicates that one should expect the protein to be localized to the nucleus at some point. In untreated cells this was not observed and only partial nuclear localization was observed in colcemid treated cells. Previous analysis of the KCTD8 protein indicates that the protein contains three leucine-rich sites that are characteristic of nuclear export signals [10]. To ensure that the protein was not imported into the nucleus and then exported at some point prior to visualization of the cells, the transfected cells were treated with leptomycin, an inhibitor of nuclear export [14, 15]. All leptomycin treated cells examined exhibited the same localization pattern as in the untreated cells, indicating that the protein had not been imported into the nucleus then exported prior to visualization. Therefore, under normal conditions, the KCTD8 protein binds to microtubules and is not imported into the nucleus, further supporting the hypothesis that KCTD8 binding to microtubules acts as a reservoir to sequester the protein until it is required in the nucleus, perhaps in response to some stimulus.

The study of the localization of KCTD8 in the rat retina revealed that the protein is distributed throughout the retina. Interestingly, KCTD8 is found in the nuclei of the retinal ganglion cells and is also nuclear as well as cytoplasmically localized in the inner nuclear layer, which contains nuclei of horizontal, bipolar and amacrine cells [27]. The cells of the inner nuclear layer are responsible for modifying and relaying the visual signal from the photoreceptor cells to the ganglion cells. The ganglion cells are the final output neurons of the retina and are responsible for sending the visual signal to the brain via the optic nerve. Although the GFP-KCTD8 localization studies in untreated COS-7 cells did not display nuclear localization, it is clear that in the dark-reared rat retina, KCTD8 is nuclear localized in a subset of cells. The nuclear localization of KCTD8 in the retinal ganglion cells as well as the previous finding that KCTD8 is expressed in the rat brain suggests that KCTD8 may have a neuronal function.

In addition to the nuclear localization observed in the inner retina, KCTD8 was also shown to co-localize with α-tubulin throughout the inner and outer retina. Co-immunoprecipitation experiments confirmed the physical interaction between KCTD8 and α-tubulin in the retina. Recently, it has been found that arrestin binds to microtubules in the photoreceptor inner segments in the dark and is translocated to the photoreceptor outer segments in response to light stimulus [28-30]. It is hypothesized that this microtubule binding serves to sequester arrestin in the dark-adapted photoreceptors in order to physically keep arrestin away from rhodopsin. Although the significance of the interaction between KCTD8 and microtubules has not been determined, a similar method of sequestration may be possible. This correlates with the cell culture localization results in cells treated with colcemid, which suggests that the binding of KCTD8 to microtubules may act to sequester the protein in the cytoplasm to prevent nuclear accumulation. Therefore, in addition to the nuclear localization of KCTD8 in the ganglion cells and inner nuclear layer, the protein may also translocate to other areas of the retina in response to some stimulus. Although this remains to be tested, the most likely trigger of

KCTD8 translocation from the microtubules to another area of the retina would be a light stimulus. However, it is also plausible, being that this gene was originally isolated from a screen for genes involved in light-induced retinal degeneration [10], that cellular stress may also induce translocation of the KCTD8 protein. These aspects will be discussed in Chapter 5.

The results presented here are contrary to what one would expect for a potassium channel tetramerization domain protein; however, they are none the less interesting. The finding that KCTD8 binds to microtubules as a possible mechanism of sequestration adds it to the growing number of microtubule-associated proteins [22] and further strengthens the role of microtubules as more than just maintainers of cell structure. Understanding the purpose of the association between KCTD8 and microtubules and what stimulus is necessary to invoke nuclear localization will provide additional clues to the function of this gene. In addition, the presence of the BTB/POZ/T1 domain, a known protein-protein interaction motif, at the N-terminal region of the protein suggests that KCTD8 may be involved in binding other proteins. Analyzing KCTD8 for potential interacting partners may also provide additional clues as to the function of KCTD8 and the importance of the microtubule association.

Figure 4.1 - GFP-tagged KCTD8 expression constructs for cell transfections.

A) The pEGFP-C1 expression vector was used for insertion of the wild-type and mutated KCTD8 cDNAs for synthesis of GFP-fusion proteins in transfected cells. B) Schematic representation of constructs containing the full-length open reading frame (ORF) of KCTD8 (dark blue) tagged to an in-frame amino-terminal GFP tag (green) positioned downstream of a cytomegalovirus (CMV) promoter (white). The first amino acid position of each NLS is shown below the wild-type construct and the NLSs are shown schematically in light blue. Mutations in the NLSs are shown in red text.

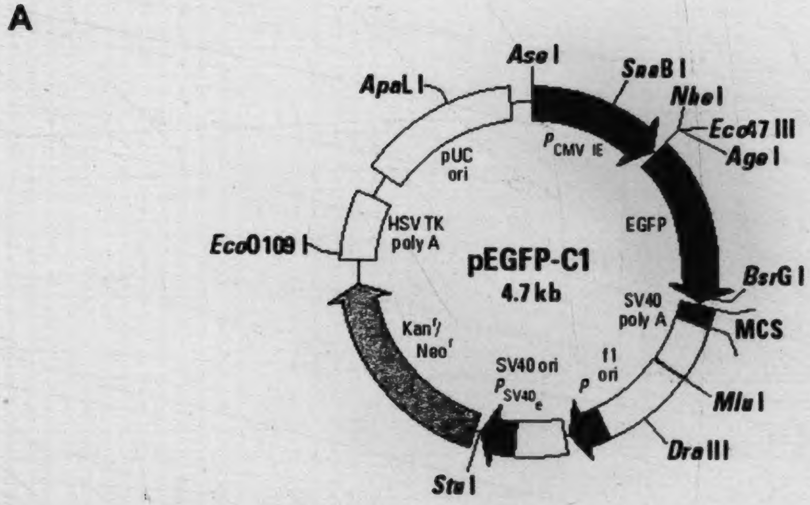
A
Ase I
SnaB I
Nhe I
Eco47 III
Age I
ApaL I
pUC ori
$P_{CMV\ IE}$
EGFP
HSV TK poly A
Eco0109 I
pEGFP-C1
4.7 kb
Bsr G I
SV40 poly A
MCS
Kan^r/ Neo^r
SV40 ori
P_{SV40_e}
f1 ori
P
Mlu I
Dra III
Stu I

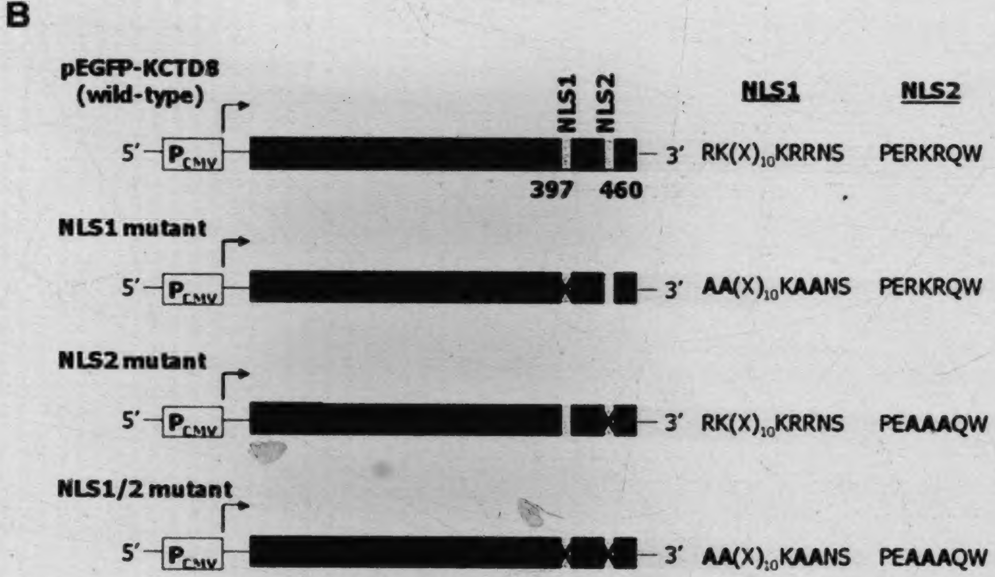
B
pEGFP-KCTD8 (wild-type)
NLS1
NLS2
NLS1
NLS2
5′
P_{CMV}
3′
RK(X)$_{10}$KRRNS
PERKRQW
397
460
NLS1 mutant
5′
P_{CMV}
3′
AA(X)$_{10}$KAANS
PERKRQW
NLS2 mutant
5′
P_{CMV}
3′
RK(X)$_{10}$KRRNS
PEAAAQW
NLS1/2 mutant
5′
P_{CMV}
3′
AA(X)$_{10}$KAANS
PEAAAQW

Figure 4.2 - Immunoblot analysis of GFP-KCTD8 fusion proteins expressed in COS-7 cells transfected with wild-type and mutant pEGFP-KCTD8 constructs.
Total cell lysates from transfected COS-7 cells were subjected to western blot analysis and probed with either anti-GFP antibody (panel A) or an affinity purified anti-KCTD8 antibody (panel B). Lanes: 1, protein extracts from mock transfected COS-7 cells (negative control); 2, protein extracts from the empty pEGFP-C1 vector transfected cells (GFP positive control); 3, protein from pEGFP-KCTD8 wild-type transfected cells; 4, protein from cells transfected with pEGFP-NLS1 mutant construct; 5, protein from cells transfected with pEGFP-NLS2 mutant construct; 6, protein from cells transfected with the double mutant pEGFP-NLS1/2 construct. Approximate size, in kilodaltons (kDa), of the resulting bands are shown to the left of the blots. Sizes are estimated based on the protein size marker. β-actin is shown as a loading control.

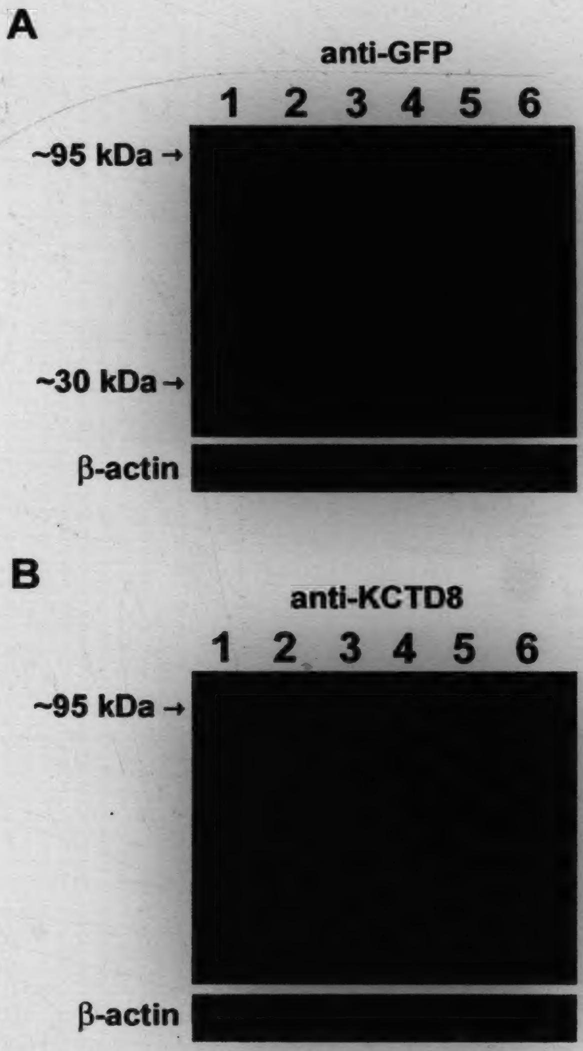
A
anti-GFP
1 2 3 4 5 6
~95 kDa →
~30 kDa →
β-actin
B
anti-KCTD8
1 2 3 4 5 6
~95 kDa →
β-actin

Figure 4.3 - Representative immunofluorescent images showing the subcellular localization of wild-type and mutant GFP-tagged KCTD8 fusion proteins in transfected COS-7 cells.

Control transfections from mock transfected cells are shown in panels A-C and transfected cells expressing the pEGFP-C1 vector are shown in panel D-F. Wild-type GFP-KCTD8 overexpressing cells are shown in panels G-I. Transfections with the mutant pEGFP-KCTD8 cDNA constructs containing sequence alterations in the putative NLSs are shown in panels J-L (NLS1 mutant), panels M-O (NLS2 mutant), and panels P-R (NLS1/2 double mutant). Subcellular localization of the GFP-KCTD8 fusion proteins is shown in panels A, D, G, J, M, and P by GFP fluorescence (green). The second column shows the propidium iodide staining (red) of the nuclei for each transfected cell (B, E, H, K, N, and Q). Overlaid images from the first two columns are shown in column three (C, F, I, L, O, and R).

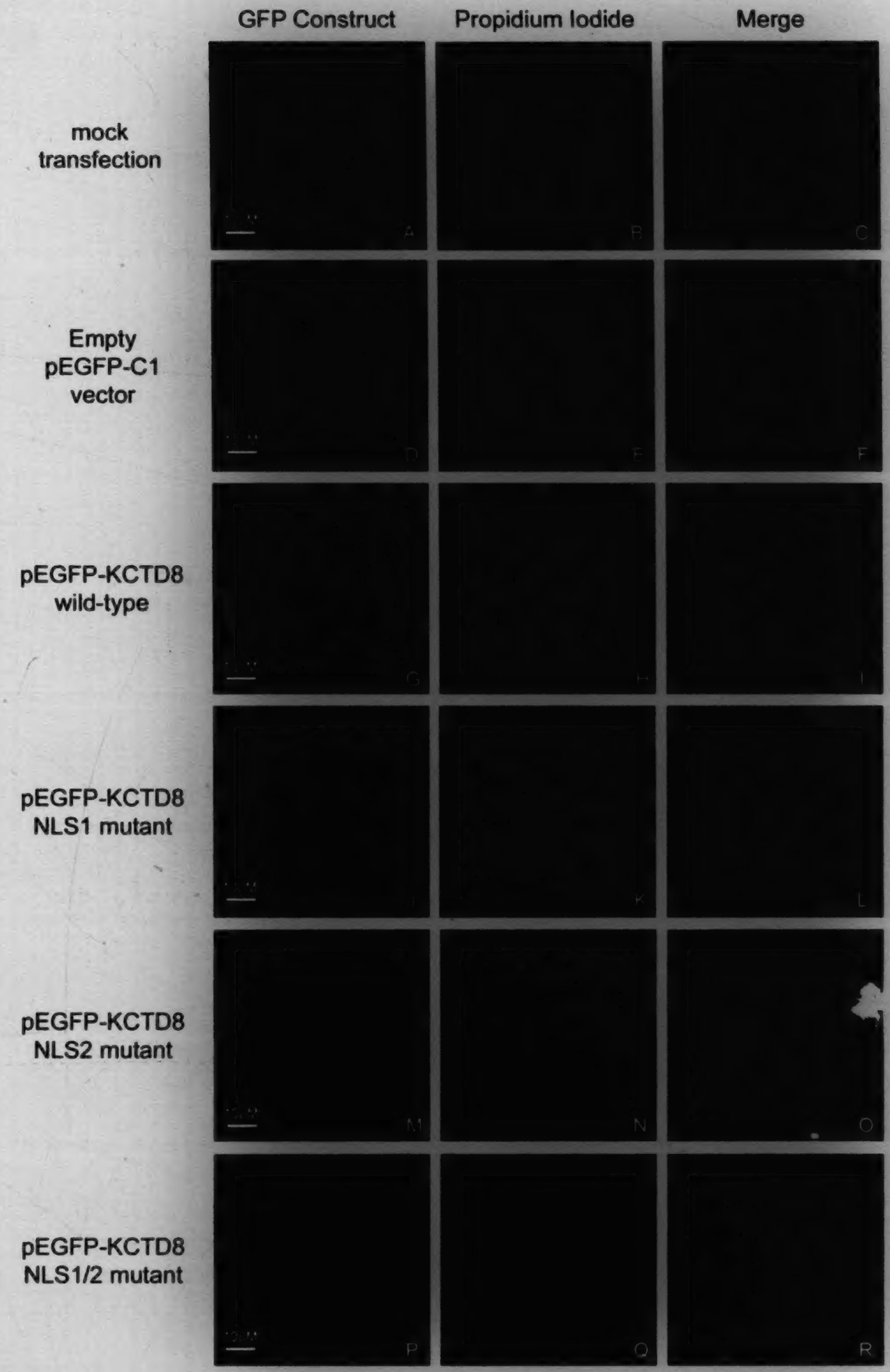
GFP Construct
Propidium Iodide
Merge
mock transfection
Empty pEGFP-C1 vector
pEGFP-KCTD8 wild-type
pEGFP-KCTD8 NLS1 mutant
pEGFP-KCTD8 NLS2 mutant
pEGFP-KCTD8 NLS1/2 mutant
A
B
C
D
E
F
G
H
I
K
L
M
N
O
P
Q
R

Figure 4.4 - Analysis of cellular localization of wild-type and mutant GFP-KCTD8 fusion protein in transfected COS-7 cells treated with leptomycin.

Transiently transfected COS-7 cells overexpressing the wild-type GFP-KCTD8 are shown in panels G-I. Cells overexpressing the pEGFP-KCTD8 construct with the first NLS (NLS1) mutated are shown in panels J-L. Cell transfected with the mutant KCTD8 construct with the second NLS mutated (NLS2) are shown in panels M-O. Cells overexpressing the double mutant construct (NLS1/2) are shown in panels P-R. Images of control transfections are shown in panels A-C (mock transfected cells) and panels D-F (cell transfected with the empty pEGFP-C1 vector). Subcellular localization of the GFP-KCTD8 fusion proteins is shown in panels A, D, G, J, M, and P by GFP fluorescence (green). All cells were treated, post-transfection, with 20 nM leptomycin to prevent nuclear export. The second column shows the propidium iodide staining (red) of the nuclei for each transfected cell (B, E, H, K, N, and Q). Overlaid images from the first two columns are shown in column three (C, F, I, L, O, and R).

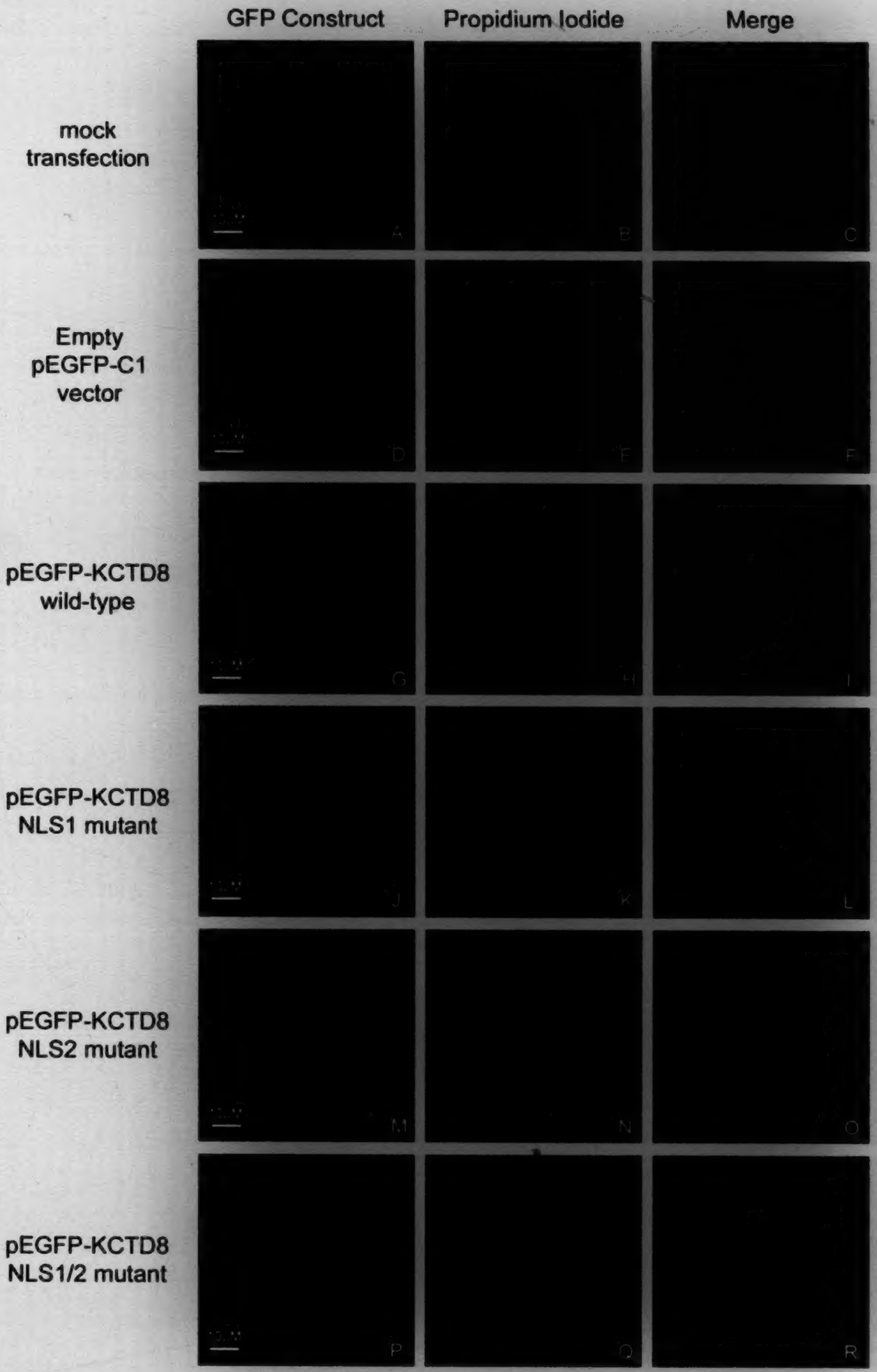
GFP Construct
Propidium Iodide
Merge
mock transfection
Empty pEGFP-C1 vector
pEGFP-KCTD8 wild-type
pEGFP-KCTD8 NLS1 mutant
pEGFP-KCTD8 NLS2 mutant
pEGFP-KCTD8 NLS1/2 mutant
A
B
C
D
E
F
G
H
I
J
K
L
M
N
O
P
Q
R

Figure 4.5 – Representative immunofluorescent images of COS-7 cells labeled with various cellular markers.

Transiently transfected COS-7 cells expressing the wild-type GFP-KCTD8 are shown in panels E-H and GFP-KCTD8 with both NLSs mutated (NLS1/2) are shown in panels I-L (green). Mock transfected cells (A-D) are shown to indicate labeling with each subcellular marker in the absence of GFP expression. Panels A, E, and I are labeled with the ER marker ER-Tracker™ Blue-White DPX (blue). Panels B, F, and J are labeled with a Golgi marker, BODIPY® TR ceramide (red), and the nuclei and stained with DAPI (blue). Cells in panels C, G, and K were labeled with MitoTracker Red CMXRos dye to visualize the mitochondria (red); nuclei were stained with Hoechst 33342 dye (blue). Panels D, H, and L were immunolabeled with mouse anti-vimentin antibody and detected with an Alexa Fluor 568 secondary antibody to visualize intermediate filaments (red); nuclei were stained with DAPI (blue).

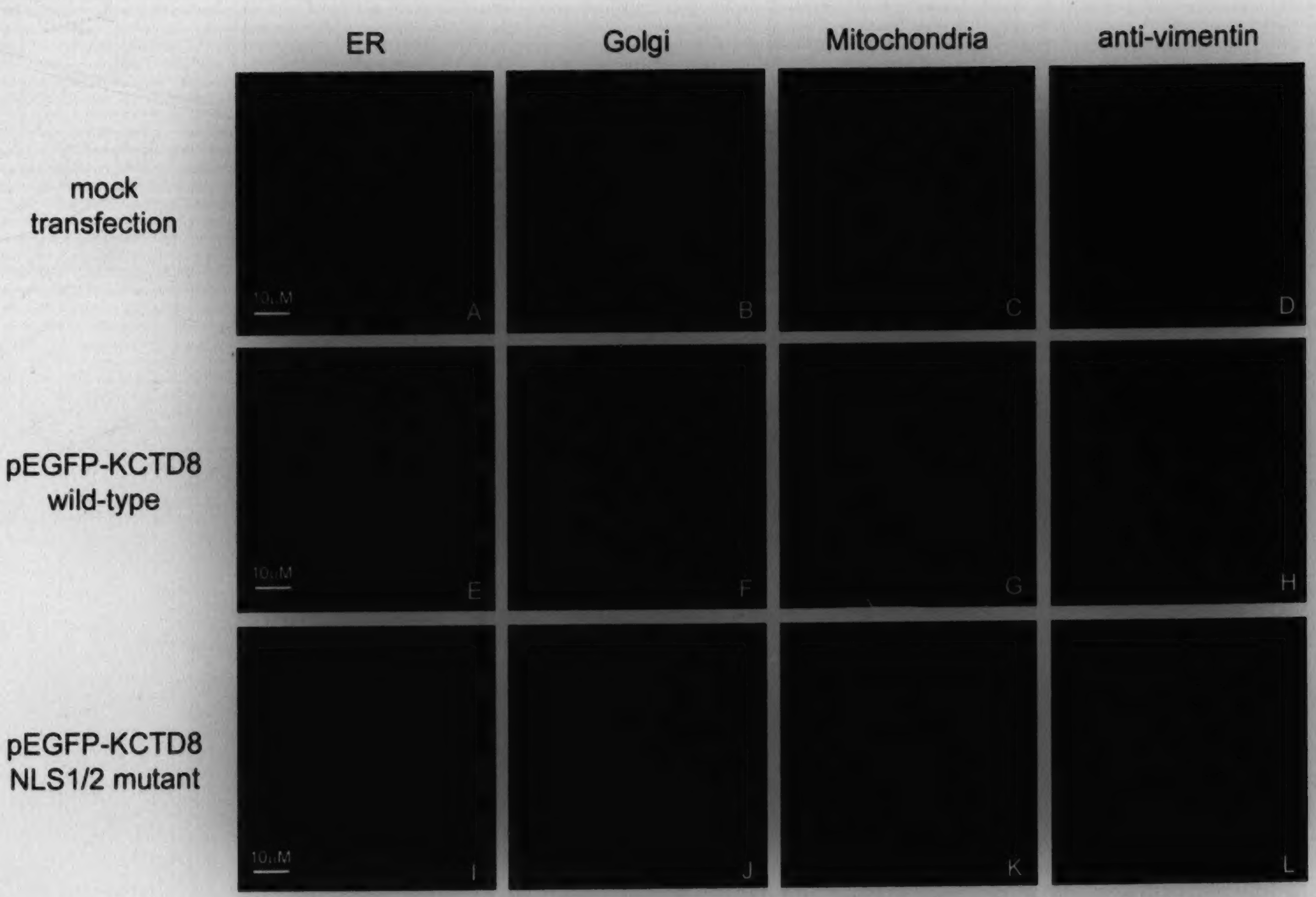
ER
Golgi
Mitochondria
anti-vimentin
mock transfection
pEGFP-KCTD8 wild-type
pEGFP-KCTD8 NLS1/2 mutant
10μM
A
B
C
D
10μM
E
F
G
H
10μM
I
J
K
L

Figure 4.6 - Representative immunofluorescent images showing co-localization of the wild-type GFP-KCTD8 with α-tubulin.

Transiently transfected COS-7 cells expressing the wild-type GFP-KCTD8 are shown in panels D and F and GFP-KCTD8 with both NLS signals mutated (NLS1/2) are shown in panels G and I. Mock transfected cells (A-C) are shown as a control. The first column (A, D and G) shows the subcellular localization of the GFP-KCTD8 fusion proteins by the autofluorescence of GFP (green). Cells shown in panels B, E and H were labeled with an anti-α-tubulin antibody and detected with an Alexa Fluor 568-conjugated secondary antibody (red). Overlaid images from the first two columns are shown in column three (C, F and I). Note the co-localization of the KCTD8 wild-type protein with α-tubulin (panel F, yellow signal) and the absence of co-localization in the cells expressing the NLS1/2 mutant construct (panel I).

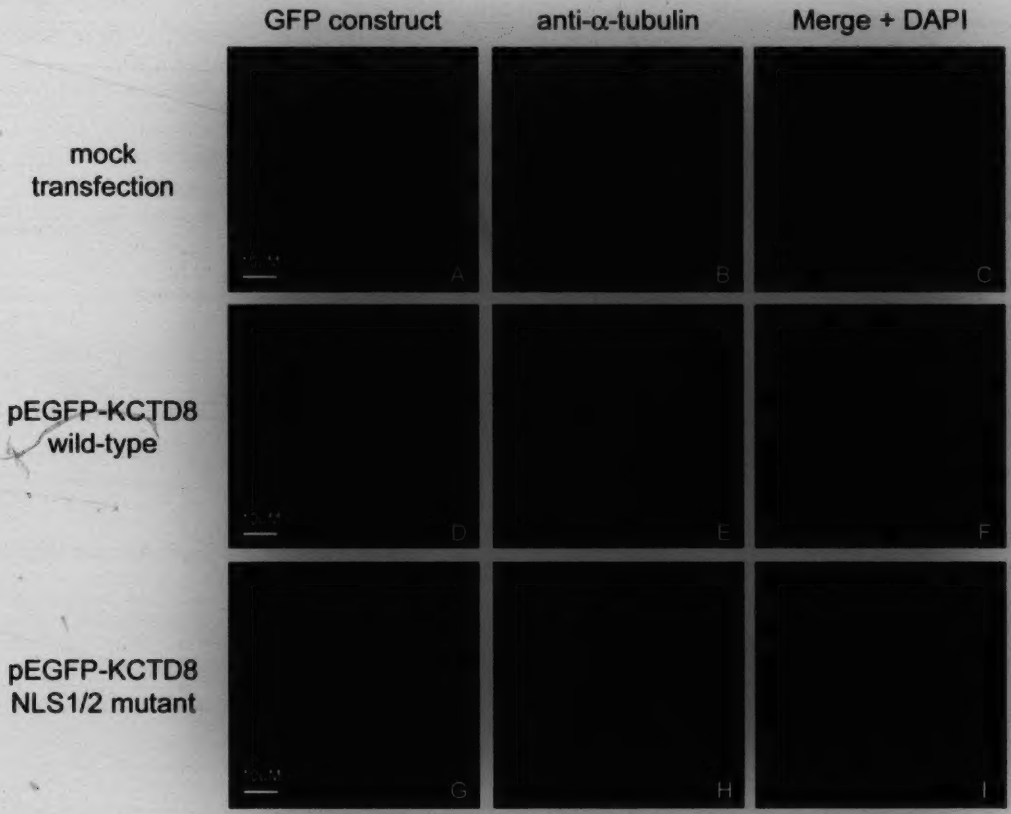

Figure 4.7 - Co-immunoprecipitation (co-IP) showing association of KCTD8 with α-tubulin in transfected COS-7 cells.

Homogenates of COS-7 cells transiently transfected with wild-type or mutant KCTD8 were subjected co-immunoprecipitation using an affinity purified anti-KCTD8 antibody. The eluate from each co-IP was split in half and subjected to SDS-PAGE and western blot analysis (A and B, lanes 7-12) to make two identical blots. The lanes in both panels for eluted protein after co-IP are as follows: 7) mock transfected; 8) pEGFP-C1 empty vector; 9) wild-type GFP-KCTD8; 10) GFP-KCTD8 NLS1 mutant; 11) GFP-KCTD8 NLS2 mutant; 12) GFP-KCTD8 NLS1/2 double mutant. Input lysates used in the co-IP experiment were also subjected to western blot analysis to ensure that equal amounts of each protein were used in the co-IP (A and B, lanes 1-6). The lanes in both panels for the input protein are as follows: 1) mock transfected; 2) pEGFP-C1 empty vector; 3) wild-type GFP-KCTD8; 4) GFP-KCTD8 NLS 1 mutant; 5) GFP-KCTD8 NLS2 mutant; 6) GFP-KCTD8 NLS1/2 double mutant. A) Analysis using anti-GFP antibody. B) Analysis with anti-α-tubulin antibody.

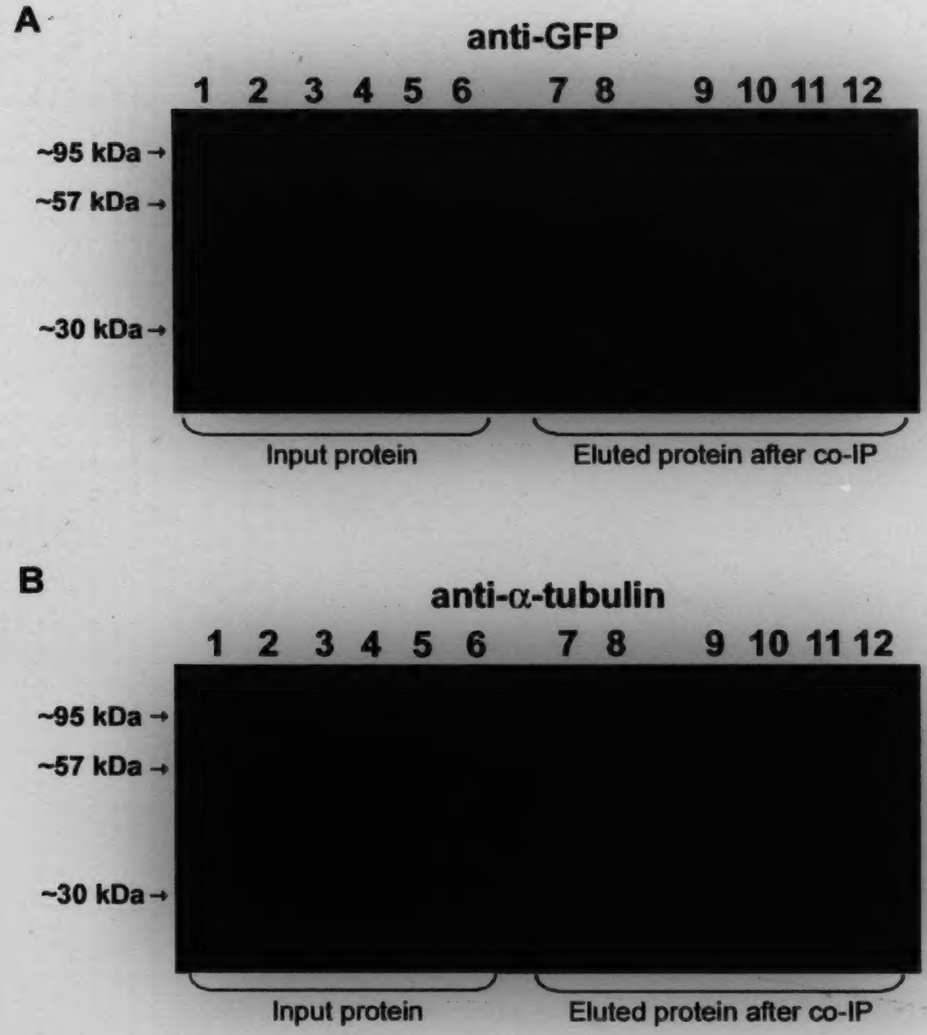
A
anti-GFP
1 2 3 4 5 6 7 8 9 10 11 12
~95 kDa →
~57 kDa →
~30 kDa →
Input protein
Eluted protein after co-IP
B
anti-α-tubulin
1 2 3 4 5 6 7 8 9 10 11 12
~95 kDa →
~57 kDa →
~30 kDa →
Input protein
Eluted protein after co-IP

Figure 4.8 - Representative images showing subcellular localization of colcemid treated COS-7 cells transfected with wild-type and mutant GFP-KCTD8 fusion proteins.

Images from control transfections are shown in panels A-C (mock transfected cells) and panels D-F (pEGFP-C1 empty vector transfected cells). COS-7 cells exogenously expressing the wild-type GFP-KCTD8 are shown in panels G-I. Cells transfected with the double mutant construct (GFP-KCTD8 NLS1/2) are shown in panels J-L. Cells overexpressing the GFP fusion proteins (green) were either untreated (A, D, G, and J), treated with 2 μM colcemid (B, E, H, and K) or 5 μM colcemid (C, F, I, and L). Nuclei were stained with propidium iodide (red).

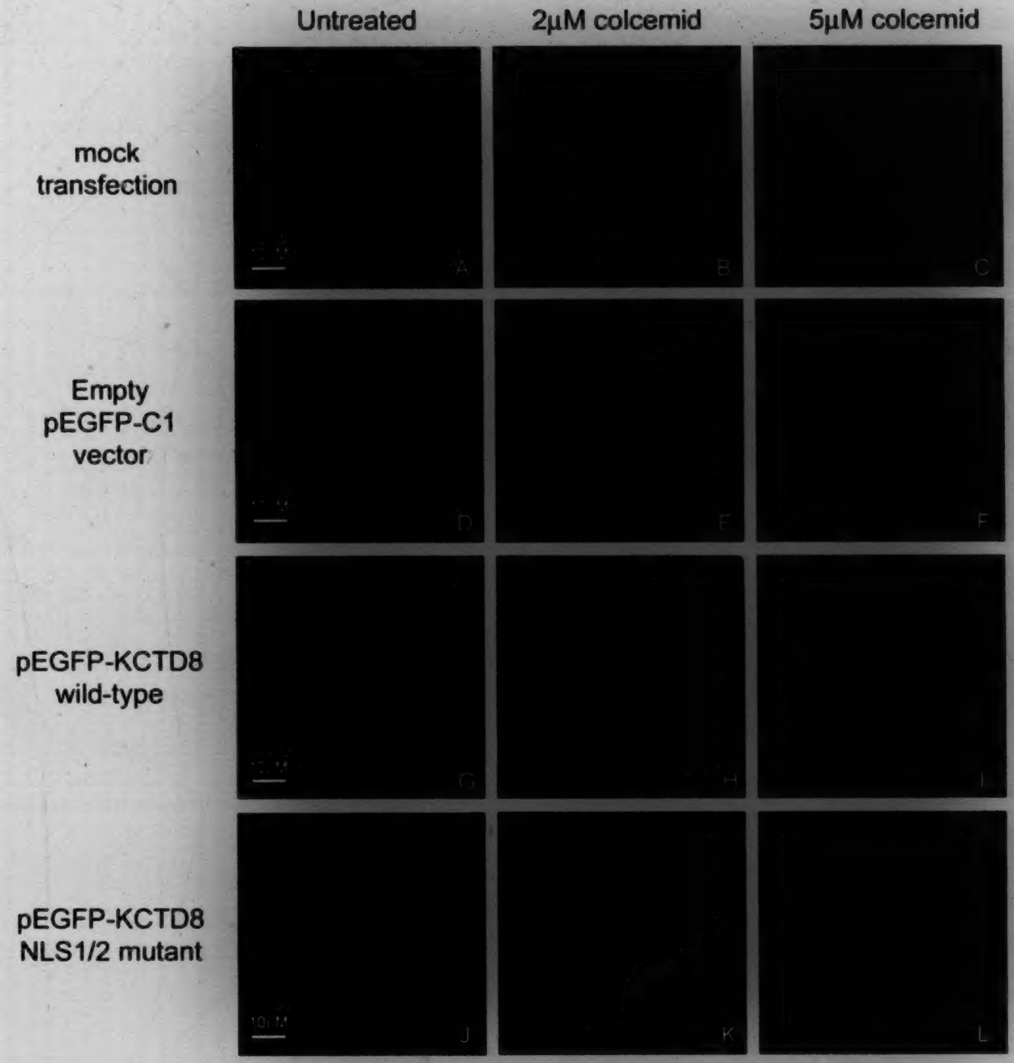
Untreated
2µM colcemid
5µM colcemid
mock transfection
Empty pEGFP-C1 vector
pEGFP-KCTD8 wild-type
pEGFP-KCTD8 NLS1/2 mutant
A
B
C
D
E
F
G
H
I
10µM
J
K
L

Figure 4.9 – Optical sections of wild-type and mutant KCTD8 transfected COS-7 cells treated with 5 μM colcemid.

Serial optical sections were taken through the z-plane of the cells. Images are in consecutive order from left to right, top to bottom. Cells transfected with wild-type pEGFP-KCTD8 construct are shown in panel A and cells transfected with the double mutant pEGFP-KCTD8 NLS1/2 construct are shown in panel B. GFP expression is shown in green and nuclei stained with propidium iodide are shown in red. Note the presence of the yellow merge signal within the nuclei of the wild-type pEGFP-KCTD8 transfected cells (panel A, indicated by arrowheads).

A wild-type pEGFP-KCTD8, 5 μM colcemid

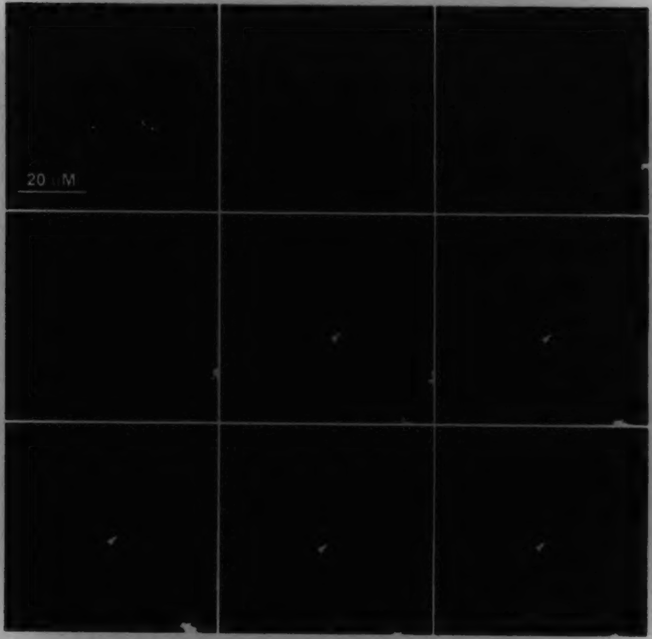

B pEGFP-KCTD8 NLS1/2, 5 μM colcemid

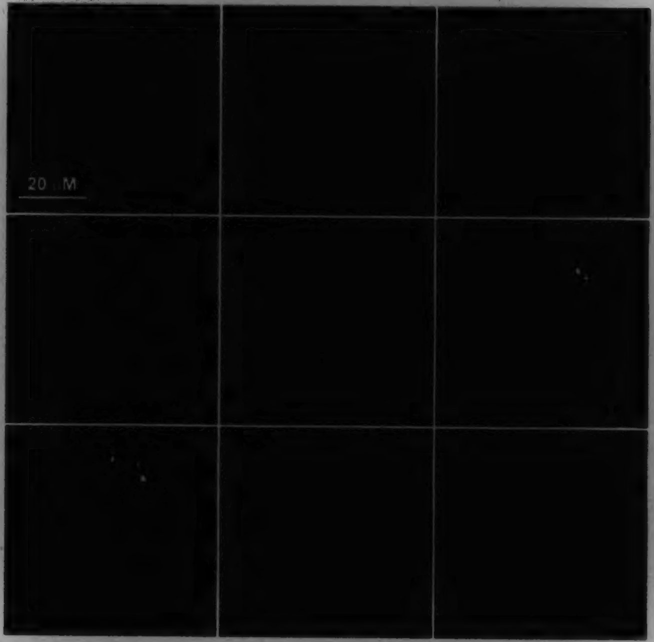

Figure 4.10 - Immunohistochemical localization of KCTD8 in the rat retina.

Single labeling of KCTD8 in retinas from rats reared in strictly dark conditions. Retina sections in Panels A, D and G were labeled with a rabbit anti-KCTD8 polyclonal antibody and detected with an Oregon Green 514 secondary antibody (green). Nuclei in Panels B, E, H, and K are stained with propidium iodide (red). The third column (Panels C, F, I, and L) are overlaid images from first two columns. Panels D, E, F, G, H and I are 2X magnifications of Panels A, B, and C in order to better show the ganglion cell layer and inner nuclear layer (Panels D, E, and F) and the outer nuclear layer and the photoreceptor cell layer (Panels G, H, and I). Note the nuclear localization of KCTD8 in the ganglion cells (Panel F, indicated with arrowheads) and the nuclear as well as cytoplasmic localization of KCTD8 in the inner nuclear layer (Panel F, indicated with asterisks). Control immunohistochemical localization with only the secondary antibody (no primary antibody) is shown in panels J and L. The signal for the ONL in panels G, H, and I appears brighter than in panels A, B, and C due to adjustment of the focal plane and a slight adjustment in the signal intensity. The various retinal layers are labeled as follows: GCL, ganglion cell layer; IPL, inner plexiform layer; INL, inner nuclear layer; OPL, outer plexiform layer; ONL, outer nuclear layer; IS, photoreceptor inner segments; OS, photoreceptor outer segments; RPE, retinal pigment epithelium.

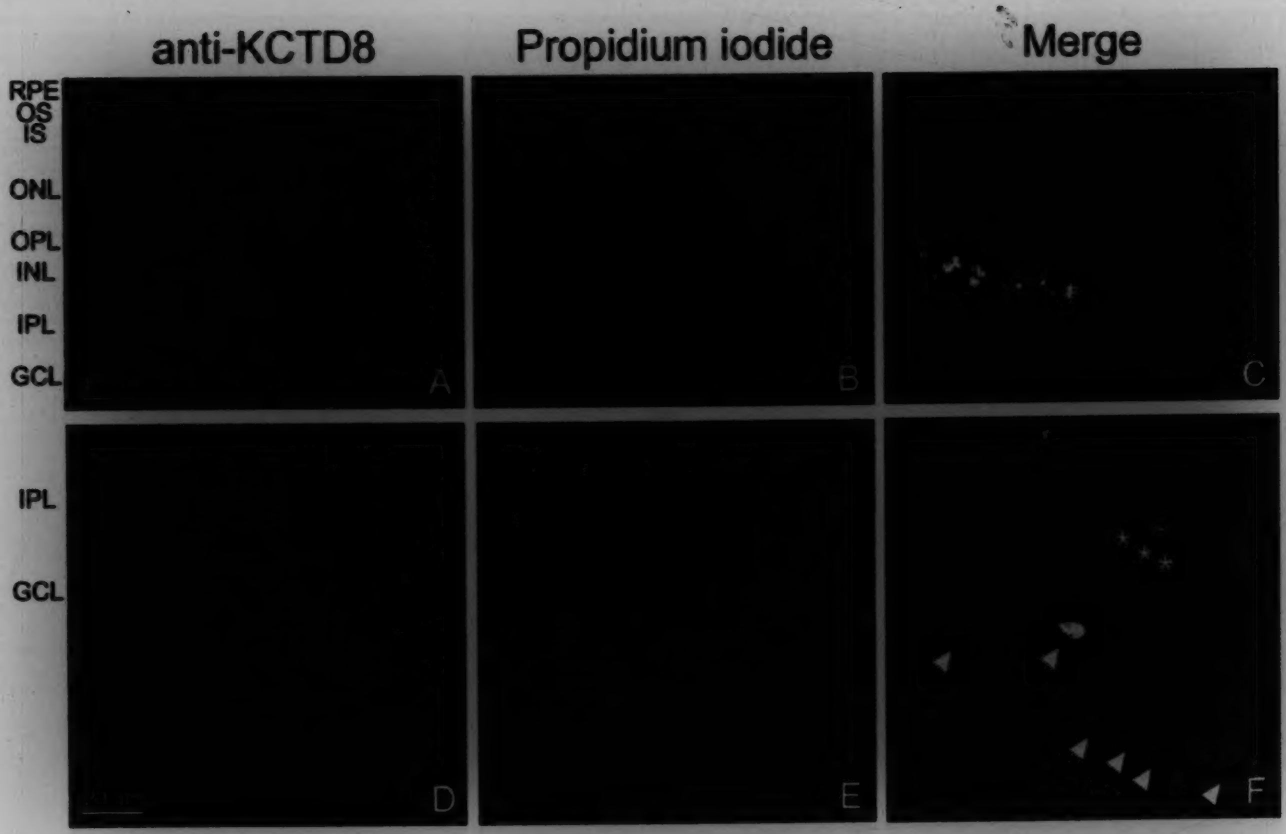
anti-KCTD8
Propidium iodide
Merge
RPE
OS
IS
ONL
OPL
INL
IPL
GCL
A
B
C
IPL
GCL
D
E
F

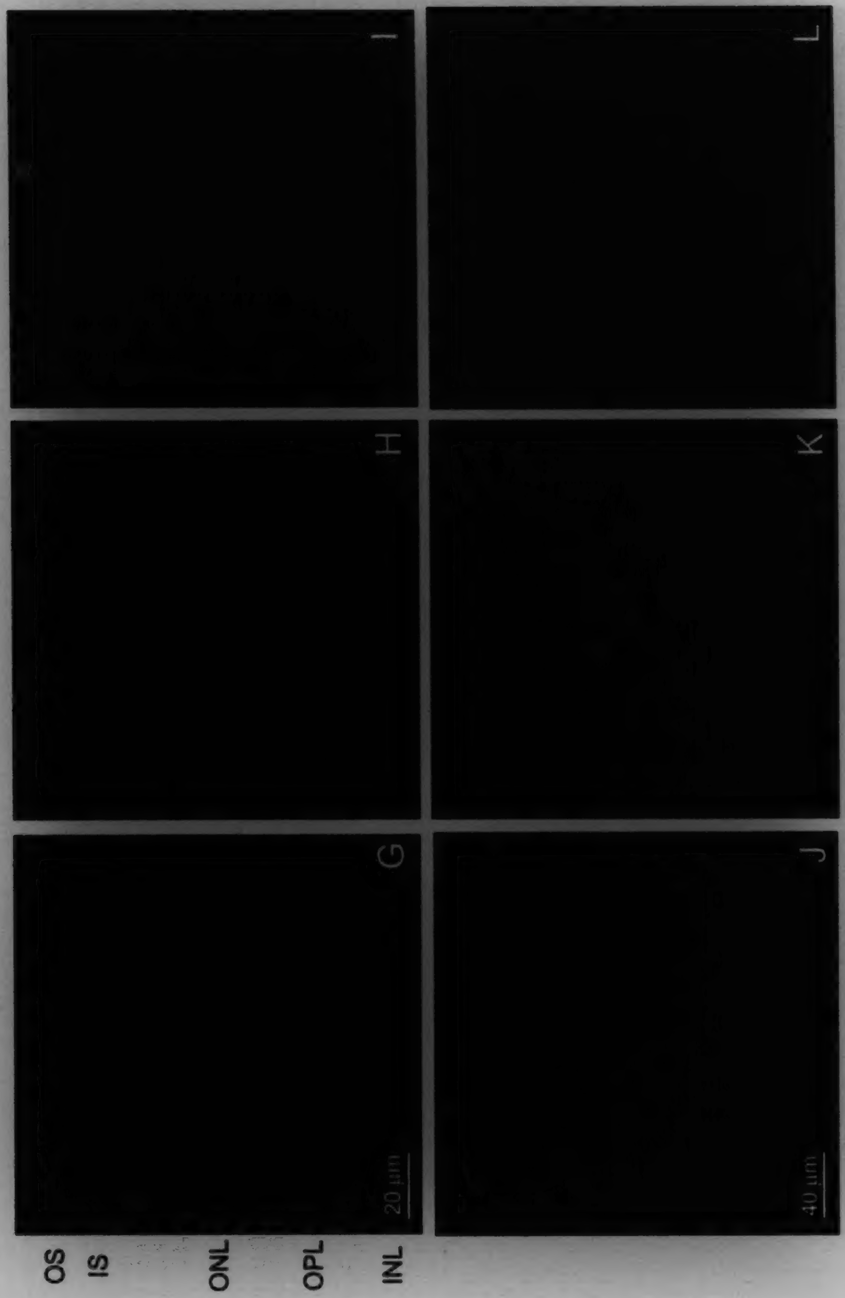
G
H
I
J
K
L
20 µm
40 µm
OS
IS
ONL
OPL
INL

Figure 4.11 - Co-localization of KCTD8 with α-tubulin in the dark-reared rat retina. The retina section in Panel A was labeled with a mouse anti-α-tubulin antibody and detected with an Alexa Fluor 488 polyclonal antibody (green). A retina section labeled with rabbit anti-KCTD8 polyclonal antibody and detected with a Cy3-conjugated secondary antibody (red) is shown in Panel B. In panel C, Hoechst stained nuclei are shown in blue. Panels A, B and C were overlaid to generate panel D. Co-localization of α-tubulin and KCTD8 is shown by the yellow signal in the merged Panel D. Control immunohistochemical staining with only the respective secondary antibodies is shown in Panels E, and F with Hoechst stained nuclei shown in panel G. The overlay of panels E, F, and G are shown in panel H. The various retinal layers are labeled as follows: GCL, ganglion cell layer; IPL, inner plexiform layer; INL, inner nuclear layer; OPL, outer plexiform layer; ONL, outer nuclear layer; IS, photoreceptor inner segments; OS, photoreceptor outer segments; RPE, retinal pigment epithelium.

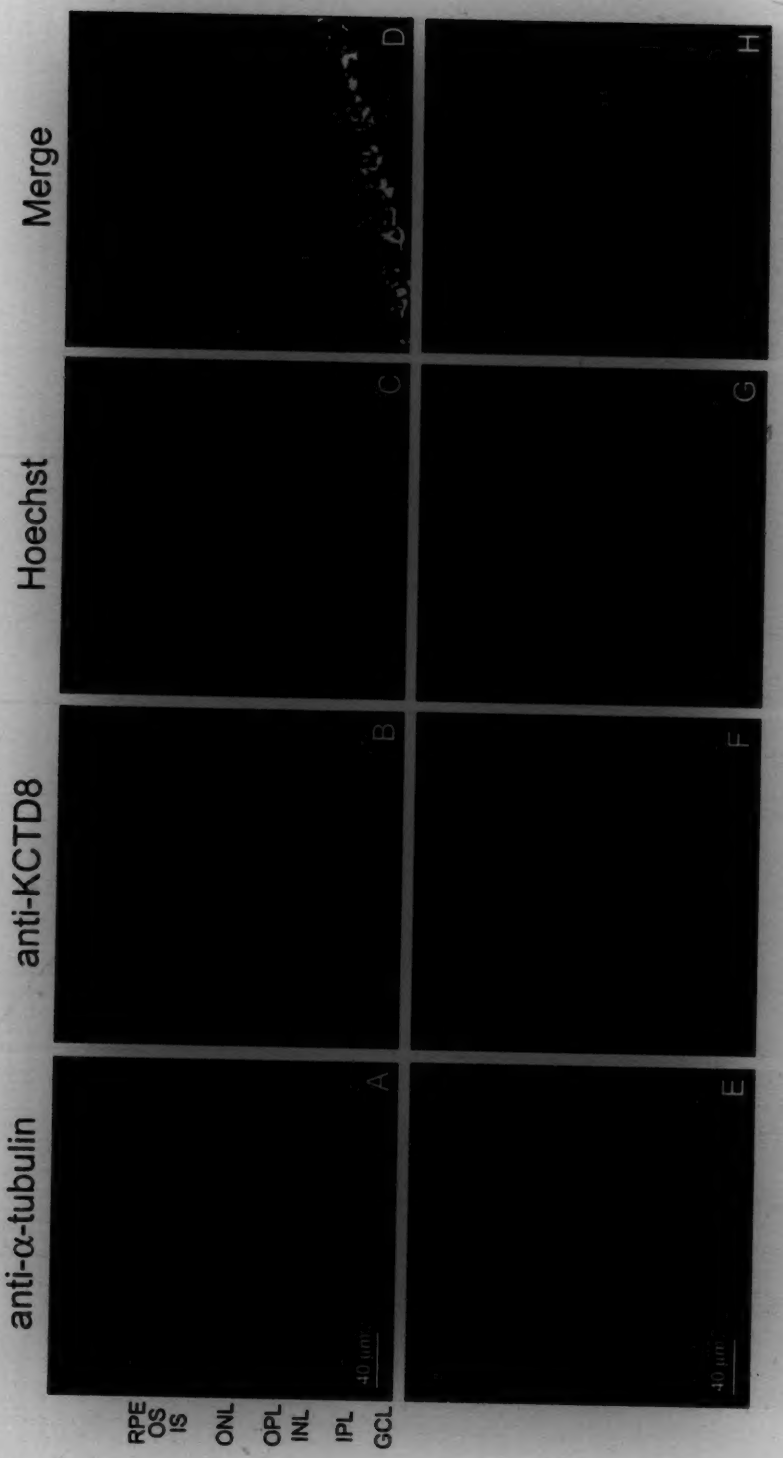
anti-α-tubulin
anti-KCTD8
Hoechst
Merge
A
B
C
D
E
F
G
H
40 µm
40 µm
RPE
OS
IS
ONL
OPL
INL
IPL
GCL

Figure 4.12 - Co-immunoprecipitation showing association of α-tubulin with KCTD8 in the dark-reared rat retina.

Retinal cell lysates were subjected to co-immunoprecipitation using an affinity purified rabbit anti-KCTD8 antibody or another rabbit polyclonal antibody as a control (anti-T-cadherin). The eluate from the co-IP was subjected to SDS-PAGE and western blot analysis and then probed with a mouse anti-α-tubulin antibody. Lanes 1, 2 and 3 are the input proteins used in the co-IP experiment. Lane 1 is negative control containing RIPA buffer with no protein. Lane 2 is the rat retinal cell lysate and Lane 3 is cell lysate from rat brain. Lanes 4-7 are the eluted proteins after the co-IP experiment. Lane 4 is the co-IP of the RIPA buffer (no protein) with the KCTD8 antibody (negative control). Lane 5 is the co-IP with the KCTD8 antibody of the retinal cell lysate. Lane 6 is the co-IP with the T-cadherin antibody of the retinal cell lysate (control for non-specific binding of rabbit antibodies). Lane 7 is the co-IP with the KCTD8 antibody of the brain cell lysate. Sizes, in kilodaltons (kDa), of α-tubulin (57 kDa) and the rabbit heavy chain IgG (55 kDa) are shown to the left of the blot. Arrowheads indicate the band corresponding to α-tubulin in lanes 5 and 7. The input protein and the eluted protein after co-IP were loaded on the same gel, however a shorter exposure time was taken for the input proteins.

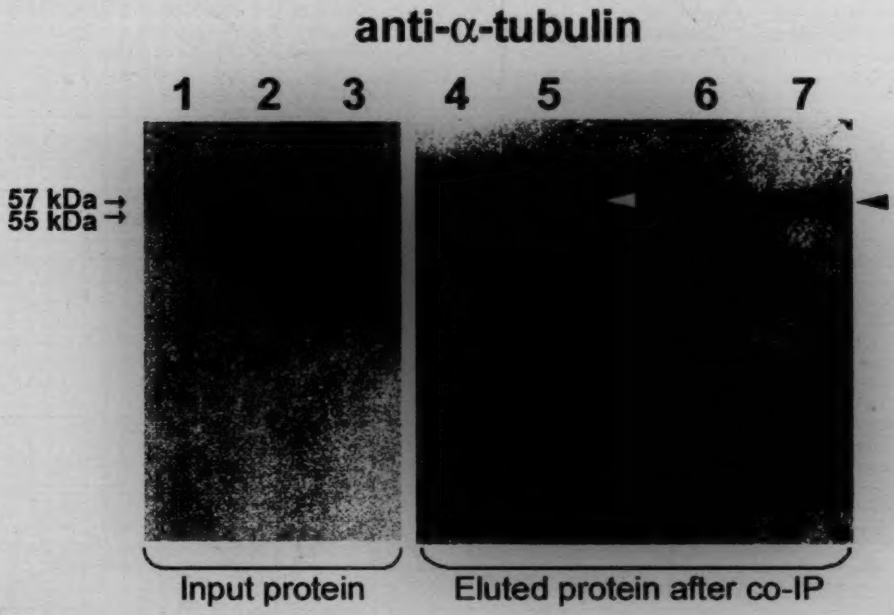

4.5 REFERENCES

1. Bixby, K.A., Nanao, M.H., Shen, N.V., Kreusch, A., Bellamy, H., Pfaffinger, P.J. and Choe, S. (1999) Zn2+-binding and molecular determinants of tetramerization in voltage-gated K+ channels. *Nat Struct Biol,* **6,** 38-43.
2. Li, M., Jan, Y.N. and Jan, L.Y. (1992) Specification of subunit assembly by the hydrophilic amino-terminal domain of the Shaker potassium channel. *Science,* **257,** 1225-30.
3. Shen, N.V. and Pfaffinger, P.J. (1995) Molecular recognition and assembly sequences involved in the subfamily-specific assembly of voltage-gated K+ channel subunit proteins. *Neuron,* **14,** 625-33.
4. Aravind, L. and Koonin, E.V. (1999) Fold prediction and evolutionary analysis of the POZ domain: structural and evolutionary relationship with the potassium channel tetramerization domain. *J Mol Biol,* **285,** 1353-61.
5. Di Marcotullio, L., Ferretti, E., De Smaele, E., Argenti, B., Mincione, C., Zazzeroni, F., Gallo, R., Masuelli, L., Napolitano, M., Maroder, M., Modesti, A., Giangaspero, F., Screpanti, I., Alesse, E. and Gulino, A. (2004) REN(KCTD11) is a suppressor of Hedgehog signaling and is deleted in human medulloblastoma. *Proc Natl Acad Sci U S A,* **101,** 10833-8.
6. Tomaru, T., Satoh, T., Yoshino, S., Ishizuka, T., Hashimoto, K., Monden, T., Yamada, M. and Mori, M. (2006) Isolation and characterization of a transcriptional cofactor and its novel isoform that bind the deoxyribonucleic acid-binding domain of peroxisome proliferator-activated receptor-gamma. *Endocrinology,* **147,** 377-88.
7. Zhou, J., Ren, K., Liu, X., Xiong, X., Hu, X. and Zhang, J. (2005) A novel PDIP1-related protein, KCTD10, that interacts with proliferating cell nuclear antigen and DNA polymerase delta. *Biochim Biophys Acta,* **1729,** 200-3.
8. Resendes, B.L., Kuo, S.F., Robertson, N.G., Giersch, A.B., Honrubia, D., Ohara, O., Adams, J.C. and Morton, C.C. (2004) Isolation from cochlea of a novel human intronless gene with predominant fetal expression. *J Assoc Res Otolaryngol,* **5,** 185-202.

9. Kelln, R.M., Organisciak, D.T., Darrow, R., Wong, P. (In preparation) Identification and characterization of T-cadherin, isolated by a differential screening strategy to identify genes involved in light-induced retinal degeneration.

10. Kelln, R., Darrow, R., Organisciak, D.T., Wong, P. (In preparation) Identification and characterization of rat KCTD8.

11. Papazian, D.M. (1999) Potassium channels: some assembly required. *Neuron,* **23,** 7-10.

12. Chalfie, M., Tu, Y., Euskirchen, G., Ward, W.W. and Prasher, D.C. (1994) Green fluorescent protein as a marker for gene expression. *Science,* **263,** 802-5.

13. Bradford, M.M. (1976) A rapid and sensitive method for the quantitation of microgram quantities of protein utilizing the principle of protein-dye binding. *Anal Biochem,* **72,** 248-54.

14. Ullman, K.S., Powers, M.A. and Forbes, D.J. (1997) Nuclear export receptors: from importin to exportin. *Cell,* **90,** 967-70.

15. Wolff, B., Sanglier, J.J. and Wang, Y. (1997) Leptomycin B is an inhibitor of nuclear export: inhibition of nucleo-cytoplasmic translocation of the human immunodeficiency virus type 1 (HIV-1) Rev protein and Rev-dependent mRNA. *Chem Biol,* **4,** 139-47.

16. Rieder, C.L. and Palazzo, R.E. (1992) Colcemid and the mitotic cycle. *J Cell Sci,* **102 (Pt 3),** 387-92.

17. Vasiliev, J.M., Gelfand, I.M., Domnina, L.V., Ivanova, O.Y., Komm, S.G. and Olshevskaja, L.V. (1970) Effect of colcemid on the locomotory behaviour of fibroblasts. *J Embryol Exp Morphol,* **24,** 625-40.

18. Vasiliev, J.M., Gelfand, I.M. and Guelstein, V.I. (1971) Initiation of DNA synthesis in cell cultures by colcemid. *Proc Natl Acad Sci U S A,* **68,** 977-9.

19. Gamse, J.T., Kuan, Y.S., Macurak, M., Brosamle, C., Thisse, B., Thisse, C. and Halpern, M.E. (2005) Directional asymmetry of the zebrafish epithalamus guides dorsoventral innervation of the midbrain target. *Development,* **132,** 4869-81.

20. Giannakakou, P., Sackett, D.L., Ward, Y., Webster, K.R., Blagosklonny, M.V. and Fojo, T. (2000) p53 is associated with cellular microtubules and is transported to the nucleus by dynein. *Nat Cell Biol,* **2,** 709-17.

21. Lam, M.H., Thomas, R.J., Loveland, K.L., Schilders, S., Gu, M., Martin, T.J., Gillespie, M.T. and Jans, D.A. (2002) Nuclear transport of parathyroid hormone (PTH)-related protein is dependent on microtubules. *Mol Endocrinol,* **16,** 390-401.

22. Campbell, E.M. and Hope, T.J. (2003) Role of the cytoskeleton in nuclear import. *Adv Drug Deliv Rev,* **55,** 761-71.

23. Alexandrova, N., Niklinski, J., Bliskovsky, V., Otterson, G.A., Blake, M., Kaye, F.J. and Zajac-Kaye, M. (1995) The N-terminal domain of c-Myc associates with alpha-tubulin and microtubules in vivo and in vitro. *Mol Cell Biol,* **15,** 5188-95.

24. Niklinski, J., Claassen, G., Meyers, C., Gregory, M.A., Allegra, C.J., Kaye, F.J., Hann, S.R. and Zajac-Kaye, M. (2000) Disruption of Myc-tubulin interaction by hyperphosphorylation of c-Myc during mitosis or by constitutive hyperphosphorylation of mutant c-Myc in Burkitt's lymphoma. *Mol Cell Biol,* **20,** 5276-84.

25. Ziegelbauer, J., Shan, B., Yager, D., Larabell, C., Hoffmann, B. and Tjian, R. (2001) Transcription factor MIZ-1 is regulated via microtubule association. *Mol Cell,* **8,** 339-49.

26. Salman, H., Abu-Arish, A., Oliel, S., Loyter, A., Klafter, J., Granek, R. and Elbaum, M. (2005) Nuclear Localization Signals Induce Molecular Delivery along Microtubules. *Biophys J,* **89,** 2134-2145.

27. Oyster, C.W. (1999) The human eye: structure and function. In. Sinauer Associates, Sunderland, MA, pp. 60-61; 545-648.

28. Nair, K.S., Hanson, S.M., Kennedy, M.J., Hurley, J.B., Gurevich, V.V. and Slepak, V.Z. (2004) Direct binding of visual arrestin to microtubules determines the differential subcellular localization of its splice variants in rod photoreceptors. *J Biol Chem,* **279,** 41240-8.

29. Nair, K.S., Hanson, S.M., Mendez, A., Gurevich, E.V., Kennedy, M.J., Shestopalov, V.I., Vishnivetskiy, S.A., Chen, J., Hurley, J.B., Gurevich, V.V. and Slepak, V.Z. (2005) Light-dependent redistribution of arrestin in vertebrate rods is an energy-independent process governed by protein-protein interactions. *Neuron,* **46,** 555-67.

30. Peterson, J.J., Orisme, W., Fellows, J., McDowell, J.H., Shelamer, C.L., Dugger, D.R. and Smith, W.C. (2005) A role for cytoskeletal elements in the light-driven translocation of proteins in rod photoreceptors. *Invest Ophthalmol Vis Sci,* **46,** 3988-98.

Chapter 5

Subcellular localization of the KCTD8 protein in response to oxidative stress

5.1 INTRODUCTION

The localization of a protein to a specific subcellular compartment as well as changes in subcellular localization can be an important component regulating proper protein function in a given cell. In addition, mislocalization of mutated proteins can indicate whether putative functional domains actually play a role in cellular localization. The functionality of a nuclear localization signal (NLS) in many proteins containing them has been assayed by comparing the cellular localization of the wild-type protein to a version of the protein in question that has the NLS(s) mutated. *In vitro* studies have shown that some proteins with NLSs can be nuclear localized under normal conditions, or cytoplasmically localized under normal conditions and in response to some stimuli, such as changes in phosphorylation, microtubule disruption, and/or apoptosis, become nuclear localized [1-7].

We have applied a similar methodology to the study of the rat potassium channel tetramerization domain containing 8 gene (KCTD8). Initial characterization of the gene identified two putative NLSs in the C-terminus of the protein [8]. Bioinformatic analysis of the protein localization using PSORT [9] and pTARGET [10] indicated that the protein is likely to be nuclear localized with 94% and 100% confidence, respectively. KCTD8 in normal, untreated cells, is associated with α-tubulin and microtubules and is localized in the cytoplasm of the cell [11]. In contrast, analysis of the KCTD8 protein with both NLSs mutated showed uniform punctate localization throughout the cytoplasm that did not co-localize with α-tubulin. Depolymerization of microtubules with colcemid resulted in irregular punctate cytoplasmic localization of wild-type KCTD8, most likely as a result of KCTD8 being bound to depolymerized microtubules. In addition to the punctate cytoplasmic localization, wild-type KCTD8 was also found to be nuclear localized following colcemid treatment suggesting that KCTD8 is bound to microtubules as a method of sequestering the protein until it is required in the nucleus. This suggests that the transport of KCTD8 from the cytoplasm to the nucleus is regulated in a stimulus specific manner. Such regulated nuclear transport has been found for proteins such as NF-κB, p53 and c-myc, which remain sequestered in the cytoplasm and get transported into the nucleus in response to changes in the cellular environment or cellular stimuli [1, 5, 7, 12].

KCTD8 was initially isolated as a differentially expressed gene from a light-induced retinal degeneration (LIRD) cDNA library [13]. In LIRD in rats, light is used to induce an oxidative stress mediated apoptotic cell death that underlies the loss of the photoreceptor cells in the retina [14, 15]. We, therefore, hypothesize that cellular stress mediates the transport of KCTD8 into the nucleus. To test this hypothesis, we transfected pEGFP-KCTD8 constructs into COS-7 cells and then examined the subcellular localization of wild-type and NLS mutant KCTD8 proteins in these cells after exposing them to a stimulus that generates oxidative stress. Three different chemicals known to impart an oxidative stress environment were used: hydrogen peroxide; paraquat; and staurosporine [16-19].

In order to determine if there are changes in the cellular localization of KCTD8 over the course of retinal degeneration we also examined the expression of KCTD8 during LIRD in rats as well as over the course of degeneration in a genetic model of retinal degeneration, the Royal College of Surgeons (RCS) rats. RCS rats are a spontaneous animal model of retinal disease with a mutation in the receptor tyrosine kinase gene *Mertk* [20]. This mutation leads to a reduced ability of the RPE to phagocytose shed photoreceptor outer segments, resulting in the accumulation of debris in the subretinal space, which potentially generates cytotoxic and genotoxic lipid-derived aldehydes and free radicals [20-22]. As a result, photoreceptor cells undergo apoptosis and complete photoreceptor cell loss is observed by 3 months of age [23, 24]. Changes in cellular localization of wild-type and mutant GFP-KCTD8 proteins between normal and degenerating retinal tissue was analyzed by immunohistochemistry. The results presented here provide additional insights into the general function of KCTD8 in the cell as well as during retinal degeneration.

5.2 MATERIALS AND METHODS

5.2.1 KCTD8 subcloning and site-directed mutagenesis

The subcloning of KCTD8 and the introduction of the mutations in the NLS sites is described in Chapter 4 (pg. 120).

5.2.2 Mammalian cell culture and transfection

COS-7 cells were grown to confluence and transfected with either the wild-type pEGFP-KCTD8 construct, the single (pEGFP-KCTD8 NLS1; pEGFP-KCTD8 NLS2) or double NLS mutant (pEGFP-KCTD8 NLS1/2) constructs, or the empty pEGFP-C1 vector. The cell culture transfections were performed as in Chapter 4 (pg. 122).

5.2.3 Cell treatments and immunocytochemistry

For all treatments, the concentrations and length of incubation used were based on published studies using COS-7 cells [18, 25, 26]. Cells transfected with the GFP constructs were treated with either:

1) **Paraquat** (methyl viologen, 1,1'-dimethyl-4,4'-bipyridylium) (Sigma-Aldrich, St. Louis, MO): Paraquat was administered at three different concentrations (100μM, 200μM and 300μM). Paraquat treatments were performed 24 or 18 hours post-transfection of the cells, and the treatment itself was carried out for 6 or 48 hours, respectively, at 37°C. Untreated control cells were left to incubate for the same length of time at 37°C so that both the untreated and treated cells would be fixed at the same time post-transfection.
2) **Hydrogen peroxide** (H_2O_2) (Sigma-Aldrich, St. Louis, MO): For hydrogen peroxide treatments, concentrations of 300 μM, 600 μM and 1 mM were used. Cells were treated at 24 hours post-transfection for 6 hours at 37°C. Untreated control cells were left to incubate for 6 hours at 37°C so that both the untreated and treated cells would be fixed at the same time post-transfection.
3) **Staurosporine** (Sigma-Aldrich, St. Louis, MO): Treatment with staurosporine was done at a low (1μM) or a high (3μM) concentration. Cells were treated at 24 hours post-transfection for 6 hours at 37°C. Untreated control cells were left to incubate for 6 hours at 37°C so that both the untreated and treated cells would be fixed at the same time post-transfection.

Following each treatment, cells were washed in cold phosphate-buffered saline (PBS - 10 mM sodium phosphate, 140 mM NaCl, and 1 mM $MgCl_2$, pH 7.4) and then fixed in absolute methanol for 15 minutes at -10°C. The fixed cells were washed again in cold PBS and the nuclei were stained with propidium iodide (Molecular Probes, Carlsbad, CA) according to the manufacturer's instructions. The cells were then mounted in Vectashield mounting medium (Vector Laboratories Inc., Burlingame, CA) and analyzed by fluorescent microscopy using a Nikon Eclipse E800 epifluorescence microscope with filters B-2A to visualize the GFP fluorescence and G-2A to visualize the propidium iodide.

Images were overlaid in Photoshop 7.0 (Adobe Systems Inc., USA) and slight adjustments in levels were performed to reduce background fluorescence, if necessary. Cell nuclei diameter measurements were taken using Photoshop 7.0 and compared to the size of the 10 μm size marker to determine nuclei size for the treated and untreated cells.

5.2.4 Animals

Light treatments of male albino Sprague-Dawley rats were performed as described in Chapter 3 (pg. 82). Dark-reared Sprague-Dawley rats (raised under conditions of no light) were use as controls. Fixation and frozen sectioning of the retinal tissue was performed as in Chapter 4 (pg. 125).

Pigmented RCS rats (bred on a Long-Evans background) were maintained in cyclic-light and raised to 2 or 6 months of age before sacrifice in CO_2 chambers. Adult Sprague-Dawley rats raised under cyclic-light conditions were used as controls. The retinas were excised and fixation was performed as above. 9 μm retinal sections were cut for both the RCS rats and the wild-type albino control rats at –20°C and placed onto Fisher Superfrost Plus slides (Fisher, Nepean, ON). Slides were stored at –80°C until use.

5.2.5 Immunohistochemistry

Immunohistochemistry on the dark-reared and light-treated retina sections was performed as in Chapter 4 (pg. 125-126).

For the wild-type cyclic-reared and RCS rats, blocking and washes were performed as per the dark-reared and light-treated retinas. The KCTD8 primary antibody was diluted 1:100 in blocking buffer. The goat anti-rabbit Alexa Fluor 488 secondary antibody (Molecular Probes) was applied at a 1:300 dilution for 1 hour in blocking solution. The final washes and mounting of the slides was performed as in Chapter 4 (pg. 126).

5.2.6 Statistical analysis

Data were analyzed by Student's t-test.

5.3 RESULTS

5.3.1 Cell treatments result in nuclear condensation and characteristic pyknotic nuclei

The concentrations used for hydrogen peroxide, paraquat, and staurosporine were based on published results using COS-7 cells, which showed that these concentrations could induce an oxidative stress environment and cause apoptosis [18, 25, 26]. To ensure that the cells were sufficiently stressed by the chemical treatments in order to induce an apoptotic response we analyzed the cells for nuclear condensation, a hallmark of classical apoptosis [27, 28]. Comparison of treated cells to untreated cells shows nuclear condensation for all treated cells except those treated with paraquat for 6 hours and the cells treated with 100 μM paraquat for 48 hours (Figure 5.1 and Figure 5.2). With the hydrogen peroxide treatments and the 48 hour paraquat treatments, an increase in the chemical concentration resulted in more significant nuclear shrinkage (Figure 5.1 and Figure 5.2A and 5.2D). For the staurosporine treatments, both the 1 μM and the 3 μM concentrations resulted in similar nuclear condensation morphology and nuclear diameter (Figure 5.1 and Figure 5.2B).

5.3.2 Oxidative stress results in nuclear localization of wild-type KCTD8

To examine the effect of cellular stress on the subcellular localization of the wild-type and NLS mutant KCTD8 proteins, transiently transfected COS-7 cells were treated with either hydrogen peroxide, paraquat or staurosporine and the GFP-KCTD8 protein localization was observed by immunofluorescence microscopy.

Hydrogen peroxide treatment concentrations used in the current study result in growth-arrest (300μM) and apoptosis (600μM, 1mM) [18, 25]. None of the transfected cells treated with the lowest concentration of hydrogen peroxide resulted in nuclear localization of either the wild-type of mutant GFP-KCTD8 proteins. The localization patterns observed for the wild-type (Figures 5.3G and 5.3I), NLS1 mutant (Figures 5.3J and 5.3L), NLS2 mutant (Figures 5.3M and 5.3O), and NLS1/2 mutant KCTD8 proteins (Figures 5.3P, and 5.3R) treated with 300μM hydrogen peroxide were similar to those observed in the untreated, transfected cells (refer to Chapter 4, Figure 4.3).

For the wild-type pEGFP-KCTD8 transfected cells treated with 600 μM hydrogen peroxide, approximately 5% of the cells displayed nuclear localization of the wild-type KCTD8 protein (Figure 5.4G and 5.4I), however, the majority (95%) of the wild-type pEGFP-KCTD8 transfected cells displayed the filamentous cytoplasmic localization of the KCTD8 protein seen in untreated cells (refer to Chapter 4, Figure 4.3). The single and double NLS mutant pEGFP-KCTD8 construct transfected cells treated with 600 μM hydrogen peroxide displayed only the filamentous or punctate cytoplasmic localization of the mutant GFP-KCTD8 proteins (Figures 5.4J, 5.4L, 5.4M, 5.4O, 5.4P and 5.4R). The highest concentration of hydrogen peroxide, 1 mM, also resulted in approximately 5% of the wild-type pEGFP-KCTD8 transfected cells displaying nuclear localization of the KCTD8 protein (Figure 5.5A and 5.5C). Treatment with 600 μM hydrogen peroxide also showed that approximately 95% of the wild-type pEGFP-KCTD8 transfected cells displayed the filamentous cytoplasmic localization of the GFP-KCTD8 protein observed in untreated cells (refer to Chapter 4, Figure 4.3). All cells transfected with the single or double NLS mutant pEGFP-KCTD8 constructs displayed the filamentous or punctate cytoplasmic localization of the mutant GFP-KCTD8 proteins (Figure 5.5D, 5.5F, 5.5G, 5.5I, 5.5J, and 5.5L) similar to that of the untreated cells. Interestingly, for the control transfections consisting of mock transfected cells and cells transfected with the empty pEGFP-C1 vector, there were no cells present on the slides after the 1 mM hydrogen peroxide treatment suggesting that the highest concentration of hydrogen peroxide used had a killing effect on these cells.

A second method of eliciting an oxidative stress environment was to treat the cells with paraquat. Paraquat is a potent oxidative-stress inducer that mediates the generation of activated oxygen and/or oxidation of NADPH and reduced glutathione [16, 29-31]. Three different concentrations, 100 μM, 200 μM and 300 μM, of paraquat were used to treat the transfected cells. Initial paraquat treatments were performed for six hours to maintain consistency between the hydrogen peroxide treatments and the paraquat treatments. A six hour paraquat treatment of the transfected cells resulted in no change in the subcellular localization for either the wild-type or NLS mutant GFP-KCTD8 proteins (Figure 5.6), even with the highest, 300 μM, concentration of paraquat (Figure 5.6C, 5.6F, 5.6I, 5.6L, 5.6O, and 5.6R). The morphology of the six hour paraquat treated cells is similar to that seen for the untreated cells and does not resemble nuclear pyknosis, which is characteristic of apoptosis, seen in the 300 μM, 600 μM and 1 mM hydrogen peroxide treated cells (Figure 5.1, Figure 5.2A and 5.2C).

Since paraquat is known to induce oxidative stress, we tested to see if the six hour incubation with paraquat was not long enough to cause a significant oxidative stress environment. Published studies have incubated COS-7 cells at the concentrations we use for up to 48 hours to induce a higher degree of cell loss; therefore we increased the paraquat treatment time to 48 hours [25]. Treatment with 100 μM paraquat for 48 hours in our experiments did not result in any nuclear condensation (Figure 5.1, Figure 5.2C) or cause any change in the subcellular localization of the GFP-KCTD8 wild-type or mutant proteins when compared to untreated cells (Figure 5.7). For the transfected cells treated with 200 μM paraquat, the wild-type GFP-KCTD8 protein displayed nuclear localization in approximately 5% of the transfected cells (Figure 5.8G and 5.8I). In contrast, both of the single NLS mutant pEGFP-KCTD8 constructs as well as the NLS1/2 double mutant pEGFP-KCTD8 construct displayed only the filamentous or punctate cytoplasmic localization (Figure 5.8J, 5.8L, 5.8M, 5.8O, and 5.8P and 5.8R). Treatment with the highest concentration of paraquat, 300 μM, approximately 10% of the wild-type pEGFP-KCTD8 transfected cells showed apparent nuclear localization of the GFP-KCTD8 protein (Figure 5.9G and 5.9I). As for the NLS1 and NLS2 single mutant pEGFP-KCTD8 transfected cells as well as the NLS1/2 double mutant pEGFP-KCTD8 transfected cells, 300 μM paraquat treatment resulted in the filamentous or punctate cytoplasmic localization of the mutant GFP-KCTD8 proteins (Figures 5.9J, 5.9L, 5.9M, 5.9O, 5.9P and 5.9R). The transfected cells treated with 200 μM and 300 μM paraquat displayed nuclear condensation similar to that seem with the higher concentrations of hydrogen peroxide (Figure 5.1, Figure 5.2D), indicating that the 48 hour paraquat treatment was inducing an oxidative stress environment leading to apoptosis.

A third agent, staurosporine, was used to induce an oxidative stress environment in our cell culture system. Staurosporine treatment leads to protein kinase inhibition, mitochondrial dysfunction, oxidative stress mediated neurotoxicity, and apoptosis [19, 32-38]. pEGFP-KCTD8 wild-type transfected cells treated with either the low (1 μM) concentration (Figure 5.10D and 5.10F) or the high (3 μM) concentration (Figure 5.11G and 5.11I) of staurosporine demonstrated nuclear localization of the KCTD8 protein in approximately 5% of the cells. Cells transfected with either of the single NLS mutant pEGFP-KCTD8 constructs displayed strictly cytoplasmic localization of the mutant GFP-KCTD8 protein with both the low (Figure 5.10G, 5.10I, 5.10J, and 5.10L) and the high (Figure 5.11J, 5.11L, 5.11M, and 5.11O) staurosporine treatments. Cells transfected with the double NLS1/2 mutant pEGFP-KCTD8 construct and treated with 1 μM or 3 μM staurosporine also displayed only punctate cytoplasmic localization of the double mutant GFP-KCTD8 protein (Figure 5.10M and 5.10O; Figure 5.11P and 5.11R). In all transfections with the mutant constructs, the cytoplasmic localization was similar to that seen in untreated cells (Chapter 4, Figure 4.3). There was no difference in the number of cells displaying cytoplasmic versus nuclear localization between the low and the high concentrations of staurosporine treated, wild-type pEGFP-KCTD8 transfected cells. The only appreciable difference between the two concentrations of staurosporine was a noticeable reduction in overall cell number when the cells were treated with the higher concentration of staurosporine. In comparing staurosporine treated cells to untreated cells there was a noticeable difference in cell nuclei size resulting in the staurosporine treated nuclei being approximately half the size of the untreated cell nuclei (Figure 5.2B). Cells treated with staurosporine tended to condense, reducing both the size of the nucleus (Figure 5.1 and Figure 5.2B) and the size of the cytoplasm, and take on the characteristic of an apoptotic cell [27, 28].

In all pEGFP-KCTD8 wild-type transfected and treated cells, pyknotic nuclei were observed in cells that also displayed cytoplasmic localization. In other words, not all pyknotic cells displayed nuclear localization of KCTD8.

5.3.3 KCTD8 becomes nuclear localized in response to cellular stress and degeneration in the retina

Analysis of KCTD8 localization in the retina indicated that KCTD8 is nuclear localized in the ganglion cell layer of dark-reared retinas as well as the light exposed retinas (Figure 5.12C, 5.12G, 5.12K, 5.12O, and 5.12S, indicated by arrowheads). KCTD8 is also localized in the nuclei of the inner nuclear layer in all the light treated retinas. In all light exposures analyzed, KCTD8 is localized in the cytosol throughout the cellular layers of the retina including the inner segments of the photoreceptor cells. With the 4 hour and 8 hour light treatments, KCTD8 is nuclear localized in a subset of nuclei in the outer nuclear layer, which contains the nuclei of the photoreceptor cells (Figure 5.12H and 5.12L, indicated by arrows).

We previously showed that KCTD8 co-localizes with α-tubulin in the cytosol of cells in culture and in dark-reared rat retinas [11]. To examine if this KCTD8 – α-tubulin association is altered after light exposure, retinal sections from dark-reared as well as light exposed rats were immunolabeled with a KCTD8 antibody and an α-tubulin antibody. Our results here confirm that KCTD8 and α-tubulin co-localize in the dark-reared as well as light-exposed retinas throughout the various layers of the retina (Figure 5.13D, 5.13H, 5.13L, 5.13P, and 5.13T; yellow merge signal). As expected, the only regions in which α-tubulin and KCTD8 do not co-localize are in the nuclei of select cells in the ganglion cell layer, the inner nuclear layer, and the outer nuclear layer.

To study localization of KCTD8 in an inherited form of retinal degeneration as opposed to an induced form, immunohistochemistry was performed on retinal sections from 2 month (Figure 5.14D) and 6 month (Figure 5.14G) old RCS rats. As a control, retina sections from wild-type cyclic-reared animals were also immunolabeled with KCTD8 (Figure 5.14A). The KCTD8 localization in the wild-type cyclic-reared retinas is similar to that seen for the dark-reared retinas. KCTD8 is cytoplasmically localized throughout the various cellular layers of the retina with nuclear localization seen primarily in the ganglion cells, as well, some cells in the inner nuclear layer display nuclear localization (Figure 5.14A and 5.14C). In the 2 month old RCS retina (Figure 5.14D, 5.14E, and 5.14F), there is a thinning of the outer nuclear layer and the photoreceptor inner and outer segments (Figure 5.14E and 5.14F). With respect to

KCTD8 localization, there is an increase in nuclear localization in the inner nuclear layer (Figure 5.14D and 5.14F) as compared to the wild-type control. The immunolabeling is still observed in the ganglion cell nuclei of the 2 month RCS rat retina. In the 6 month old RCS retina (Figure 5.14G, 5.14H and 5.14I), the outer nuclear layer and photoreceptor inner and outer segments have degenerated and, as shown in Figure 5.14H and 5.14I, there is a drastic thinning of those layers to the point that they are barely visible. The immunolabeling with KCTD8 appeared to show an increase in nuclear localization of KCTD8 in the inner nuclear layer as compared to the 2 month old RCS retina and the wild-type retina (Figure 5.14G and 5.14I). The 6 month old RCS retina shows a more pronounced detection of KCTD8 in ganglion cell nuclei than in the 2 month old RCS retina or the wild-type retina. In none of the retinas analyzed was there nuclear localization in the outer nuclear layer.

5.4 DISCUSSION

The process of LIRD is known to involve a rhodopsin-mediated oxidative stress environment that leads to the degeneration of the photoreceptor cells, the light sensing cells of the retina [15, 39-42]. As such, it is plausible to hypothesize that the nuclear localization of KCTD8 may be in response to an oxidative stress environment. In the current chapter we have demonstrated that wild-type KCTD8 translocates from the cytoplasm to the nucleus in response to an oxidative stress environment. In all treatments, a subset of cells displayed nuclear localization of the wild-type KCTD8 protein with the remainder of the cells displaying the cytoplasmic localization similar to that observed in untreated cells.

Hydrogen peroxide mediates the reduction of hydroxyl radicals and therefore is a well known inducer of oxidative stress [18]. Depending on the concentration of hydrogen peroxide used, proliferating mammalian cells can exhibit a broad range of responses anywhere from a protective effect to growth-arrest to apoptosis and, at very high concentrations, cells will undergo necrosis. At the concentrations used in this study, the lowest concentration is expected to result in growth arrest whereas the two higher concentrations should result in an apoptotic environment in the cultured cells [18]. In light of our results, we can conclude that cellular growth arrest does not mediate nucleocytoplasmic transport of KCTD8. In contrast, the higher concentrations of hydrogen peroxide that are known to induce active cell death in COS-7 cells resulted in nuclear localization of the wild-type KCTD8 protein in a subset of transfected cells, suggesting that oxidative stress and/or apoptosis triggers nuclear localization of KCTD8. Interestingly, with the highest concentration of hydrogen peroxide (1 mM), none of the mock transfected cells or the cells transfected with the pEGFP-C1 vector survived. However, cells transfected with either the wild-type pEGFP-KCTD8 construct or the NLS mutant pEGFP-KCTD8 constructs did survive, suggesting that the KCTD8 protein may confer a protective effect. This preliminary finding of a potential protective role of KCTD8 will need to be confirmed by further research.

Paraquat, a common herbicide, imparts its toxicity through the formation of superoxide anions, which then leads to production of additional reactive oxygen species such as hydrogen peroxide and hydroxyl radicals [17, 43]. As such, the mode of action for both paraquat and hydrogen peroxide are similar, resulting in the production of toxic hydroxyl radicals by Haber-Weiss and Fenton reactions [44, 45]. Initial experiments were carried out with a 6 hour treatment of paraquat to maintain consistency between the incubation times with hydrogen peroxide. In all transfected cultured cells treated for 6 hours with paraquat, no change in subcellular localization of the KCTD8 protein was noticed. Since both paraquat and hydrogen peroxide have similar modes of action we expected that paraquat and hydrogen peroxide treatment would give similar results. The incubation time for paraquat was increased to 48 hours to see if a longer exposure had an affect [25]. With the increased exposure time, transfected cells treated with the higher concentrations of paraquat (200 μM and 300 μM), resulted in nuclear localization of the wild-type KCTD8 protein in some of the transfected cells. As well, an increase in the wild-type KCTD8 protein nuclear localization was observed with increased paraquat concentration. The results with the 48 hour paraquat treatment confirm the results observed with the hydrogen peroxide treatment indicating that the wild-type KCTD8 protein can become nuclear localized in response to an oxidative stress environment in the cell.

Staurosporine induces oxidative stress mediated apoptosis via protein kinase inhibition [19, 32]. All concentrations of staurosporine used in the current study resulted in the observation of the wild-type KCTD8 protein being nuclear localized in a subset of pEGFP-KCTD8 transfected cells. These results, in combination with the observations of the hydrogen peroxide and paraquat treated cells, indicate that regardless of the source of the oxidative stress, the wild-type KCTD8 protein appears to be transported from the cytoplasm to the nucleus in a subset of the cells.

Cells transfected with either the single or double NLS mutant pEGFP-KCTD8 constructs, with or without exposure to mediators of oxidative stress, did not result in nuclear localization of the mutant KCTD8 protein. This suggests that both NLS signals present in the KCTD8 protein are required to localize the protein to the nucleus in response to oxidative stress.

Retinal degeneration in rats as a result of exposure to intense light is known to involve an oxidative stress mediated pathway resulting in apoptosis of photoreceptor cells [15]. A concomitant increase in heme oxygenase-1 levels in response to prolonged light exposures confirms the finding that photo-oxidative stress is involved in light damage [41, 46]. As such, localization of KCTD8 in retinas from rats exposed to increasing durations of light should allow us to determine if KCTD8 becomes translocated to the nucleus in response to either light or oxidative stress. In both dark-reared and light exposed retinas we found that KCTD8 localizes to ganglion cells, the cells responsible for transmitting the visual signal to the brain [47]. The presence of KCTD8 in the nuclei of retinal ganglion cells in the dark-reared retina as well as the retina during LIRD suggests that nuclear localization of KCTD8 in the ganglion cell layer is not light dependent. Due to the high oxygen partial pressure in the retina [48], even under resting conditions, it is still plausible that the localization of KCTD8 in the ganglion cell nuclei is in response to the basal level of oxidative stress in the resting retina. Since KCTD8 is not present in the nuclei of every ganglion cell, it is also possible that the cells displaying KCTD8 nuclear localization may be related to the subset of ganglion cells that are intrinsically photosensitive and function to regulate circadian rhythms [49-52]. This could be tested by performing immunohistochemistry with both the KCTD8 antibody and an antibody to melanopsin, the visual pigment of intrinsically photosensitive retinal ganglion cells [50], and analyzing for co-localization.

KCTD8 and α-tubulin co-localize in light exposed and dark-reared retinas. This suggests that KCTD8 in the retina, like KCTD8 in our cell culture experiments, is bound to microtubules and sequestered in the cytoplasm of cells. With the shorter light exposures of 4 and 8 hours, KCTD8 becomes nuclear localized in a subset of the photoreceptor cells. The nuclear localization observed in the nuclei of the photoreceptor cells after 4 and 8 hours of light treatment appears to be in response to the retinal degeneration occurring at these time points and not the presence of the light stimulus. If the response was directly related to light exposure, all the light treated retinas would have resulted in the same KCTD8 localization profile in the outer nuclear layer. The 16 hour light treatment as well as the 12 hour light treatment, 24 hour recovery retinas, however, do not show nuclear localization of KCTD8 in the outer nuclear layer.

The 4 and 8 hour time points in LIRD represent early phases of photoreceptor degeneration that we have named the commitment and execution phases, respectively [46]. It is proposed that at 4 hours of light exposure there is a change in gene expression that commits the photoreceptor cell to undergo apoptosis. With 8 hours of light exposure, the gene expression is believed to change such that there is an induction of genes involved in the actual process of apoptosis. Based on the nuclear localization of KCTD8 in the outer nuclear layer at these time points, it is possible that KCTD8 gets transported to the nucleus in response to early apoptotic signals. It is also possible that the various KCTD8 protein isoforms have multiple functions such that one is cytoplasmically localized under normal conditions and another isoform becomes nuclear localized in response to apoptosis. At present, it is unclear whether this nuclear localization in the outer nuclear layer functions to facilitate the apoptotic process or conversely, functions in an anti-apoptotic and cell protective mechanism. The localization of KCTD8 in ganglion cell nuclei in the absence of LIRD would argue against a strict role in apoptosis or a response to an active cell death environment unless KCTD8 is a multi-functional protein that has a role in both normal cellular function as well as during apoptosis. As mentioned above, this multi-functionality may be a result of the multiple KCTD8 protein isoforms performing different functions.

Unlike the LIRD model system, the RCS rat is an inherited retinal degeneration model, which contains a deletion mutation affecting the ability of the retinal pigment epithelium to phagocytose shed photoreceptor outer segments [20, 53]. This leads to a build up of debris that is believed to result in cytotoxicity and generation of free radicals with the end result being photoreceptor cell death [20, 22]. In the wild-type cyclic-reared retina used in the RCS study, the localization pattern of KCTD8 is similar to that seen for the dark-reared retinas in the LIRD model. This confirms that cellular localization of KCTD8 is not affected by low-level light stimulus. In both the 2 month and 6 month old RCS retinas, immunolabeling is observed in all retinal layers present, the ganglion cell layer, inner plexiform layer, the inner nuclear layer, and the cytoplasm of the outer nuclear layer (2 month RCS retina only). The nuclear localization of KCTD8 in both the ganglion cells and the inner nuclear layer appears to be more pronounced in the 6 month old RCS retina as compared to both the 2 month old RCS retina and the wild-type control retina. This apparent increased nuclear localization in the inner nuclear layer may be in response to the remodeling of the neural retina as a result of the almost complete loss of photoreceptor cells.

The RCS rat as well as the LIRD rat model both result in loss of photoreceptor cells via apoptosis. The main difference between the two model systems is that the LIRD model also involves phototoxicity, which exacerbates the cell death process. The presence of nuclear localized KCTD8 in the outer nuclear layer of the 4 and 8 hour light treated retinas, as opposed to the observed lack of KCTD8 nuclear localization in the outer nuclear layer of the 2 month old RCS rat, suggests that nuclear localization of KCTD8 in the photoreceptor nuclei may be in response to the phototoxicity brought about by the light treatment.

In response to the cell death of the photoreceptor cells, both the RCS rat retina and the LIRD retina undergo stereotypical phase three remodeling which involves restructuring of the neuronal retina following loss of the sensory retina [54]. Although neuronal cell death occurs in this restructuring process, many of the ganglion, amacrine, and bipolar cells located in the inner nuclear layer survive and also express molecular signatures characteristic of normal cells [55]. With the complete loss of the photoreceptor cells in the 6 month old RCS retina, detection of light by the photoreceptor cells is not possible. Being that the ganglion cells appear to function normally after complete loss of the photoreceptor cells, the increase in ganglion cell nuclear localization of KCTD8 seen in the 6 month old RCS retina may be related to the intrinsically photosensitive ganglion cells that regulate circadian rhythm compensating for the lack of circadian entrainment by the photoreceptor cells.

In both the mammalian cell culture and the retinal degeneration localization studies presented here, only a subset of cells experiencing an oxidative stress environment exhibited nuclear localization, suggesting that the nuclear localization of KCTD8 is highly regulated. Regulated nuclear localization of proteins in a cell is necessary for cellular function. A growing number of proteins that require a specific stimulus for nuclear import have been identified [56]. Many of these types of regulated nuclear localization have been found for transcription factors in which tight control of nuclear localization is necessary for normal cellular function. This is the case for the transcription factor NF-κB, in which intermolecular masking of the NF-κB p65 NLS by IκB results in the cytoplasmic retention of the protein until the NLS is unmasked by phosphorylation of IκB [57, 58]. In the case of p53, a combination of a functional microtubule network and DNA damage or cell stress results in nuclear accumulation of the protein [12, 59, 60]. Disruption of the microtubule network results in impaired nuclear accumulation of p53 due to microtubules facilitating the nuclear accumulation of p53 [12]. Microtubules are also important in the case of the transcriptional regulator c-myc in which they function to sequester and regulate the protein [1]. Phosphorylation of c-myc during mitosis or in response to oncogenic mutations disrupts the association of c-myc with microtubules allowing free c-myc to accumulate in the nucleus [2, 61].

It is clear from our results that KCTD8 can be added to this growing list of highly regulated nuclear localized proteins. In addition to the cytoplasmic retention of KCTD8, additional factors such as those identified for NF-κB, p53, and c-myc may affect its complete nuclear localization. One plausible factor is nuclear localization signal masking. The binding alone of KCTD8 to α-tubulin and microtubules may mask the NLS sites preventing the KCTD8 protein from entering the nucleus. In both untreated and treated cultured cells, the NLS1/2 double mutant KCTD8 protein does not co-localize with α-tubulin suggesting that the NLS sites are important for the interaction of KCTD8 with α-tubulin. Masking of the NLS sites in KCTD8 may also be due to native protein folding in the cell. Under normal conditions, the protein may adopt a conformation that masks the

NLS sites making recognition by the import proteins impossible. Finally, the nuclear localization signals may be masked by phosphorylation within or close to the NLSs, which inactivates the signals through charge or conformational effects. Previous analysis of the KCTD8 protein identified a number of potential phosphorylation sites in the protein, a few of which are within and surround the NLS sites [8]. Whether these predicted sites are actually phosphorylated *in vivo* remains to be determined; however, this provides a further potential mechanism of regulated nuclear import of KCTD8.

It is clear that the process of nuclear localization of KCTD8 is not as straightforward as a simple recognition of the NLS sites and import into the nucleus. Nuclear import of KCTD8 appears to be regulated by cytoplasmic anchoring and a specific trigger or process, possibly multiple triggers or processes, are required to dissociate the protein or transport the protein along the microtubules to the nucleus. Sequestration of the protein to the microtubules may act to serve as a reservoir of readily accessible KCTD8 protein that can be rapidly transported to the nucleus in response to cellular stress, apoptosis, or some additional trigger. In this study we are able to show that treatments resulting in cellular stress and apoptosis were successful in localizing the KCTD8 protein to the nucleus in a subset of cells, both in mammalian cell culture and animal models of retinal degeneration. Either the nuclear localization of KCTD8 is very tightly regulated, such that only certain cells exhibiting some specific signal trigger KCTD8 to enter, or perhaps there are additional cellular triggers not yet discovered that fully localize KCTD8 to all cells.

Figure 5.1 – Comparison of nuclear morphology of untreated cells with cells treated with hydrogen peroxide, paraquat and staurosporine.

Nuclear condensation is a hallmark of classical apoptosis [27, 28]. As such, cells were stained with propidium iodide to visual the nucleus. Note the nuclear condensation in all treatments except for all 6 hour paraquat treatments and the 100 μM 48 hour paraquat treatment.

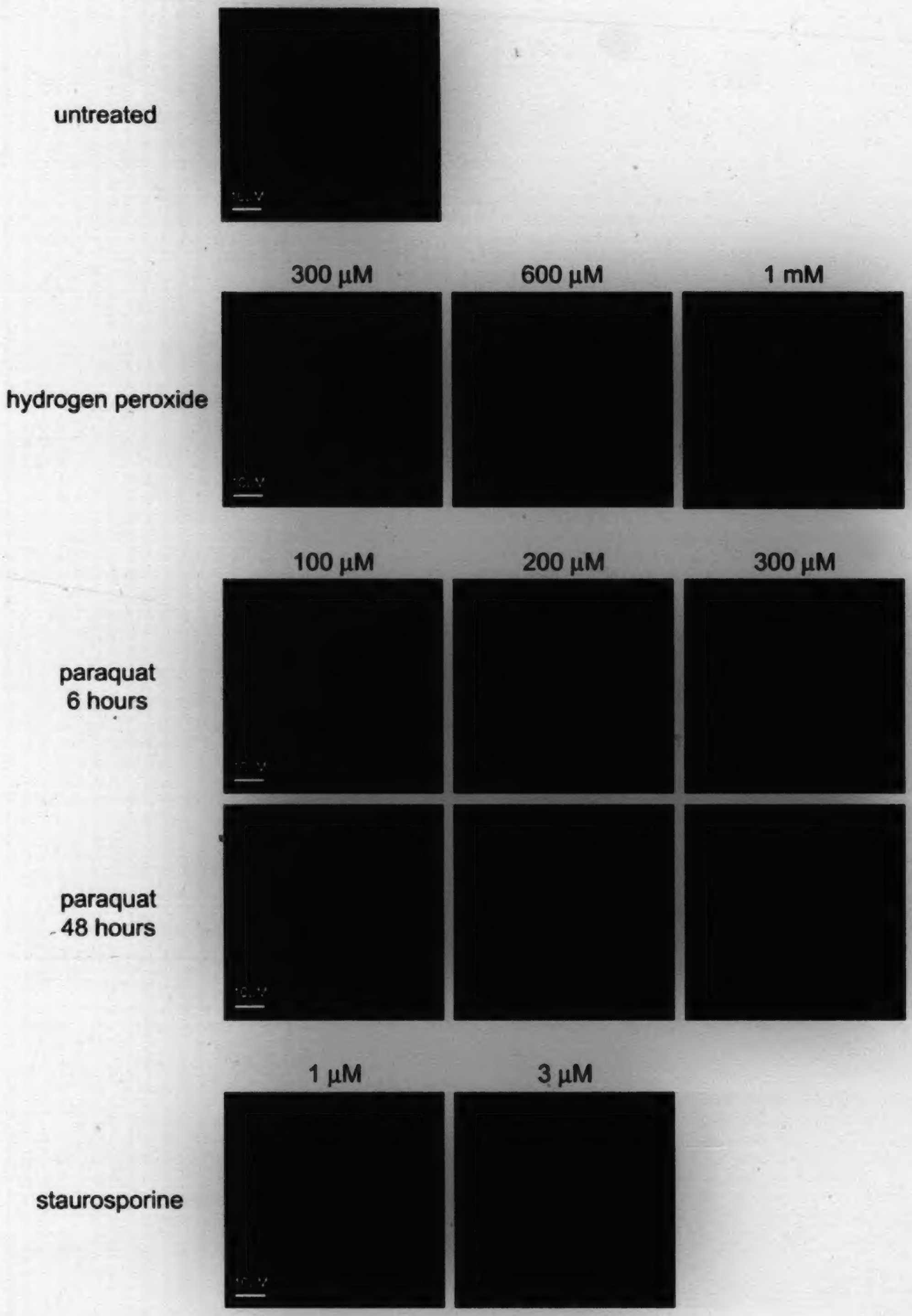
untreated
300 µM
600 µM
1 mM
hydrogen peroxide
100 µM
200 µM
300 µM
paraquat
6 hours
paraquat
48 hours
1 µM
3 µM
staurosporine

Figure 5.2 – Comparison of cell nuclei diameter when COS-7 cells are treated with hydrogen peroxide, staurosporine and paraquat.

Cell nuclei diameter measurements were taken using Adobe Photoshop and compared to the size of the 10 um size marker to determine nuclei size for cells treated with increasing concentrations of A) hydrogen peroxide for 6 hours; B) staurosporine for 6 hours; C) paraquat for 6 hours; D) paraquat for 48 hours. Each bar represents the mean ± the standard deviation of twenty cell measurements. * Significantly different from untreated COS-7 cells at $p<0.05$. ** Significantly different from untreated COS-7 cells at $p<0.001$.

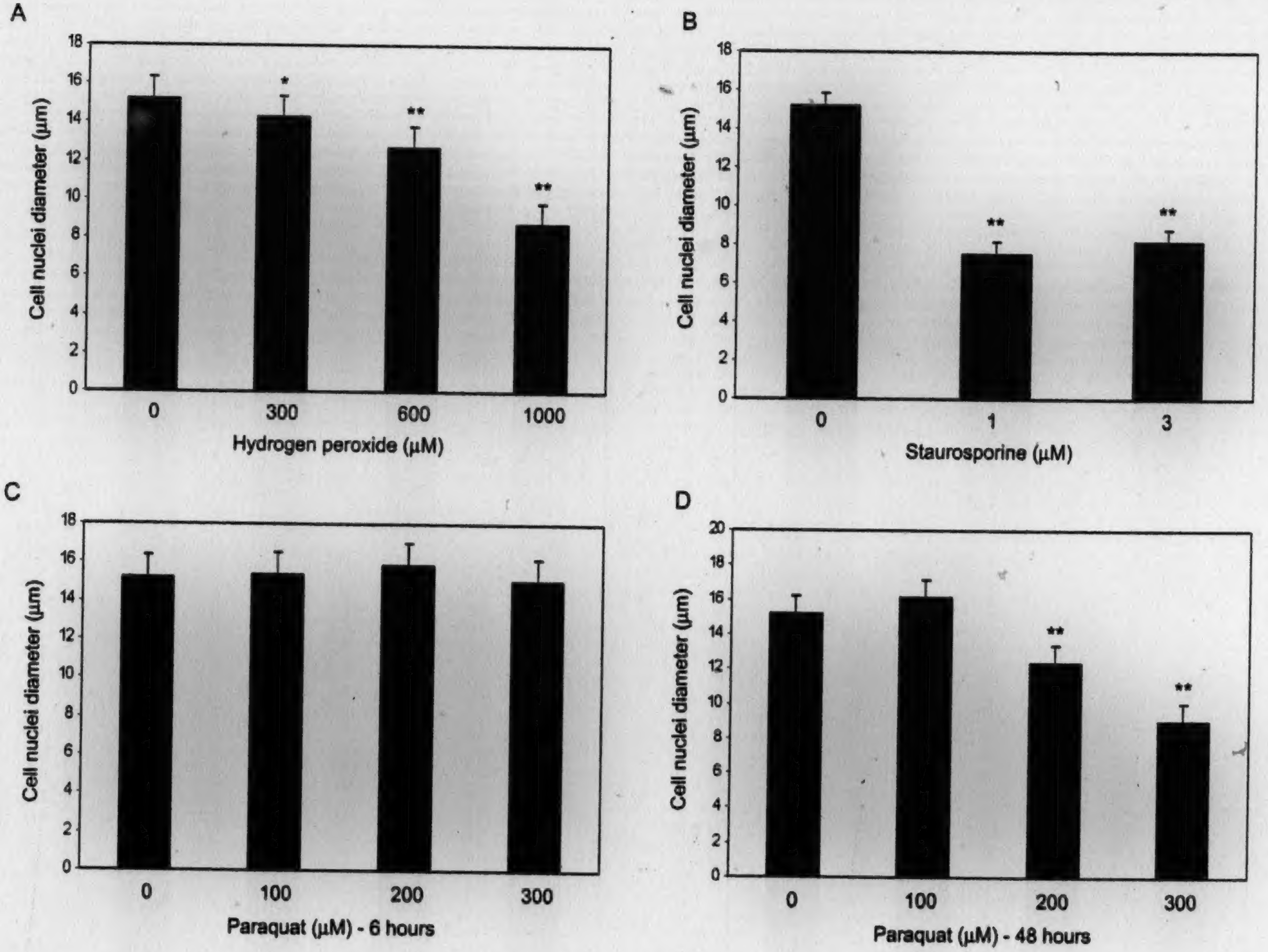
A
Cell nuclei diameter (µm)
18
16
14
12
10
8
6
4
2
0
*
**
**
0
300
600
1000
Hydrogen peroxide (µM)
B
Cell nuclei diameter (µm)
18
16
14
12
10
8
6
4
2
0
**
**
0
1
3
Staurosporine (µM)
C
Cell nuclei diameter (µm)
18
16
14
12
10
8
6
4
2
0
0
100
200
300
Paraquat (µM) - 6 hours
D
Cell nuclei diameter (µm)
20
18
16
14
12
10
8
6
4
2
0
**
**
0
100
200
300
Paraquat (µM) - 48 hours

Figure 5.3 – Immunofluorescent images of COS-7 cells transfected with wild-type and NLS mutant pEGFP-KCTD8 constructs and treated with 300 μM hydrogen peroxide for 6 hours.

Transfected cells overexpressing wild-type GFP-KCTD8 are shown in panels G-I. Control transfections are shown in panels A-C (mock-transfected cells) and panels D-F (empty pEGFP-C1 vector transfected cells). Cells transfected with the single NLS mutant constructs are shown in panels J-L (pEGFP-KCTD8 NLS1 mutant) and panels M-O (pEGFP-KCTD8 NLS2 mutant). Cells overexpressing the double NLS mutant construct, pEGFP-KCTD8 NLS1/2, are shown in panels P-R. The subcellular distribution of the GFP-KCTD8 fusion proteins are shown in panels A, D, G, J, M and P by the autofluorescence of GFP (green). Cells shown in the second column, panels B, E, H, K, N, and Q, were stained with propidium iodide (red) to visualize the nuclei of the cells. Images from column one and column two were overlaid to generate the images in the third column (panels C, F, I, L, O, and R). Note the lack of nuclear localization in any of the pEGFP-KCTD8 transfected cells.

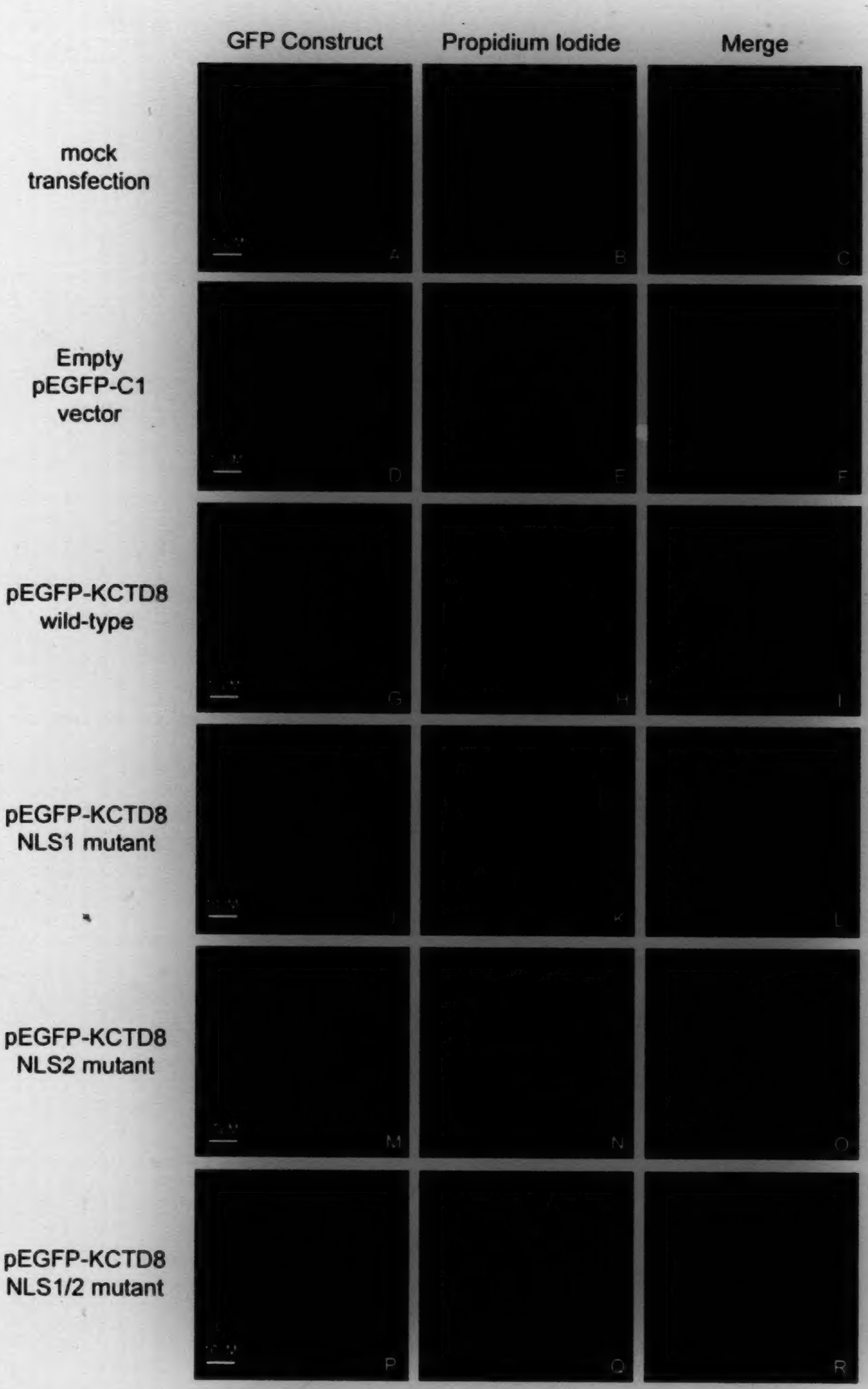
GFP Construct
Propidium Iodide
Merge
mock transfection
Empty pEGFP-C1 vector
pEGFP-KCTD8 wild-type
pEGFP-KCTD8 NLS1 mutant
pEGFP-KCTD8 NLS2 mutant
pEGFP-KCTD8 NLS1/2 mutant
A
B
C
D
E
F
G
H
I
J
K
L
M
N
O
P
Q
R

Figure 5.4 – Immunofluorescent images of COS-7 cells transfected with wild-type and NLS mutant pEGFP-KCTD8 constructs and treated with 600 μM hydrogen peroxide for 6 hours.

Transfected cells overexpressing wild-type KCTD8 are shown in panels G-I. Control transfections are shown in panels A-C (mock-transfected cells) and panels D-F (empty pEGFP-C1 vector transfected cells). Cells transfected with the single NLS mutant constructs are shown in panels J-L (pEGFP-KCTD8 NLS1 mutant) and panels M-O (pEGFP-KCTD8 NLS2 mutant). Cells overexpressing the double NLS mutant construct, pEGFP-KCTD8 NLS1/2, are shown in panels P-R. The subcellular distribution of the GFP-KCTD8 fusion proteins are shown in panels A, D, G, J, M and P by the autofluorescence of GFP (green). Cells shown in the second column, panels B, E, H, K, N, and Q, were stained with propidium iodide (red) to visualize the nuclei of the cells. Propidium iodide staining in panels N and Q was too faint to show up after the image capture; therefore, there is no propidium iodide stained nuclei in these panels. Images from column one and column two were overlaid to generate the images in the third column (panels C, F, I, L, O, and R). Note the apparent nuclear localization of the wild-type GFP-KCTD8 protein in panel I and the absence of nuclear localization for all three NLS mutant proteins (panels L, O, and R).

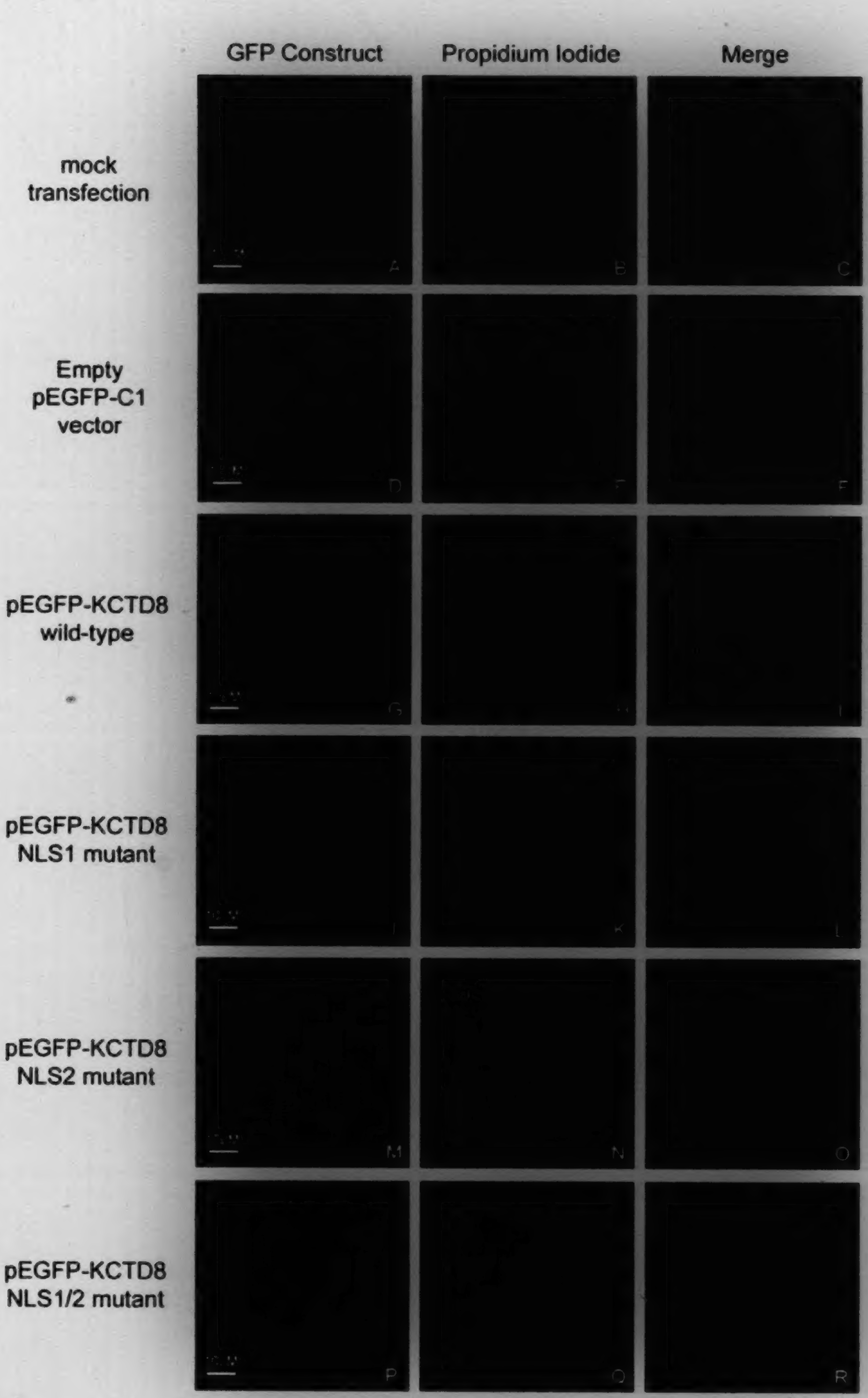
GFP Construct
Propidium Iodide
Merge
mock transfection
Empty pEGFP-C1 vector
pEGFP-KCTD8 wild-type
pEGFP-KCTD8 NLS1 mutant
pEGFP-KCTD8 NLS2 mutant
pEGFP-KCTD8 NLS1/2 mutant
A
B
C
D
E
F
G
H
I
J
K
L
M
N
O
P
Q
R

Figure 5.5 – Immunofluorescent images of COS-7 cells transfected with wild-type and NLS mutant pEGFP-KCTD8 constructs and treated with 1 mM hydrogen peroxide for 6 hours.

Transfected cells overexpressing wild-type KCTD8 are shown in panels A-C. Cells transfected with the single NLS mutant constructs are shown in panels D-F (pEGFP-KCTD8 NLS1 mutant) and panels G-I (pEGFP-KCTD8 NLS2 mutant). Cells overexpressing the double NLS mutant construct, pEGFP-KCTD8 NLS1/2, are shown in panels J-L. The subcellular distribution of the GFP-KCTD8 fusion proteins is shown in panels A, D, G, and J by the autofluorescence of GFP (green). Cells shown in the second column, panels B, E, H, and K, were stained with propidium iodide (red) to visualize the nuclei of the cells. Propidium iodide staining in panels E and K was too faint to show up after the image capture; therefore, there is no propidium iodide stained nuclei in these panels. Images from column one and column two were overlaid to generate the images in the third column (panels C, F, I, and L). Control transfections, mock transfected and transfected with the empty pEGFP-C1 vector, are not shown due to absence of cells in these transfections. Note the apparent nuclear localization of the wild-type EGFP--KCTD8 protein in panel C and the absence of nuclear localization for all three NLS mutant proteins (panels F, I and L).

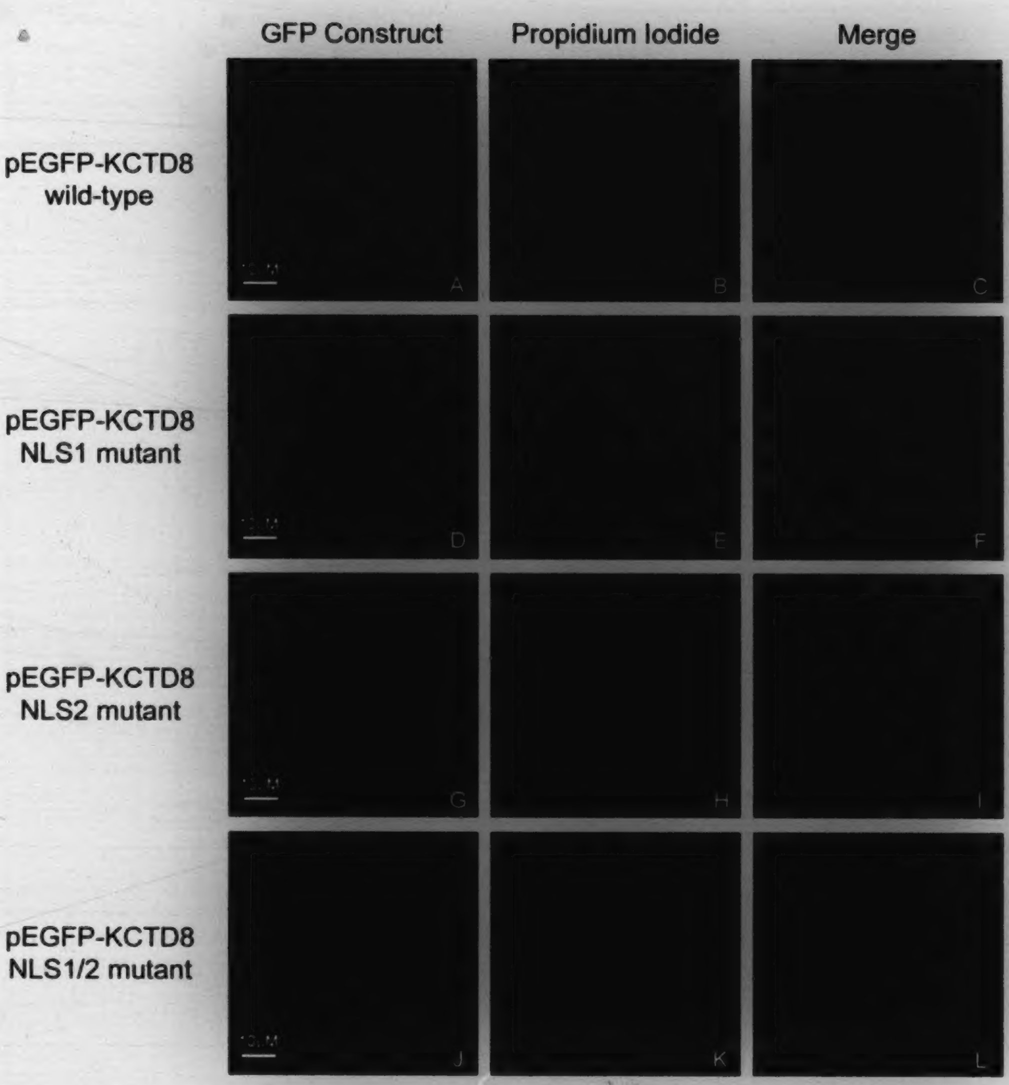
GFP Construct
Propidium Iodide
Merge
pEGFP-KCTD8 wild-type
pEGFP-KCTD8 NLS1 mutant
pEGFP-KCTD8 NLS2 mutant
pEGFP-KCTD8 NLS1/2 mutant
A
B
C
D
E
F
G
H
I
J
K
L

Figure 5.6 – Representative immunofluorescent images showing the subcellular localization of wild-type and NLS mutant GFP-tagged KCTD8 constructs in cells treated with 100 µM, 200 µM or 300 µM paraquat for 6 hours.

Transiently transfected COS-7 cells expressing pEGFP-KCTD8 wild-type (panels G-I), pEGFP-KCTD8 with the first NLS mutated (panels J-L), pEGFP-KCTD8 with the second NLS mutated (panels M-O), and pEGFP-KCTD8 with both NLS signals mutated (panels P-R). The subcellular distribution of the GFP-KCTD8 fusion proteins is shown by the autofluorescence of GFP (green). Transfections from mock transfected cells (panels A-C) as well as cells transfected with the empty pEGFP-C1 construct (panels D-F) are shown as controls. The first column shows transfected cells treated with 100 µM paraquat for 6 hours (A, D, G, J, M, and P); the second column shows transfected cells treated with 200 µM paraquat for 6 hours (B, E, H, K, N, Q); column three shows transfected cells treated with 300 µM paraquat for 6 hours (C, F, I, L, O, and R). Cells were stained with propidium iodide (red) to indicate the nuclei. Note the lack of nuclear localization in cells transfected with either the wild-type or NLS mutant pEGFP-KCTD8 constructs.

6

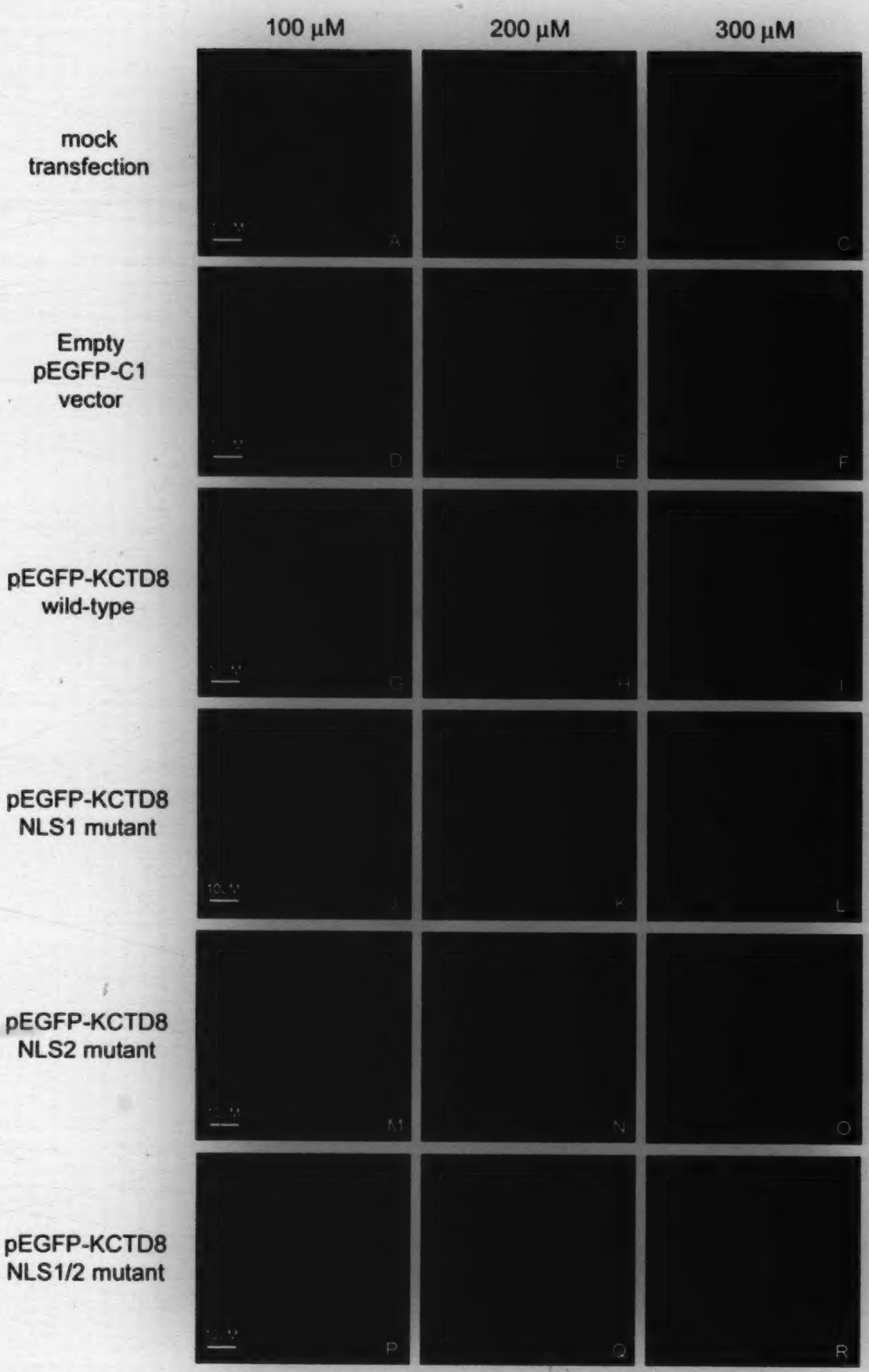
100 μM
200 μM
300 μM
mock transfection
Empty pEGFP-C1 vector
pEGFP-KCTD8 wild-type
pEGFP-KCTD8 NLS1 mutant
pEGFP-KCTD8 NLS2 mutant
pEGFP-KCTD8 NLS1/2 mutant
10μM
A
B
C
D
E
F
G
H
I
J
K
L
M
N
O
P
Q
R

Figure 5.7 – Representative images showing subcellular localization of COS-7 cells transfected with wild-type and mutant pEGFP-KCTD8 constructs and treated with 100 μM paraquat for 48 hours.

Control transfections from mock transfected cells are shown in panels A-C and transfected cells expressing the pEGFP-C1 vector are shown in panel D-F. Wild-type GFP-KCTD8 overexpressing cells are shown in panels G-I. Transfections with the mutant GFP-KCTD8 cDNA constructs containing sequence alterations in the putative NLSs are shown in panels J-L (NLS1 mutant), panels M-O (NLS2 mutant), and panels P-R (NLS1/2 double mutant). Subcellular localization of the GFP-KCTD8 fusion proteins is shown in panels A, D, G, J, M, and P by GFP fluorescence (green). The second column shows the propidium iodide staining (red) of the nuclei for each transfected cell (B, E, H, K, N, and Q). Overlaid images from the first two columns are shown in column three (C, F, I, L, O, and R). Note the lack of nuclear localization in cells transfected with the pEGFP-KCTD8 constructs.

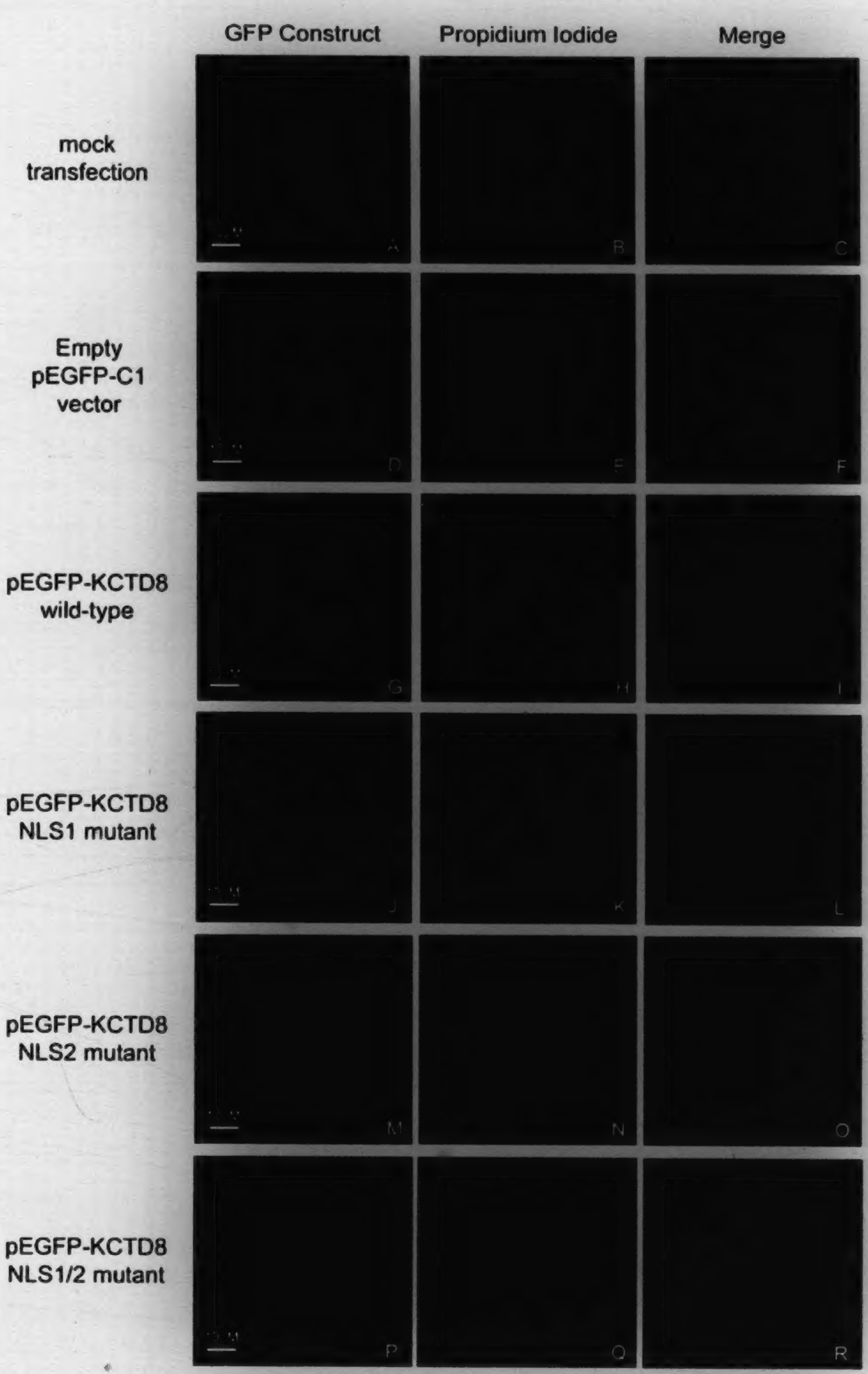
GFP Construct
Propidium Iodide
Merge
mock transfection
Empty pEGFP-C1 vector
pEGFP-KCTD8 wild-type
pEGFP-KCTD8 NLS1 mutant
pEGFP-KCTD8 NLS2 mutant
pEGFP-KCTD8 NLS1/2 mutant
A
B
C
D
E
F
G
H
I
J
K
L
M
N
O
P
Q
R

Figure 5.8 - Representative images showing subcellular localization of COS-7 cells transfected with wild-type and mutant pEGFP-KCTD8 constructs and treated with 200 μM paraquat for 48 hours.

Control transfections from mock transfected cells are shown in panels A-C and transfected cells expressing the pEGFP-C1 vector are shown in panel D-F. Wild-type GFP-KCTD8 overexpressing cells are shown in panels G-I. Transfections with the mutant GFP-KCTD8 cDNA constructs containing sequence alterations in the putative NLSs are shown in panels J-L (NLS1 mutant), panels M-O (NLS2 mutant), and panels P-R (NLS1/2 double mutant). Subcellular localization of the GFP-KCTD8 fusion proteins is shown in panels A, D, G, J, M, and P by GFP fluorescence (green). The second column shows the propidium iodide staining (red) of the nuclei for each transfected cell (B, E, H, K, N, and Q). Overlaid images from the first two columns are shown in column three (C, F, I, L, O, and R). Note the apparent nuclear localization of the wild-type GFP-KCTD8 protein (panel I).

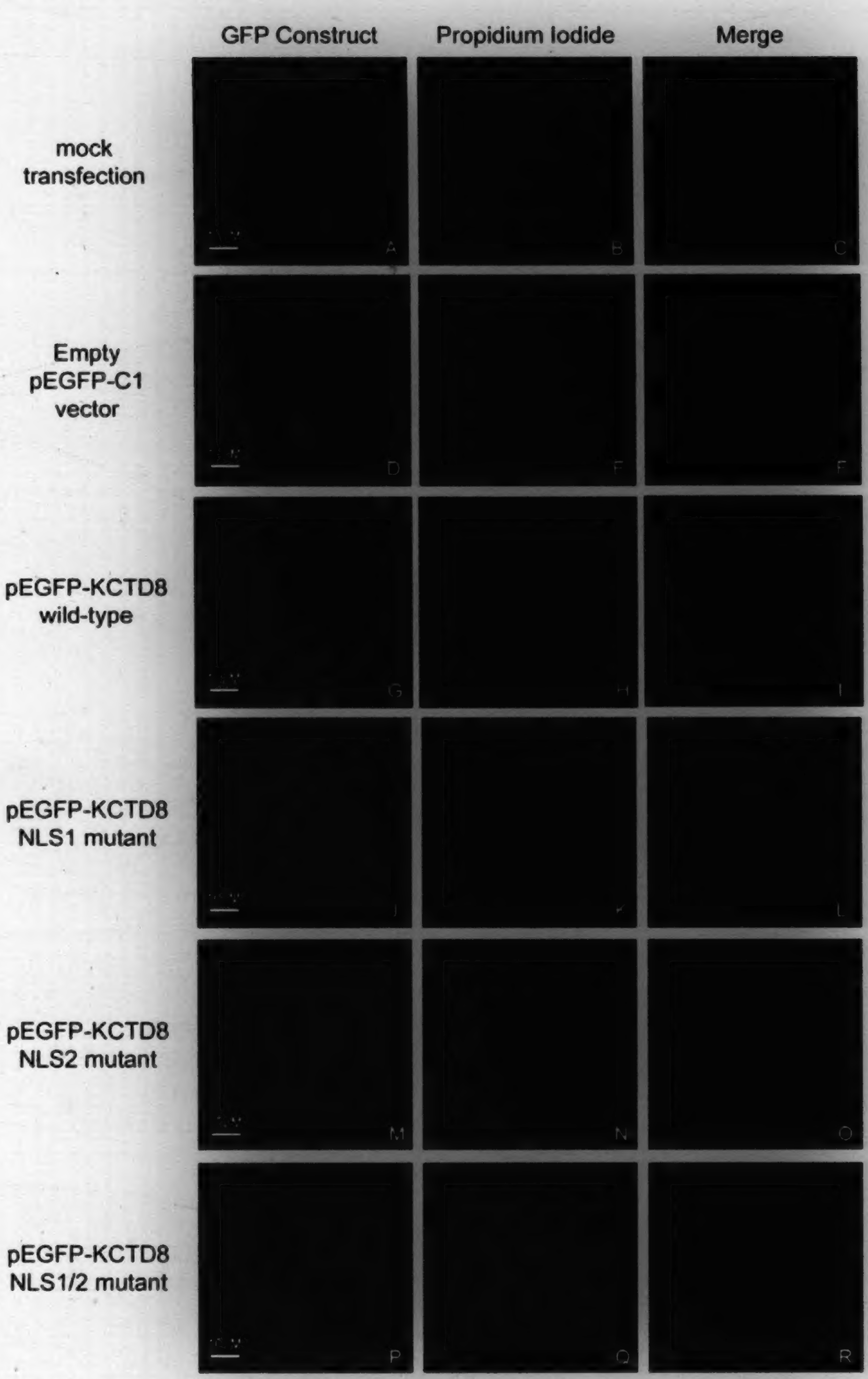
GFP Construct
Propidium Iodide
Merge
mock transfection
Empty pEGFP-C1 vector
pEGFP-KCTD8 wild-type
pEGFP-KCTD8 NLS1 mutant
pEGFP-KCTD8 NLS2 mutant
pEGFP-KCTD8 NLS1/2 mutant
A
B
C
D
E
F
G
H
I
J
K
L
M
N
O
P
Q
R

Figure 5.9 – Representative images showing subcellular localization of COS-7 cells transfected with wild-type and mutant pEGFP-KCTD8 constructs and treated with 300 μM paraquat for 48 hours.

Control transfections from mock transfected cells are shown in panels A-C and transfected cells expressing the pEGFP-C1 vector are shown in panel D-F. Wild-type GFP-KCTD8 overexpressing cells are shown in panels G-I. Transfections with the mutant GFP-KCTD8 cDNA constructs containing sequence alterations in the putative NLSs are shown in panels J-L (NLS1 mutant), panels M-O (NLS2 mutant), and panels P-R (NLS1/2 double mutant). Subcellular localization of the GFP-KCTD8 fusion proteins is shown in panels A, D, G, J, M, and P by GFP fluorescence (green). The second column shows the propidium iodide staining (red) of the nuclei for each transfected cell (B, E, H, K, N, and Q). Overlaid images from the first two columns are shown in column three (C, F, I, L, O, and R). Note the apparent nuclear localization of the wild-type GFP-KCTD protein (panel I) and the absence of nuclear localization for all three NLS mutant proteins (panels L, O, and R).

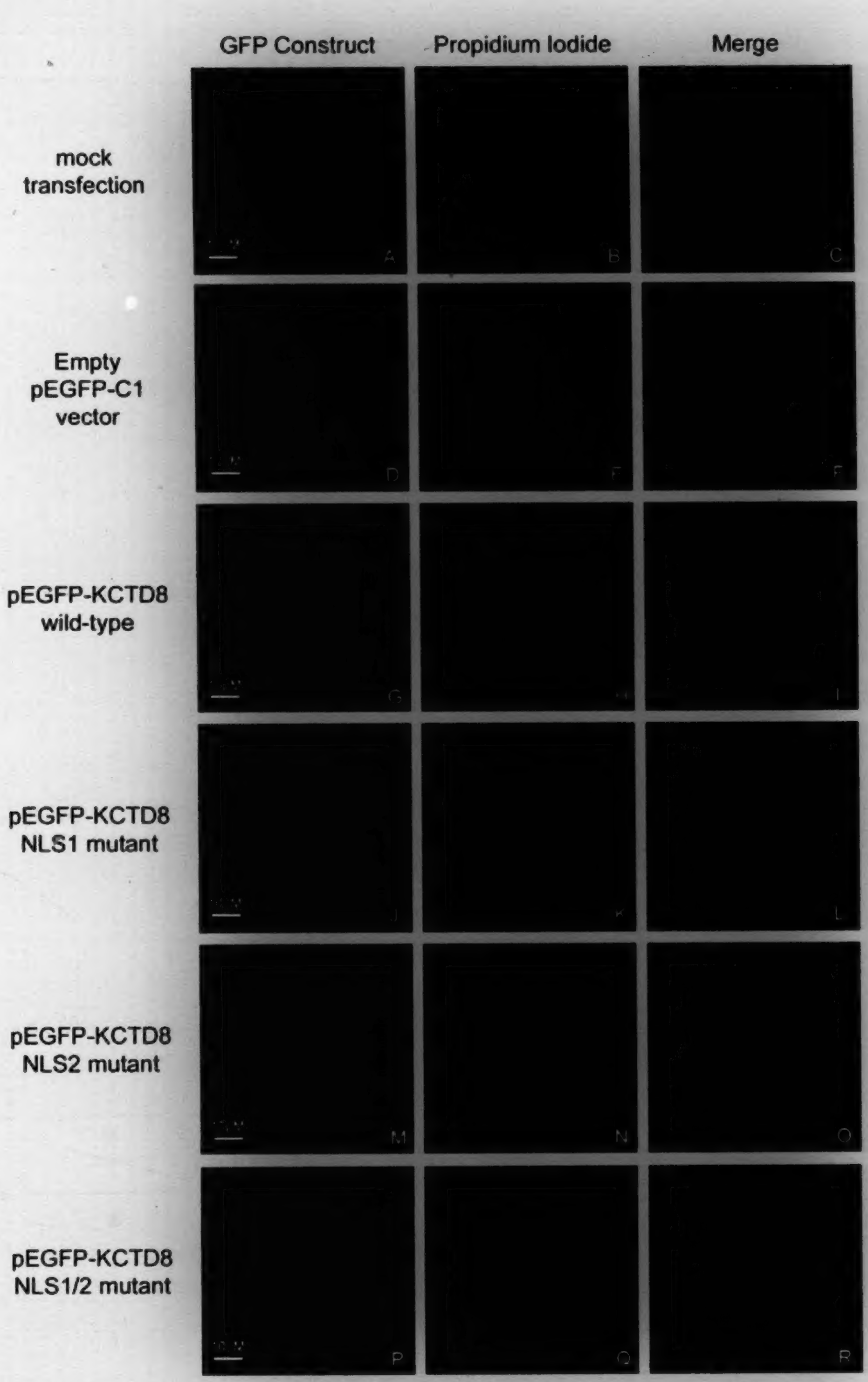
GFP Construct
Propidium Iodide
Merge
mock transfection
Empty pEGFP-C1 vector
pEGFP-KCTD8 wild-type
pEGFP-KCTD8 NLS1 mutant
pEGFP-KCTD8 NLS2 mutant
pEGFP-KCTD8 NLS1/2 mutant
A
B
C
D
E
F
G
H
I
J
K
L
M
N
O
P
Q
R

Figure 5.10 – Analysis of cellular localization of wild-type and NLS mutant GFP-KCTD8 fusion proteins in transfected COS-7 cells treated with 1 μM staurosporine. Transiently transfected cells overexpressing the wild-type GFP-KCTD8 are shown in panels D-F. Cells overexpressing the pEGFP-KCTD8 construct with the first NLS (NLS1) mutated are shown in panels G-I. Cell transfected with the mutant pEGFP-KCTD8 construct with the second NLS mutated (NLS2) are shown in panels J-L. Cells overexpressing the double mutant construct (NLS1/2) are shown in panels M-O. Images of control transfections are shown in panels A-C (cell transfected with the empty pEGFP-C1 vector). Mock transfected cells are not shown due to lack of cells on the slide. Subcellular localization of the GFP-KCTD8 fusion proteins due to autofluorescence of GFP (green) is shown in the first column (panels A, D, G, J, and M). The second column shows the propidium iodide staining (red) of the nuclei for each transfected cell (panels B, E, H, K, and N). Note that propidium iodide staining for panels H, K, and N is very faint but still present. Overlaid images from the first two columns are shown in column three (panels C, F, I, L, and O). Note the nuclear localization of the wild-type GFP-KCTD8 protein in panel F and the absence of nuclear localization for all three NLS mutant proteins (panels I, L and O).

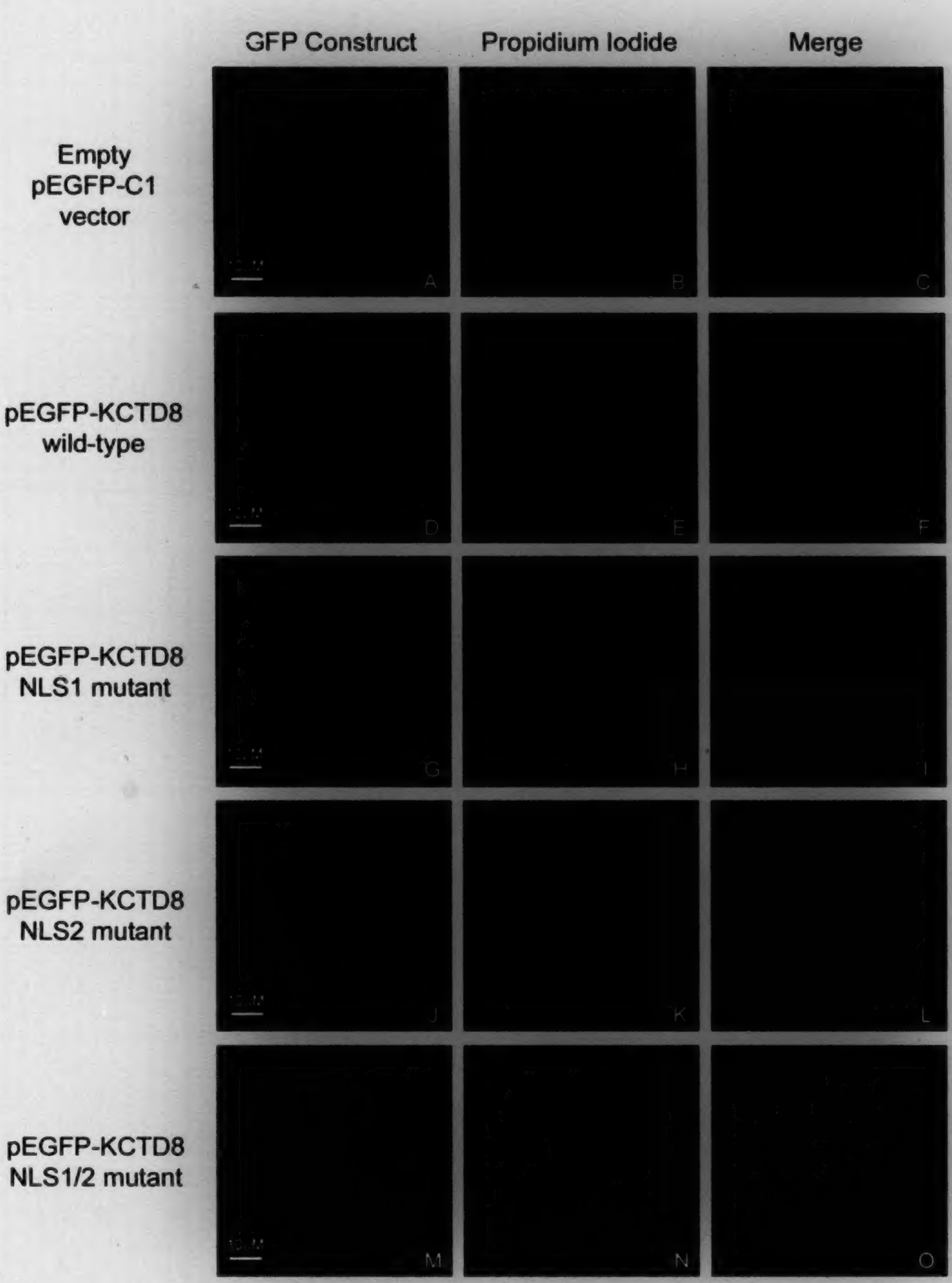
GFP Construct
Propidium Iodide
Merge
Empty pEGFP-C1 vector
pEGFP-KCTD8 wild-type
pEGFP-KCTD8 NLS1 mutant
pEGFP-KCTD8 NLS2 mutant
pEGFP-KCTD8 NLS1/2 mutant
A
B
C
D
E
F
G
H
I
J
K
L
M
N
O

Figure 5.11 – Analysis of cellular localization of wild-type and NLS mutant GFP-KCTD8 fusion proteins in transfected COS-7 cells treated with 3 μM staurosporine. Transiently transfected cells overexpressing the wild-type GFP-KCTD8 are shown in panels G-I. Cells overexpressing the pEGFP-KCTD8 construct with the first NLS (NLS1) mutated are shown in panels J-L. Cell transfected with the mutant pEGFP-KCTD8 construct with the second NLS mutated (NLS2) are shown in panels M-O. Cells overexpressing the double mutant construct (NLS1/2) are shown in panels P-R. Images of control transfections are shown in panels A-C (mock transfected cells) and panel D-F (cell transfected with the empty pEGFP-C1 vector). Subcellular localization of the GFP-KCTD8 fusion proteins due to autofluorescence of GFP (green) are shown in the first column (panels A, D, G, J, M, and P). The second column shows the propidium iodide staining (red) of the nuclei for each transfected cell (panels B, E, H, K, N, and Q). Overlaid images from the first two columns are shown in column three (panels C, F, I, L, O and R). Note the nuclear localization of the wild-type GFP-KCTD8 protein in panel I and the absence of nuclear localization for all three NLS mutant proteins (panels L, O, and R).

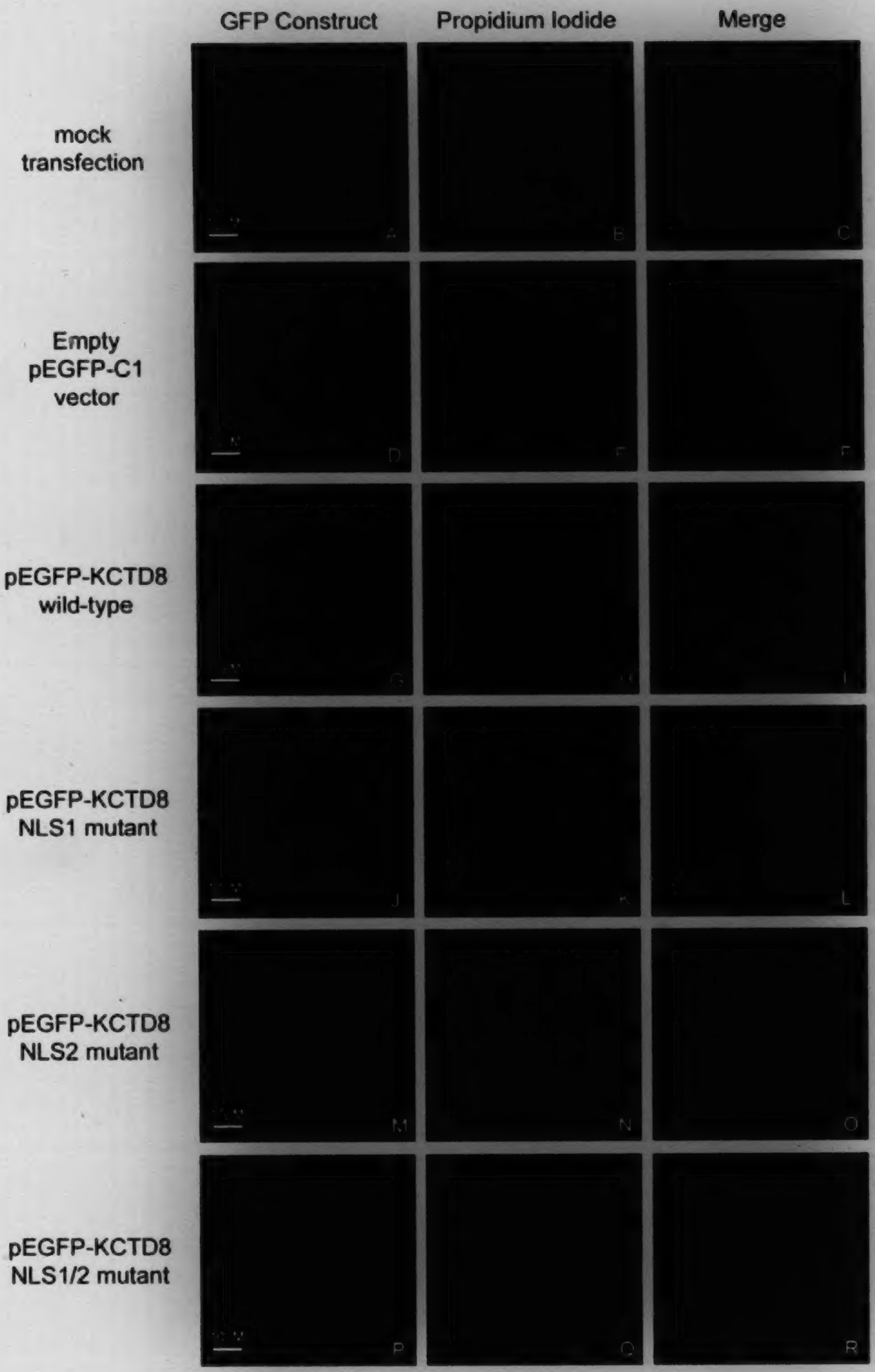
GFP Construct
Propidium Iodide
Merge
mock transfection
Empty pEGFP-C1 vector
pEGFP-KCTD8 wild-type
pEGFP-KCTD8 NLS1 mutant
pEGFP-KCTD8 NLS2 mutant
pEGFP-KCTD8 NLS1/2 mutant
A
B
C
D
E
F
G
H
I
J
K
L
M
N
O
P
Q
R

Figure 5.12 – Immunohistochemical localization of KCTD8 in dark-reared and light-induced retinal degenerative rat retinas.

Retina sections from dark-reared rats (0 hour light treatment) or rats exposed to increasing durations of light followed by zero hours dark recovery or 24 hours dark recovery were labeled with a rabbit anti-KCTD8 polyclonal antibody and detected with an Oregon Green 514 secondary antibody (green) (panels A, E, I, M, and Q). Nuclei in panels B, F, J, N, R and V are stained with propidium iodide (red). The third column (panels C, G, K, O, S, and W) are overlaid images from the first two columns. The fourth column, panels D, H, L, P and T, are 100X magnifications of the retina sections to better show the outer nuclear layer and photoreceptor cells. Note the nuclear localization of KCTD8 in the ganglion cells of dark-reared retinas (panel C, indicated with arrowheads) as well as light-treated retinas (panels G, K O, and S, indicated with arrowheads) and the nuclear localization of KCTD8 in the outer nuclear layer of 4 hour and 8 hour light-treated retinas (panels H and L, indicated with arrows). In addition, nuclear as well as cytoplasmic localization of KCTD8 is seen in the inner nuclear layer throughout the various light treatments (panels C, G, K, O, and S). Control immunohistochemical staining with only the secondary antibody (no primary antibody) is shown in panels U and W. The retinal layers are labeled as follows: GCL, ganglion cell layer; IPL, inner plexiform layer; INL, inner nuclear layer; OPL, outer plexiform layer; ONL, outer nuclear layer; IS, photoreceptor inner segments; OS, photoreceptor outer segments; RPE, retinal pigment epithelium. In panels A, E, I, M, Q, and U the size bar = 40 µm. In panels D, H, L, P and T the size bar = 20 µm.

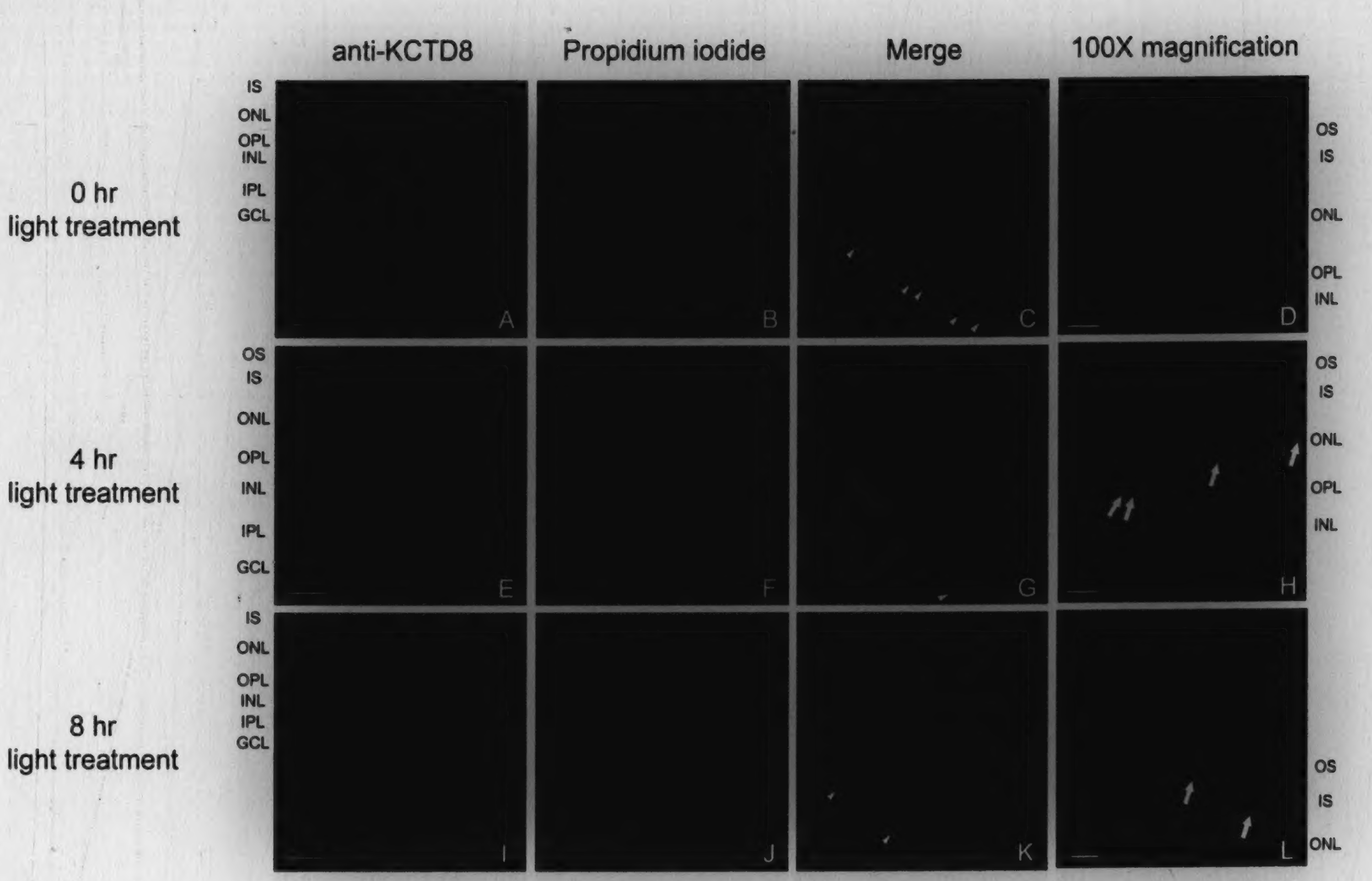
anti-KCTD8
Propidium iodide
Merge
100X magnification
0 hr
light treatment
4 hr
light treatment
8 hr
light treatment
IS
ONL
OPL
INL
IPL
GCL
OS
IS
ONL
OPL
INL
IPL
GCL
IS
ONL
OPL
INL
IPL
GCL
A
B
C
D
E
F
G
H
I
J
K
L
OS
IS
ONL
OPL
INL
OS
IS
ONL
OPL
INL
OS
IS
ONL

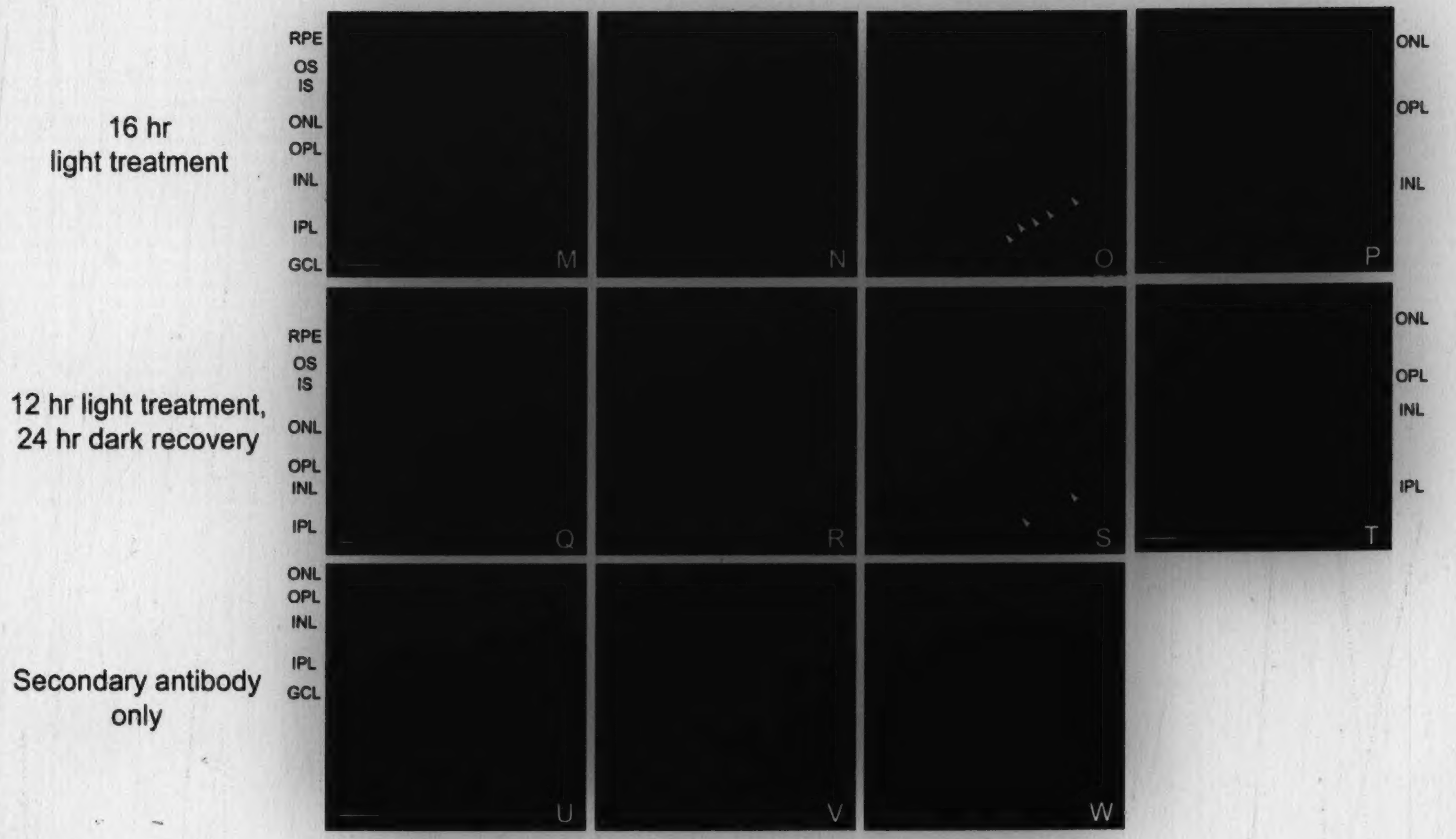
16 hr light treatment
12 hr light treatment, 24 hr dark recovery
Secondary antibody only
RPE
OS
IS
ONL
OPL
INL
IPL
GCL
M
N
O
P
Q
R
S
T
U
V
W

Figure 5.13 – Co-localization of KCTD8 with α-tubulin in dark-reared and light-induced retinal degenerative rat retinas.

Retinal sections in panels A, E, I, M, and Q were labeled with a mouse anti-α-tubulin antibody and detected with an Alexa Fluor 488 polyclonal antibody (green). Retina sections labeled with rabbit anti-KCTD8 polyclonal antibody and detected with a Cy3-conjugated secondary antibody (red) are shown in panel B, F, J, N, and R. Hoechst-stained nuclei (blue) are shown in panels C, G, K, O, S, and W. Panels from the first three columns were overlaid to generate the merge column (panels D, H, L, P, and T). Co-localization of α-tubulin and KCTD8 is shown by the yellow signal in the merged panels. Control immunohistochemical staining with only the respective secondary antibodies is shown in Panels U and V with the merged image shown in panel X. The various retinal layers are labeled as follows: GCL, ganglion cell layer; IPL, inner plexiform layer; INL, inner nuclear layer; OPL, outer plexiform layer; ONL, outer nuclear layer; IS, photoreceptor inner segments; OS, photoreceptor outer segments; RPE, retinal pigment epithelium. The size bars in panels A, E, I, M, Q, and U = 40 μm.

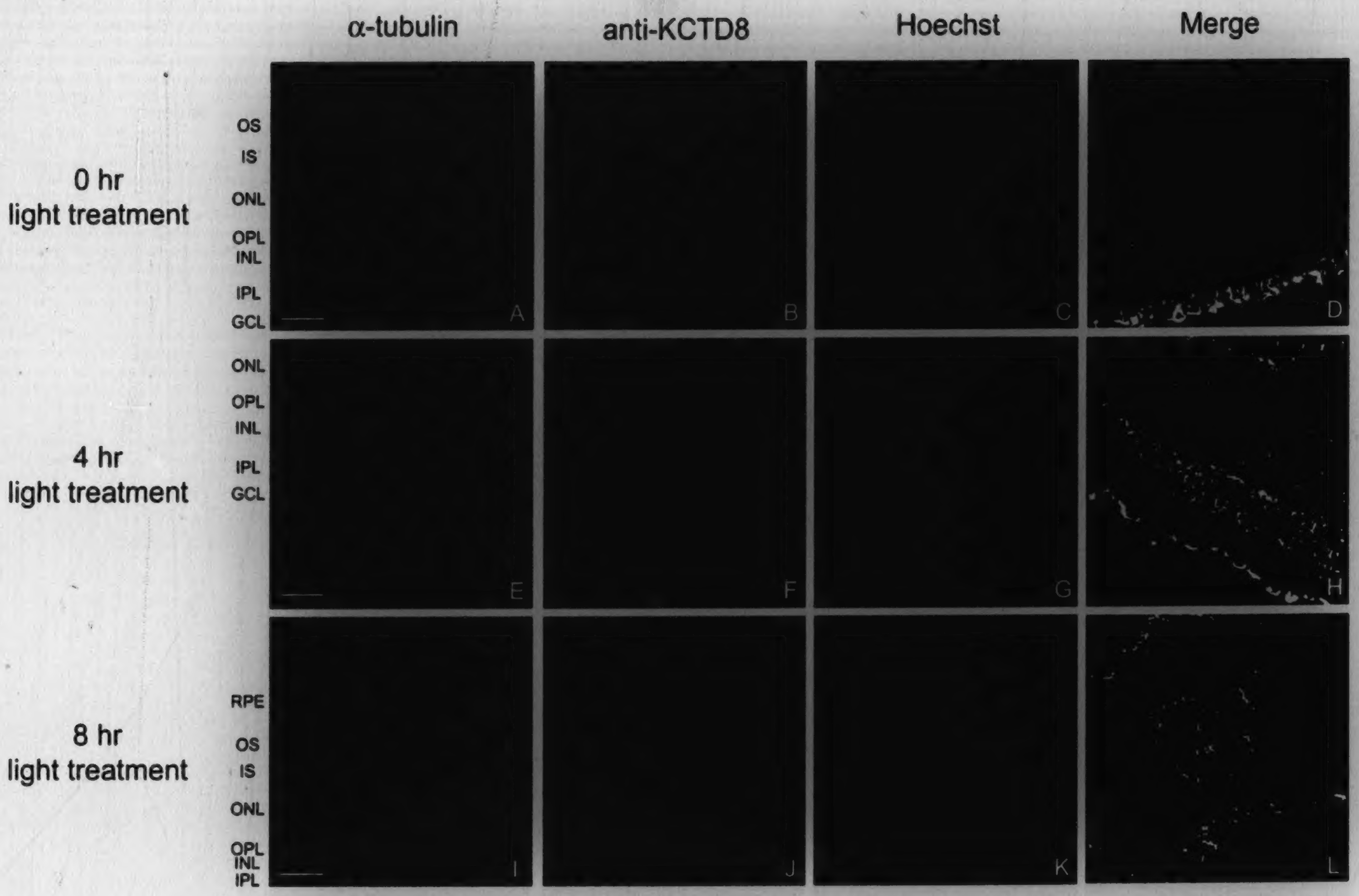
α-tubulin
anti-KCTD8
Hoechst
Merge
0 hr
light treatment
4 hr
light treatment
8 hr
light treatment
OS
IS
ONL
OPL
INL
IPL
GCL
ONL
OPL
INL
IPL
GCL
RPE
OS
IS
ONL
OPL
INL
IPL
A
B
C
D
E
F
G
H
I
J
K
L

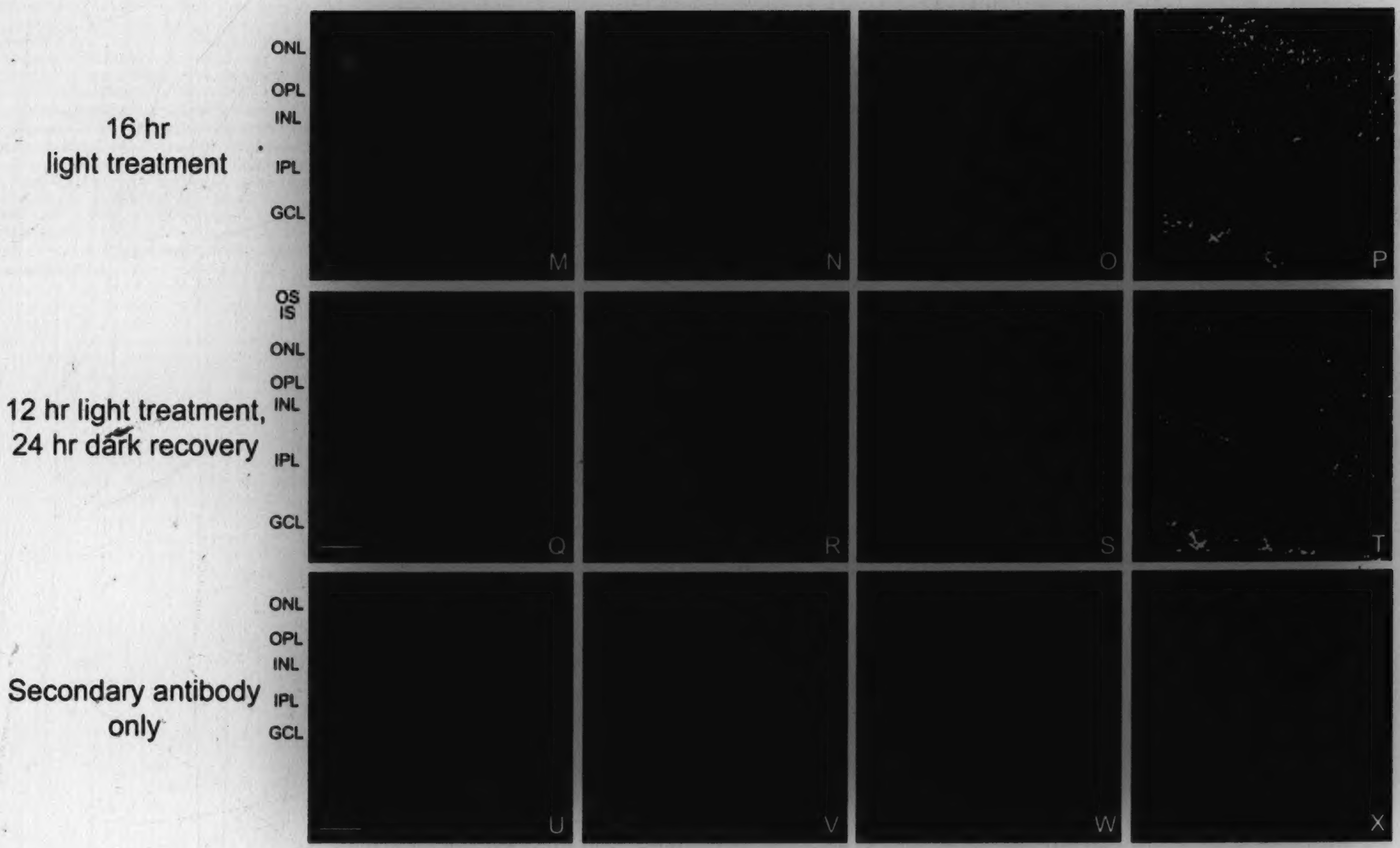
16 hr
light treatment
ONL
OPL
INL
IPL
GCL
M
N
O
P
12 hr light treatment,
24 hr dark recovery
OS
IS
ONL
OPL
INL
IPL
GCL
Q
R
S
T
Secondary antibody
only
ONL
OPL
INL
IPL
GCL
U
V
W
X

Figure 5.14 – Immunolocalization of KCTD8 in wild-type and RCS rat retinas. Retina sections of wild-type rats (panels A), 2 month old (panel D) and 6 month old (panel G) RCS rats were labeled with rabbit anti-KCTD8 polyclonal antibody and detected with a goat anti-rabbit Alexa Fluor 488 secondary antibody (green). Nuclei were stained with propidium iodide (red) (panels B, E, and H). Note the loss of the outer nuclear layer and photoreceptor cells by 6 months of age, which is characteristic of RCS retinas. In addition, there is an increase in nuclear staining of KCTD8 in the inner nuclear layer of the 2 month and 6 month RCS retina as compared to the wild-type retina (as shown by the yellow merged signal in panels C, F and I). The retinal layers are labeled as follows: GCL, ganglion cell layer; IPL, inner plexiform layer; INL, inner nuclear layer; OPL, outer plexiform layer; ONL, outer nuclear layer; IS, photoreceptor inner segments; OS, photoreceptor outer segments; RPE, retinal pigment epithelium.

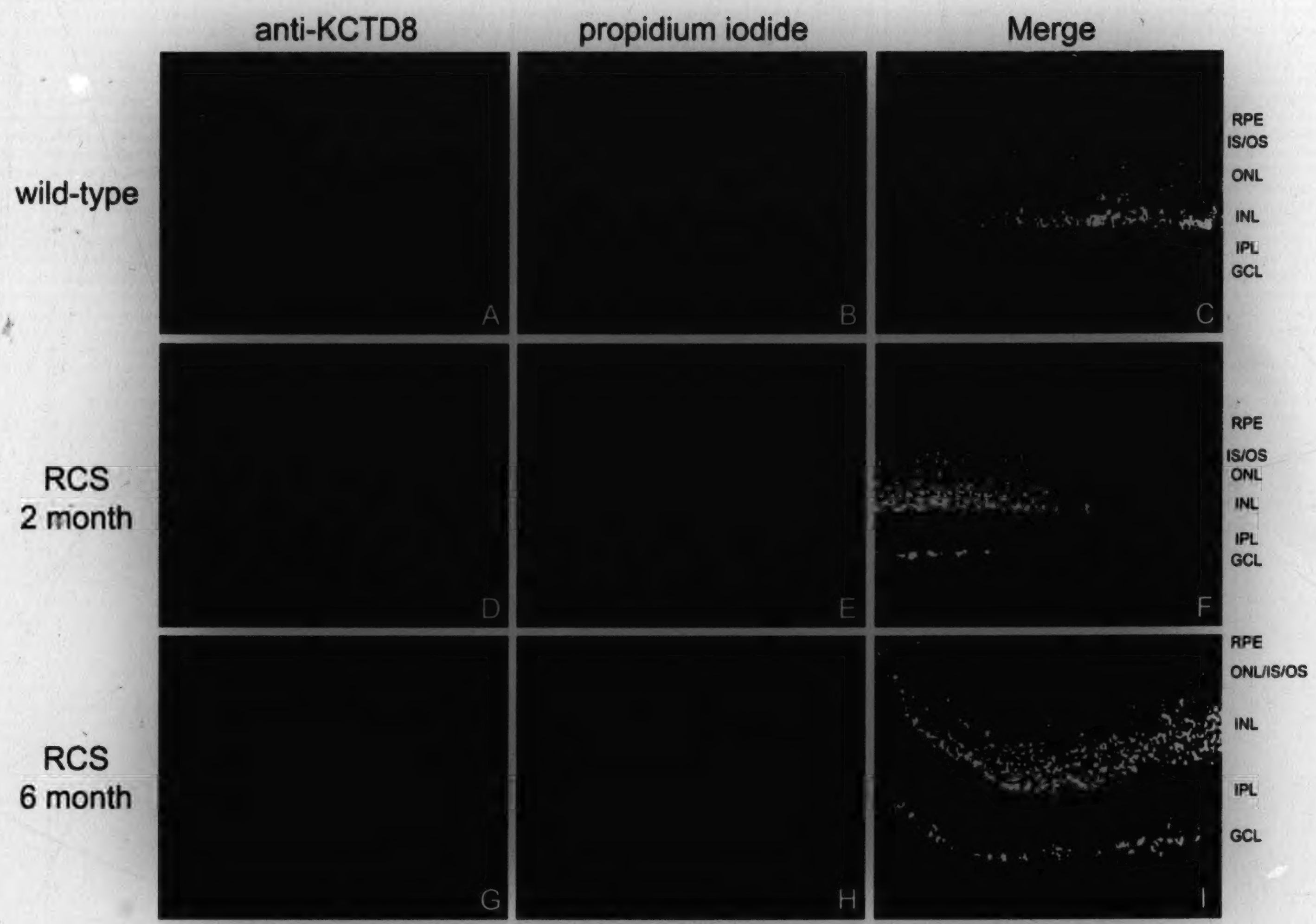
anti-KCTD8
propidium iodide
Merge
wild-type
RCS
2 month
RCS
6 month
A
B
C
D
E
F
G
H
I
RPE
IS/OS
ONL
INL
IPL
GCL
RPE
IS/OS
ONL
INL
IPL
GCL
RPE
ONL/IS/OS
INL
IPL
GCL

5.5 REFERENCES

1. Alexandrova, N., Niklinski, J., Bliskovsky, V., Otterson, G.A., Blake, M., Kaye, F.J. and Zajac-Kaye, M. (1995) The N-terminal domain of c-Myc associates with alpha-tubulin and microtubules in vivo and in vitro. *Mol Cell Biol,* **15,** 5188-95.
2. Niklinski, J., Claassen, G., Meyers, C., Gregory, M.A., Allegra, C.J., Kaye, F.J., Hann, S.R. and Zajac-Kaye, M. (2000) Disruption of Myc-tubulin interaction by hyperphosphorylation of c-Myc during mitosis or by constitutive hyperphosphorylation of mutant c-Myc in Burkitt's lymphoma. *Mol Cell Biol,* **20,** 5276-84.
3. Ziegelbauer, J., Shan, B., Yager, D., Larabell, C., Hoffmann, B. and Tjian, R. (2001) Transcription factor MIZ-1 is regulated via microtubule association. *Mol Cell,* **8,** 339-49.
4. Jans, D.A., Xiao, C.Y. and Lam, M.H. (2000) Nuclear targeting signal recognition: a key control point in nuclear transport? *Bioessays,* **22,** 532-44.
5. Kaffman, A. and O'Shea, E.K. (1999) Regulation of nuclear localization: a key to a door. *Annu Rev Cell Dev Biol,* **15,** 291-339.
6. Furukawa-Hibi, Y., Kobayashi, Y., Chen, C. and Motoyama, N. (2005) FOXO transcription factors in cell-cycle regulation and the response to oxidative stress. *Antioxid Redox Signal,* **7,** 752-60.
7. Ferrando-May, E. (2005) Nucleocytoplasmic transport in apoptosis. *Cell Death Differ,* **12,** 1263-1276.
8. Kelln, R., Darrow, R., Organisciak, D.T., Wong, P. (In preparation) Identification and characterization of rat KCTD8.
9. Reinhardt, A. and Hubbard, T. (1998) Using neural networks for prediction of the subcellular location of proteins. *Nucleic Acids Res,* **26,** 2230-6.
10. Guda, C. and Subramaniam, S. (2005) pTARGET [corrected] a new method for predicting protein subcellular localization in eukaryotes. *Bioinformatics,* **21,** 3963-9.
11. Kelln, R.M., Vasireddy, V., Chrenek, M.A., Darrow, R., Organisciak, D.T., Ayyagari, R., Wong, P. (In preparation) KCTD8 binds to microtubules in vivo and in vitro in an nuclear localization signal dependent manner.

12. Giannakakou, P., Sackett, D.L., Ward, Y., Webster, K.R., Blagosklonny, M.V. and Fojo, T. (2000) p53 is associated with cellular microtubules and is transported to the nucleus by dynein. *Nat Cell Biol,* **2,** 709-17.

13. Kelln, R.M., Organisciak, D.T., Darrow, R., Wong, P. (In preparation) Identification and characterization of T-cadherin, isolated by a differential screening strategy to identify genes involved in light-induced retinal degeneration.

14. Organisciak, D.T., Darrow, R.M., Jiang, Y.I., Marak, G.E. and Blanks, J.C. (1992) Protection by dimethylthiourea against retinal light damage in rats. *Invest Ophthalmol Vis Sci,* **33,** 1599-609.

15. Organisciak, D.T., Kutty, R.K., Leffak, M., Wong, P., Messing, S., Wiggert, B., Darrow, R.M. and Chader, G.J. (1995) Oxidative damage and responses in retinal nuclei arising from intense light exposure. In *Degenerative Diseases of the Retina.* Plenum Press, New York, pp. 19-26.

16. Bus, J.S. and Gibson, J.E. (1984) Paraquat: model for oxidant-initiated toxicity. *Environ Health Perspect,* **55,** 37-46.

17. Autor, A.P. (1977) *Biochemical mechanisms of paraquat toxicity.* Academic Press, New York.

18. Davies, K.J. (1999) The broad spectrum of responses to oxidants in proliferating cells: a new paradigm for oxidative stress. *IUBMB Life,* **48,** 41-7.

19. Pong, K., Doctrow, S.R., Huffman, K., Adinolfi, C.A. and Baudry, M. (2001) Attenuation of staurosporine-induced apoptosis, oxidative stress, and mitochondrial dysfunction by synthetic superoxide dismutase and catalase mimetics, in cultured cortical neurons. *Exp Neurol,* **171,** 84-97.

20. D'Cruz, P.M., Yasumura, D., Weir, J., Matthes, M.T., Abderrahim, H., LaVail, M.M. and Vollrath, D. (2000) Mutation of the receptor tyrosine kinase gene Mertk in the retinal dystrophic RCS rat. *Hum Mol Genet,* **9,** 645-51.

21. Herron, W.L., Riegel, B.W., Myers, O.E., Rubin, M.L. (1968) Retinal dystrophy in the rat - A pigment epithelial disease. *Invest Ophthalmol Vis Sci,* **13,** 585-604.

22. Jones, B.W. and Marc, R.E. (2005) Retinal remodeling during retinal degeneration. *Exp Eye Res,* **81,** 123-37.

23. Strauss, O., Stumpff, F., Mergler, S., Wienrich, M. and Wiederholt, M. (1998) The Royal College of Surgeons rat: an animal model for inherited retinal degeneration with a still unknown genetic defect. *Acta Anat (Basel),* **162,** 101-11.

24. Tso, M., Zhang, C., Abler, A., Chang, C., Wong, F., Chang, G. and Lam, T. (1994) Apoptosis leads to photoreceptor degeneration in inherited retinal dystrophy of RCS rats. *Invest. Ophthalmol. Vis. Sci.,* **35,** 2693-2699.

25. Shimizu, K., Fujino, T., Ando, K., Hayakawa, M., Yasuda, H. and Kikugawa, K. (2003) Overexpression of oxidized protein hydrolase protects COS-7 cells from oxidative stress-induced inhibition of cell growth and survival. *Biochem Biophys Res Commun,* **304,** 766-71.

26. Wolter, K.G., Hsu, Y.T., Smith, C.L., Nechushtan, A., Xi, X.G. and Youle, R.J. (1997) Movement of Bax from the cytosol to mitochondria during apoptosis. *J Cell Biol,* **139,** 1281-92.

27. Kerr, J.F., Wyllie, A.H. and Currie, A.R. (1972) Apoptosis: a basic biological phenomenon with wide-ranging implications in tissue kinetics. *Br J Cancer,* **26,** 239-57.

28. Hacker, G. (2000) The morphology of apoptosis. *Cell Tissue Res,* **301,** 5-17.

29. Yang, W.L. and Sun, A.Y. (1998) Paraquat-induced cell death in PC12 cells. *Neurochem Res,* **23,** 1387-94.

30. Dodge, A.D. (1971) The mode of action of the bipyridylium herbicides, paraquat and diquat. *Endeavour,* **30,** 130-5.

31. Suntres, Z.E. (2002) Role of antioxidants in paraquat toxicity. *Toxicology,* **180,** 65-77.

32. Kabir, J., Lobo, M. and Zachary, I. (2002) Staurosporine induces endothelial cell apoptosis via focal adhesion kinase dephosphorylation and focal adhesion disassembly independent of focal adhesion kinase proteolysis. *Biochem J,* **367,** 145-55.

33. Tamaoki, T., Nomoto, H., Takahashi, I., Kato, Y., Morimoto, M. and Tomita, F. (1986) Staurosporine, a potent inhibitor of phospholipid/Ca++dependent protein kinase. *Biochem Biophys Res Commun,* **135,** 397-402.

34. Matsumoto, H. and Sasaki, Y. (1989) Staurosporine, a protein kinase C inhibitor interferes with proliferation of arterial smooth muscle cells. *Biochem Biophys Res Commun,* **158,** 105-9.

35. Yanagihara, N., Tachikawa, E., Izumi, F., Yasugawa, S., Yamamoto, H. and Miyamoto, E. (1991) Staurosporine: an effective inhibitor for Ca2+/calmodulin-dependent protein kinase II. *J Neurochem,* **56,** 294-8.

36. Fallon, R.J. (1990) Staurosporine inhibits a tyrosine protein kinase in human hepatoma cell membranes. *Biochem Biophys Res Commun,* **170,** 1191-6.

37. Badwey, J.A., Erickson, R.W. and Curnutte, J.T. (1991) Staurosporine inhibits the soluble and membrane-bound protein tyrosine kinases of human neutrophils. *Biochem Biophys Res Commun,* **178,** 423-9.

38. Elliott, L.H., Wilkinson, S.E., Sedgwick, A.D., Hill, C.H., Lawton, G., Davis, P.D. and Nixon, J.S. (1990) K252a is a potent and selective inhibitor of phosphorylase kinase. *Biochem Biophys Res Commun,* **171,** 148-54.

39. Noell, W.K., Walker, V.S., Kang, B.S. and Berman, S. (1966) Retinal damage by light in rats. *Investigative Ophthalmology,* **5,** 450-472.

40. Noell, W.K., Organisciak, D.T., Ando, H., Braniecki, M.A. and Durlin, C. (1987) Ascorbate and dietary protective mechanisms in retinal light damage of rats: electrophysiological, histological and DNA measurements. *Prog Clin Biol Res,* **247,** 469-83.

41. Kutty, R.K., Kutty, G., Wiggert, B., Chader, G.J., Darrow, R.M. and Organisciak, D.T. (1995) Induction of heme oxygenase 1 in the retina by intense visible light: suppression by the antioxidant dimethylthiourea. *Proc Natl Acad Sci U S A,* **92,** 1177-81.

42. Organisciak, D.T., Darrow, R.A., Barsalou, L., Darrow, R.M. and Lininger, L.A. (1999) Light-induced damage in the retina: differential effects of dimethylthiourea on photoreceptor survival, apoptosis and DNA oxidation. *Photochem Photobiol,* **70,** 261-8.

43. Pasi, A. (1978) *The Toxicity of Paraquat, Diquat, and Morfamquat*. Hans Huber, Bern.

44. Haber, F., Weiss, J. (1934) The catalytic decomposition of hydrogen peroxide by iron salts. *Proc. R. Soc.*, **147**, 332-351.

45. Kehrer, J.P. (2000) The Haber-Weiss reaction and mechanisms of toxicity. *Toxicology,* **149,** 43-50.

46. Wong, P., Ulyanova, T., Organisciak, D.T., Bennett, S., Lakins, J., Arnold, J.M., Kutty, R.K., Tenniswood, M., vanVeen, T., Darrow, R.M. and Chader, G. (2001) Expression of multiple forms of clusterin during light-induced retinal degeneration. *Current Eye Research,* **23,** 157-165.

47. Oyster, C.W. (1999) The human eye: structure and function. In. Sinauer Associates, Sunderland, MA, pp. 60-61; 545-648.

48. Steinberg, R.H. (1987) Monitoring communications between photoreceptors and pigment epithelial cells: effects of "mild" systemic hypoxia. Friedenwald lecture. *Invest Ophthalmol Vis Sci,* **28,** 1888-904.

49. Hannibal, J., Hindersson, P., Knudsen, S.M., Georg, B. and Fahrenkrug, J. (2002) The photopigment melanopsin is exclusively present in pituitary adenylate cyclase-activating polypeptide-containing retinal ganglion cells of the retinohypothalamic tract. *J Neurosci,* **22,** RC191.

50. Hattar, S., Liao, H.W., Takao, M., Berson, D.M. and Yau, K.W. (2002) Melanopsin-containing retinal ganglion cells: architecture, projections, and intrinsic photosensitivity. *Science,* **295,** 1065-70.

51. Gooley, J.J., Lu, J., Chou, T.C., Scammell, T.E. and Saper, C.B. (2001) Melanopsin in cells of origin of the retinohypothalamic tract. *Nat Neurosci,* **4,** 1165.

52. Provencio, I., Rodriguez, I.R., Jiang, G., Hayes, W.P., Moreira, E.F. and Rollag, M.D. (2000) A novel human opsin in the inner retina. *J Neurosci,* **20,** 600-5.

53. Bok, D. and Hall, M.O. (1971) The role of the pigment epithelium in the etiology of inherited retinal dystrophy in the rat. *J Cell Biol,* **49,** 664-82.

54. Marc, R.E., Jones, B.W., Watt, C.B. and Strettoi, E. (2003) Neural remodeling in retinal degeneration. *Prog Retin Eye Res,* **22,** 607-55.

55. Jones, B.W., Watt, C.B., Frederick, J.M., Baehr, W., Chen, C.K., Levine, E.M., Milam, A.H., Lavail, M.M. and Marc, R.E. (2003) Retinal remodeling triggered by photoreceptor degenerations. *J Comp Neurol,* **464,** 1-16.

56. Jans, D.A. and Hubner, S. (1996) Regulation of protein transport to the nucleus: central role of phosphorylation. *Physiol Rev,* **76,** 651-85.

57. Woronicz, J.D., Gao, X., Cao, Z., Rothe, M. and Goeddel, D.V. (1997) IkappaB kinase-beta: NF-kappaB activation and complex formation with IkappaB kinase-alpha and NIK. *Science,* **278,** 866-9.

58. Mercurio, F., Zhu, H., Murray, B.W., Shevchenko, A., Bennett, B.L., Li, J., Young, D.B., Barbosa, M., Mann, M., Manning, A. and Rao, A. (1997) IKK-1 and IKK-2: cytokine-activated IkappaB kinases essential for NF-kappaB activation. *Science,* **278,** 860-6.

59. Kastan, M.B., Onyekwere, O., Sidransky, D., Vogelstein, B. and Craig, R.W. (1991) Participation of p53 protein in the cellular response to DNA damage. *Cancer Res,* **51,** 6304-11.

60. Inoue, T., Wu, L., Stuart, J. and Maki, C.G. (2005) Control of p53 nuclear accumulation in stressed cells. *FEBS Lett,* **579,** 4978-84.

61. Luscher, B. and Eisenman, R.N. (1992) Mitosis-specific phosphorylation of the nuclear oncoproteins Myc and Myb. *J Cell Biol,* **118,** 775-84.

Chapter 6

Summary and Conclusions

6.1 SUMMARY AND CONCLUSIONS

Retinal degeneration occurs by apoptosis, which involves altered gene expression to initiate and carry out the apoptotic cascade [1]. However, the molecular mechanisms involved in retinal cell death are not well understood. The work described in this thesis represents the steps taken to further our understanding of the process of retinal degeneration and more generally, the process of apoptosis. From the initial isolation of a cDNA clone representing the partial sequence of a novel gene, to determining how the encoded protein performs under normal conditions as well as conditions of cell stress and LIRD, provides us with further avenues to explore and enhances our understanding of retinal cell death.

The first hypothesis I set out to test was that LIRD is a multifaceted process involving numerous changes in the molecular phenotype of the retina. In an effort to better understand the process of LIRD and identify the numerous molecular changes I performed a differential cDNA library screen (Chapter 2). A number of differentially expressed genes that help define the retinal degeneration molecular phenotype were isolated from this screen. The myriad of genes isolated from this screen, as well as the functional clustering of these genes, provide us with a sense of the molecular environment at that particular state of retinal degeneration. A number of clones isolated corresponded to the crystallin gene family, which have been found to play a role in protecting the retina from light damage [2, 3]. It is clear from the clones isolated that after 16 hours of light exposure the retina is undergoing cell death and molecular changes are taking place in order to protect the retina or facilitate the process of retinal cell death. Ideally, the full functional characterization of each gene isolated from the cDNA library screen would provide us with better insight into the degeneration process. Unfortunately, this would encompass numerous years of work and is beyond the scope of this thesis. The benefit of using the cDNA library screening approach outlined in chapter 2 is the potential identification of novel genes which have either not been characterized or genes that have not been previously found to be expressed during retinal degeneration.

In the current thesis I choose to follow my initial findings by further characterizing two genes, T-cadherin and KCTD8, which were isolated from the cDNA library screen and had not previously been shown to be involved over the course of retinal degeneration. The characterization of T-cadherin was undertaken in response to the growing number of cadherin family members implicated in retinal disease [4-10]. My findings, combined with research indicating that overexpression of T-cadherin protects against oxidative stress induced apoptosis [11], suggest that T-cadherin is upregulated during the stress response phase of LIRD and may function to protect the retina from oxidative stress leading to apoptosis. In addition, the localization of T-cadherin to the Müller cells of the retina provide further support for a signaling mechanism between the intact inner retina and the degenerating outer retina to either protect the retina or facilitate the cell death process.

The main focus of the thesis, encompassing chapters 3, 4 and 5, is based on my hypothesis that alterations in expression and localization of KCTD8 define one aspect of the molecular phenotype of LIRD. KCTD8 was isolated as a partial cDNA clone from the cDNA library screen and the use of RACE and *in silico* analysis provided me with further avenues to explore with respect to the characterization of the gene and the prediction of its biological function in general and in relation to retinal degeneration. Most notable in my preliminary characterization of the KCTD8 protein sequence was the presence of two putative nuclear localization signals (NLSs) and a conserved N-terminal BTB/POZ/T1 domain. Further analysis of KCTD8 focused on determining the functionality of the two putative NLSs.

While the exact purpose of multiple NLSs in a protein is not fully known it is believed that nuclear targeting sequences may be of varying strengths or potencies such that some NLSs may be more efficient at targeting a protein to the nucleus [12]. Thus, combining multiple NLSs on a protein would be expected to enhance the nuclear localization [12]. We hypothesized that since KCTD8 contained two putative NLSs, the protein would be directed to the nucleus. To determine the functionality of the NLSs within the KCTD8 protein under normal conditions, I studied the subcellular localization of wild-type and NLS mutant GFP-tagged KCTD8 proteins. Contrary to my hypothesis, I found that under normal conditions, *in vitro*, the wild-type KCTD8 protein is not localized to the nucleus; however, disrupting the NLSs did result in aberrant cytoplasmic localization. In addition, I discovered that wild-type KCTD8 co-localizes and binds to microtubules in mammalian cell culture and in the retina.

Due to the involvement of oxidative stress in retinal degeneration and because KCTD8 was isolated from a screen for genes involved in retinal degeneration, I hypothesized that an oxidative stress cellular trigger was needed to localize wild-type KCTD8 to the nucleus. I tested this hypothesis by treating KCTD8 transfected mammalian cells with chemicals known to induce oxidative stress. As well, I analyzed changes in cellular localization during retinal degeneration. In general I observed only a small percentage of cells showing nuclear localized KCTD8 in mammalian cell culture and in the retina. From my results it became clear that the nuclear localization of KCTD8 is not as straightforward as first thought. Based on the presence of three conserved nuclear export signals (NES) in the KCTD8 protein, I tested whether the protein was imported into the nucleus and then exported back to the cytoplasm before visualization by chemically inhibiting nuclear export. While I saw no change from untreated cells, suggesting that the protein remained cytoplasmically localized, it is possible that the treatment I used was not sufficient to inhibit nuclear export. A method in which to confirm this hypothesis would be to mutate the NESs using the same methodology to mutate the NLSs. Transfecting mammalian cells with the KCTD8 protein containing mutant NESs would allow us to better analyze the possible transient nucleocytoplasmic localization of KCTD8.

There are a multitude of factors that can regulate nuclear localization of proteins such as phosphorylation, inter- and intramolecular masking, and the presence of competing targeting signals [13, 14]. In the case of phosphorylation, NLSs can be masked by the presence of phosphorylation within or nearby the NLSs [15]. As well, the NLS target sequence recognition by import proteins can be modulated by phosphorylation, as is the case with importin α/β1-recognized NLSs of T-ag and the *Drosophila* morphogen Dorsal [16-18]. Phosphorylation has been found to increase the binding of the NLS sites to importin α/β by about 100-fold, in the case of T-ag [13]. *In silico* analysis of KCTD8 revealed 40 putative phosphorylation sites in the KCTD8 protein, a few of which are within or near the NLSs. Therefore, it is plausible that phosphorylation may play some role in the regulation of nuclear localization of KCTD8 and may explain the low number of cells I observed showing nuclear localization of KCTD8.

Phosphorylation within the protein such that it masks the NLSs is an example of intramolecular masking resulting in rendering the NLSs non-functional. In addition, masking of the NLSs due to protein conformation is also a plausible intramolecular masking affecting the recognition of the NLSs by the import proteins and resulting in the KCTD8 protein not being targeted to the nucleus. Without knowing the native conformation of the protein it is difficult to determine if this is a possibility. However, the development of antibodies that specifically detect the NLSs within the KCTD8 protein may allow the determination of whether those sites are exposed on the native protein.

There are many known examples of intermolecular masking resulting in preventing the recognition of the specific target sequences. The best characterized NLS masking protein is I-κB, which binds to the NLS present in the NF-κB p65 subunit [19, 20]. The unmasking of the NF-κB p65 NLS is a highly regulated process involving phosphorylation and proteolytic degradation to remove I-κB and expose the NLS. From my results, we know that KCTD8 binds to α-tubulin and it is possible that this association could mask the NLSs present in the KCTD8 protein. However, as discussed in chapter 4, it is more likely that the binding of KCTD8 to α-tubulin and microtubules functions as a mechanism to sequester the protein to the cytoplasm of the cell. Disruption of the microtubule network results in nuclear as well as cytoplasmic localization of KCTD8, further supporting this theory of cytoplasmic sequestration. On the contrary, the nucleocytoplasmic regulation of KCTD8 could involve the dual signal:dual location model, which suggests that competing intracellular signals could result in decreased or absent nuclear localization if the cytoplasmic signal is dominant [14]. This would imply that a separate signal, independent of the NLSs, is required to localize the protein to the microtubules and that disruption of this unknown signal would result in nuclear accumulation of KCTD8. Since my results show that the disruption of the NLSs also disrupts the microtubule binding, it may in fact be the NLSs that are mediating the binding to microtubules, which would discount the dual signal hypothesis. However, it is possible that an intermediary protein is required to tether the KCTD8 protein to the microtubules via the NLSs. Importin, which is a protein that functions in transporting NLS containing proteins to the nucleus, has been shown to bind microtubules [21] and is therefore a likely candidate to mediate the binding of KCTD8 to α-tubulin. In either case of the NLSs binding directly to microtubules or an intermediary protein binding to the microtubules, it seems unlikely that there is a second subcellular signal contained within or surrounding the NLSs that functions in a dominant fashion to inhibit nuclear localization.

Many proteins that shuttle between the cytoplasm and the nucleus are involved in signal transduction or are transcription factors that translocate to the nucleus to mediate gene expression. Regulating the nucleocytoplasmic transport of transcription factors is an important checkpoint in the control of gene expression [22]. A number of the mechanisms proposed here for the regulation of KCTD8 have been shown to function in regulating the nuclear localization of transcription factors. Although the exact function of the KCTD8 gene has not been elucidated, it is plausible that the gene functions as a transcription factor and it is tightly regulated, with respect to nuclear localization, in an effort to control gene expression. In the context of retinal degeneration, nucleocytoplasmic transport of KCTD8 may function to either inhibit retinal degeneration and protect the retina or facilitate the process of apoptosis leading to vision loss by regulating the genes involved in these processes. The association between KCTD8 and microtubules may also be important in the process of retinal degeneration since studies have shown that oxidative stress in neuronal cell lines leads to a disruption of the cytoskeleton and more specifically a depolymerization of microtubules [23, 24]. Whether the nuclear localization seen with the oxidative stress treatments is due to a breakdown in the microtubule network is a worthwhile future endeavor to explore.

One feature of KCTD8 that was not analyzed in this thesis is the functionality of the BTB/POZ/T1 domain located at the N-terminus of the protein. Since the nuclear localization of KCTD8 appears to be a tightly regulated process that could be affected by a number of factors, a worthwhile future avenue of research would be to analyze this N-terminal conserved BTB/POZ domain in order to provide additional insight into the function of KCTD8. The functionality of this conserved domain may provide clues to the factors required to bring about complete nuclear localization of KCTD8.

The BTB/POZ/T1 domain is a known protein-protein interaction motif, which can bind other proteins containing either a BTB/POZ domain or a number of other conserved domains [25]. At present there are over 200 proteins that contain this conserved domain, many of which have been shown to function as transcription factors [26]. BTB/POZ containing proteins have been found to be involved in a range of biological processes such as development [27], cell differentiation [26], homeostasis, oncogenesis [26, 28], and transcription repression/activation [29]. By analyzing binding partners of KCTD8, through techniques used to identify protein interactions such as a yeast two-hybrid screen, we will better understand the function of this gene.

Understanding the intricacies of the KCTD8 protein, such as the functionality of the NLSs, NESs, and the BTB/POZ/T1 domain, will increase our understanding of the gene in general. This knowledge of KCTD8 function can then be related to its function in the retina and during retinal degeneration. The research presented in this thesis provides numerous further avenues to explore with respect to the functional characterization of KCTD8. Gaining an understanding of the molecular mechanisms involved in the retinal response to stress will facilitate the development of new therapies to treat retinal degeneration and retinal disease.

6.2 REFERENCES

1. Reme, C.E., Grimm, C., Hafezi, F., Marti, A. and Wenzel, A. (1998) Apoptotic cell death in retinal degenerations. *Prog Retin Eye Res,* **17,** 443-64.
2. Sakaguchi, H., Miyagi, M., Darrow, R.M., Crabb, J.S., Hollyfield, J.G., Organisciak, D.T. and Crabb, J.W. (2003) Intense light exposure changes in crystallin content in retina. *Experimental Eye Research,* **76,** 131-133.
3. Organisciak, D. (2006) Genetic, Age and Light Mediated Effects on Crystallin Protein Expression in the Retina. *Photochem Photobiol.*
4. Ahmed, Z.M., Riazuddin, S., Bernstein, S.L., Ahmed, Z., Khan, S., Griffith, A.J., Morell, R.J., Friedman, T.B. and Wilcox, E.R. (2001) Mutations of the protocadherin gene PCDH15 cause Usher syndrome type 1F. *Am J Hum Genet,* **69,** 25-34.
5. Alagramam, K.N., Yuan, H., Kuehn, M.H., Murcia, C.L., Wayne, S., Srisailpathy, C.R., Lowry, R.B., Knaus, R., Van Laer, L., Bernier, F.P., Schwartz, S., Lee, C., Morton, C.C., Mullins, R.F., Ramesh, A., Van Camp, G., Hageman, G.S., Woychik, R.P. and Smith, R.J. (2001) Mutations in the novel protocadherin PCDH15 cause Usher syndrome type 1F. *Hum Mol Genet,* **10,** 1709-18.
6. Bork, J.M., Peters, L.M., Riazuddin, S., Bernstein, S.L., Ahmed, Z.M., Ness, S.L., Polomeno, R., Ramesh, A., Schloss, M., Srisailpathy, C.R., Wayne, S., Bellman, S., Desmukh, D., Ahmed, Z., Khan, S.N., Kaloustian, V.M., Li, X.C., Lalwani, A., Bitner-Glindzicz, M., Nance, W.E., Liu, X.Z., Wistow, G., Smith, R.J., Griffith, A.J., Wilcox, E.R., Friedman, T.B. and Morell, R.J. (2001) Usher syndrome 1D and nonsyndromic autosomal recessive deafness DFNB12 are caused by allelic mutations of the novel cadherin-like gene CDH23. *Am J Hum Genet,* **68,** 26-37.
7. Bolz, H., von Brederlow, B., Ramirez, A., Bryda, E.C., Kutsche, K., Nothwang, H.G., Seeliger, M., del, C.S.C.M., Vila, M.C., Molina, O.P., Gal, A. and Kubisch, C. (2001) Mutation of CDH23, encoding a new member of the cadherin gene family, causes Usher syndrome type 1D. *Nat Genet,* **27,** 108-12.
8. Sprecher, E., Bergman, R., Richard, G., Lurie, R., Shalev, S., Petronius, D., Shalata, A., Anbinder, Y., Leibu, R., Perlman, I., Cohen, N. and Szargel, R.

(2001) Hypotrichosis with juvenile macular dystrophy is caused by a mutation in CDH3, encoding P-cadherin. *Nat Genet,* **29,** 134-6.

9. Rattner, A., Smallwood, P.M., Williams, J., Cooke, C., Savchenko, A., Lyubarsky, A., Pugh, E.N. and Nathans, J. (2001) A photoreceptor-specific cadherin is essential for the structural integrity of the outer segment and for photoreceptor survival. *Neuron,* **32,** 775-86.
10. Bolz, H., Ebermann, I. and Gal, A. (2005) Protocadherin-21 (PCDH21), a candidate gene for human retinal dystrophies. *Mol Vis,* **11,** 929-33.
11. Joshi, M.B., Philippova, M., Ivanov, D., Allenspach, R., Erne, P. and Resink, T.J. (2005) T-cadherin protects endothelial cells from oxidative stress-induced apoptosis. *Faseb J,* **19,** 1737-9.
12. Dingwall, C. and Laskey, R.A. (1991) Nuclear targeting sequences--a consensus? *Trends Biochem Sci,* **16,** 478-81.
13. Jans, D.A., Xiao, C.Y. and Lam, M.H. (2000) Nuclear targeting signal recognition: a key control point in nuclear transport? *Bioessays,* **22,** 532-44.
14. Roberts, B.L., Richardson, W.D. and Smith, A.E. (1987) The effect of protein context on nuclear location signal function. *Cell,* **50,** 465-75.
15. Jans, D.A. and Hubner, S. (1996) Regulation of protein transport to the nucleus: central role of phosphorylation. *Physiol Rev,* **76,** 651-85.
16. Briggs, L.J., Stein, D., Goltz, J., Corrigan, V.C., Efthymiadis, A., Hubner, S. and Jans, D.A. (1998) The cAMP-dependent protein kinase site (Ser312) enhances dorsal nuclear import through facilitating nuclear localization sequence/importin interaction. *J Biol Chem,* **273,** 22745-52.
17. Xiao, C.Y., Hubner, S. and Jans, D.A. (1997) SV40 large tumor antigen nuclear import is regulated by the double-stranded DNA-dependent protein kinase site (serine 120) flanking the nuclear localization sequence. *J Biol Chem,* **272,** 22191-8.
18. Hubner, S., Xiao, C.Y. and Jans, D.A. (1997) The protein kinase CK2 site (Ser111/112) enhances recognition of the simian virus 40 large T-antigen nuclear localization sequence by importin. *J Biol Chem,* **272,** 17191-5.

19. Mercurio, F., Zhu, H., Murray, B.W., Shevchenko, A., Bennett, B.L., Li, J., Young, D.B., Barbosa, M., Mann, M., Manning, A. and Rao, A. (1997) IKK-1 and IKK-2: cytokine-activated IkappaB kinases essential for NF-kappaB activation. *Science,* **278,** 860-6.

20. Woronicz, J.D., Gao, X., Cao, Z., Rothe, M. and Goeddel, D.V. (1997) IkappaB kinase-beta: NF-kappaB activation and complex formation with IkappaB kinase-alpha and NIK. *Science,* **278,** 866-9.

21. Smith, H.M. and Raikhel, N.V. (1998) Nuclear localization signal receptor importin alpha associates with the cytoskeleton. *Plant Cell,* **10,** 1791-9.

22. Vandromme, M., Gauthier-Rouviere, C., Lamb, N. and Fernandez, A. (1996) Regulation of transcription factor localization: fine-tuning of gene expression. *Trends Biochem Sci,* **21,** 59-64.

23. Allani, P.K., Sum, T., Bhansali, S.G., Mukherjee, S.K. and Sonee, M. (2004) A comparative study of the effect of oxidative stress on the cytoskeleton in human cortical neurons. *Toxicol Appl Pharmacol,* **196,** 29-36.

24. Hinshaw, D.B., Miller, M.T., Omann, G.M., Beals, T.F. and Hyslop, P.A. (1993) A cellular model of oxidant-mediated neuronal injury. *Brain Res,* **615,** 13-26.

25. Albagli, O., Dhordain, P., Deweindt, C., Lecocq, G. and Leprince, D. (1995) The BTB/POZ domain: a new protein-protein interaction motif common to DNA- and actin-binding proteins. *Cell Growth Differ,* **6,** 1193-8.

26. Kelly, K.F. and Daniel, J.M. (2006) POZ for effect--POZ-ZF transcription factors in cancer and development. *Trends Cell Biol,* **16,** 578-87.

27. Zollman, S., Godt, D., Prive, G.G., Couderc, J.L. and Laski, F.A. (1994) The BTB domain, found primarily in zinc finger proteins, defines an evolutionarily conserved family that includes several developmentally regulated genes in Drosophila. *Proc Natl Acad Sci U S A,* **91,** 10717-21.

28. Nakayama, K., Nakayama, N., Davidson, B., Sheu, J.J., Jinawath, N., Santillan, A., Salani, R., Bristow, R.E., Morin, P.J., Kurman, R.J., Wang, T.L. and Shih, I.M. (2006) A BTB/POZ protein, NAC-1, is related to tumor recurrence and is essential for tumor growth and survival. *Proc Natl Acad Sci U S A.*

29. Bardwell, V.J. and Treisman, R. (1994) The POZ domain: a conserved protein-protein interaction motif. *Genes Dev,* **8,** 1664-77.